Development of Cathodic Electrocatalysts for Use in Low Temperature H_2/O_2 Fuel Cells with an Alkaline Electrolyte

Contract No. NASW-1233

Q-8

Eighth Quarterly Report
Covering
July 1, 1965 - June 30, 1967

for
National Aeronautics and Space Administration
Headquarters, Washington, D. C.

Tyco Laboratories, Inc.
Bear Hill
Waltham, Massachusetts 02154

DEVELOPMENT OF CATHODIC ELECTROCATALYSTS FOR USE IN LOW TEMPERATURE H_2/O_2 FUEL CELLS WITH AN ALKALINE ELECTROLYTE

Contract No. NASW-1233

Q-8

Eighth Quarterly Report
Covering
July 1, 1965 - June 30, 1967

by
J. Giner
J. Parry
L. Swette
R. Cattabriga

for
National Aeronautics and Space Administration
Headquarters, Washington, D. C.

NOTICE

This report was prepared as an account of Government sponsored work. Neither the United States, nor the National Aeronautics and Space Administration (NASA), nor any person acting on behalf of NASA:

A) Makes any warranty or representation, expressed or implied, with respect to the accuracy, completeness, or usefulness of the information contained in this report, or that the use of any information, apparatus, method, or process disclosed in this report may not infringe privately owned rights; or

B) Assumes any liabilities with respect to the use of, or for damages resulting from the use of any information, apparatus, method or process disclosed in this report.

As used above, "person acting on behalf of NASA" includes any employee or contractor of NASA, or employee of such contractor, to the extent that such employee or contractor of NASA, or employee of such contractor prepared, disseminates, or provides access to, any information pursuant to this employment or contract with NASA or his employment with such contractor.

Requests for copies of this report should be referred to:

National Aeronautics and Space Administration
Office of Scientific and Technical Information
Attn: AFSS-A
Washington, D. C. 20546

CONTRACT OBJECTIVES

The research under contract NASW-1233 is directed towards the development of an improved oxygen electrode for use in alkaline H_2/O_2 fuel cells. The work is being carried out for the National Aeronautics and Space Administration, with Mr. E. Cohn as technical monitor. Principal investigators are Dr. J. Giner, and Dr. J. Parry.

CONTENTS

CONTENTS (Cont.)

SECTION 3

Interstitial Compounds of Group VIII Metals
(Porous Electrodes)

CONTENTS (Cont.)

SUMMARY AND CONCLUSIONS

In the first phase of this program (section I of this report), a survey was carried out on the intrinsic activity of the transition metals; selected transition metal alloys and intermetallic compounds; and transition metal carbides, nitrides, borides and silicides for the electrochemical reduction of oxygen. Subsequently, a more detailed study was made of materials shown to be of interest in the initial survey. These included (section 11) gold alloys of the precious metals, intermetallic compounds of gold and titanium, nonstoichiometric TiO_2, silver magnesium alloys, Os and Pt/Os alloys, silicon carbide and barium tantalate. Measurements made on finely divided interstitial compounds of group VIII metals prepared by the Bureau of Mines are described in section 111.

SECTION I

A summary of the data obtained in the survey is presented in Table II (pages 12-20); the principal conclusions to be made from it are as follows:

A. The Elements

The activity for the reduction of O_2 was Pt ~ Os ~ Pd > Au ~ Ag > Mn > C. Of the remaining elements Fe, Re, Ir, and Rh were active below +675 mv; Ni, Ti, and Cu were active below +360 mv on the DHE scale.

Metals most active for oxygen reduction were generally those with easily reduced surface oxides. The principal exception was manganese: A substantial O_2 reduction current was observed on MnO_2 at about +900 mv.

B. Alloys and Intermetallic Compounds of Transition Metals

The materials examined were alloys of transition metals. They are discussed under four groupings, alloys of (1)platinum, (2) nickel, (3) Ti, Zr, Hf, and (4) Ta.

1. Platinum Alloys

Alloys of platinum with base metals were generally less active than platinum, although a number of alloys equalled platinum in activity, e. g. Pt_2Ta and PtMn.

Alloys of platinum with metals that corroded in the pure state often developed a roughened or etched surface. However, the extent of corrosion was far less than that for the pure, base metal. For example, Pt_2Nb corroded at a substantially smaller rate than Nb; similarly, Pt_3Co did not form the surface oxides found with pure cobalt. Alloys showing corrosion (e. g. PtNb) may show a high apparent activity because of surface roughening.

2. Nickel Alloys

Of the nickel-based metal alloys studied, only those with manganese and cobalt were significantly active for the reduction of O_2. In the former system the activity is associated with manganese. The activity of $NiCo_2$ is probably due *to* the formation of a surface layer of nickel-cobalt spinel. The activity is enhanced by holding the starting potential above + 1200 mv, where Co^{+3} is formed. Apparently Co^{+3} is reduced to Co^{+2} below +750 mv and the activity noted above this potential disappears below +750 mv. Returning the electrode to high potentials restores its performance. This effect was not observed for pure cobalt due to excessive corrosion current.

One of the more interesting characteristics of nickel alloys is the effectiveness of nickel in suppressing corrosion of the alloyed constituents. These effects were observed for alloys of at least 50 wt % nickel and either Mn, Co, Al, Nb, or Mo.

3. Titanium, Zirconium, and Hafnium Alloys

The corrosion behavior of these alloys was similar to that of nickel. No pronounced enhancement of O_2 activity was noted for alloys containing base metals. In fact, the small amount of activity associated with nickel was inhibited in Zr_2Ni and suppressed in $TiNi_3$.

The activity of $TiPt_3$ was less than that of platinum, while Ti_3Au was more active for the reduction of O_2 than gold, being comparable to platinum. The surface area of Ti_3Au increased with time, apparently yielding a surface having a higher Ti/Au ratio than the bulk material had. In spite of the higher surface concentration of nonnoble metal, activity of the sample also increased. $ZrAu_3$, richer in gold than is Ti_3Au, showed a lower activity than gold itself and a stable surface. (See also section II.)

4. Tantalum Alloys

The performance of alloys of tantalum showed very little interaction between the metals; i.e. the corrosion and O_2 activity were approximately that expected from a mixture of the pure metals. $TaPt_2$ and $TaPd_3$ are esseiitially as active as platinum and palladium, respectively.

C. Carbides and Nitrides of the Transition Metals

The carbides and nitrides showed, in general, greater activity than the parent metal; even when the metal itself was inert (e.g. Zr, Hf, TaCr) the carbide showed some activity for O_2 reduction. The highest activities were observed for TiN, VC, Fe_2C, Ni_3C. The latter two materials are discussed in detail in section III.

D. Borides and Silicides of the Transition Metals

The borides and silicides were characterized by rapid corrosion at O_2 reduction potentials. Exceptions were Ni_2B and Ni_3B, which experienced slight corrosion, and Pt_2B, which was resistant. The activities of these three materials were no greater than those of the parent metals.

SECTION II

A. Gold Alloys of Ag, Pd, and Pt

The rate of oxygen reduction was measured on gold, platinum, palladium and silver, and the alloys Au/Pd, Au/Pt, and Au/Ag at 10% increments of composition. The activity of the Au/Ag alloys decreased progressively as the silver content was increased. The Au/Pt alloys showed an almost constant activity over the whole composition range; the Au/Pd alloys, however, showed a broad maximum of activity (i. e. greater than that of the Au/Pt alloys) over the composition range. The order of activity was Au/Pd > Au/Pt > Au/Ag. For the 1:1 alloys the following potentials (E_{50}) were recorded at i = 50 $\mu a/cm^2$: Au/Pd - 926 mv, Au/Pt - 878 mv, Au/Ag - 856 mv, all *vs.* RHE. An interesting feature of the results is that at 25°C palladium (E_{50} = 922 mv *vs.* RHE) is more active than Pt (E_{50} = 880 mv *vs.* RHE). At 75°C these figures were 915 mv for Pd and 903 mv for Pt. In other words at 75°C and 50 $\mu a/cm^2$ Pd was more active (12 mv less polarization) than Pt.

B. Titanium, Nonstoichiometric TiO_2 and Gold Alloys of Titanium

The initial survey on solid electrodes showed Ti_3Au to have an activity comparable to platinum. In finely divided form the Ti_3Au iiiter-metallic corroded rapidly and subsequently demonstrated low activity probably due to the formation of TiO_2. Two approaches were adopted in an attempt to take advantage of the activity displayed by titanium gold intermetallics. One was a more exteiisive study to understand the electro-chemistry of titanium and TiO_2 better, particularly in its nonstoichiometric form which has an electronic conductivity several orders of magnitude greater than the stoichiometric form. The second approach was to look at other alloys of titanium and gold. The studies of titanium and non-stoichiometric TiO_2 showed that thin films of the nonstoichiometric oxide on titanium will cathodically reduce O_2 at potentials of 550 mv, 200 mv,

more positive than on the passive stoichiometric TiO_2 film normally formed. Measurements on single crystals of nonstoichiometric TiO_2 showed that the nonstoichiometric forms of reasonable conductivity (e. g. $TiO_{1.8}$) are stable (i. e. they do not revert to TiO_2 stoichiometry) under the experimental conditions of oxygen reduction. However, titanium powder oxidized under conditions that should give rise to a nonstoichiometric oxide produced on electrode of high ohmic resistance and negligible activity.

The other alloys of titanium examined were TiAu ($E_{\frac{1}{2}}$ = 745 mv vs. RHE), $TiAu_2$ ($E_{\frac{1}{2}}$ = 725 mv vs. RHE), $Ti(Rh_{1.5}Au_{1.5})$ ($E_{\frac{1}{2}}$ = 825 mv vs. RHE), and $TiPt_3$ ($E_{\frac{1}{2}}$ = 820 mv vs. RHE). The $E_{\frac{1}{2}}$ value for Ti_3Au was 810 mv vs. RHE. The corrosion resistance of these materials was superior to Ti_3Au, particularly TiAu which showed no anodic current under N_2 and no surface roughening during the experimental measurements.

C. Silver Magnesium Alloys

The enhanced intrinsic activity claimed in the literature for Ag 1.5% Mg alloys compared with pure Ag was not confirmed. The higher activity that we measured for the alloy was directly related to an increase in surface roughness.

D. Os and Pt/Os Alloys

Initial measurements indicating an activity for O_2 reduction on Os greater than that of Pt were not reproduced for either pure Os metal or a Pt/Os alloy. The activity was essentially the same as that of Pt.

E. Silicon Carbide Single Crystals

The 6H-α silicon carbide single crystal is of interest since opposite faces are monatomic and present either silicon or carbon atoms on polishing. The behavior of these faces would be expected to be similar or different, depending on the relative importance of continuum or atomic properties in the catalytic activity of this crystal. The two surfaces behave differently. Notably the first reduction current observed on the carbon side occurs at 525 mv vs. RHE and on the silicon side at 375 mv, suggesting that continuum factors are not dominant in this case.

F. Barium Tantalate

$BaTaO_3$ mounted in gold was tested for O_2 reduction activity. The results were indistinguishable from those of pure gold.

SECTION III

Interstitial compounds of Fe, Ni and Co in finely divided form were prepared by the Bureau of Mines. These were made up as plastic bonded electrodes and tested at Tyco in 35% KOH at 70°C for activity as O_2 fuel cell electrodes. The activity observed is summarized in Table XVI (page 129). The best performances observed in terms of current at 600 mv were iron carbide -32 ma/cm^2, iron nitrocarbide -68 ma/cm^2, iron carbonitride -3 ma/cm^2, nickel carbide -94 ma/cm^2, nickel cobalt carbide -125 ma/cm^2, nickel nitrocarbide -68 ma/cm^2, and nickel cobalt nitrocarbide -49 ma/cm^2. Of the nickel cobalt materials the pattern of activity was 3 Ni/Co > Ni/Co > Ni/3 Co. All the cobalt carbide samples tested corroded rapidly. The level of activity of nickel carbide did not compare favorably with samples of nickel carbide (290 ma/cm^2) and nickel cobalt carbide (350 ma/cm^2) prepared by acetate decomposition in the laboratory. The most likely explanation for this difference is variation in the physical characteristics, particularly the porosity of the catalyst. Carbides and nitrocarbides of Raiiey alloys of nickel and cobalt with silver, gold and palladium showed greater activity (up to 180 ma/cm^2), but this was generally less than that observed for the uiicarbided alloy; e. g. NiAuPd which gave a current of 315 ma/cm^2 at 750 mv.

The level of activity observed with the interstitial compounds of iron and nickel prepared by the Burear of Mines (excluding those containing a precious metal) does not yet meet the requirements of a practical fuel cell catalyst. Nickel and nickel/cobalt carbides have demonstrated high activity, but reproducibility in terms of good electrode performance was not alwasy obtained. If high activity nickel carbide catalysts could be

prepared coiisisteiitly and with reasonable electrode life, these materials would constitute catalysts of practical interest even though their performance is some 100 mv below that of platinum.

SECTION 1

SURVEY OF THE INTRINSIC ACTIVITY OF CATALYSTS FOR THE CATHODIC REDUCTION OF OXYGEN (SOLID ELECTRODES)

I. INTRODUCTION

The selection of alloys for experimental investigation as electrocatalysts for oxygen reduction must be carried out in a systematic way. Random selection is a questionable procedure, since the number of possible systems is extremely large. For example, even if one restricts the choice to about 30 transition metals that are generally good catalysts, there are about 400 binary systems, 4,000 ternary systems, 28,000 quaternary systems, and so on, for a total of about a hundred million systems. If we consider that, in addition, there are distinct intermetallics and that even solid solutions of different concentration may have qualitatively different properties, it is clear that in the available time we can study only a tiny fraction of the possible compositioiis.

The intrinsic factor which determines the reactivity of an oxygen electrode is its atomic composition and the subordinate crystal structure. The composition ultimately determines both the desirable properties (viz. electrocatalytic activity for reduction of oxygen) and the undesirable properties (viz. corrosion or other time-dependent failure mechanisms which limit the efficiency or life of the electrode). The electrode activity may be an inherent characteristic of the pure electrode surface, or it may be conditioned by reactions with the electrolyte, e. g. through specific adsorption or ions.

Previous work on catalysts has been treated within a theoretical framework based on a consideration of two extreme points of view concerning the source of surface activity. According to one view (which can be called

the "atomic approach"), the reactivity is determined by the intrinsic chemical properties of the individual surface atoms and is only slightly influenced by the neighboring atoms in the crystal bulk. The other extreme view (which can be called the "continuum approach") is that reactivity is determined primarily by the electronic energy states of the material as a whole, with the specific atomic chemistry being secondary. This approach has been used extensively to interpret chemisorption and catalysts on transition metal alloys where the surface activity has been correlated with d-band occupancy.

The oxygen reaction is admittedly a more complex process, the mechanism of which (i. e. the precise sequence and relative rates of the various elementary steps) still remains unresolved[1]. However, there is ample evidence for the existence of a special kind of oxygen-metal interaction during the electrolytic reduction of oxygen, even if knowledge of the precise nature of this interaction is scanty.

There is also little doubt that the disruption of the oxygen-to-oxygen bond is the slowest step in the over-all process and that hydrogen peroxide appears as an intermediate or by-product during reduction in alkaline solutions . Without going into the details of the reaction, we can thus safely assume that (a) electronic factors play an important role in the kinetics and (b) geometric factors are probably also involved in the catalytic breaking of the oxygen bond.

Catalysts were selected with both the "continuum" and "atomic" approaches in mind. Alloys of noble metals (Pt, Au) – which are good catalysts for O_2 reduction – with base metals were investigated, as well as alloys containing only base metals. The materials examined encompass a variety of crystal types; a partial listing is given in Table I. The validity of the continuum approach to the electrocatalysis of oxygen reduction would be established by alterations on the noble metal activity through alloy formation and/or by the development of high activity through alloying of low activity base metals.

TABLE I

Structure and Stoichiometry of Selected Alloys

Stoichiometry	Structure	Alloy
A_3B	"β W"	Ti_3Au
		Nb_3Pt
		Mo_3Pt
A_2B	$CuAl_2$ type	Zr_2Ni
	$MoSi_2$ type	Ti_2Cu
AB	C_5Cl type	TiCo
	AuCl - B19	NbPt
AB_2	Laves Phases	TaV_2
		HfW_2
		$TiCr_2$
	C.P. phases	Pt_2Ta
		Pt_2Nb
AB_3	$AuCu_3$ type	Pt_3Ti
		Pt_3Co
	41	Pt_3Zr
	12 lsh	Ni_3Ti
		Pt_3Ta
		$TaIr_3$
	2 lsh	$ZrAu_3$
		$TiCu_3$
	3 lsh	Pt_3V
AB_n n> 3		Ni_4Mo
Variable	δ	NbPt
	μ	TaNi

II. EXPERIMENTAL

A. Introduction

A convenient method of testing a material for corrosion resistance and catalytic activity was to use it as a solid ingot. As such, it could be mounted in an alkali resistant resin and tested potentiostatically as a rotating disc electrode run consecutively in N_2- and O_2- saturated KOH-solution.

By potentiostatic measurement of the corrosion current under an inert atmosphere, it was possible to measure the corrosion rate over the whole potential region relevant to an oxygen electrode.

The advantages of this method are that the samples can be prepared with relative ease and have well-defined surfaces. They could therefore be tested unequivocally for corrosion and for O_2-activity under well-defined transport conditions (Levich equation). The main disadvantage of the method is the sensitivity of the electrode, with its low roughness factor, to poisoning by impurities. This disadvantage is minimized by the high electrode potential at which O_2 is reduced and by continuous surface renewal due to the small corrosion current present in most cases. The low concentration of surface defects on solid electrodes, in contrast to that on dispersed electrodes, may lead to lower specific activity, but this difference is probably irrelevant in a comparative study of the relative activity of a series of materials.

B. Testing of Solid Ingots as Rotating Discs

1. Preparation of the Disc Electrode

Carefully weighed mixtures of pure elements were arc-melted in a furnace with six water-cooled copper heaters (each one-inch in diameter), using a tungsten tip under an argon atmosphere. A Ti getter was fired before each run in order to eliminate traces of O_2. A maximum of six ingots weighing 5 to 10 grams could be obtained in one run.

If the alloy or compound was formed peritectically (i. e. during solidification the composition of the solid phase differs from the composition of the liquid phase), the ingot was annealed, generally overnight, at a convenient temperature. If the alloy or compound was formed congruently (i. e. the solidifying phase had the same composition as the molten phase), the ingot could be used without any subsequent thermal treatment.

The ingots were button shaped when removed from the furnace and were cut with a boron carbide or chromonel saw in order to expose two parallel, flat, circular faces. One part of the sawed button was used for metallographic analysis, according to standard procedures.

The part of the button with the two parallel, flat, circular planes was incorporated as shown in Fig. la with "Koldmount," (an acrylic resin – including methylmethacrylate monomer – used for metallographic work, which erroded less than 0.05 mg/cm^2 in 2N KOH at 80°C over a period of 80 hrs). This arrangement, besides isolating the electrical contact to the electrode from the electrolyte, also constituted an ideal configuration for controlling precisely mass transport to the electrode.

Electrical contact to the button was made by screwing a metal rod down on a spring-loaded contact in the threaded shaft of the Koldmount. The rod, spring, and contact were gold-plated and the rod was covered with heat shrinkable Teflon tubing (Fig. la). The electrode assembly was mounted in a Sargent 600 rpm synchronous motor designed for voltammetry with solid electrodes. Contact between the stirring rod and the fixed lead was made by dipping a wire into a pool of mercury in the hollow top of the rod.

A series of ductile materials was also tested in a demountable assembly described by Stern and Makrides[2], with only Teflon and glass exposed to the solution (Fig. lb). Ductile materials tested in both electrode assemblies gave basically the same results. This confirms that the acrylic resin used in the rotating disc had no poisoning effect on the results.

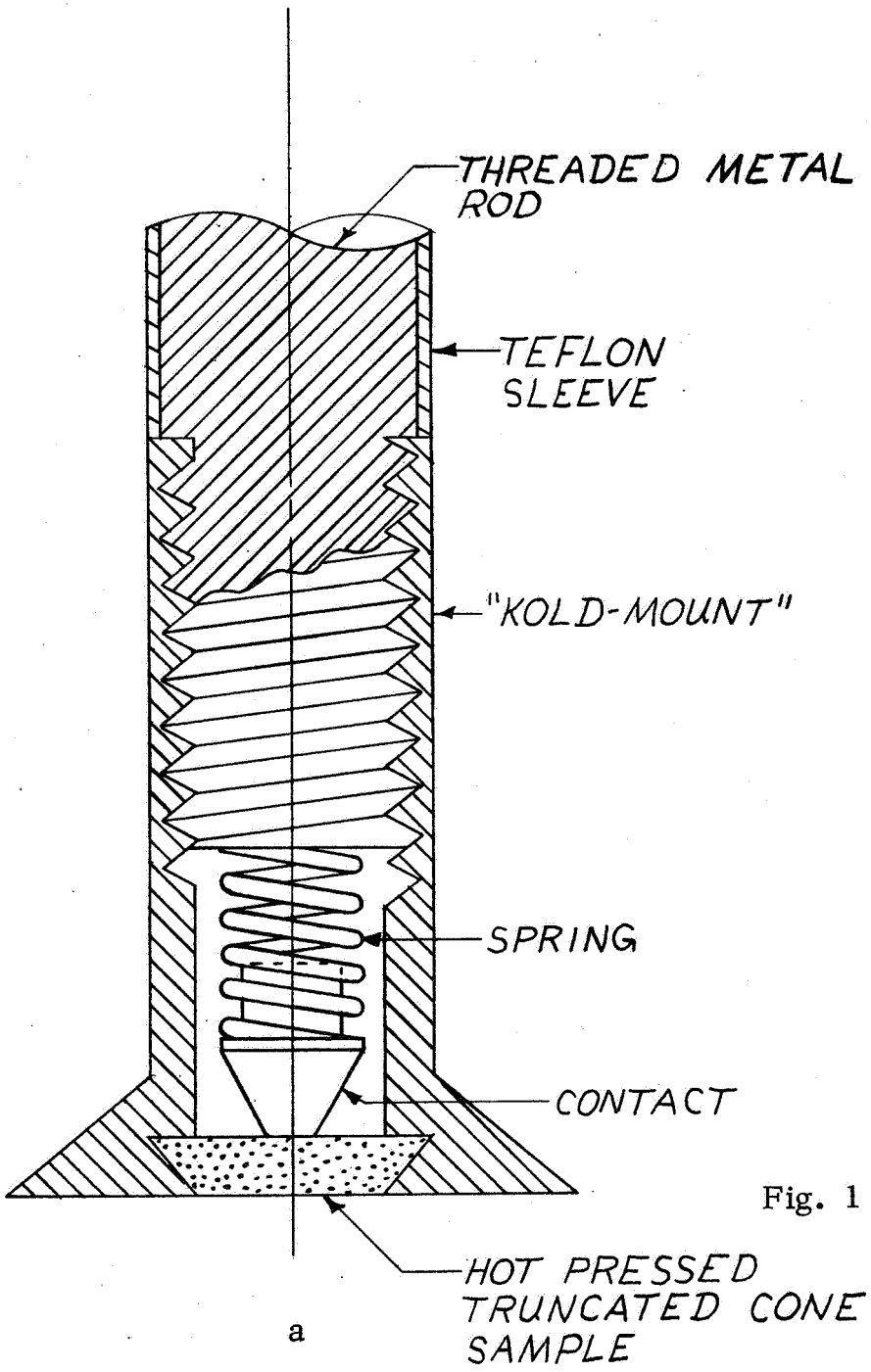
4 X ACTUAL
THREADED METAL ROD
TEFLON SLEEVE
"KOLD-MOUNT"
SPRING
CONTACT
HOT PRESSED TRUNCATED CONE SAMPLE

a

Fig. 1

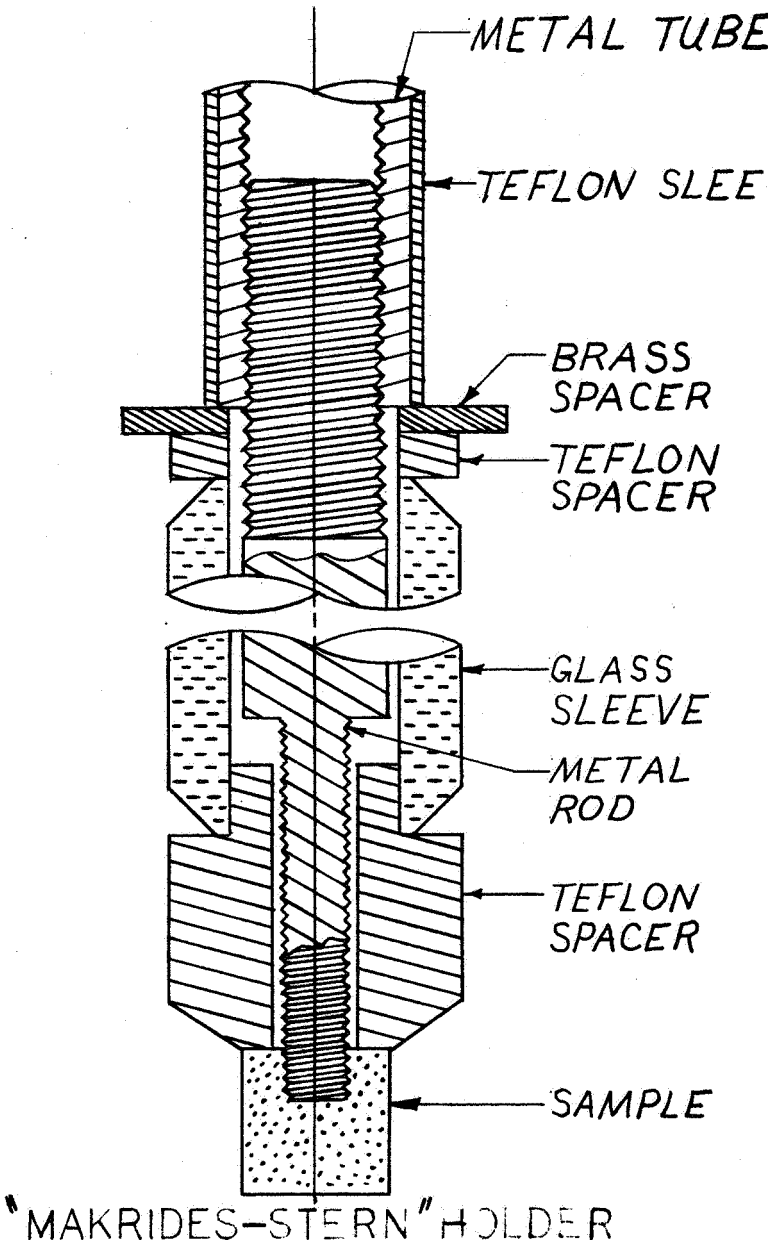
METAL TUBE
TEFLON SLEE
BRASS SPACER
TEFLON SPACER
GLASS SLEEVE
METAL ROD
TEFLON SPACER
SAMPLE
"MAKRIDES-STERN" HOLDER

FIG. 1

2. Test Cell

The cell shown in Fig, 2 was used. In this cell all the frits were eliminated since they dissolve in caustic solution, The lack of a frit between working and counter electrodes did not introduce a significant error, since during the cathodic oxygen reduction (with oxygen saturated solution) only oxygen was evolved at the counter electrode. The hydrogen evolved at the counter electrode during the corrosion test (N_2-saturated solution) which could dissolve and reach the working electrode was largely swept by nitrogen and therefore did not contribute significantly to the measured current.

The reference electrode was a Dynamic Hydrogen Electrode (DHE)[3] which under the cell-operating condition adopted a potential 30 mv ± 5 mv negative to the RHE.

The temperature of the cell was regulated ± 0.5°C by a heating mantle and a regulator with a temperature sensor inside the electrolyte. A temperature of 75°C was selected for the experiments.

The electrolyte concentration was set at 2M KOH after preliminary experiments with 35% (8.4 M) KOH. This concentration had a more favorable transport factor (D x C) than 8.3 M KOH solutions used in fuel cells. Since the screening electrolyte was milder, the chalices of missing a possible catalyst were reduced.

3. Electrochemical Measurements

i(E)-curves were generated by imposing a linear potential scan on the working electrode by means of a slow linear potential signal to a Wenking potentiostat. The slow function generator was constructed with two standard batteries, two 10 turn, 10 K potentiometers, and a synchronous motor (Insco Corp. , Croton, Mass.). The motor has a basic speed of 4 rpm and six gear ratios of 1:1, 2:1, 5:1, 10:1, 20:1, and 50:1. By changing these gear ratios and the peak voltage, scanning rates from 10 mv/min to 800 mv/min could be obtained. For the initial routine screening, a rate of 50 mv/min was selected.

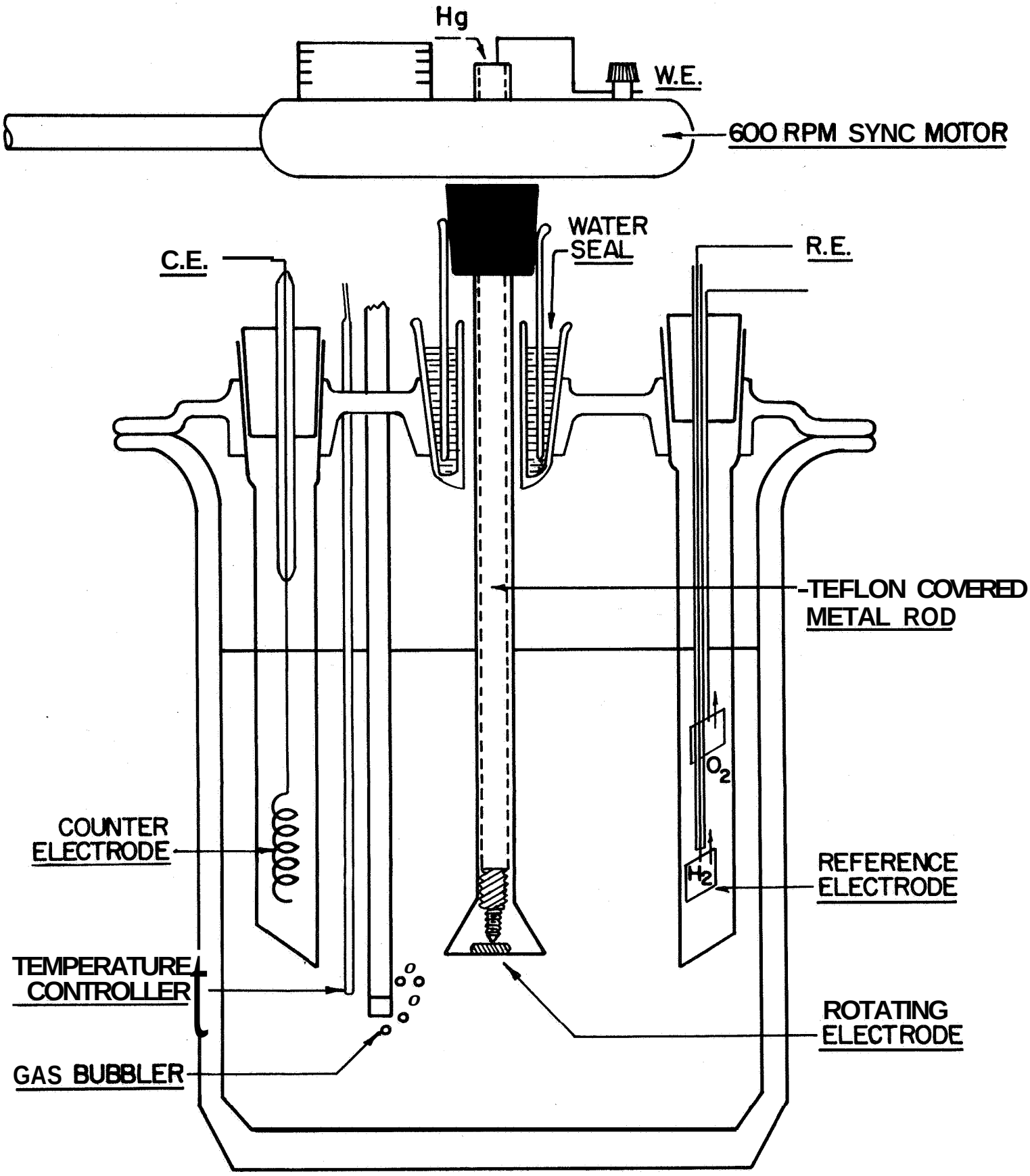

ROTATING ELECTRODE CELL Fig. 2

The current-potential curve was recorded directly on an x-y recorder. Current-time curves at constant potential for relatively long times could be recorded on the same recorder by using the slow function generator to feed the y-axis of the recorder,

Before an activity test experiment, the corrosion current under inert gas (N_2) was measured at a series of potentials. This corrosion current had to be measured with stirring in order to subtract it quantitatively from the O_2 reduction current. It was also measured without stirring in order to apply the results to a practical electrode. Also, the possibility of a decrease of the corrosion rate with time had to be investigated. As long as the corrosion current was small compared with the expected O_2-current, the O_2-curve was run, even if the corrosion rate was higher than useful for a practical cell.

In order to ascertain whether an observed performance represented the intrinsic activity of a material aiid not a mere increase of the surface area, the real surface area of the electrode had to be estimated. The only practical method of doing this during screening of a large number of flat electrodes was by measuring the double layer capacity of the electrode.

For the capacity measuremeiits a method was selected in which a triangular wave of 50 cycles/sec and a peak-to-peak voltage of 100 mv (i. e. a sweep rate of 10 volts/sec), biased by a convenient dc voltage, was fed to the signal input of the potentiostat. The dc voltage was selected so that Faradaic currents were avoided. If the electrode behaves as a perfect capacitor (no Faradaic or ohmic resistance), the small triangular potential wave is transformed into a square current wave, with a peak-to-peak value which is proportional to the electrode capacity and therefore to the real surface.

Procedure

The following procedure was used for routine screening:

(1) N_2 Saturation

A freshly prepared 2M KOH solution was saturated with pure nitrogen for at least 45 minutes. The electrode was kept iiiside the cell but not exposed to the electrolyte until N_2 saturation was complete.

(2) Corrosion i(E)-Curve

The electrode was introduced into the solution at a potential of E = 0 mv. The potential scan was initiated within a minute at a rate of 50 mv/min and 600 rpm rotation. The potential scan was reversed between E = 0.8 volt and E = 1.23 volts, depending on the extent of corrosion in this range. If there was a high corrosion rate at the lower potentials, higher potentials were still investigated since there could be a region of passivation in the potential range of interest.

At several points of the i(E)-curve, stirring was stopped for 1 or 2 minutes without stopping the potential sweep (in order to observe the effect of stirring on corrosion).

(3) Measurements of the Double Layer Capacity

At several points in the i(E)-curve under N_2, the recording was interrupted and a double layer capacity measurement was made as described above.

The electrode potential was never left uncontrolled in order to control the history of the electrode from the moment it was immersed in solution. If, in addition to the i(E)-curve, the electrode had to be left for some time at a known potential, the time at this potential was kept as short as possible and noted. The electrode was removed from the solution during extended periods of inactivity, and any attached electrolyte was removed by rotating the electrode in the gas phase for a short time (about half a minute).

(4) O_2-Saturation

If the corrosion current was within tolerable limits, the test for O_2-activity was carried out. The electrode was removed from the system and repolished, and the solution was saturated with O_2 (at least 45 min).

(5) i(E)-Curve for O_2-Reduction

The repolished sample was introduced into the electrolyte at a high, passive potential where possible, but below any current wave

(usually between 0. 8 volt and **1. 23** volt), and the i(E)-curve was initiated in the direction of decreasing potentials. At E = 0, the direction of the potential sweep was reversed,

(6) Measurements of the double layer capacity in the region of the limiting current were necessary when doubts existed about the real surface increase during recording of the i(E)-curve.

(7) After recording the i(E)-curves, a micrograph of the electrode surface was taken and the sample was filed for subsequent study.

(8) The data presented in tabular form are corrected to the reversible hydrogen electrode (RHE) in the same electrolyte by subtracting 30 $\pm$ 5 mv from the recorded potentials (DHE).

C. Presentation of Data

Table II lists the following information for the transition elements and alloys and intermetallic compounds: $E_{\frac{1}{2}}$, the half wave potential; E_2, the potential at which cathodic current was first observed; i_L, the limiting current density; and C, the double layer capacities of the electrode. The significance of these measurements in defining the activities of a catalyst is established below. The detailed results from which these figures were derived were presented in the Fourth Quarterly Report[4]. Comment is also made in Table II on the corrosion (anodic currents) observed for the electrode measured in the absence of O_2.

The reduction of oxygen is an irreversible process, and in the absence of concentration polarization, the current potential curve is described by

$$i = i_o \exp \left(\frac{\alpha z F}{RT} \eta\right) \qquad (1)$$

where i_o is the exchange current, α the transfer coefficient, $z = \frac{n}{\nu}$ where n is the number of electrons involved in the electrode reaction

TABLE II

Master Table of Activity for O_2 Reduction and Corrosion Resistance

ELEMENTS	$E_{\frac{i}{2}}$ mv	E_i mv	$i_L \mu a/cm^2$	$C \mu f/cm^2$	Corrosion
Ag	760	900	1800	60	
Au	785	900	1340	96	
co					Corrodes
Cr		~200			Corrodes
Cu					Corrodes
Fe	300	645	780	52	
Graphite	370	810	390	410	
Hf					Inert
Ir	544	675	705	176	
Mn	820	900	150	604	Extensive oxide formation
Mo					Corrodes
Nb					Corrodes
Ni	<90	340	500	26	
OS	375	810	250	75	
Pd	835	900	1200	95	
Pt	845	925	1350	115	
Re	340	820	600	350	
Rh	545	820	1370	340	
Ru	545	670	1000		
Ta					Inert
Ti	160	250	600	100	Corrosion >950
V					Corrodes
W					Corrodes
Zr					Inert

ALLOYS AND INTERMETALLIC COMPOUNDS

	$E_{\frac{1}{2}}$mv	$E_i$mv	$i_L \mu a/cm^2$	$C\mu f/cm^2$	Corrosion
$AuNb_3$	825	910	582		some corrosion
AlNi	130	300	800	17	
$AlNi_3$	100	700	225	18	
AlNiCo	175	400	140	212	slight corrosion
Al_3NiCo_2					corrodes
AuPd					see separate
AuPt					section
$Au_{1.5}Rh_{1.5}Ti$	825	920	658	225	slight Corrosion
AuTi	745	925	746	51	
Au_2Ti .	725	800	665	47	
$AuTi_3$	810	910	698	70	some corrosion
AuV_3					corrodes
Au_3Zr	575	875	360	22	slight corrosion
$AuZr_3$					corrodes
CoAlNi	175	400	140	212	slight corrosion
Co_2Al_3Ni					corrodes
$CoHf_2$					inert
Co_2Ni	810	880	500	87	slight corrosion
$CoPt_3$	815	900	680	133	some corrosion
CoTi					corrodes
Cr_2Ta					inert, corrosion >850mv
Cr_2Ti	130	270	1000	41	
Cr_4Ti					inert
CuTi					corrodes
$CuTi_2$	180	250	240	41	some corrosion
Cu_3Ti					corrodes
Fe_2Ta	230	390	1600	420	some corrosion
Hf_2Co					inert
$HfMo_2$					corrodes
HfW_2					corrodes
Ir_3Ti	550	750	1280	375	

ALLOYS AND INTERMETALLIC COMPOUNDS (cont.)

	$E_{\frac{1}{2}}$ mv	E_i mv	$i_L \mu a/cm^2$	$C \mu f/cm^2$	Corrosion
MnNi(2:1)					extensive oxide formation
MnNi(1:1)	150	820	1430	163	slight corrosion
MnPt(3:1)	820	920		1400	some corrosion
Mo_2Hf					corrodes
$MoNi_4$	150	250	600	19	slight corrosion
MoPt	560	810	1700	350	some corrosion
Mo_3Pt					corrodes
Mo_2Zr					corrodes
Nb_3Au	825	910	582		some corrosion
$NbPt_2$	810	860	1320	133	
NbPt	840	920	1400	820	some corrosion
$NbNi_3$	200	800	910	17	
NiAl	130	300	800	17	
Ni_3Al	100	700	225	18	
NiAlCo	175	400	140	212	slight corrosion
$NiCo_2Al$					corrodes
NiMn(1:1)	150	820	1430	163	slight corrosion
NiMn(1:2)					extensive oxide formation
Ni_4Mo	150	250	600	19	slight corrosion
Ni_3Nb	200	800	910	17	
Ni_2P	210	810	1550	27	slight corrosion
NiTa	120	225	410	30	
Ni_2Ta	175	280	575	80	
Ni_3Ta	160	720	630	65	
Ni_3Ti	90	260	200	15	
$NiZr_2$					inert
PdAg					see separate
PdAu					section
PdPt	840	900	1500	140	
Pd_3Ta	835	890	1250	180	slight corrosion
$PdZr_2$	730	830	1000	68	
Pt_3Co	815	900	680	133	some corrosion

ALLOYS AND INTERMETALLIC COMPOUNDS (cont,)

	$E_{\frac{1}{2}}$ mv	E_i mv	i_L μa/ cm^2	Cμf/ cm2	Corrosion
PtMo	560	810	1700	350	some corrosion
$PtMo_3$					corrodes
PtMn	820	920	1400		some corrosion
PtNb	840	920	1400	820	some corrosion
Pt_2Nb	810	860	1320	133	
$PtNb_3$					corrodes
PtPd	840	900	1500	140	
Pt_2Ta	840	900	1205	112	
Pt_3Ta	840	890	1280		some corrosion
Pt_3Ti	820	870	1003	132	
Pt_3V	820	880	1000	132	some corrosion
$Rh_{1.5}Au_{1.5}Ti$	825	920	658	225	slight corrosion
Rh_3Ti	610	920	1266	129	slight corrosion
$TaCr_2$					inert-corrosion >850mv
$TaFe_2$	230	390	1600	420	some corrosion
TaNi	120	225	410	30	
$TaNi_2$	175	280	575	80	
$TaNi_3$	160	720	630	65	
$TaPd_3$	835	890	1250	180	slight corrosion
$TaPt_2$	840	920	1205	112	
$TaPt_3$	840	890	1280		slight corrosion
TaV_2					corrodes
TiAu	745	925	746	51	
$TiAu_2$	725	800	665	47	
$TiAu_{1.5}Rh_{1.5}$	825	920	658	225	
Ti_3Au	810	910	698	70	some corrosion
TiCo					corrodes
$TiCr_2$	130	270	1000	41	
$TiCr_4$					inert
TiCu					corrodes
Ti_2Cu	180	250	240	41	some corrosion

ALLOYS AND INTERMETALLIC COMPOUNDS (cont.)

	$E_{\frac{1}{2}}$ mv	E_i mv	i_L μa/cm^2	Cμf/cm^2	Corrosion
$TiCu_3$					corrodes
$TiIr_3$	550	750	1280	375	
$TiNi_3$	90	260	200	15	
$TiPt_3$	820	870	1000	132	
$TiRh_3$	610	920	1266	129	
VPt_3	820	880	1000	132	some corrosion
V_2Ta					corrodes
V_3Au					corrodes
W_2Hf					corrodes
W_2Zr					corrodes
Zr_3Au					corrodes
$ZrAu_3$	575	875	360	22	slight corrosion
$ZrMo_2$					
Zr_2Ni					inert
Zr_2Pd	730	830	1000	68	
ZrW_2					corrodes

TABLE II (cont.)

INTERSTITIAL COMPOUNDS - BORIDES AND SILICIDES

Electrode	Corrosion Behavior	E_I for O_2 Reduction
TiB_2	corrodes	<+200
Ti_5Si_3	corrodes	<+200
$TiSi_2$	corrodes	<+700 mv
ZrB_2	high corrosion current	----
$ZrSi_2$	high corrosion current	----
VB_2	high corrosion current	----
VSi_2	high corrosion current	----
NbB	high corrosion current	----
NbB_2	high corrosion current	----
$NbSi_2$	corrodes less than NbB, by order of magnitude	----
TaB	high corrosion current	----
TaB_2	high corrosion current	----
Ta_5Si_3	low corrosion current	----
$TaSi_2$	higher corrosion current	----
CrB	Cathodic current above +300; Anodic current below +700	----
CrB_2	similar to CrB	
Cr_5B_3	similar to CrB	
Cr_2B	low corrosion currents	low O_2 currents

Electrode	Corrosion Behavior	E_I for O_2 Reduction
Cr_3B	similar to Cr_2B	----
Cr_4B	siinilar to Cr_2B	----
$CrSi_2$	very low corrosion below lv	----
Cr_3Si	very low corrosion below lv	----
MoB	high corrosion currents above + 200	----
MoB_2	high corrosion currents above + 200	----
$MoSi_2$	high corrosion currents above + 200 (lower than MoB)	----
WB	high corrosion currents above + 100	----
W_2B	high corrosion currents above + 100	----
W_2B_5	high corrosion currents above + 100	----
WSi_2	high corrosion currents above 0	----
$MnSi_2$	high corrosion currents	
$CoSi_2$	corrosion	
Ni_2B	stable	+250
Ni_3B	stable	+150
Pt_2B	stable	+875
B_4C	stable	low +200

TABLE II (cont.)

INTERSTITIAL COMPOUNDS-CARBIDES AND NITRIDES

	E_i*mv	i $\mu a/cm^2$ at 500 mv	i $\mu a/cm^2$* at 150mv	C $\mu f/cm^2$	Corrosion
Ti	+250	----	0.24	100	
TiN	+770	0.27	1.13	540	
TiC	+820	0.1	0.26	220	
Zr	----	----	----	----	inert
ZrN	----	----	----	435	
ZrC	+400	----	0.48	46	
Hf	----	----	----	2	
HfN	+500	----	.01	----	
HfC	+500	----	0.80	17	
V	----	corrosion	----	----	corrodes
VN	+180			>500	
VC	+820	0.27	0.50	61	
Nb	~270	corrosion	1.0	----	
NbN	~270	----	0.4	----	
NbC	+600	0.29	1.1	169	
Ta	inert	----	----	----	
TaN	+100	corrodes	----	----	
TaC	+630	0.15	1.0	----	
Cr	+200	----	.01	22	
Cr_2N	+400	----	.01	266	
Cr_3C_2	+600	0.3	1.1	----	

* The E-i characteristics do not permit unequivocal definition of $E_{\frac{1}{2}}$ or i_L for most of these materials.

	$E_i$mv	i μa/cm^2 at 500mv	i μa/cm^2 at 150mv	Cμf/cm2	
Mo	----	----	----	----	corrodes
Mo_2C	----	----	----	----	corrodes
W	----	----	----	----	corrodes
WC	----	----	----	----	corrodes
WC-co	----	----	----	----	corrodes
Fe	+645	0. 14	0.70	52	
Fe_2C	+770	0.42	0.88	28	
Ni					
Ni_3N		Separate Section			
Ni_3C					
Carbon (graphite)	+820	0.55	0.56	410	

and ν the stoichiometric number, F is Faraday's constant, R the gas constant, and T the absolute temperature,

If, in addition to activation polarization, concentration polarization appears due to O_2 depletion at the electrode, equation **(1)** converts to:

$$i = i_o \left(\frac{C^E}{C^B} \right)^{z'} \exp \left(\frac{\alpha z F}{RT} \right) \eta \qquad (2)$$

where C^E and C^B are the concentrations of oxygen at the electrode and in the bulk of the solution, respectively, and z' the stoichiometric factor[5] for the oxygen molecule in the reduction reaction.

Equation (2) can be rewritten as

$$\eta = \frac{RT}{\alpha z F} \ln \frac{i}{i_o} + \frac{z' RT}{\alpha z F} \ln \left(\frac{C^B}{C^E} \right) \qquad (3)$$

It can be easily demonstrated that in case of diffusion-controlled limiting current (as is the case in most of our experiments), at the half wave potential (i. e. when $i = i_{d/2}$) $C^E = \frac{C^B}{z}$.

Equation *(3)* can then be rewritten as

$$\eta = \eta_{act} + \frac{z' RT}{\alpha z F} \ln 2 \text{ , or at } T = 75°C \qquad (4)$$

$$\eta = \eta_{act} + \frac{z'}{\alpha z} 0.018 \text{ (volt)} \qquad (5)$$

Thus, for electrodes with similar hydrodynamic conditions (as exist in our experiments) at the half wave potential of a diffusion limited wave, the overvoltage ($\eta_{\frac{1}{2}} = E_{\frac{1}{2}} - E_O$) is equal to pure activation polarization plus a small iiumerical term. This term depends on the transfer coefficient, stoichiometric factor, and stoichiometric number,

It is apparent that the half wave potential is a very appropriate quantity for comparing catalysts studied under identical conditions, since the normalization of the current to this potential is not subject to errors made in the measurement of electrode area.

In this system there are two complications which limit the rigor with which such a comparison can be made:

(1) The passivating effect of oxides and chemisorbed oxygen. Because of this effect, it is frequently found that above a given potential no current is seen, while below the potential at which the "oxide" is reduced, a very steep (purely diffusion controlled) wave appears. It is therefore possible that electrodes with little "oxide passivation" but large overvoltage due to other causes show a more negative half wave potential than do electrodes with very steep waves but with an "oxide inhibition" at low polarizations.

(2) The formation and accumulation of HO_2^- by partial reduction of O_2 during the following reaction sequence:

$$O_2 + H_2O + 2e^- \rightarrow HO_2^- + OH^- \quad (6)$$

$$HO_2^- + H_2O + 2e^- \rightarrow 3\,OH^- \quad (7)$$

It is possible in principle that an electrode with completely reversible step (6) and very irreversible step (7) (i. e. with a very low half wave potential for the 4-electron O_2-reduction over-all wave) shows much more negative half wave potential than an electrode with less reversible reaction (6) but a more reversible reaction (7).

In order to eliminate this uncertainty, we have included in the tabulation the initial potential, i.e. the potential at which a net cathodic current is observed. This value is, at best, semiqualitative since it is dependent on the sensitivity of the ammeter and the presence or absence of corrosion current. Even with these limitations, it is a good complement to the half wave potential for comparing catalyst performance.

111. RESULTS

Table II presents all the data accumulated on the activity and corrosion resistance of the elements of the transition series and of intermetallic and interstitial compounds. The intermetallic compounds are listed alphabetically for each component. Supplementary Tables III to IX group the materials in terms of activity, corrosion resistance, etc., and are discussed in detail below.

The first group (Table 111) comprises those transition elements that show activity for O_2 reduction above + 800 mv.

TABLE III

Transition Metals Active for O_2 Reduction Above + 800 mv

Mn	Ag
	Au
Pd	(C)
Pt	Os

The performance curves indicate the order of activity (based on initial potential): Os $\approx$ Pt $\approx$ Pd > Au $\approx$ Ag > Mn > C.

Of the remaining elements, Fe, Re, and Ir are active below +675 mv; Ni, Ti, and Cu are active below +360 mv.

A parallel grouping of the metals can be formed according to whether oxygen is reduced on an oxide or on "bare" metal. This correlation is shown in Table IV.

TABLE IV

Oxygen Reduction Activity vs. Surface Composition

Oxide Surface	Metal Surface
Ti	Pd
Nb	Pt
Fe	Ag
Mn	Au
Ni	Cu

The performances of the transition metals are summarized in Table V according to position in the periodic table, in Table VI, according to the potential region of activation controlled current, and in Table VII according to $E_{\frac{1}{2}}$ and E_i values.

The most active elements are those for which the metal itself catalyzes the O_2 reduction process. The low limiting currents and the slope of the performance curves for Fe, Ti, and possibly Ni and Re indicate that these materials have a low activity for the decomposition of HO_2^-. Nb also shows a two-step reduction; however, some ambiguity is introduced by corrosion.

Manganese dioxide is the one oxide which shows activity for oxygen reduction at high potentials.

TABLE V

O_2 Reduction Properties of the Elements

Group	Metal	E_i	$E_{\frac{1}{2}}$	i_1 (ma/cm^2)
IV a	Ti	250	160	0.66
	Zr		inert	
	Mf		inert	
V a	V		corrodes	
	Nb		(2 190), corrodes	1 36
	Ta		inert	
VI a	Cr	~200	< 0, corrodes > + 950	
	Mo		corrodes	
	W		corrodes	
VII B	Mn	900	~820	0.60
	Re	820	340	0.60
VIII B	Fe	640	300	0.78
	Ru	670	545	1.00
	Os	970	400	0.25
	Co		"corrodes"	
	Rh	820	545	1.37
	Ir	670	544	0.70
	Ni	340	<90	0.50
	Pd	900	835	1.2
	Pt	920	845	1.35
I a	Cu		oxide format>	1.33
	Ag	300	760	1.80
	Au	200	785	1.34
graphite		810	370	0.89

TABLE VI

Materials Active for O_2 Reduction

Potential Region of Activation Control Current

> + 700 mv			+ 700 to + 450		+ 450 to + 250				≤ + 100
Pt	$TiPt_3$	Co_2Ni	Re	MoPt	Ni*		Ti	Ti_2Cu	Cr
Pd	$TaPt_3$	$ZrAu_3$	Fe	$TaNi_3$	Cu	ZrC	Nb	$TiNi_3$	$TiCr_2$
Ag	VPt_3	Ti_3Au	Ru	$TiIr_3$	Ni_3Nb*	HfC	Ni_3Ti	$TiCr_4$	TiCo
Au	$CoPt_3$	$TaPd_3$	Ir	TiC	TiCu	NbC	NiTa	NbN	ZrN
Mn	$TaPt_2$	C		TiN	$TiCu_3$	Ni_3N*	$TaNi_2$	Cr_2	HfN
Os	$NbPt_2$	Pt_2B		VC	$TaFe_2$	Cr_5B_3 *	Ni_4Mo	Ni_2B	VN
	NbPt	$TiAu_{1.5}Rh_{1.5}$		TaC	Ni_2P		NiAl	Ni_3	TaN
	MnPt	$AuNb_3$		Cr_3	Fe_2Ta		Ni_3Al*	$_4C$	Cr_2N
	PtPd	AuTi		Fe_2C			Alnico*		TiB_2
	Pd-Ag	Au_2Ti		Ni_3C*					$TiSi_2$**
	MnNi (3:1)	$PdZr_2$		Ti_3Si					
	MnNi*			Cr_2B					

* The placement of these materials is not well defined by the data.

** Considerable corrosion also observed in this potential range.

TABLE VII

Classification of O_2 Reduction Catalysts According to $E_{\frac{1}{2}}$
(Materials Showing Activity Above + 700 mv)

Class 1 ~ 840 mv

Material		$E_{\frac{1}{2}}$
Pt	+925	+845
Pt_2Ta	920	840
Pt:Pd	900	840
Pt_3Ta	870	840
OS	810	375*
PtNb	920	840

Class 2 ~ 830 mv

Pd	900	835
$TaPd_3$	890	835
Pt_2B	875	830

Class 3 ~ 800 mv

$AuNb_3$	910	825
$Ti(Au_{1.5}Rh_{1.5})$	920	825
PtMn	920	820
Mn	900	820**

* Low $E_{\frac{1}{2}}$ due to slow reduction of HO_2^-.

** Limiting current was not observed due to oxide reduction.

TABLE VII (Cont.)

Material	E_1	$E_{\frac{1}{2}}$
Class 3 ~ 800 mv (Cont.)		
Pt_3V	880	820
Pt_3Ti	870	820
Pt_2Nb	870	820
Pt_3Co	900	815
Ti_3Au	910	810
Class 4 < 800 mv > 700 mv		
Au	900	785
Ag	900	760
AuTi	925	745
$PdZr_2$	830	730
$AuTi_2$	800	725
Class 5 < 700 mv		
MnNi (3:1)	820	700
$TiRh_3$	920	610
$ZrAu_3$	875	575
PtMo	810	560
$TiIr_3$	750	550
C	810	370
MnNi	820	150

Finally, we group together those metals which either corrode substantially or are inert over the potential range 0 to + 1200 mv. These metals are listed in Tables VIII, IX, X, and XI.

TABLE VIII

Elements Not Active as Oxygen Electrodes

Corrode	Inert
V	Zr
Nb*	Hf
Ta	Cr**
Mo	
W	
CO	

* Active where corrosion is observed

** Corrodes above +900 mv.

TABLE IX

Materials Inert Between 0 and + 1200 mv

Zr	Zr_2Ni
Hf	Hf_2Co
Ta	HfN

TABLE X

Materials Showing Anodic Current Between + 800 and + 1200 mv

Cr	Co_2NiAl_3	TiC	TaC	Cr_2B	Cr_3Si
Re	$TiCr_2$	VN	Cr_2N	Cr_3B	
OS	$TiCr_4$	VC	Cr_3C_2	Cr_4B	
Ag	$TaCr_2$	NbC	CrB	$CrSi_2$	
Rh	Ti_3Au				

TABLE XI

Materials Showing Anodic Current Below + 800 mv

V	NbPt (low)	TiCu*	ZrN	$TiSi_2$	TaB_2	W_2B
Nb	MoPt (low)	$TiCu_3$	HfC*	ZrB_2	$TaSi_2$	W_2B_5
Mo	Nb_3Pt	TiCo	NbN	$ZrSi_2$	Ta_5Si_3	WSi_2
W	Mo_3Pt	TaV_2	TaN	VB_2	CrB_2	$MnSi_2$
Co*	Co_2NiAl_3	$TaFe_2$	Mo_2C	VSi_2	Cr_5B_3	$CoSi_2$
Cu*	$ZrMo_2$	MnNi*	WC	NbB	MoB	
Mn*	$HfMo_2$		WC-co	NbB_2	MoB_2	
	ZrW_2		TiB_2	$NbSi_2$	$MoSi_2$	
	HfW_2		Ti_5Si_3	TaB	WB	

* Apparent insoluble oxide

In a number of cases, the observed corrosion behavior was other than that predicted by thermodynamics. Consider the following specific examples:

a) Vanadium corroded at negative potentials, presumably due to the formation of $HV_2O_5^-$. A slight passivation occurred at + 200 mv; the predicted transition to V_2O_5 or $H_3V_2O_7^-$ at about 600 mv was not observed.

b) Niobium is reported to be covered by an insoluble oxide at positive potentials. However, corrosion of niobium was observed above + 250 mv, presumably because of a soluble reaction product.

c) The formation of soluble WO_4^- is predicted to occur at negative potentials. However, the formation of a soluble corrosion product was not observed below + 200 mv.

The remaining transition elements show some activity for O_2 reduction. Table IX lists elements which catalyze O_2 reduction above + 800 mv.

The borides, silicides, carbides, and nitrides of the transition metals were surveyed for their corrosion behavior and their activity for catalyzing the electrochemical reduction of oxygen.

The performances of materials within each grouping is discussed in terms of modifying the properties of the parent transition metal.

In a later section of this report, we discuss a more detailed study of highly dispersed carbides, nitrides, nitrocarbides, and carbonitrides of Fe, Ni, and Co. The data presented below are, except where noted, for solid electrodes.

(a) Ti, TiN, TiC.

A slight anodic corrosion current is observed for titanium. This current is much less for TiN even though the surface area of the nitride is much greater, as indicated by the capacitance (540 $\mu f/cm^2$). Substantial corrosion of TiC is observed above +830 mv. Judging from the absence of a passivating current, the reaction product is either partly soluble or porous.

The O_2 reduction activity of TiN is substantially higher than that of Ti. The current-potential curve has two waves, implying a difference in rate for O_2 and HO_2^- reduction noted for oxide coated metals. This material was also studied with a graphite counter electrode to eliminate the possibility of contamination of TiN by dissolved platinum. No difference in activity was found.

TiC is slightly more active than titanium and some O_2 reduction current is noted at + 820 mv. However, its performance is less than that of TiN. Some of this could be ascribed to the large difference in surface area.

(b) Zr, ZrN, ZrC.

As noted previously, Zr does not corrode or reduce O_2 over the potential range studied. ZrN shows a slight activity and possibly corrosion at potentials above + 600 mv.

Corrosion is not observed for ZrC; the material shows cathodic current for O_2 reduction below + 400 mv.

(c) Hf, HfN, HfC.

Hafnium, like Zr, is inert over the potential range studied. The low capacitance (2 $\mu f/cm^2$) is consistent with an insulating oxide film. HfN is also essentially inert although there is a slight indication of activity below + 500 mv.

HfC shows an anomalous anodic current peak at + 630 mv. O_2 reduction is observed at potentials less positive than + 500 mv.

(d) V, VN, VC.

Vanadium corrodes under the conditions of the experiment, presumably with the formation of a soluble product. Anodic corrosion current is observed for VN above +180 mv, and a small amount of oxygen activity is observed below + 180 mv. These corrosion reactions are further suppressed in VC. Anodic current is observed only above +820 mv; the low capacitance (60 $\mu f/cm^2$) at + 600 mv is consistent with a stable surface. Cathodic O_2 reduction current is observed below this potential.

(e) Nb, NbN, NbC.

Niobium corrodes above + 170 mv, but is also active for O_2 reduction; a net cathodic current was observed below + 270 mv. The corrosion behavior of NbN is similar to that of the metal; the O_2 activity may be less, although this point is difficult to establish because of the corrosion current.

NbC is more resistant to corrosion than is the metal; anodic current is observed only above + 600 mv. Reduction of oxygen is observed below this potential; as with the other carbides studied, two waves are present.

(f) Ta, TaN, TaC.

Tantalum is essentially inert over the potential range studied. The nitride, on the other hand, shows substantial corrosion at potentials more positive than 0 mv. A small amount of oxygen activity is observed below + 100 mv. Corrosion is observed for TaC above + 630 mv, and O_2 reduction is observed below + 630 mv.

(g) Cr, Cr_2N, Cr_3C_2.

Chromium shows little activity for O_2 reduction and corrodes to soluble chromate above + 900 mv. The behavior of Cr_2N is essentially identical. The corrosion behavior of Cr_3C_2 is apparently more complex; anodic current is observed above + 350 mv. Net O_2 reduction activity is observed below + 600 mv.

(h) Mo, Mo_2C.

Substantial corrosion current is observed for both materials.

(i) W, WC, **94** WC - 6 Co, 80 WC - 20 Co.

The corrosion behavior of W and WC are essentially identical. This behavior appears to be somewhat suppressed by alloying with cobalt. Anodic current peaks are observed rather than continuous corrosion.

(j) Fe, Fe_2C.

Fe_2C is somewhat more active than Fe and cathodic current is observed at more positive potentials. Both limiting currents are low (~ 0.8 - 0.9 ma/ cm^2), indicating incomplete reduction of O_2. The electrical capacitances of the electrodes indicate stable surfaces on both samples.

(k) Ni, Ni_3N, Ni_3C.

It was difficult to prepare the carbide and nitrides as solid ingots; powder electrodes were therefore used; the preparative techniques are described elsewhere.

Ni_3N is slightly more active than nickel, and Ni_3C is two orders of magnitude more active than nickel. It is not clear whether this high activity is an inherent property of Ni_3C or due to a high surface area. Furthermore, the sample is not pure Ni_3C; nickel is also present as a major constituent.

The corrosion behavior of these compounds relative to the parent metals is given in Table XII. The data are qualitatively displayed in terms of increased or decreased corrosion.

TABLE XII

Relative Corrosion Behavior

Metal	Nitride	Carbide	Corrosion Level (Metal)
Ti	decreased	increased	low
Zr	small increase	small increase	none
Hf	no change	?	none
V	decrease	decrease	high
Nb	no change	decreased	high
Ta	increase	increase	none
Cr	no change	increase	at high potential
Mo	----	no change	high
W	----	no change	high

There are no systematic trends in corrosion behavior useful in predicting the behavior of other compounds or in correlating with other pertinent parameters such as O_2 activity. The corrosion rates of VC, VN, NbC, and TiN are lower than they are for the metals. However, Cr_3C_2, TiC, and TaC corrode faster than the parent materials. Apparently either porous or soluble products are formed since passivation currents are not observed. 'This effect implies that the composition of the surface oxide film normally present on the metal has been substantially altered by the presence of carbon.

The carbides are all more active than the parent metal for O_2 reduction, and some activity is found even when the metal itself is inert, e.g. Zr, Hf, Ta, and Cr. Except for the titanium compounds, the nitrides are less active than the carbides. The apparent limiting currents (at + 150 mv) for Cr_3C_2, Fe_2C, NbC, and TaC were significantly higher than for graphite, implying that the carbides are more effective in reducing HO_2^-.

The highest activities were observed for TiN, VC, Fe_2C, and Ni_3C. The relative activity of TiN may be misleading since the material had a high surface area (540 $\mu f/cm^2$). The use of VC cathodes is impractical because of corrosion at high positive potentials. Fe_2C is apparently stable over the voltage range studied so that its use is not ruled out by corrosion problems.

Corrosion currents are observed for the borides and silicides of the refractory metals. Of interest are the high corrosion rates for the borides and silicides of metals which are inert in 2N KOH, *e.g.* Zr, Hf, and Ta. Evidently, the normally passivating film of insoluble oxide is substantially modified by the nonmetallic constituent, more so than for carbon or nitrogen.

The chromium compounds are the most stable in this group, although a small amount of corrosion current is observed for the high boron-content compounds, i.e. CrB, CrB_2, and Cr_5B_3. The first two of these materials also show cathodic currents. It is tempting to assign this current to reduction of soluble chromate. However, the stirring in these experiments should remove from the surface chromate produced at high potentials.

Because of these high corrosion currents, the refractory metal borides and silicides cannot be considered as possible oxygen electrodes.

The group VIII borides studied (Ni_2B, Ni_3B, Pt_2B) were relatively resistant to corrosion, although even in the case of Pt_2B anodic current was observed at high potentials. The measurement of O_2 activity indicated no enhancement due to the presence of boron.

IV. DISCUSSION

We can consider these catalysts mainly in terms of the role of the oxide film formed on the surface during the oxygen reduction process. There are three main groups.

The first includes metals on which oxygen reduction begins only when bare metal surface becomes available - that is after substantial reduction of an oxide or chemisorbed oxygen layer. The reduction of oxygen proceeds directly to water on the bare surface with very little hydrogen peroxide accumulation. Examples of metals of this type include those of the Pt group and silver. Within this group Pt has the highest activity at low temperatures. The metals Zr, Ta, Hf, and Nb can be included in this group insofar as an oxide layer is present at all potentials and no appreciable O_2^- reduction occurs.

The next group contains elements such as Ti, Ni, Fe, and graphite. Oxygen is reduced on these materials on oxide-covered surfaces with varying degrees of reversibility. For example, reduction of oxygen on passivated Ti requires an overvoltage of about 1v, while on graphite (which is completely covered by oxygen) oxygen can be reduced to hydrogen peroxide with a high degree of reversibility.

The third group includes elements such as Mn and Co on which redox reactions of the type

$$Mn^{4+}/Mn^{3+} \text{ or } Co^{3+}/Co^{2+}$$

have specific effect on oxygen reduction. In these cases, a maximum activity is found in the range of potentials where these reactions occur. A maximum can be observed directly on pure Mn but is masked on pure cobalt by a corrosion current. It is, however, observed on Ni-Co alloys where the corrosion current is very small. The activity of the $NiCo_2$ alloy may be additionally due to a synergistic effect related to the spinel Co_2NiO_4.

Gold is a special case since it is the only metal essentially free of oxide or chemisorbed oxygen below the reversible O_2^- potential (1.23 v). Reduction of oxygen to hydrogen peroxide is virtually reversible on gold, while the further reduction of HO_2^- to water (or OH-) is slow.

In the case of the intermetallic compounds, we were principally concerned with the influence of alloy or compound formation on the intrinsic catalytic activity for the electrochemical reduction of O_2. Again for most of these we are examining the influence of the bulk catalyst composition on the surface oxide formed under the test conditions, rather than the activity of the intermetallic itself.

Our experiments show that enhancement of the catalytic properties by formation of a new phase is generally small. The catalytic properties of the components of an alloy appear to be more important than the electronic or crystallographic structure of any phase that may be formed. However, compounds or alloys may show substantially higher activity and stability than do the components. This result is generally to the effect of the electronic or crystallographic structure of the compound on the properties of the surface oxide formed during oxygen reduction on all nonnoble metals.

A substantial effect of chemical compound formation is also apparent in corrosion.

Of the specific systems studied, the intermetallic compounds of platinum and nickel and the interstitial compounds of the transition elements with carbon and nitrogen are of particular interest.

From our study of intermetallic compounds of Pt with nonnoble metals we may conclude that:

(a) Appreciable dilution by a nonnoble metal (e.g. Pt_2Ta) causes no decrease of the platinum activity for comparable surface roughness factors.

(b) Considerable surface increase can be obtained in some intermetallic compounds, probably by leaching of the nonnoble metal component. This effect may be useful in obtaining platinum particles with a high and stable surface for practical electrodes.

(c) Although addition of cobalt to nickel imparts a considerable increase in activity, $PtCo_3$ does not show a corresponding improvement. This may be due to the high intrinsic activity of Pt. This conforms to the general pattern observed, namely that no intermetallic compound tested to date shows more activity than platinum.

Nickel alloys with Co and Mn show improvement in performance over nickel. The corrosion resistance of a metal which corrodes in alkali is improved, on the other hand, by addition of Ni. This general trend was noticed for all nickel alloys; the best example was NiAl which behaved exactly as nickel.

Ti_3Au is a particularly interesting intermetallic compound. Its initial performance is higher than titanium or gold (but somewhat lower than platinum). With time, this performance increased to a level higher than platinum, but it was accompanied by a pronounced increase in double layer capacity, implying roughening of the surface. This was confirmed by electron microscopy. Analysis of the surface with an electron microprobe showed the surface exposed to the electrolyte to be more rich in titanium than was the bulk of the sample. This is discussed in more detail later.

Of the "interstitials" of the refractory metals, borides and silicides generally exhibited high corrosion currents, which eliminated them as possible oxygen electrodes in caustic electrolytes.

The nitrides and carbides are another matter, especially in the cases of VC, VN, NbC, and TiN all of which are more resistant than their parent metals. The carbides (and the nitrides to a lesser extent) are all more active for O_2^- reduction than the parent metals; some activity is found even when the metal itself is inert, for instance with Hf, Ta, and Cr.

Another example of interest is Ti and TiN. The decrease of corrosion current and of overvoltage for O_2^- reduction (about 500 mv) observed with TiN is hard to explain as a pure surface area effect and must be due to the favorable effect of an oxynitride of titanium covering the TiN surface.

SECTION 2

THE ACTIVITY OF GOLD ALLOYS OF PRECIOUS METALS AND TITANIUM; NONSTOICHIOMETRIC TiO_2, SILVER MAGNESIUM ALLOYS; OSMIUM, SILICON CARBIDE, AND BARIUM TANTALATE (SOLID ELECTRODES)

I. GOLD ALLOYS OF SILVER, PALLADIUM, AND PLATINUM

A. Introduction

These alloys are of interest because of the gradual changes in electronic configuration and lattice parameters which can be induced by alloying. In addition, some new surface oxide characteristics may appear for these alloys. It has been found that oxide layers of Pt, Pd, and Ag do not catalyze O_2-reduction to the same extent as the bare metal does. Consequently alloying with gold, which does not form surface oxides, may lend some nobie characteristics to the alloys. It should be noted, however, that the absence of an oxide layer does not ensure catalytic activity for O_2-reduction. Gold, for example, catalyzes the reduction of O_2 to HO_2^- quite reversibly but shows considerable irreversibility in the second step, the reduction of HO_2^- to OH-.

One of the purposes of this work was to try to distinguish between the electronic effects and the influence of the oxide layer. Special precautions were taken (a) to keep the composition of the surface constant (i.e. avoiding selective segregation of components), (b) to control diffusion conditions and (c) to minimize the effect of impurities.

B. Experimental

The rate of oxygen reduction was measured on gold, platinum, palladium and silver and the alloys Au/Pd, Au/Pt, and Au/Ag at 10% increments of composition. The electrodes were machined and polished cylinders 0.6 cm high and 0.6 cm diameter and were mounted in a holder described by Makrides and Stern[2]. The actual geometric surface area was determined accurately in

each case. All tests were made in 2M potassium hydroxide (Baker Analyzed) at 25°C ± 0.1°C. Further tests on selected alloys were made at 75°C. The reference electrode was a reversible H_2 electrode separated by a Teflon frit. After preliminary tests with Pt and graphite the counter electrode was changed to a large folded piece of Pd-Ag foil precharged cathodically with hydrogen in order to maintain its potential below 100 mv vs. RHE for the duration of the test. (The reason for selecting this counter electrode is discussed later.) The solution was presaturated with nitrogen for corrosion tests and with oxygen for the activity determination. The electrode was rotated at 600 rpm.

Mass transport in an electrode of the described configuration cannot be strictly defined by a simple equation such as the Levich equation for rotating disc electrodes. Consequeiitly, an experiment was performed to determine the transport contribution from the sides and the bottom of the electrode to the total current. The implications of this information are discussed in the next section.

Three experimental techniques were used to establish the characteristics of the alloys:

(1) Fast potential sweeps (500 mv/sec) carried out in the presence of a N_2 saturated solution to determine the nature of surface oxidation of the alloys.

(2) Slow sweeps (50 mv/min) in an O_2 saturated solution to define the current voltage relationship for the O_2-reduction reaction.

(3) Capacity measurements to determine the relative surface roughness.

The electrode potential was coiitrolled at all times with a potentiostat, and the signal source was either a fast or slow function generator. The E (1)-curves were followed on an X-Y recorder, or an oscilloscope in case of fast sweeps and capacity measurements.

Typical fast sweeps are shown in Figs. 3a, 3b, and 3c. The potential range for these fast sweeps was 0 to 1600 mv vs. RHE except for the gold palladium alloys. For these alloys the potential was kept above 400 mv vs. RHE to avoid the absorption of H_2 by palladium, since the subsequent oxidation of the H_2 masks the surface oxidation processes being studied, Particular precautions were taken to prevent surface roughening and changes of surface composition of the alloys. The samples were repolished for each experiment; in addition, the number of potential cycles applied to the electrode, before the fast sweeps were recorded, was restricted to four sweeps, the first three being used to align the trace on the oscilloscope. For the slow sweep, the electrode was again polished and the potential restricted to 600-1000 mv. The higher limit was set to avoid surface composition changes due to oxidation above 1000 mv, and the lower limit was intended to minimize the duration of the experiment and thus avoid accumulation of peroxide in the electrolyte. A typical example of a slow sweep curve is shown in Fig. 4.

The capacity of each electrode was measured in N_2-saturated solution prior to the O_2-reduction activity determination. The technique consisted of the application of a small triangular wave (25 mv, peak to peak) to the electrode at 600 mv vs. RHE (to conform to the potential restriction mentioned above). The resulting square wave of current was used to calculate the double layer capacity.

Effect of Impurities

Gold was chosen as the electrode material for the investigation since it allows the most sensitive measurements of side reactions.

In the initial tests, there were two unexpected features in the experimental curves. These were (1) an unusual cathodic peak in the limiting current during the return sweep (increasing potential) at 250-500 mv and (2) an anodic current, also observed with gold, at potentials > 900 mv, which varied with time and immediate past history of the system. Both of these factors were important in considering our present objectives.

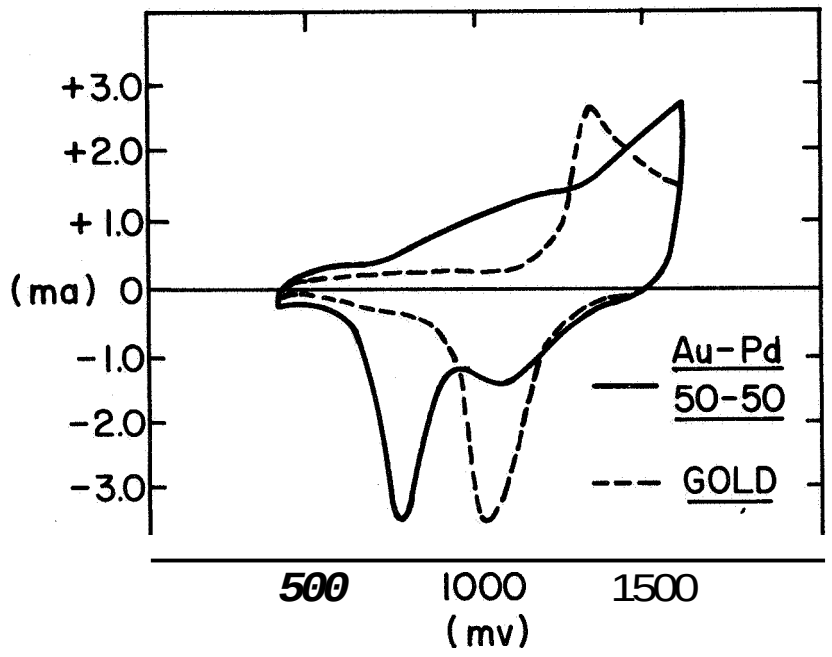

Fig. 3a

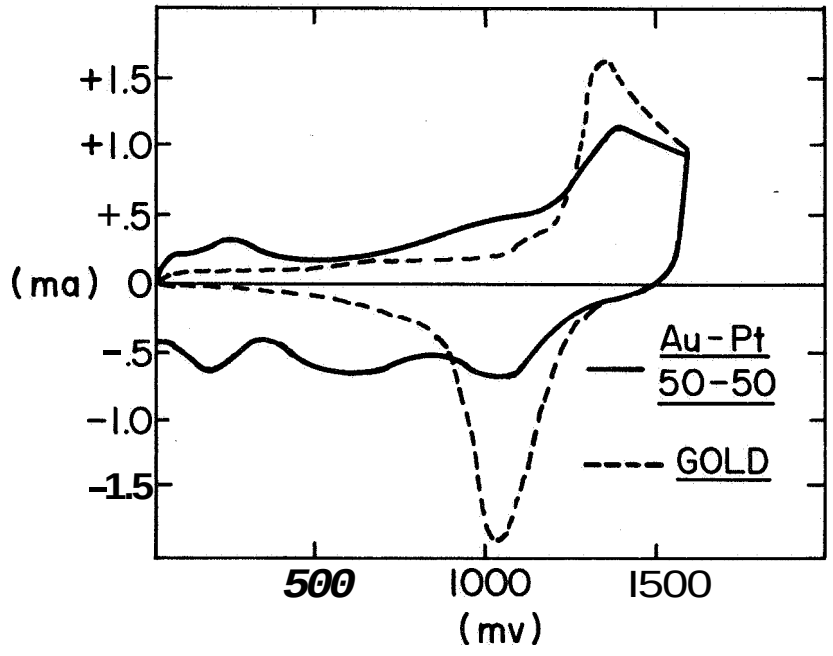

Fig. 3b

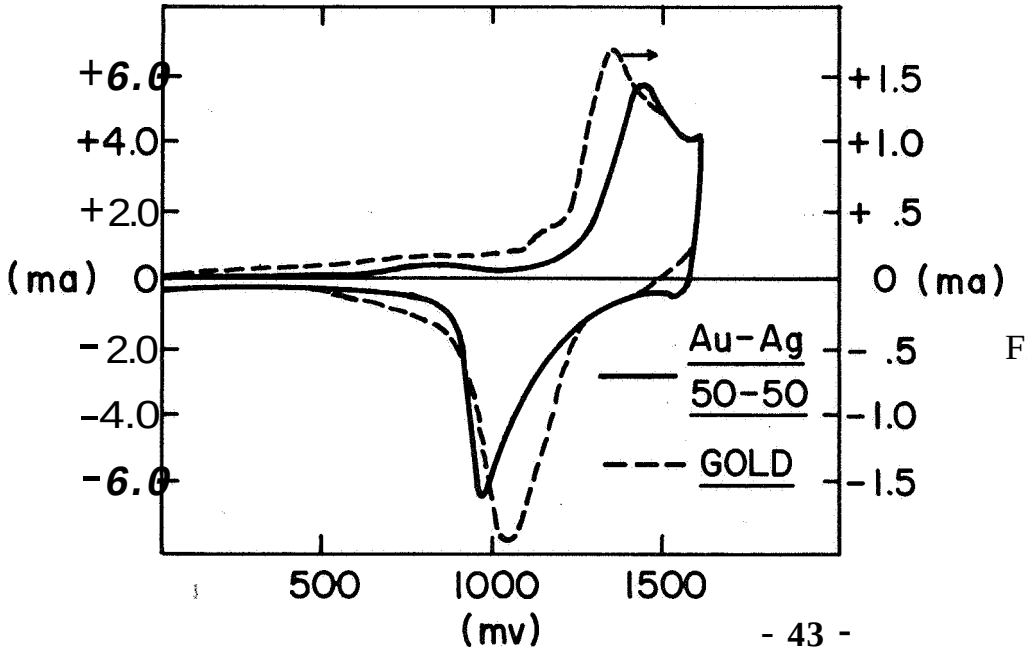

Fig. 3c

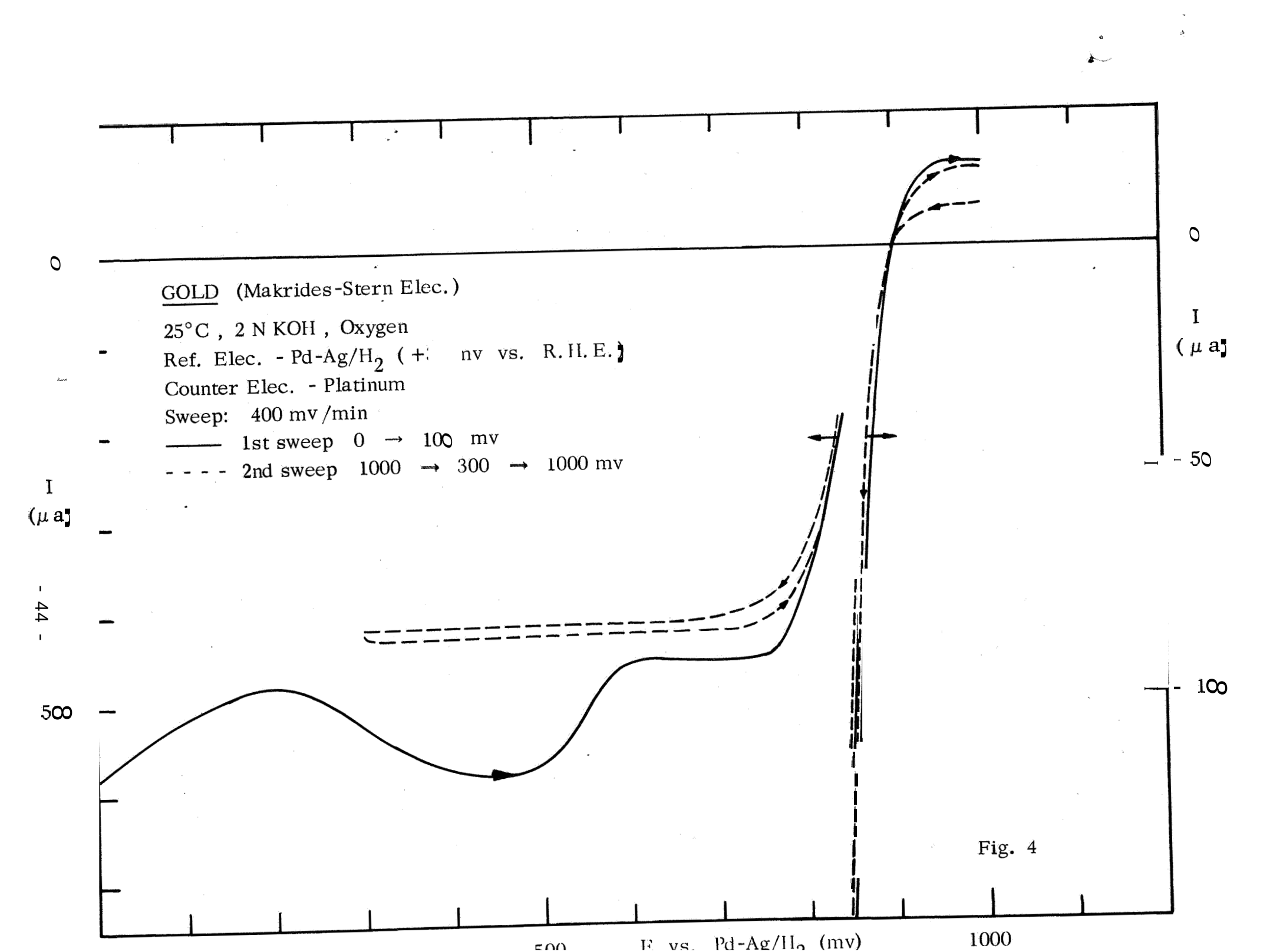
GOLD (Makrides-Stern Elec.)
25°C , 2 N KOH , Oxygen
Ref. Elec. - Pd-Ag/H2 (+ nv vs. R.H.E.)
Counter Elec. - Platinum
Sweep: 400 mv/min
1st sweep 0 → 100 mv
2nd sweep 1000 → 300 → 1000 mv
I (μa)
0
- 50
- 100
- 44 -
500
1000
E vs. Pd-Ag/H2 (mv)

Fig. 4

The peak in the limiting current was undesirable because it prevented precise definition of $E_{\frac{1}{2}}$ and because it was an indication of an impurity in solution that was actively involved in the oxygen reduction reaction. The anodic current was undesirable because it occurred in the potential region where the O_2 reduction process is activation controlled. The activation controlled region (Tafel region) of the current voltage curve is that where the surface reaction, which is dependent on the catalytic activity of the electrode, controls the over-all rate of the reduction reaction. Measurements of the rate, the current density per real square centimeter of the surface as a function of potential in this region, is a means of assessing the activity of the electrocatalyst. Therefore, the presence of a simultaneous anodic process of any magnitude restricts precise determination of the electrocatalytic activity toward the O_2 reduction process (further discussion below). Prior to making the experimental measurements on the three systems, the possible causes of the aiiodic current and the cathodic peak were investigated.

The anodic current occurred at all potentials > 800 mv under N_2. Under O_2 the anodic current was not observed until higher potentials (~ 950 mv), but it was assumed that the aiiodic reaction occurred simultaneously at the lower potentials, affecting the magnitude of the observed cathodic current. The anodic current tended to increase with time and frequently showed a sharp increase after the determination of a current voltage curve under O_2.

This behavior corresponds to the accumulation in the electrolyte of H_2O_2 (or more precisely HO_2^-) produced by the incomplete reduction of O_2. This is particularly the case when the electrode material is not a good peroxide decomposition catalyst. To check the effect of peroxide accumulation, hydrogen peroxide was added to the electrolyte to make a 10^{-3}M solution. The anodic current increased by a factor of 10^3. If it is assumed that the current is diffusion controlled, then the anodic currents usually observed correspond to a solution 10^{-6}M in peroxide. This level of concentration may occur under the normal operating conditions, particularly since the electrode is at low positive potentials for quite long periods during the slow sweep measurements. A large

gold scavenger electrode was introduced to the system and maintained at a potential of 1000 mv vs. RHE, in order to consume accumulated peroxide. However, this electrode was apparently not as efficient as was expected in the oxidation of HO_2^-, since it did not reduce the magnitude of the anodic current, possibly because of poor transport of HO_2^- to its surface.

The anodic currents have been minimized by working with fresh electrolyte for every determination, by conducting the measurements in the shortest possibly time, and by using a restricted potential range for the slow sweep studies (see below) thereby reducing the amount of peroxide produced.

The cathodic peak in the limiting current of O_2-reduction to HO_2^- is a catalytic peak. It did not appear when the potential was maintained above 300 mv vs. RHE. Furthermore, the current peak never exceeded the theoretical limiting current to be expected from reduction of O_2 to H_2O. This suggests that the effect was possibly due to the complete reduction of O_2 to OH- catalyzed by a metal deposited at the low potential. Kronenberg[6] has reported a 1M solution of KOH containing 1-10 ppm of Fe, Ag, Cu and Cr. For iron, a 5 ppm impurity level corresponds to a 10^{-4}M solution.

Another source of impurities that was considered was the counter electrode. Initially, Pt was excluded from the system because of its possible dissolution and deposition on the surface of the working electrode, which could change its character, including oxygen film formation at lowered potentials. Measurements carried out with a graphite counter electrode indicated that it contained leachable impurities. Gold was excluded on the same basis as Pt. Any gold deposited on the working electrode would not show the difference in activity expected of Pt but could give rise to a continuously changing surface composition in the case of the alloys. The system selected for the counter electrode was a large piece of Ag/Pd foil charged with H_2. The anodic process that occurs to complement the cathodic reduction of O_2 is hydrogen oxidation, and since this occurs at < 100 mv vs. RHE, no metal dissolution can occur.

C. Results

A typical E-log i curve is presented in Fig. 5. The linearity of the curve for over a decade of current suggests that in this particular region the rection is activation controlled,

The activities of the complete range of alloys are presented in Figs. 6 and 7 at the potential corresponding to a particular current density in the Tafel region; the current was normalized for the real surface area of the electrodes using the double layer capacities measured previously. Also shown in Fig. 8 are the activities defined in terms of potential at a constant current density (per geometric square centimeter). The pattern of activity is the same.

The order of activity was Au/Pd > Au/Pt > Au/Ag; for the 1:1 alloys the following E_i values were recorded for i = 50 $\mu a/cm^2$: Au/Pd - 926 mv, Au/Pt - 878 mv, Au/Ag - 856 mv vs. RHE. The Au/Pd series exhibit a flat maximum of activity over the range 70/30 - Au/Pd to 30/70 - Au/Pd; the Au/Pt and Au/Ag alloys show, with some scatter, a steady transition from the activity of one pure component to the other. The activity patterns are approximately the same at 75°C (Fig. 9). The enhanced activity of the Au/Pd alloys is not unexpected and has been reported in the literature[7,8]. An interesting feature of these results is that at 25°C pure Pd (E_{50} = 922 mv vs. RHE) is more active than pure Pt (E_{50} = 880 mv vs. RHE). As the temperature was increased from 25°C to 75°C, the activity (E_{50}) of pure Pt increased from 880 to 903 mv, while that of Pd decreased from 922 to 915 mv. In other words, at 75°C and 50 $\mu a/cm^2$ Pd was still somewhat more positive (12 mv) than Pt.

An important reason why Pd has not been extensively used in practical fuel cells is that it is known to corrode at a significant rate at positive potentials in KOH (or in acid) at 75°C and above. The aiiodic current observed at 1000 mv was 3 $\mu a/cm^2$ for Pd compared with 1 $\mu a/cm^2$ for Pt, though no great significance should be attached to the absolute value of these figures. It is therefore of considerable interest to note that the activity of Pd is

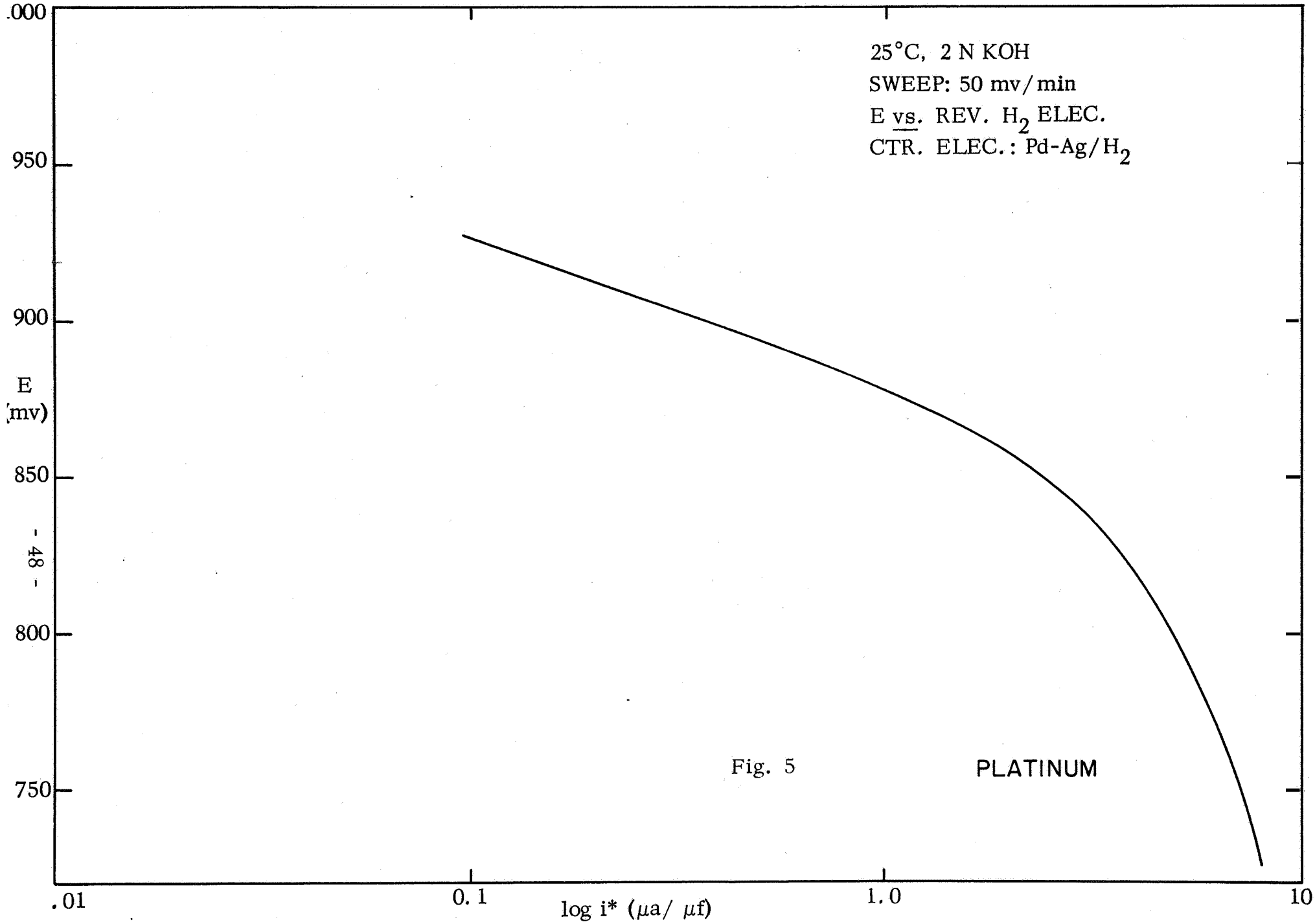
25°C, 2 N KOH
SWEEP: 50 mv/min
E vs. REV. H_2 ELEC.
CTR. ELEC.: Pd-Ag/H_2
.000
950
900
E (mv)
850
800
750
.01
0.1
1.0
10
log i* (μa/ μf)
PLATINUM

Fig. 5

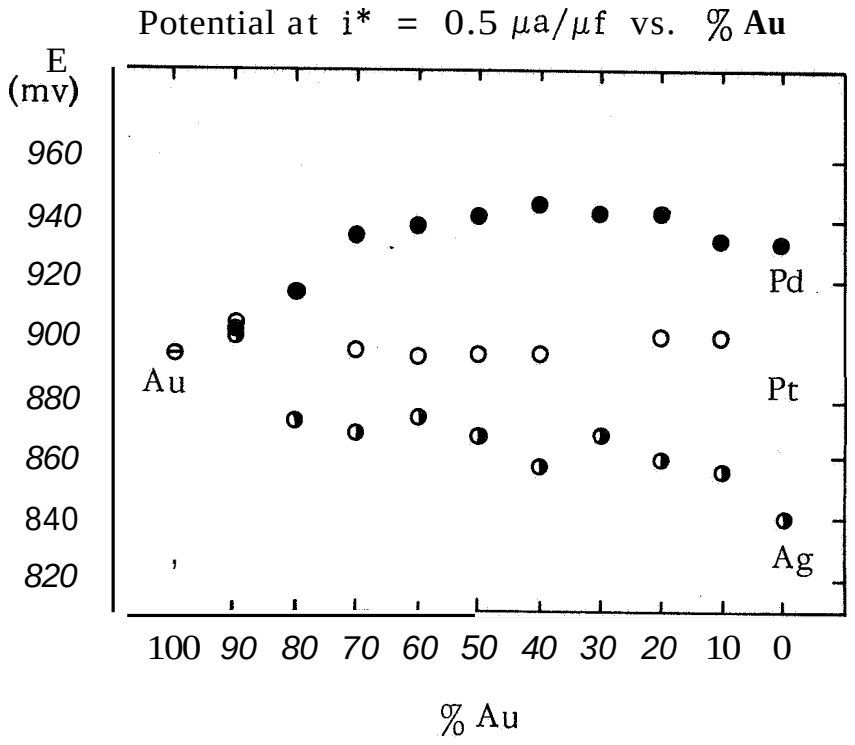
Potential at i* = 0.5 μa/μf vs. % Au
E
(mv)
960
940
920
900
880
860
840
820
Au
Pd
Pt
Ag
100 90 80 70 60 50 40 30 20 10 0
% Au

Fig. 6

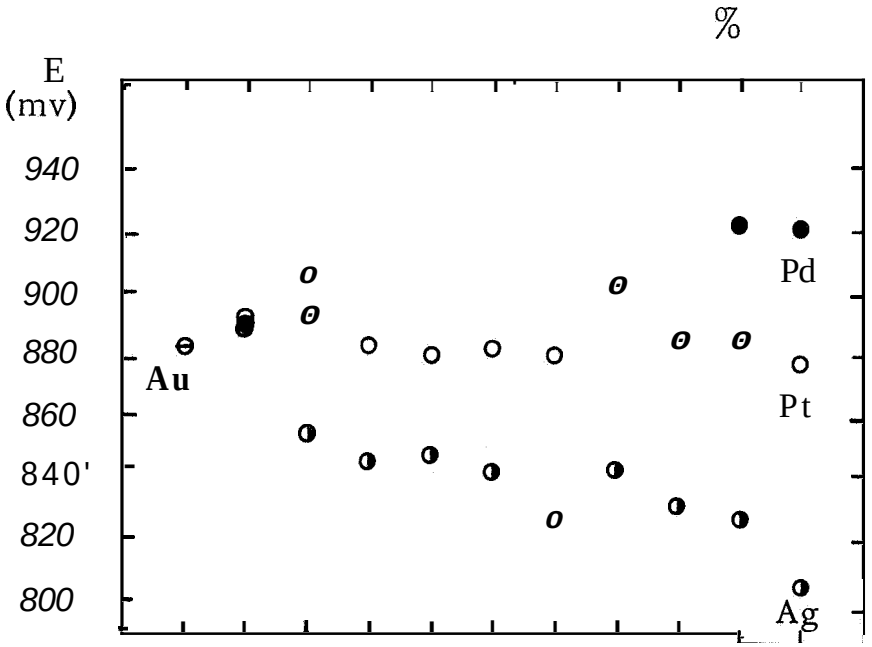
%
E
(mv)
940
920
900
880
860
840'
820
800
Au
Pd
Pt
Ag

Fig. 7

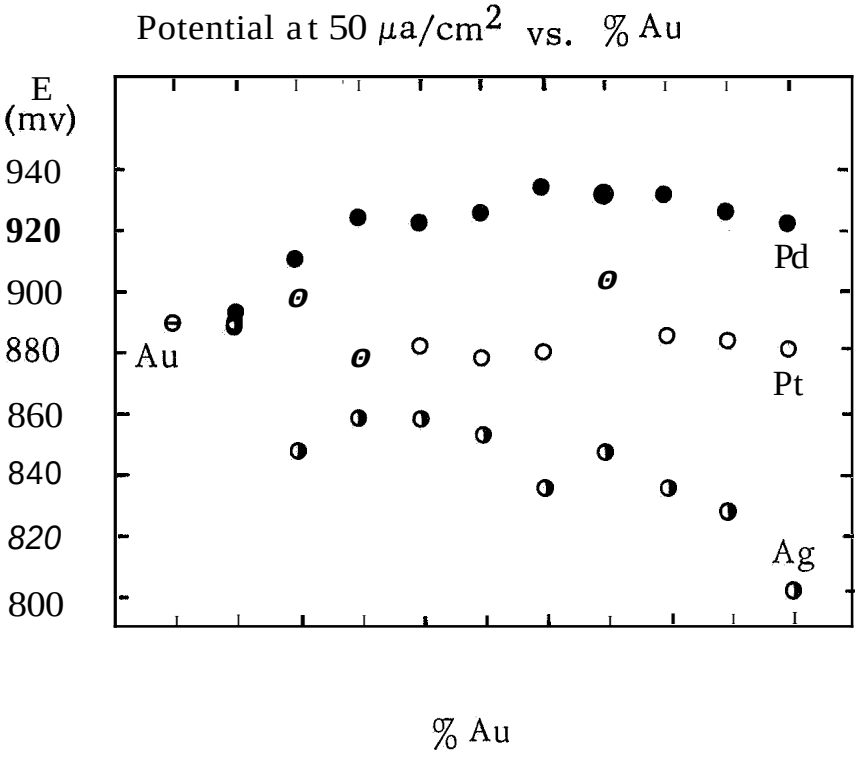
Potential at 50 μa/cm² vs. % Au
E
(mv)
940
920
900
880
860
840
820
800
Au
Pd
Pt
Ag
% Au

Fig. 8

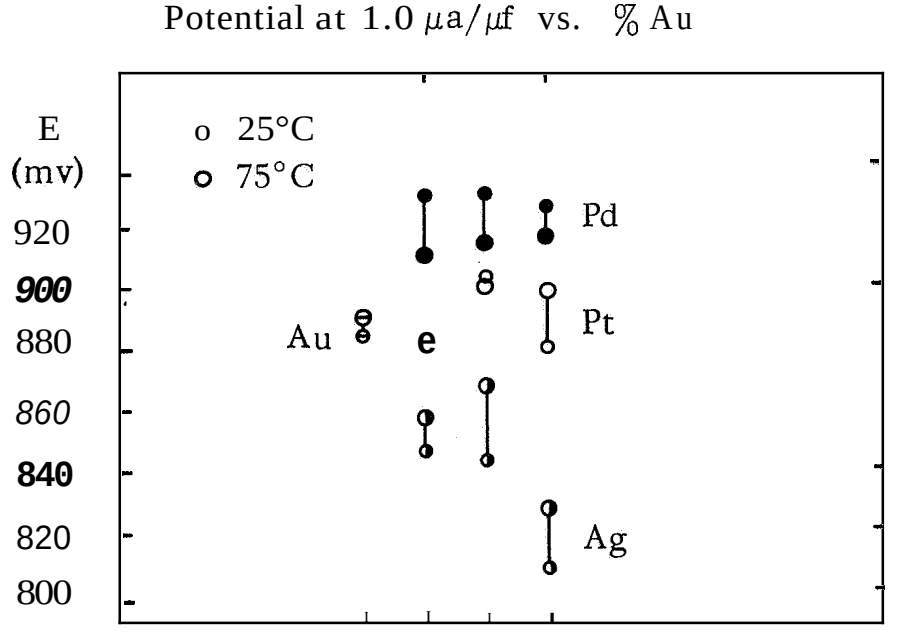
Potential at 1.0 μa/μf vs. % Au
E
(mv)
o 25°C
o 75°C
920
900
880
860
840
820
800
Au
Pd
Pt
Ag

Fig. 9

maintained or even enhanced in the gold alloys up to 70% Au, particularly since it might be expected that the corrosion resistance of the alloys would be better than that of pure Pd, as is the case for the Ni alloys of Mn and Co[4]. The level of activity, compared with Pt, shown by these gold alloys of palladium warrants further examination in a practical form as finely divided catalysts,

In the fast potential sweeps separate peaks for the O_2 desorption process (cathodic current) are observed on the Au/Pd and Au/Pt alloys (Figs. 10-12), the relative magnitudes changing with the alloy composition. This indicates that for the most part, as shown in our study of intermetallic compounds, the componeiit metals retain their individual characteristics with respect to oxide reduction and do not exhibit any composite properties. There is less differentiation of peaks, except in magnitude, among the Au/Ag alloys since the pure metals under these conditions behave in a similar manner. Another indication that the component metals retain their individual characteristics is the observed differences in limiting current density for 10% additions of Ag, Pd, or Pt. At room temperature the reduction of O_2 on gold proceeds oiily to peroxide at low polarization, whereas platinum, palladium, and silver are all effective peroxide decomposition catalysts. It is interesting to note that the limiting currents are doubled for only a 10% addition of these components to Au. See Table XIII.

D. Future Work

We have started to examine the behavior of highly dispersed catalysts of Au/Pd alloys. The initial results show that 30/70 Au/Pd alloy to have higher activity (at low current densities) than has a Pt electrode made in an identical manner. So far, the 70-30 and 60-40 Au/Pd alloys have shown lower activity than has Pt.

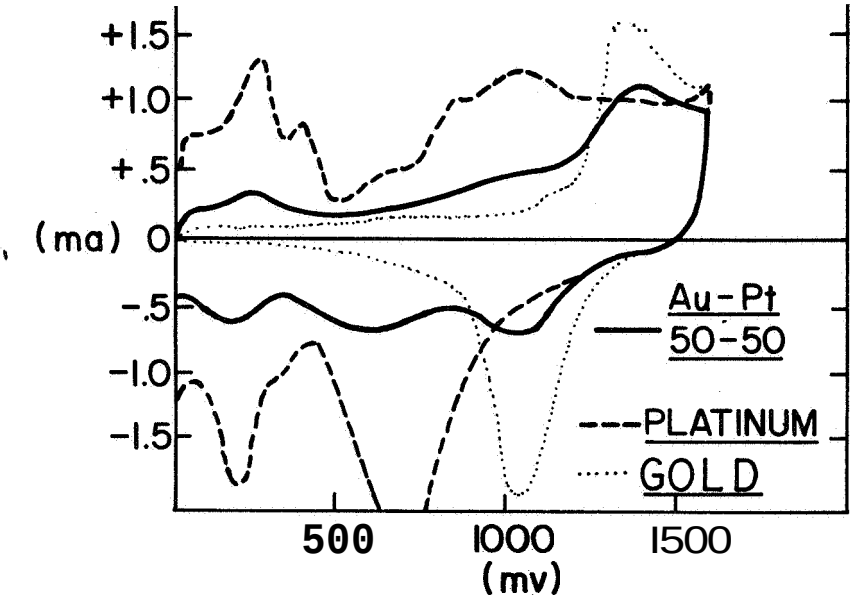

Fig. 10

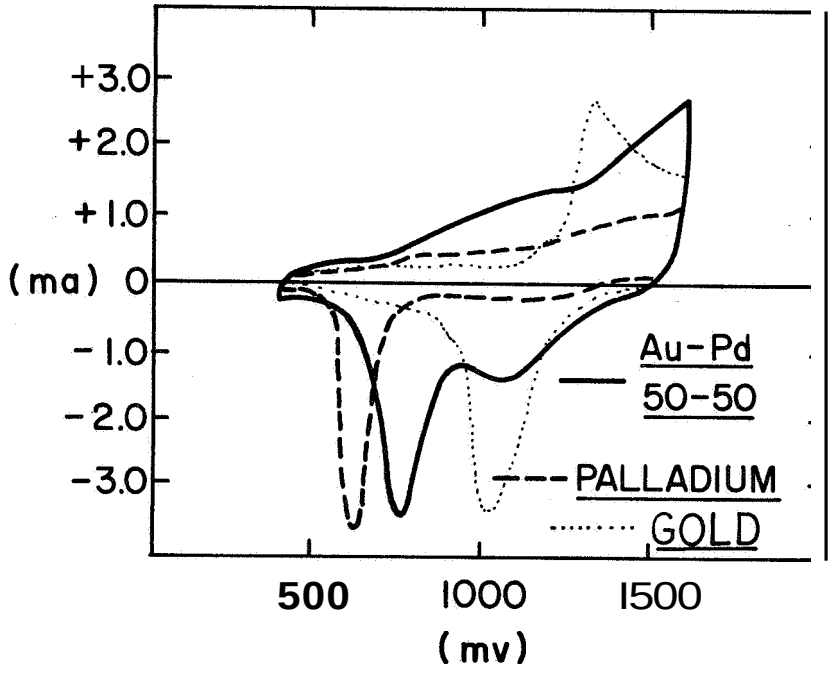

Fig. 11

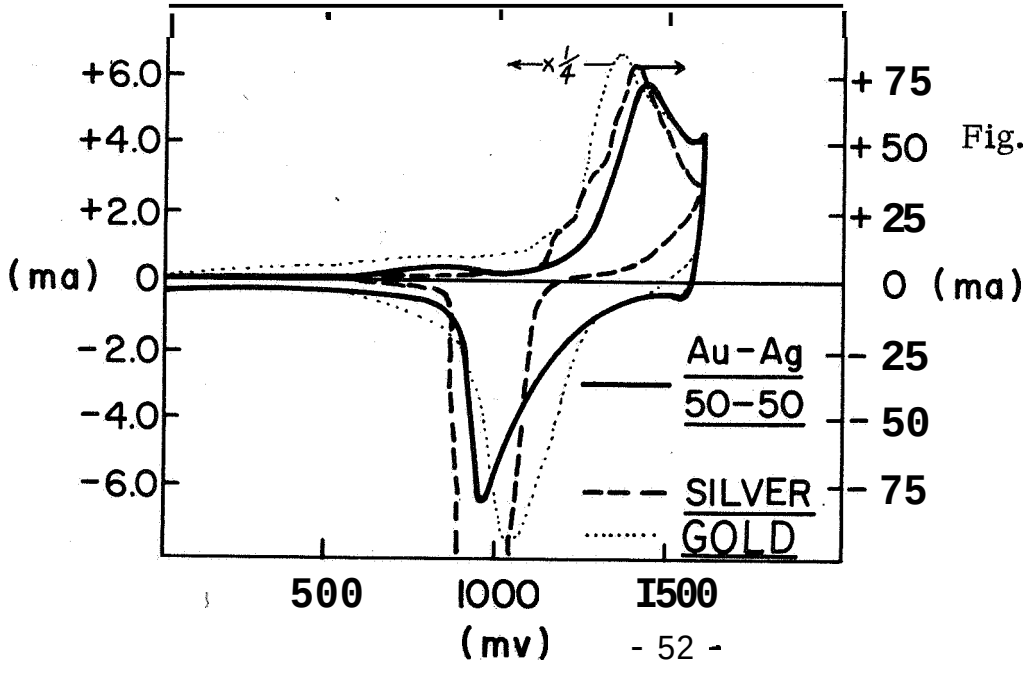

Fig. 12

TABLE XIII

Activities of Platinum, Palladium,
and Silver Alloys of Gold

Atom % Au	Au-Pt		Au-Pd		Au-Ag	
	i_L/A ($\mu a/cm^2$)	$E_{\frac{1}{2}}$ (mv)	i_L/A ($\mu a/cm^2$)	$E_{\frac{1}{2}}$ (mv)	i_L/A ($\mu a/cm^2$)	$E_{\frac{1}{2}}$ (mv)
100	340 (Au)	860				
90	623	820	558	840	508	825
80	766	826	662	860	491	750
70	636	787	781	877	650	755
60	615	804	637	877	675	750
50	599	795	845	873	701	739
40	763	785	1006	880	634	717
30	808	837	1037	876	693	737
20	686	795	984	878	623	728
10	802	787	926	877	628	713
	676 (Pt)	780	1000 (Pd)	854	436 (Ag)	700

II. TITANIUM, NONSTOICHIOMETRIC TiO_2 AND GOLD ALLOYS OF TITANIUM

A. Introduction

As noted in section I the intermetallic compound Ti_3Au shows considerable catalytic activity for the reduction of oxygen; it was subject to some corrosion. A comparison of the activity of Ti_3Au and Pt_2 as solid electrodes is given in Fig. 13. Titanium nitride, probably the oxynitride when tested, also shows greater activity than pure titanium. However, when attempts were made to run powdered forms of Ti_3Au and TiN as floating electrodes, they were unsuccessful because of oxidation of the catalyst to a nonconductive state (see below).

It has been suggested that the activity of the Ti_3Au intermetallic in solid form may in part be due to the formation of a iioiistoichiometric phase of titanium dioxide by the chemical and/or electrochemical environment to which it is subjected in testing. The nonstoichiometric form is characterized by having a conductivity ($TiO_{1.75} = 10^2 \Omega^{-1}cm^{-1}$) that is much greater than TiO_2 ($10^{-10}\Omega^{-1}cm^{-1}$)[8]. Therefore, since the electrochemistry of pure gold is reasonably well defined, we have turned our attention to a more detailed study of the electrochemistry of titanium, and more especially nonstoichiometric titanium dioxide.

A literature survey of the titanium oxygen system with emphasis on the preparation of nonstoichiometric oxides and their resistivity, catalytic activity, and electrochemical behavior showed some interesting properties.

Douglass, St. Pierre, and Spieser[9] report that attempts to nitride TiO_2 with NH_3 in Ar at 900-1070°C resulted in the reduction of the oxide to form successively $TiO_{1.96}$, Ti_9O_{17}, Ti_8O_{15}, Ti_7O_{13}, Ti_2O_3, aiid TiO with the eventual formation of some TiN. This is in contrast to the reports of Gilles, Lejus, and Colonguy[10] where no oxynitride was detectable by X-ray analysis. Hollander and Castro[11] have prepared nonstoichiometric oxides of titanium by the reduction of single crystals of TiO_2 (rutile) by H_2 in Ar at 600 - 1000°C. In this case, the conductivity was measured as a function of crystal orientation and was found to be markedly anisotropic; the maximum

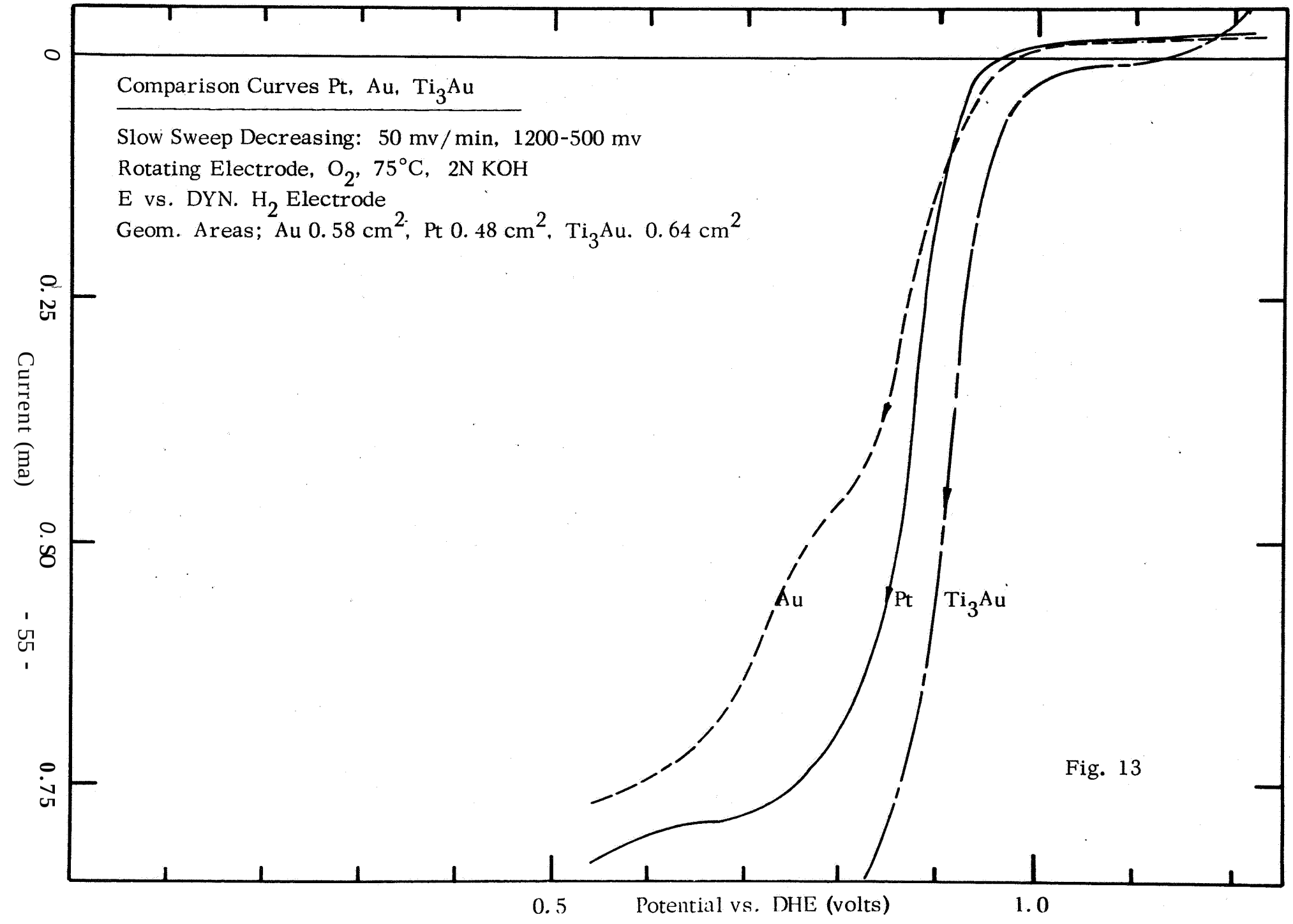
Comparison Curves Pt, Au, Ti_3Au
Slow Sweep Decreasing: 50 mv/min, 1200-500 mv
Rotating Electrode, O_2, 75°C, 2N KOH
E vs. DYN. H_2 Electrode
Geom. Areas; Au 0.58 cm^2, Pt 0.48 cm^2, Ti_3Au. 0.64 cm^2
Au
Pt
Ti_3Au
0
0.25
0.50
0.75
Current (ma)
0.5
Potential vs. DHE (volts)
1.0

Fig. 13

ratio for the coiiductivities along the a and c planes ρ_a/ρ_c was reported as 10,000:1. This fact is used to explain previous discrepancies in measured conductivities that were reported in the literature. Dorin and Tartakovskaya[12] have reported the preparation of the nonstoichiometric oxide by heating TiO_2 with Ti in an inert atmosphere at 700-1100° C. Boltaks, Veseniii, and Salunina[13] have used H_2 and CO in the presence of C as reducing agents and report material of higher conductivity from the H_2 reduction. They stress that the material prepared from CO and carbon contained no residual carbon or carbide.

Measuremeiits of conductivity as a function of composition have been made by Greener[14], Ariya and Bogdanova[15] (also as a fuiiction of temperature), Morin[16], Sawai, Terada, Okamura and Ueno[17], and Boltaks et al.[13]. The conductivity of TiO_x is greatly increased by the incorporation of WO_3 in the oxide lattice[18].

The catalytic activity of TiO_x (anatase structure) towards the oxidation of CO has been related to the defect structure by Long and Tiechiier[19] and to conductivity for oxidation processes by Mysanikov[20].

For titanium metal oxidized in 1N NaOH + 0.1N H_2O_2, Mazza, Mussoni, and Trasatti[21] describe the black (oxide) coating as 200-300 mv more noble than titanium with respect to the oxygen and peroxide reactions; the black is identified as an oxygen deficient oxide. They conclude, in general, that the black favorably influences electrodic behavior. In a further paper Mazza[22] attributes the formation of the black in the presence of H_2O_2 to the dissolution of a subvaleiit ion which subsequently forms the nonstoichiometric oxide. Dean and Hornstein[23] have related the oxygen content of TiO_x to its rest potential in solution, while a survey of the anodic behavior of TiO, Ti_2O_3, and titanium nitrides and carbides has been made by Smirnov, Ivanovskii, and Krasnov[24].

A considerable amount of information is available on the corrosion of Ti under widely varying conditions, This is best summarized in the potential-pH diagram for the Ti-H_2O system by Schmets and Pourbaix[25]. A phase diagram for the Ti-TiO_2 system has been constructed by DeVries and Roy[26].

With regard to Ti_3Au, it is interesting to note that Philipsborn and Laves[27] have described an induced $\beta \rightarrow \alpha$ phase transition (Cr_3Si or βW type to Cu_3Au type) on remelting in the presence of small amounts of oxygen, nitrogen, or carbon; the transformation is described as irreversible.

B. Experimental

The experimental work described here consists of measurements on highly dispersed Ti_3Au, pure titanium metal, and nonstoichiometric single crystals of TiO_2.

Ti_3Au powder was prepared by grinding glass brittle ingots in an agate mortar and pestle and sieving for -325 mesh particles. A porous electrode was fabricated from about 50 mg of this powder and 20% Teflon on a nickel screen. An attempt was made to operate this electrode on oxygen in the floating electrode apparatus. It was found, however, that the electrode began evolving gas immediately upon immersion in solution. The powder, initially gray-gold, turned bluish-black and expanded significantly in volume. The currents observed were only nominally larger than those of the platinum wire clamps of the electrode holder itself.

In order to obtain a more coherent electrode for electrochemical tests, some of the original Ti_3Au powder was boiled in **2N** KOH for 7 hours, at which time gas evolution ceased. A BET analysis of the resultant powder yielded 133 m^2/gm of surface area. The electrical resistance of the compressed powder was of the order of 200 KΩ. An electrode made from the material showed no gain in performance over the original electrode.

Chemical analysis of the powder for Au and Ti showed Ti 22.75% and Au 56.3% by wt. This indicates a loss of 44.5 wt % Ti, if it is assumed that there was no loss of gold. The balance of the analysis, taken to be oxygen, gives a formula $Au\ Ti_{1.65}O_{4.5}$, an oxygen content in excess of the TiO_2 stoichiometry.

For the tests performed with titanium, it was decided that a Makrides-Stern electrode configuration would be more suitable than the

"Koldmount" device used in previous tests. The cylinder of titanium was machined from (99.9%) titanium rod. Runs were made in 2N KOH at 25°C in N_2 and then O_2-saturated solution; the electrode was rotated at 600 RPM; potentials were measured vs. reversible hydrogen electrode in the same solution; H_2-charged Pd-Ag was used as the counter electrode.

For the experiments with the single crystal of TiO_2, a rutile boule was bought from the National Lead Company. Its crystallographic orientation (important because of the marked anisotropy of the conductivity) was determined using the Laue X-ray diffraction method, prior to cutting into small samples 3/8" square and 3/16" thick for testing as rotating electrodes. Two samples were prepared with the working face perpendicular to the c-axis, (001) plane, and two with the working face perpendicular to the a-axis, (010) plane. The boule as received was blue and translucent, indicating that it was in a partially reduced (nonstoichiometric) state. The first tests were carried out on the as-received crystals for which the specific resistivity was measured as 23 Ω-cm.

In view of the marked anisotropy of conductivity, it was difficult to make good electrical contact with the sample in the Koldmount rotating electrode structure. For the crystal with the working face perpendicular to the c-axis, a point or ring contact was soon demonstrated to be insufficient because of the low conductivity parallel to the plane of the contact face. The first approach was to vapor-plate gold on to the face of the crystal opposite to the working face. However, it was found that the contact point broke through the gold film on assembly, and no real reduction in contact resistance was achieved. Good contact was eventually made when the gold was protected by a conducting silver-epoxy cement. (The vapor-plated gold was retained in addition to the silver cement in order to be able to remove the epoxy cement from the crystal at the end of the experimental measurements. This is essential since the crystal is to be reduced at 800-1000°C in hydrogen[17], conditions under which decomposition of the epoxy cement would take place with possible contamination of the crystal.)

The current voltage curves obtained for the rotating electrodes of Ti and TiO_2 are interpreted in the manner described in the first section of this report (Part II C).

C. Results

The first measurements on titanium metal were made with a sweep from 1000 to 0 mv at 50 mv/min. O_2-reduction current was first observed at 400 mv. The diffusion limited current was not reached above zero mv. The corrosion current observed under nitrogen was of the order of 10-20 $\mu a/cm^2$.

In the second run (Fig. 14) the potential sweep was extended from -600 mv to +1600 mv, and the sweep rate was increased to 1 volt/min. It can be seen in this figure that the O_2 diffusion limiting current has not reached a plateau even at -300 mv. Figure 15 shows a rerun of the sweep under N_2 on a more sensitive scale. Figures 16, 17, and 18 illustrate the effects on O_2-reduction of sweeping through different potential ranges. The reaction obviously occurs on an oxide layer down to potentials of -450 mv. The hysteresis becomes greater when the sweep is extended to -600 mv (Fig. 16), but the surface may still retain some oxide. When the sweep is extended to -900 mv or held at -600 mv, O_2-reduction is apparently taking place on a clean titanium metal surface, as indicated by the large hysteresis and the exceptionally flat diffusion current plateau (Fig. 18).

The paper of Bianchi, Mazza, and Trasatti[21] asserts that in alkaline solutions of hydrogen peroxide, the "black oxide" is formed in preference to the passive oxide film. We examined the behavior of this black oxide in the potential region of O_2 reduction. The titanium electrode was exposed in the first case to 0.1 molar peroxide solution for 120 hours. The potential (vs. RHE same solution) was recorded and the change is shown in Fig. 19. The potential rise observed should indicate, according to Bianchi, et al.. that passivation rather than "black oxide" formation had occurred. The electrode when examined, was in fact a light bluish-gray rather than black. This

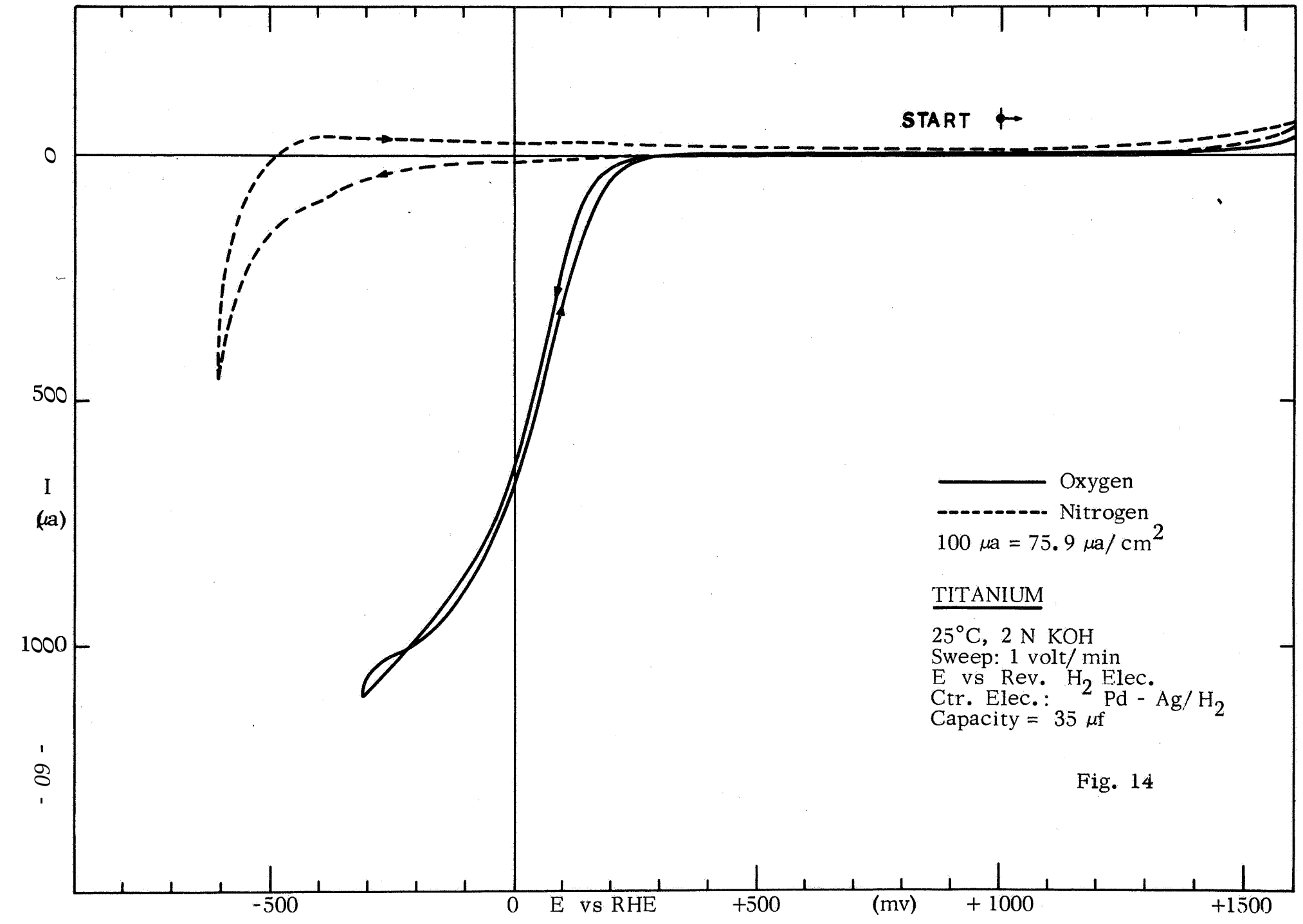
START
0
500
1000
I
(μa)
-500
0
E vs RHE
+500
(mv)
+ 1000
+1500
Oxygen
Nitrogen
100 μa = 75.9 μa/ cm2
TITANIUM
25°C, 2 N KOH
Sweep: 1 volt/ min
E vs Rev. H2 Elec.
Ctr. Elec.: Pd - Ag/ H2
Capacity = 35 μf

Fig. 14

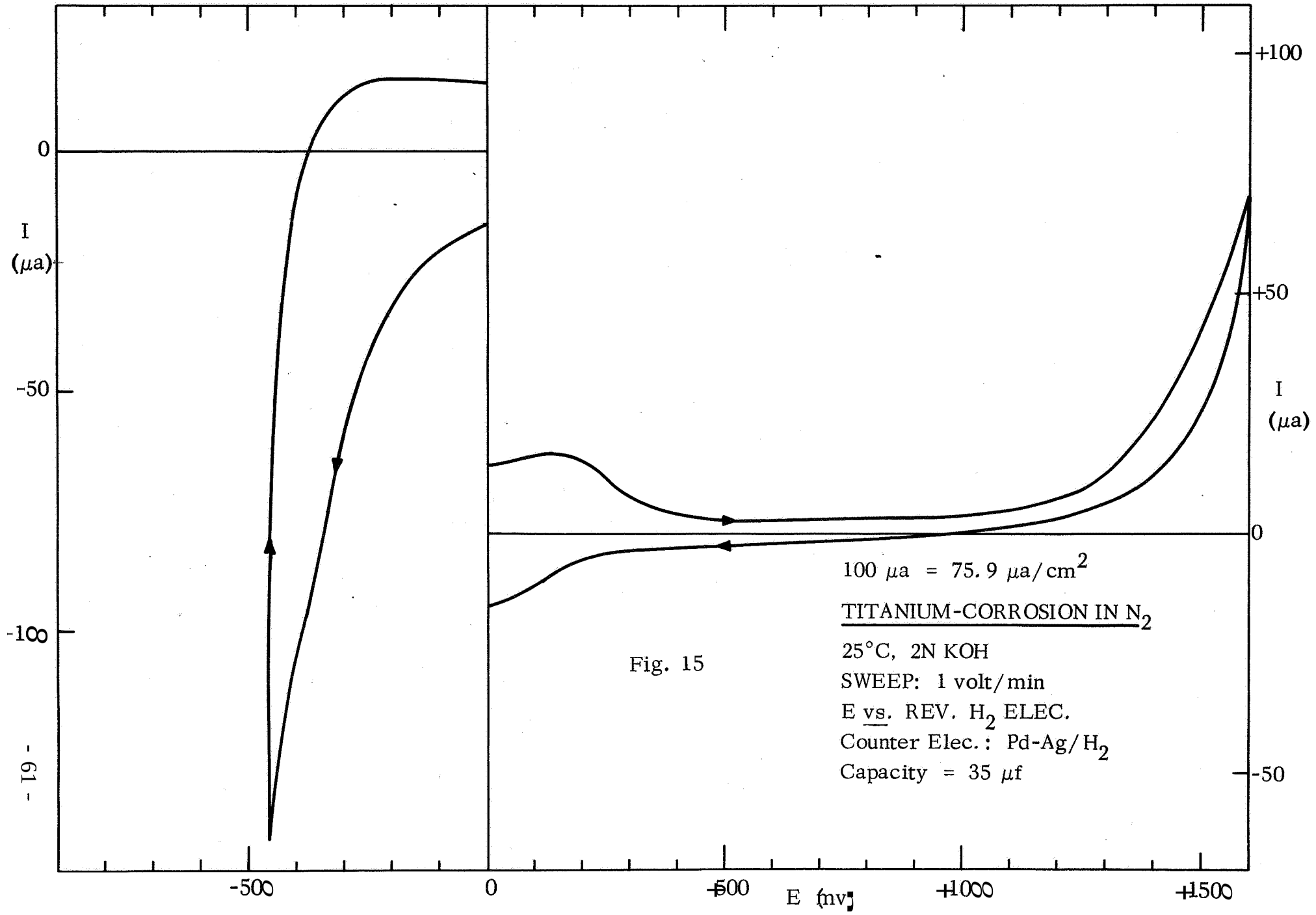

100 μa = 75.9 μa/cm^2

TITANIUM-CORROSION IN N_2

25°C, 2N KOH
SWEEP: 1 volt/min
E vs. REV. H_2 ELEC.
Counter Elec.: Pd-Ag/H_2
Capacity = 35 μf

Fig. 15

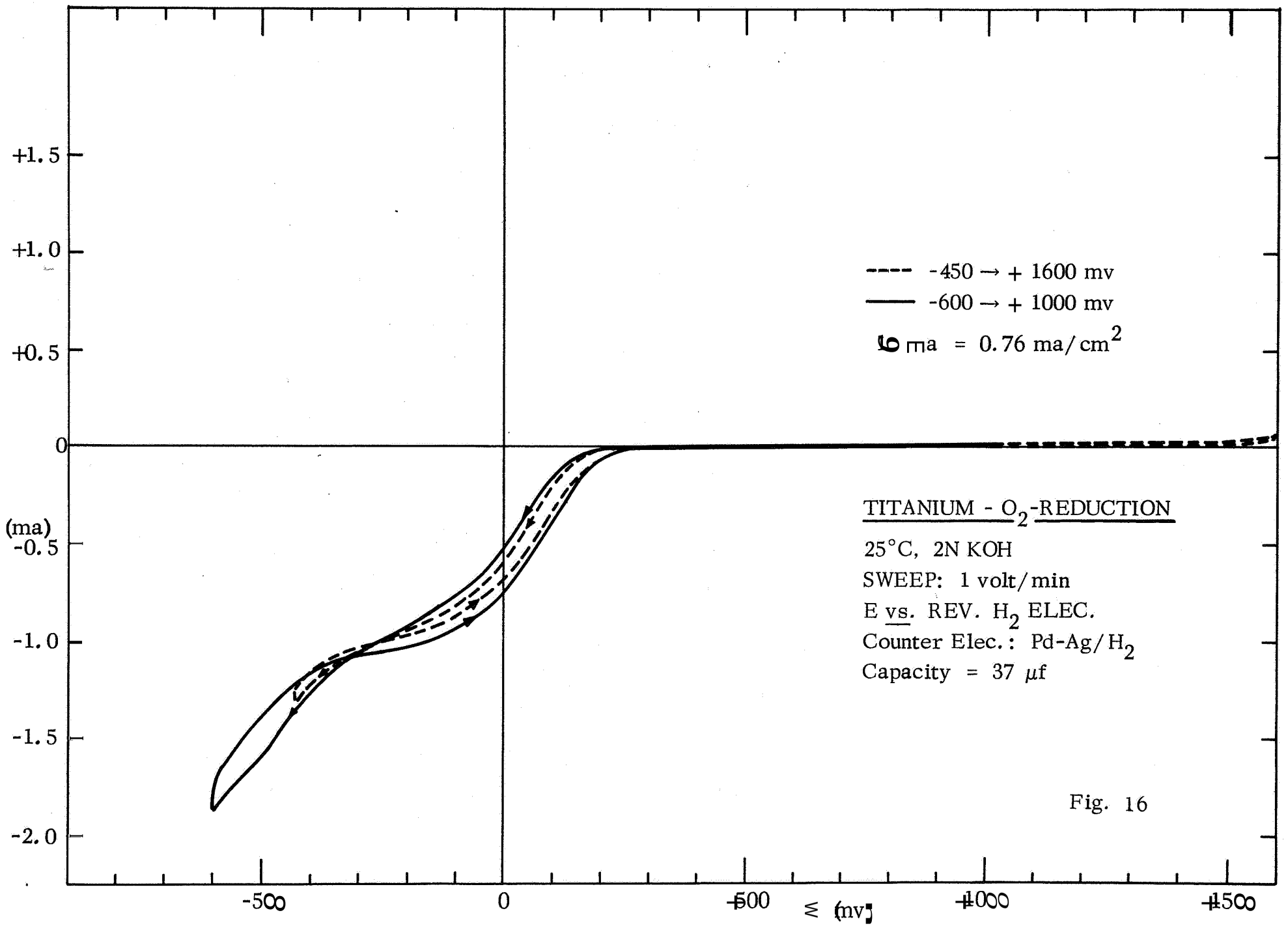
+1.5
+1.0
+0.5
0
-0.5
-1.0
-1.5
-2.0
(ma)
-500
0
+500
+1000
+1500
E (mv)
---- -450 → + 1600 mv
—— -600 → + 1000 mv
6 ma = 0.76 ma/cm²
TITANIUM - O2-REDUCTION
25°C, 2N KOH
SWEEP: 1 volt/min
E vs. REV. H2 ELEC.
Counter Elec.: Pd-Ag/H2
Capacity = 37 μf

Fig. 16

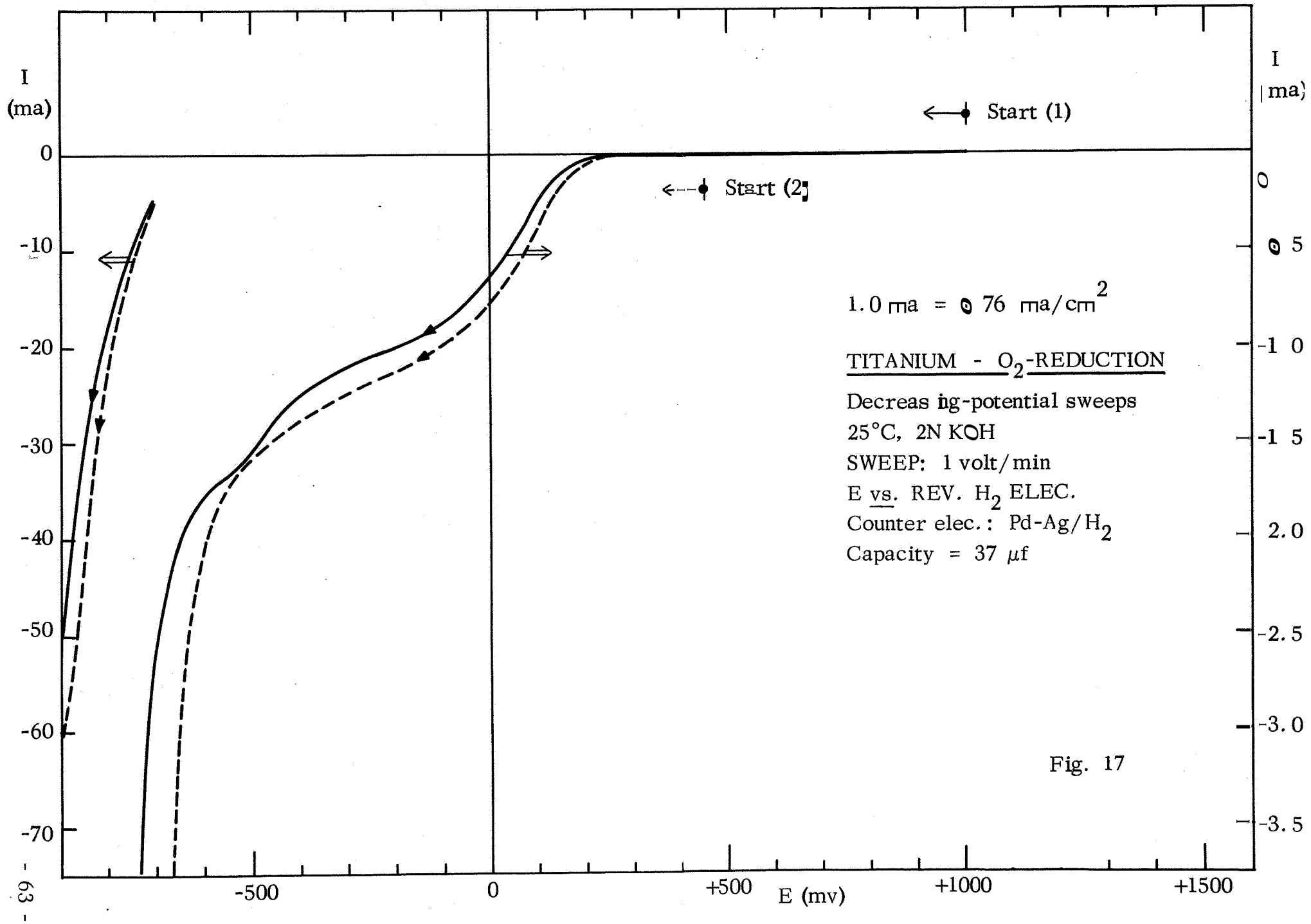
I (ma)
0
-10
-20
-30
-40
-50
-60
-70
-500
0
+500
E (mv)
+1000
+1500
I (ma)
0
0 5
-1 0
-1 5
2.0
-2.5
-3.0
-3.5
Start (1)
Start (2)
1.0 ma = 0 76 ma/cm2
TITANIUM - O2-REDUCTION
Decreas ing-potential sweeps
25°C, 2N KOH
SWEEP: 1 volt/min
E vs. REV. H2 ELEC.
Counter elec.: Pd-Ag/H2
Capacity = 37 μf

Fig. 17

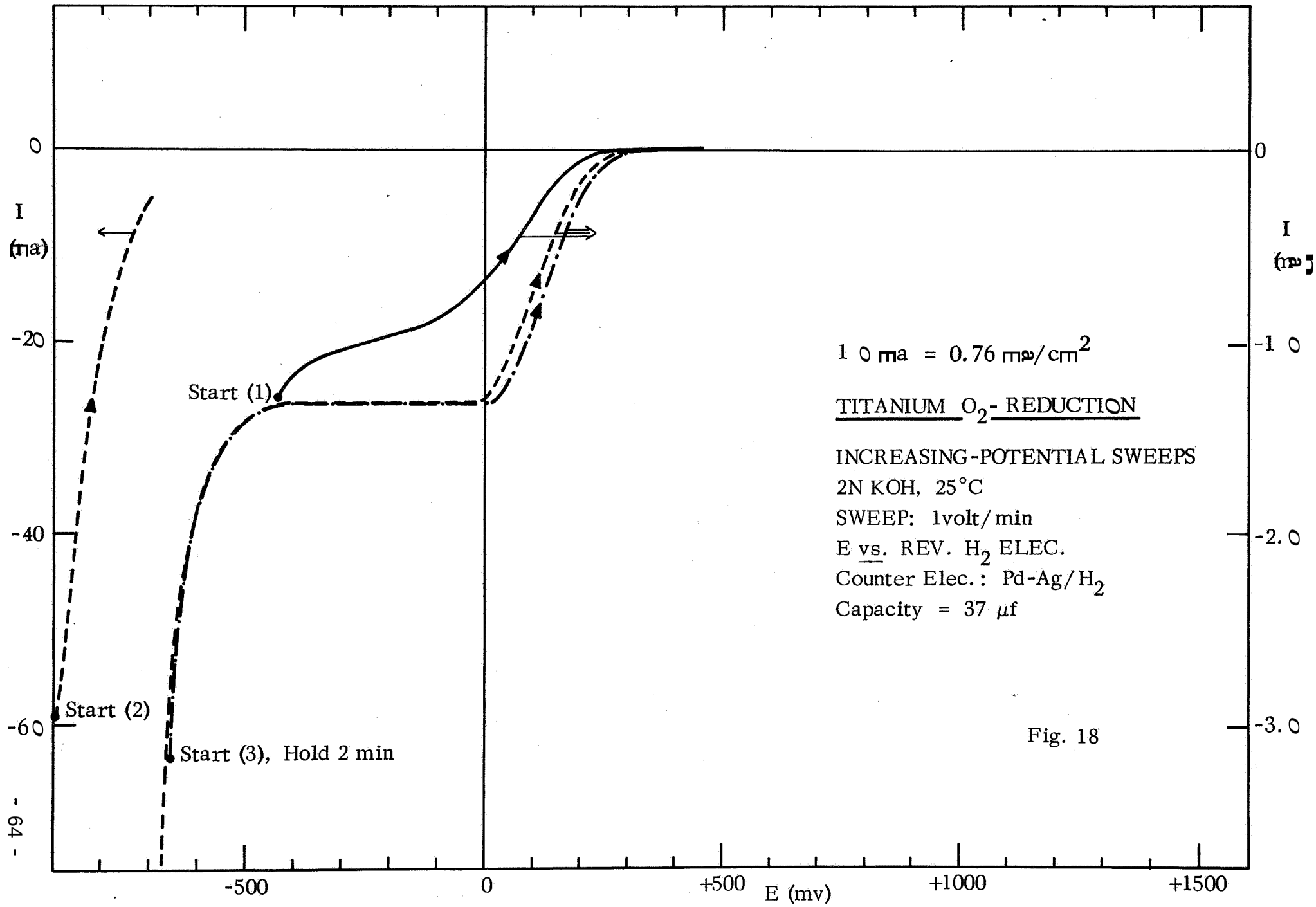
0
-20
-40
-60
I (ma)
0
-10
-20
-30
I (ma)
Start (1)
Start (2)
Start (3), Hold 2 min
-500
0
+500
+1000
+1500
E (mv)
10 ma = 0.76 ma/cm2
TITANIUM O2- REDUCTION
INCREASING-POTENTIAL SWEEPS
2N KOH, 25°C
SWEEP: 1volt/min
E vs. REV. H2 ELEC.
Counter Elec.: Pd-Ag/H2
Capacity = 37 μf

Fig. 18

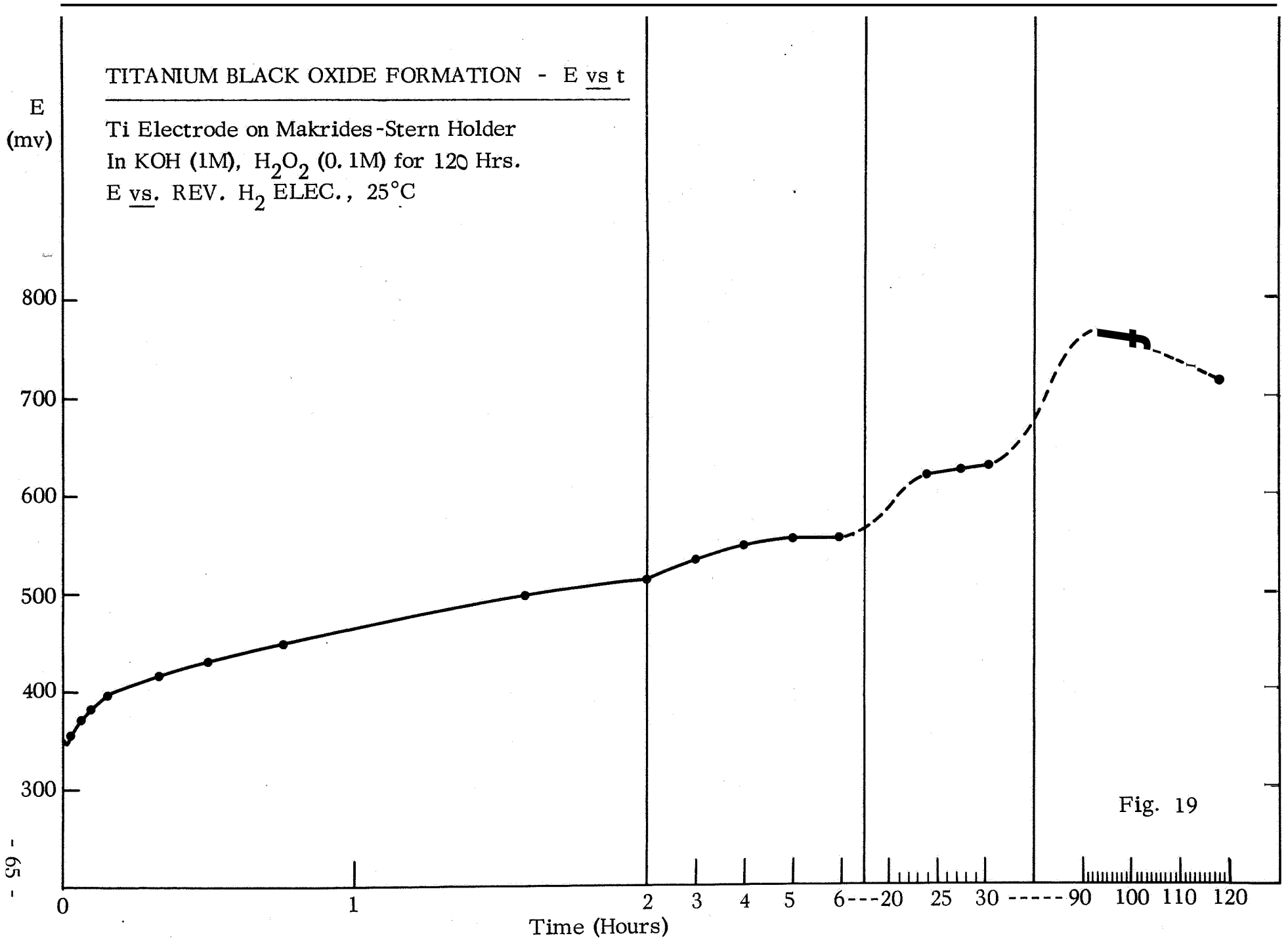
TITANIUM BLACK OXIDE FORMATION - E vs t
Ti Electrode on Makrides-Stern Holder
In KOH (1M), H_2O_2 (0.1M) for 120 Hrs.
E vs. REV. H_2 ELEC., 25°C
E
(mv)
800
700
600
500
400
300
0
1
2
3
4
5
6---20
25
30 -----90
100
110
120
Time (Hours)

Fig. 19

electrode was then tested for O_2-reduction activity; the results compared with smooth titanium are shown in Fig. 20. The potential at which O_2-reduction occurs is shifted to more positive values, $E_{\frac{1}{2}}$ by about 70 mv and E_1 by about 200 mv. The double layer capacity increases by a factor of approximately two. An extended potential sweep is shown in Fig. 21 for comparison with Fig. 20.

In a subsequent experiment the peroxide concentration was increased to 1M. An attempt was made to follow the potential change, but measurements could not be made either because of peroxide contamination of the reference electrode or because of hydrogen leakage. The electrode was left in solution for 20 hours and then tested for O_2-reduction activity. It had a heavy, adherent black film on its surface. The results are shown in Fig. 22 in comparison again to smooth titanium. The shift in potential for O_2-reduction was ~ 200 mv more positive, the double layer capacity increased by a factor of 25.

Titanium powder was exposed to 2N KOH at 100°C for five hours and then allowed to cool in the solution for ~ 15 hours. These are the conditioiis under which Ti_3Au formed a nonconductive (200,000 ohms), black powder, as reported above. The bluish-black powder obtained from titanium presently has a resistance of ~ 50 ohms. This material was made into a Teflon-bonded electrode and operated as a floating electrode in 35% KOH at 75°C. Activity for O_2-reduction was not discernible, the behavior being similar to that of the black Ti_3Au. A second sample of titanium powder was exposed to the same solution (1. OM KOH, 1. OM H_2O_2) for 120 hours. A light bluish-black powder was obtained and was tested as a PTFE bonded electrode in 35% KOH at 75°C; again there was no measurable activity.

The current voltage curves measured on single crystals of TiO_2 are shown in Figs. 23 and 24. Measurements were made on both the "a" and "c" crystals in the "as-received" condition. As described above the as-received crystal was slightly oxygen deficient but from the electrochemical behavior the stoichiometry was not far removed from TiO_2.

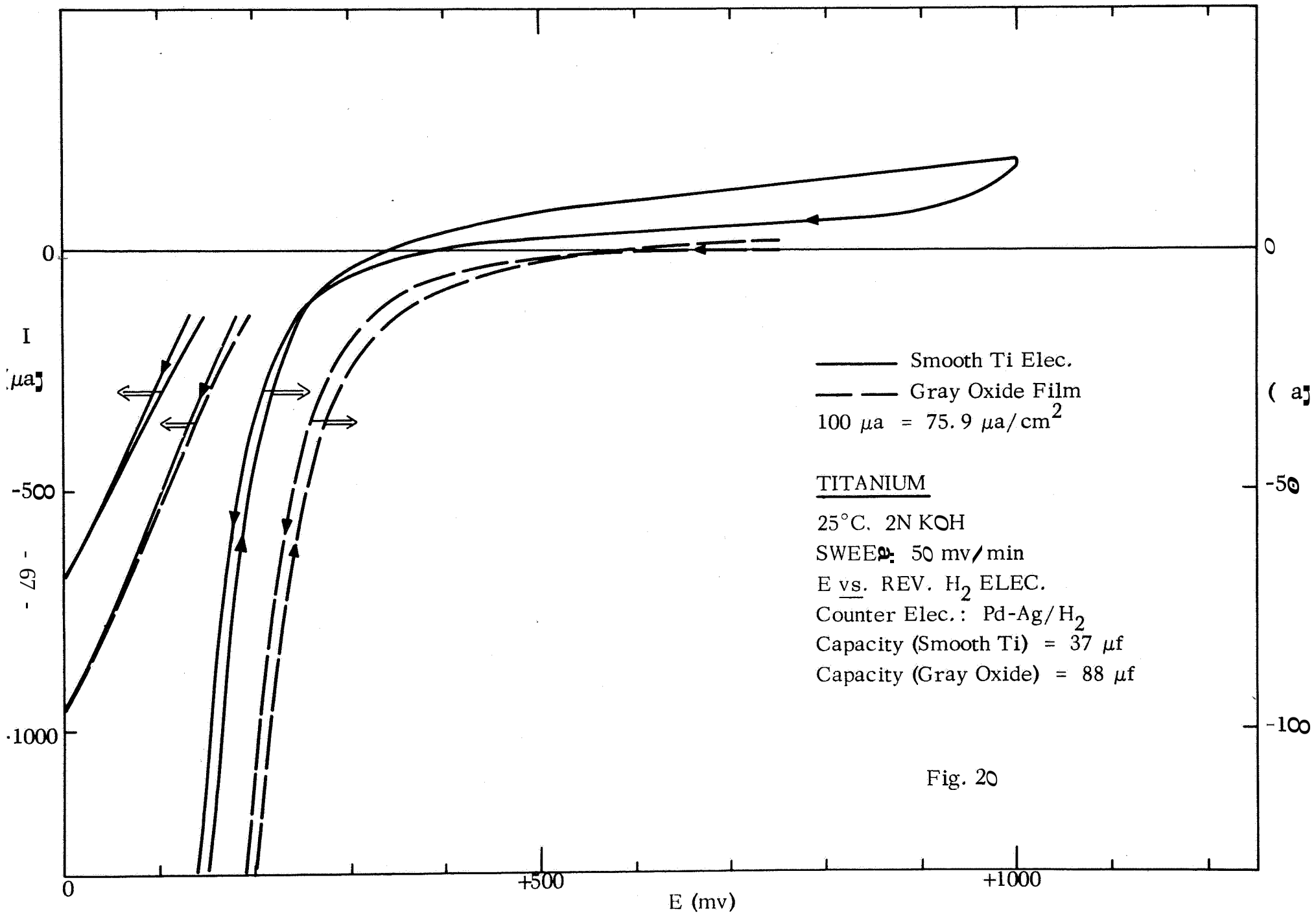
0
-500
-1000
I
(μa)
- 67 -
0
+500
+1000
E (mv)
0
-50
-100
(a
Smooth Ti Elec.
Gray Oxide Film
100 μa = 75.9 μa/cm²
TITANIUM
25°C. 2N KOH
SWEEP: 50 mv/min
E vs. REV. H2 ELEC.
Counter Elec.: Pd-Ag/H2
Capacity (Smooth Ti) = 37 μf
Capacity (Gray Oxide) = 88 μf

Fig. 20

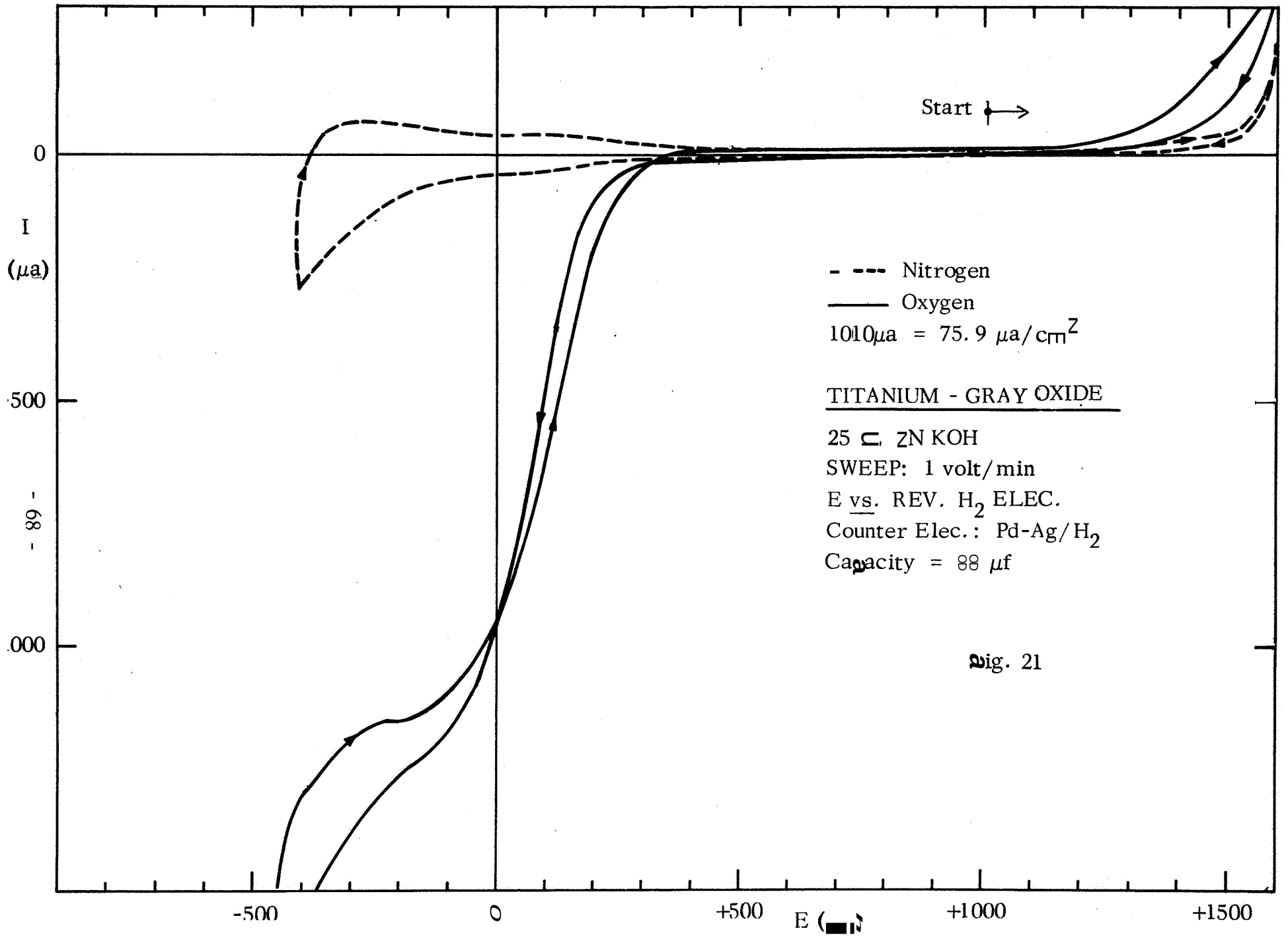
Start
0
I
(μa)
500
- 89 -
000
- - - Nitrogen
—— Oxygen
1010μa = 75.9 μa/cm²
TITANIUM - GRAY OXIDE
25 ⊏ ZN KOH
SWEEP: 1 volt/min
E vs. REV. H2 ELEC.
Counter Elec.: Pd-Ag/H2
Capacity = 88 μf
-500
0
+500
+1000
+1500

Fig. 21

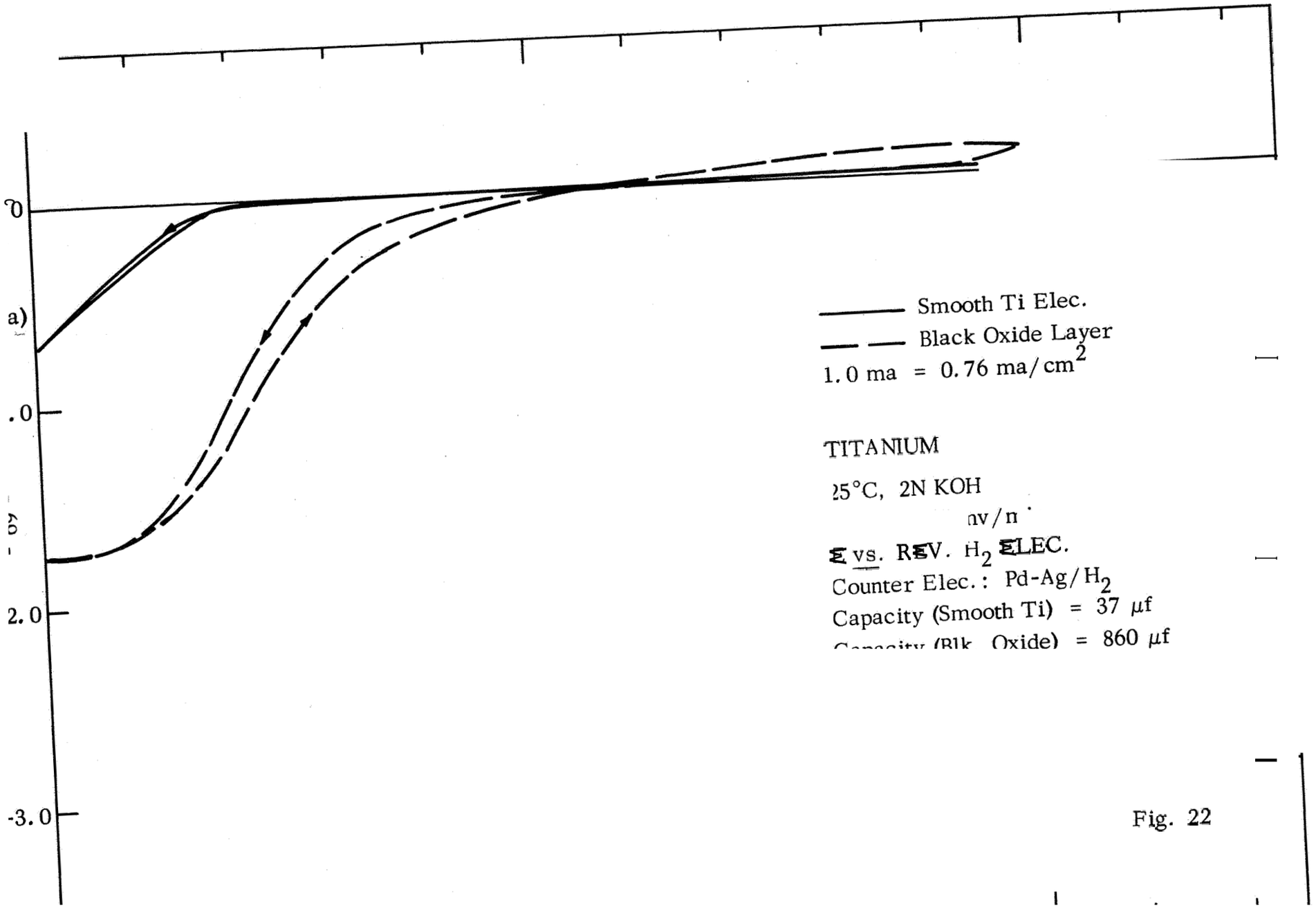
0
a)
.0
2.0
-3.0
+500
E (mv)
0
+1000
Smooth Ti Elec.
Black Oxide Layer
1.0 ma = 0.76 ma/cm²
TITANIUM
25°C, 2N KOH
mv/m
E vs. REV. H2 ELEC.
Counter Elec.: Pd-Ag/H2
Capacity (Smooth Ti) = 37 μf
Capacity (Blk Oxide) = 860 μf

Fig. 22

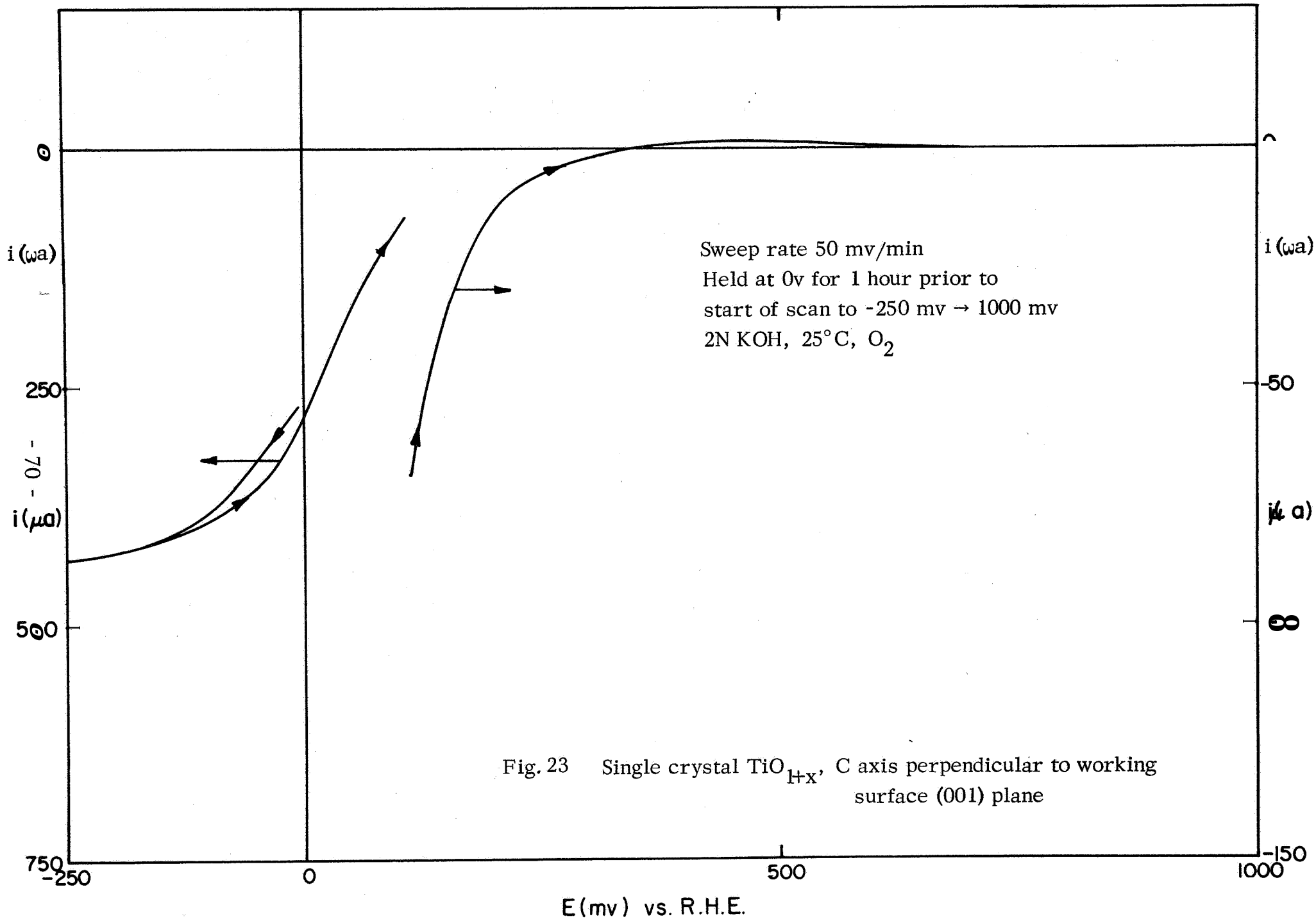

Fig. 23 Single crystal TiO_{H+x}, C axis perpendicular to working surface (001) plane

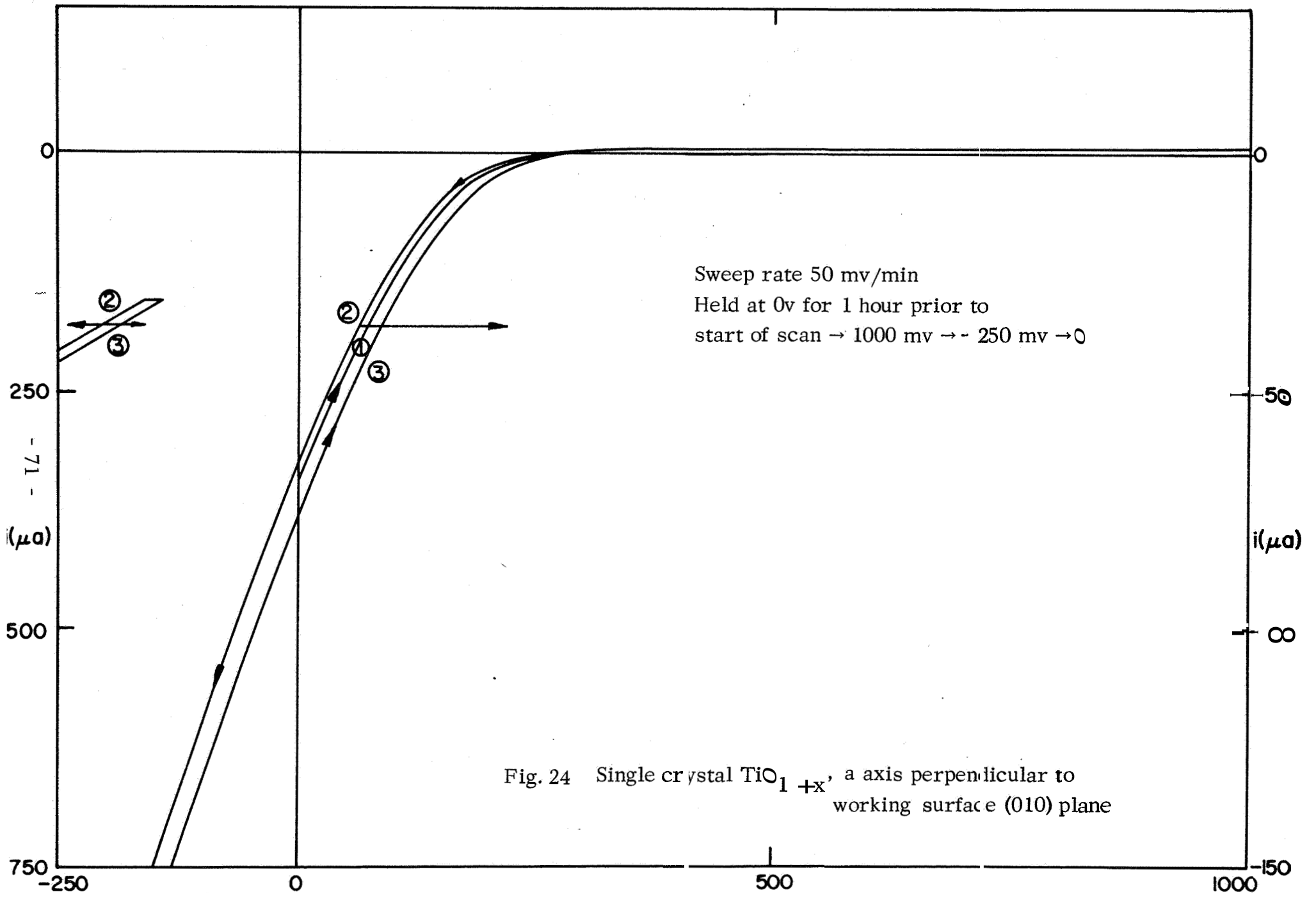

Fig. 24 Single crystal TiO_{1+x}, a axis perpendicular to working surface (010) plane

Interesting differences are already apparent between the two crystallographic orientations. The potential at which a reduction current is first discernible (E_i) is 100 mv greater for the c-axis crystal (at 375 mv vs. RHE) than for the a-axis crystal. The effect of the difference in conductivity can be seen in the less rapid increase of current with potential for the a-axis crystal below 275 mv.

The two samples were retested after reduction in H_2 at 1000°C for 3 hours. The temperature for this process was increased from room temperature to 1000°C in three hours. The cooling time was 15 hours; (these times were necessary to prevent thermal cracking).

The results for the a-axis crystals are given in Figs. 25 to 30; the initial and final runs were at 50 mv/min; the other measurements to test the effects of prepolarization were carried out at 1000 mv/min.

The resistance of this crystal (measured with a resistance meter across the electrode configuration) was about 50 ohms, which is considerably less than the original sample. The reduced sample shows an increase in activity over the original crystal. The initial cathodic current is observed in the present case at 550 mv, compared with 375 mv observed previously (Fig. **23).** The sample was subsequently swept through different potential ranges in a manner similar to the measurements made on pure titanium to check the effect of prepolarization. The results are essentially the same with one significant exception: Sweeping to -600 mv on pure titanium produces a clean metal surface and a flat diffusion current plateau on the return sweep. This was never observed on the titanium dioxide crystal.

Finally, a slow sweep was rerun at the end of this series, starting at the open circuit potential and going to 1000 mv before sweeping back to 0.0 mv (Fig. 30). The initial potential at which cathodic current is seen occurs at a higher potential, ~ 750 mv, than that at which cathodic current occurs initially, ~ 550 mv (Fig. **25).**

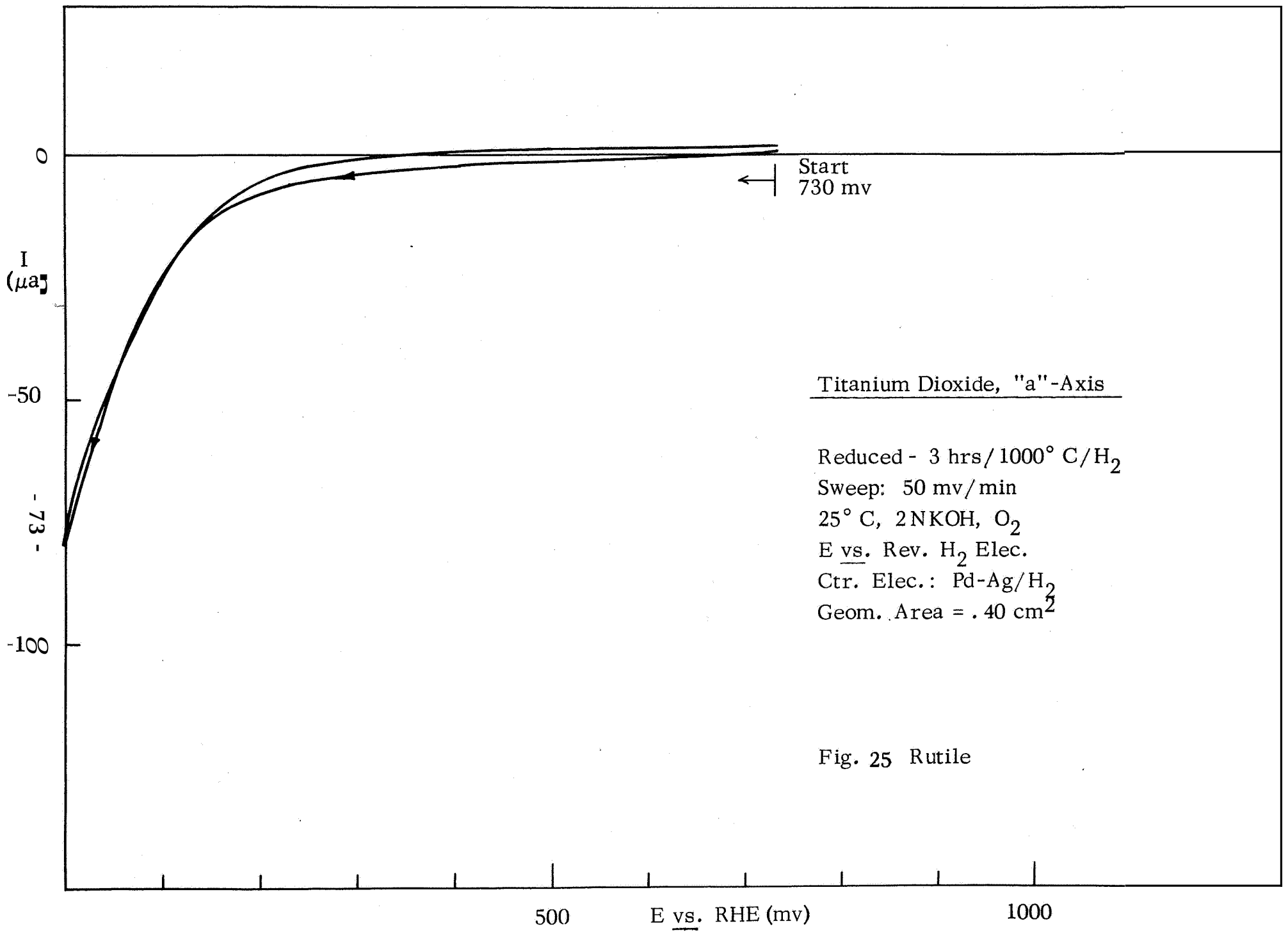

Titanium Dioxide, "a"-Axis

Reduced - 3 hrs/1000° C/H_2
Sweep: 50 mv/min
25° C, 2NKOH, O_2
E vs. Rev. H_2 Elec.
Ctr. Elec.: Pd-Ag/H_2
Geom. Area = .40 cm^2

Fig. 25 Rutile

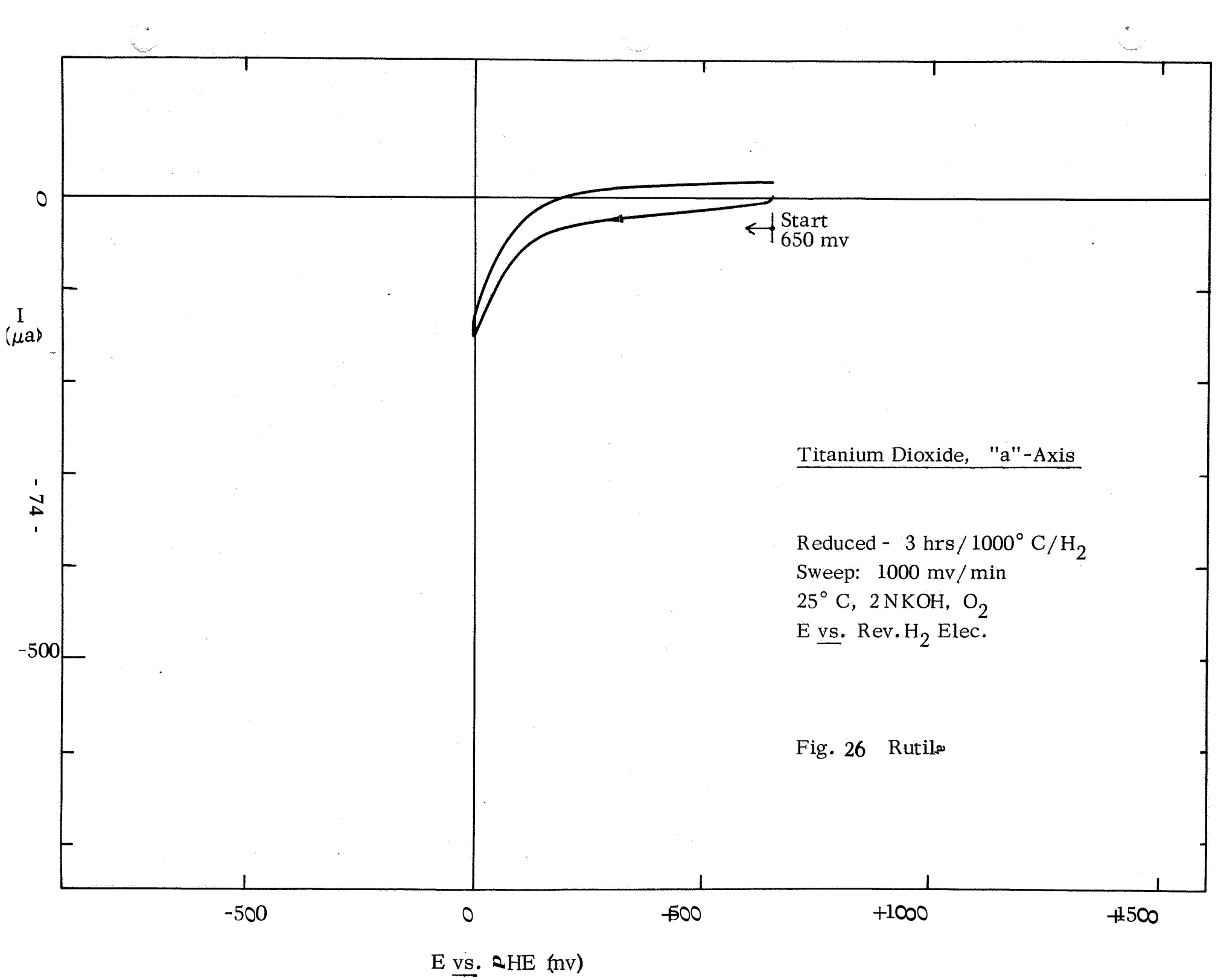

Fig. 26 Rutile

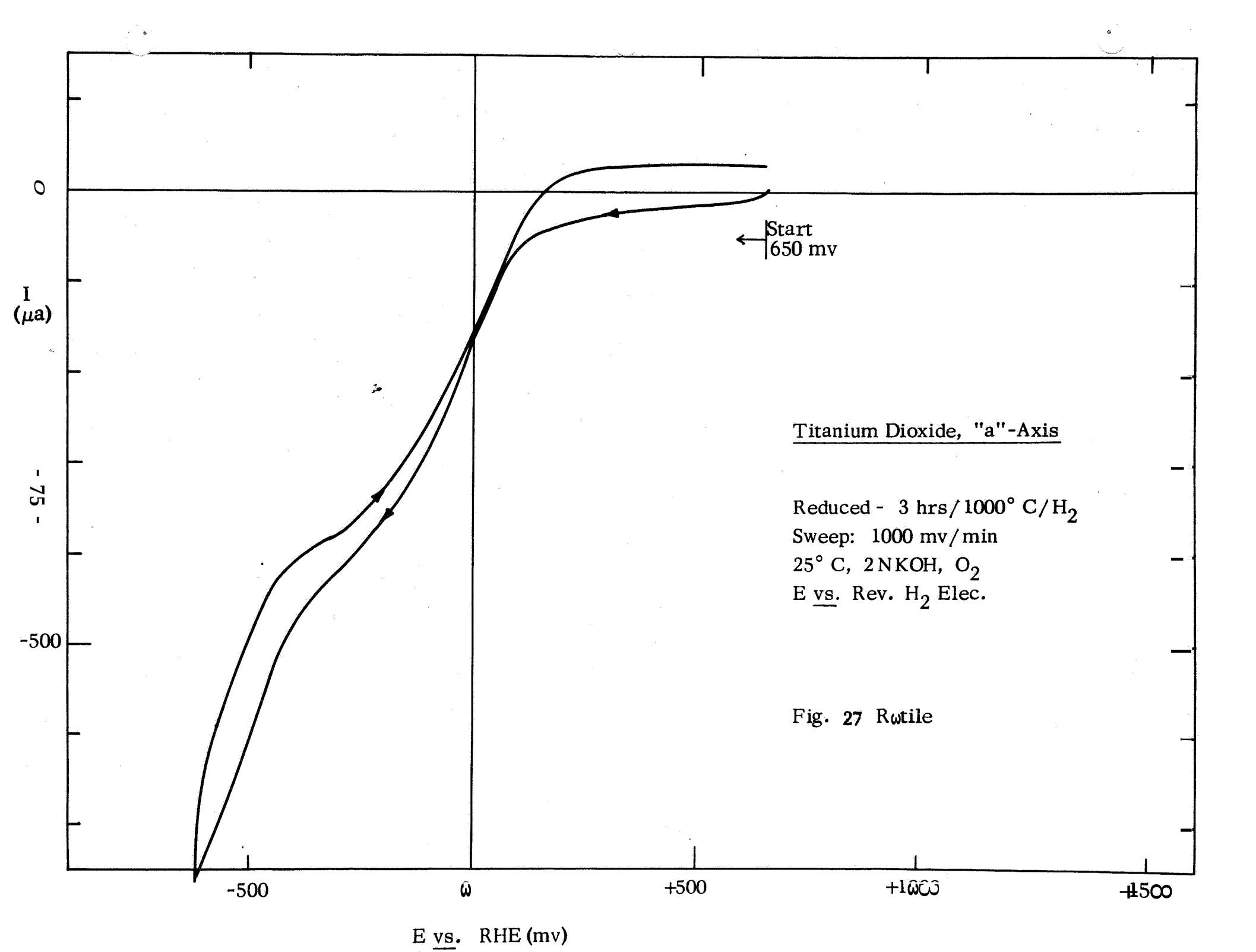

Fig. 27 Rutile

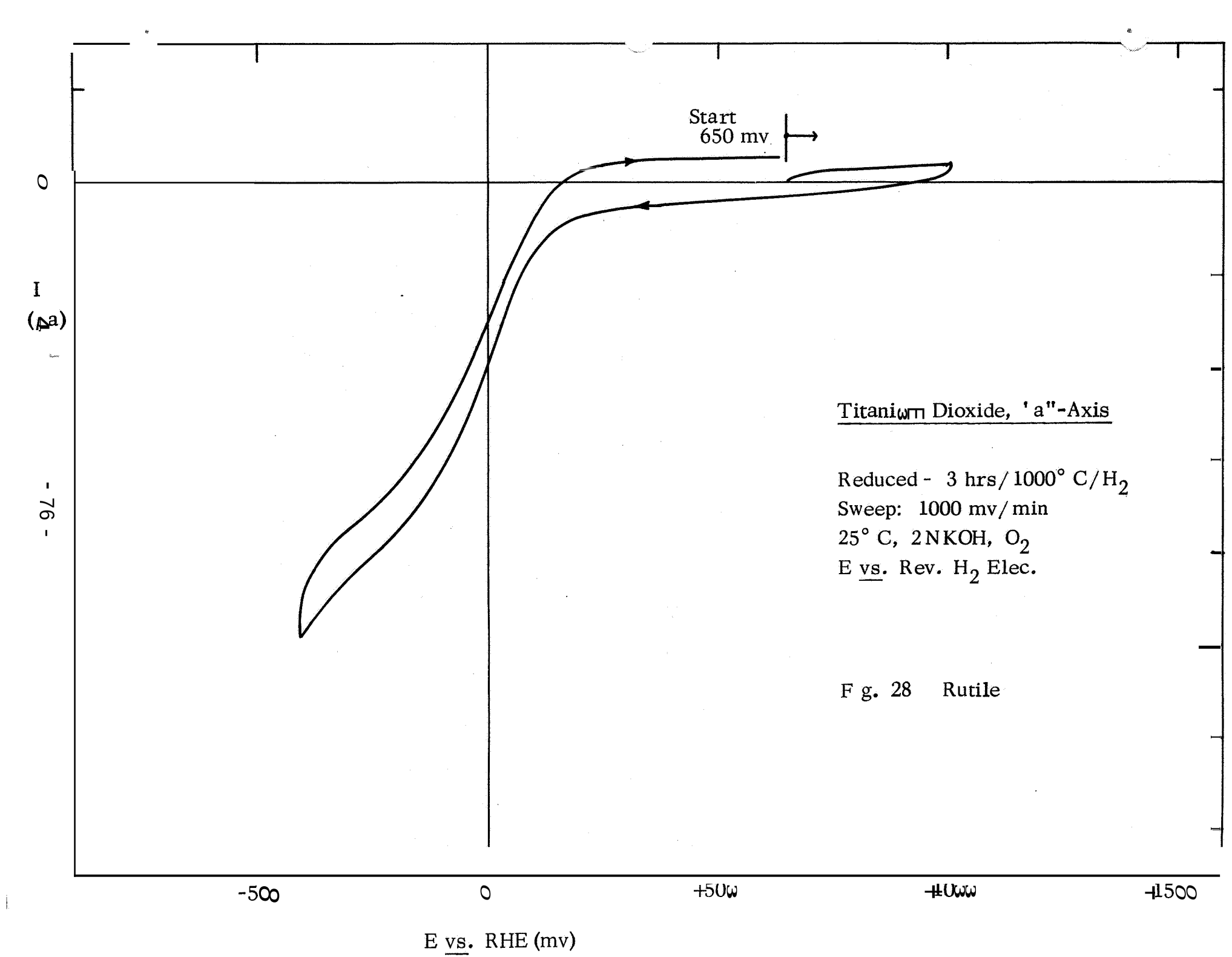
Start
650 mv
0
I
(a)
- 76 -
Titaniωm Dioxide, 'a"-Axis
Reduced - 3 hrs/1000° C/H_2
Sweep: 1000 mv/min
25° C, 2NKOH, O_2
E vs. Rev. H_2 Elec.
-500
0
+500
+1000
+1500
E vs. RHE (mv)

F g. 28 Rutile

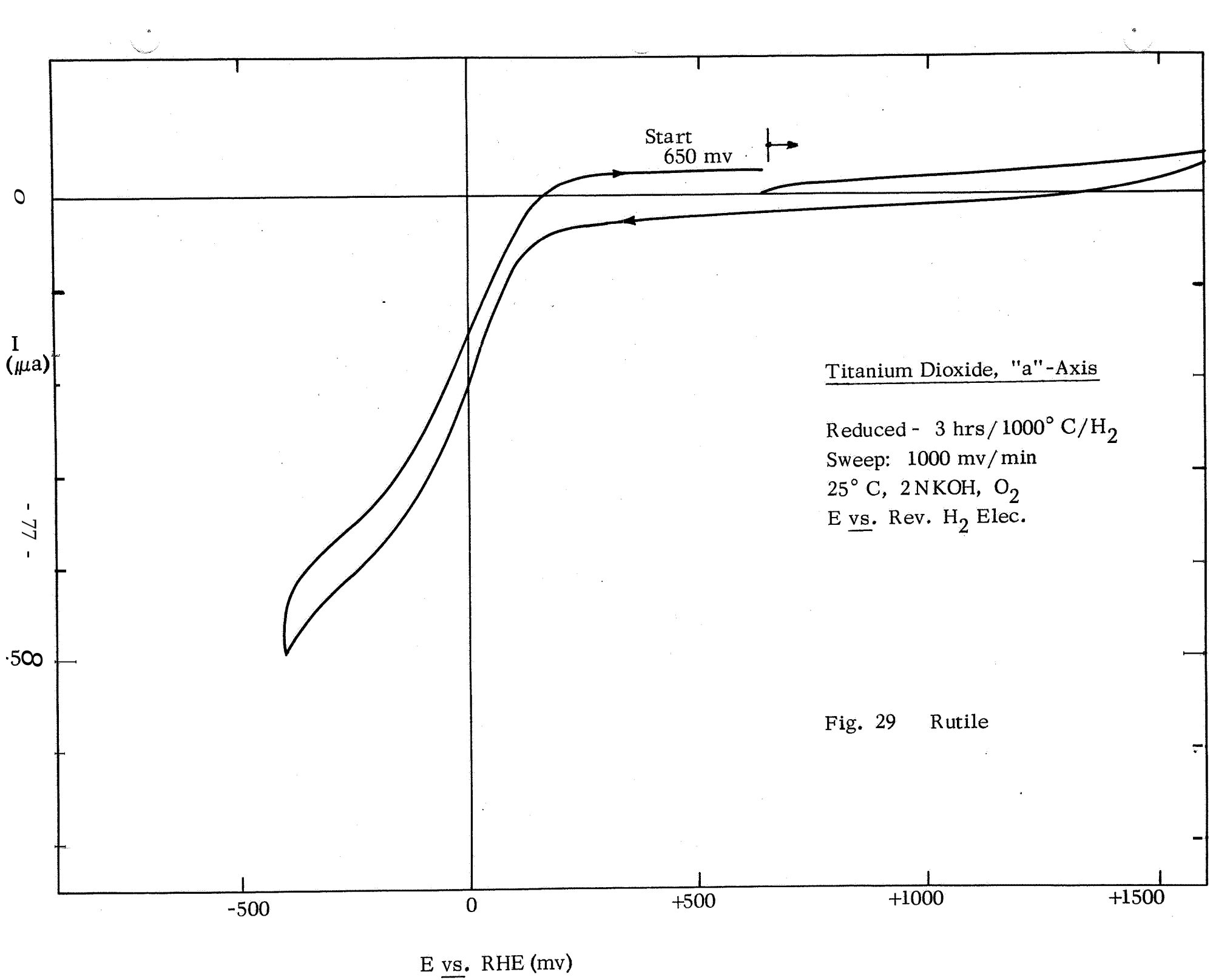

Fig. 29 Rutile

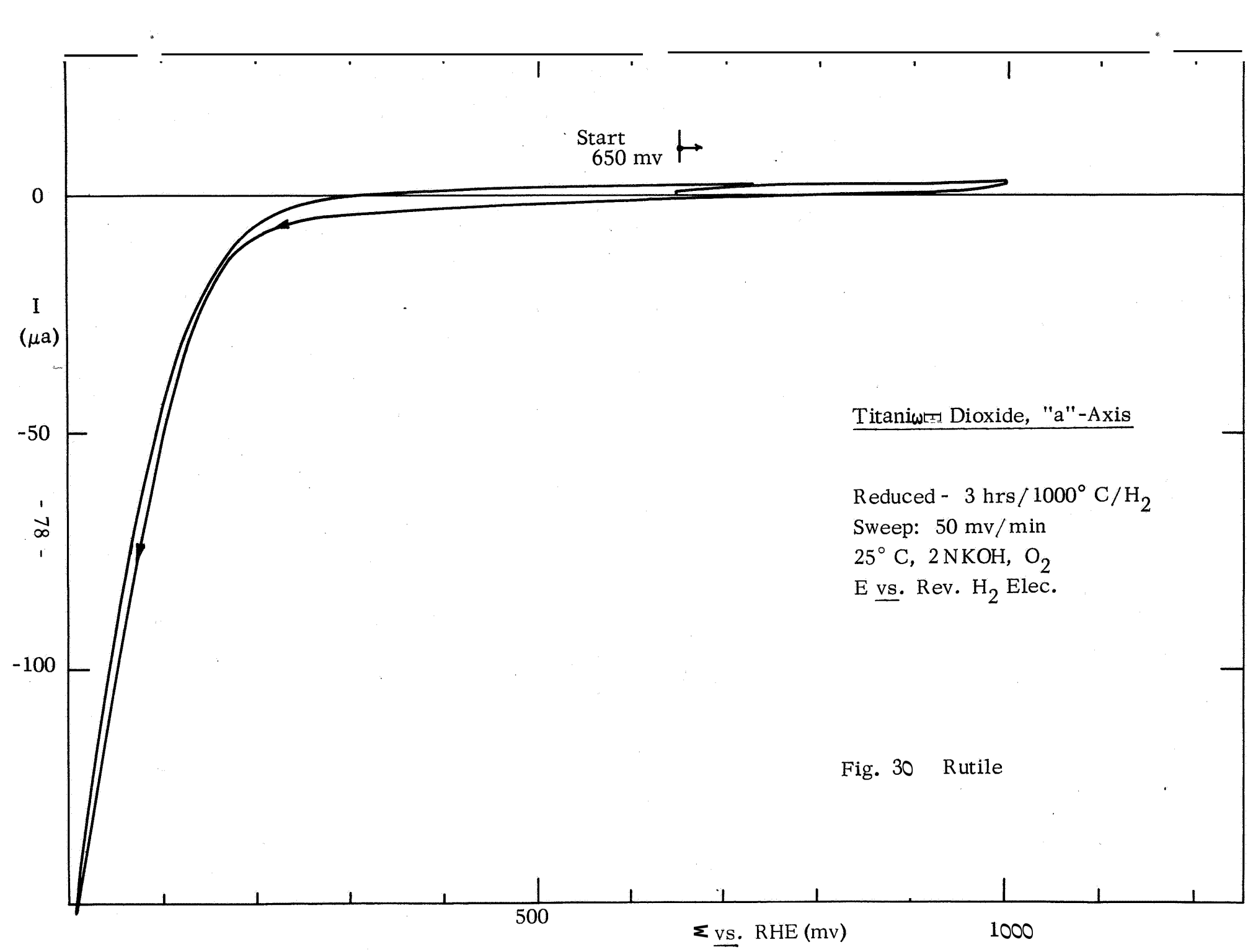

Fig. 30 Rutile

Similar measurements were made with the c-axis crystal; these are shown in Figs. 31 to 36. Cathodic current on these crystals is first observed at 850 mv, i. e. approximately 100 mv more positive than in the a-axis crystal. Prepolarization of the electrode in anodic and cathodic directions has no discernible effect.

D. Discussion

The essential points to come out of the measurements on the single crystals of TiO_2 are that the reduced form (particularly the c-axis crystals) does support a cathodic current corresponding to reduction of oxygen at potentials > 500 mv and is stable (i. e. does not revert to TiO_2 stoichiometry during the time interval of the experiments in the potential range of interest (600-1200 mv). This latter point is well demonstrated by the fact that prepolarization to both cathodic and anodic potentials beyond this range has no effect on the current voltage characteristics. The anodic (and cathodic) currents noted in the potential range 300 to 1000+ mv with the fast sweep method can be attributed to the double layer charging current, both from the dependence on the direction of the sweep and the fact that the current decays rapidly when the sweep is stopped or the sweep rate reduced (c. f. 50 mv/min sweep). The magnitude of this charging current indicates a significant roughness factor for these crystals.

The behavior of the black oxide on titanium and the nonstoichiometric TiO_2 is quite similar and that even if the absolute activities are low considerable increases can be obtained by modification of stoichiometry.

Sufficient electronic conductivity exists in the oxide to sustain relatively high rates of O_2 reduction on single crystal surfaces and on thin films on the metal surface when the total amount is small. However, this conductivity is not high enough to provide the current paths for the high currents to be expected in the finely divided form in PTFE bonded electrodes. This would account for the inactivity of the finely divided Ti_3Au electrode.

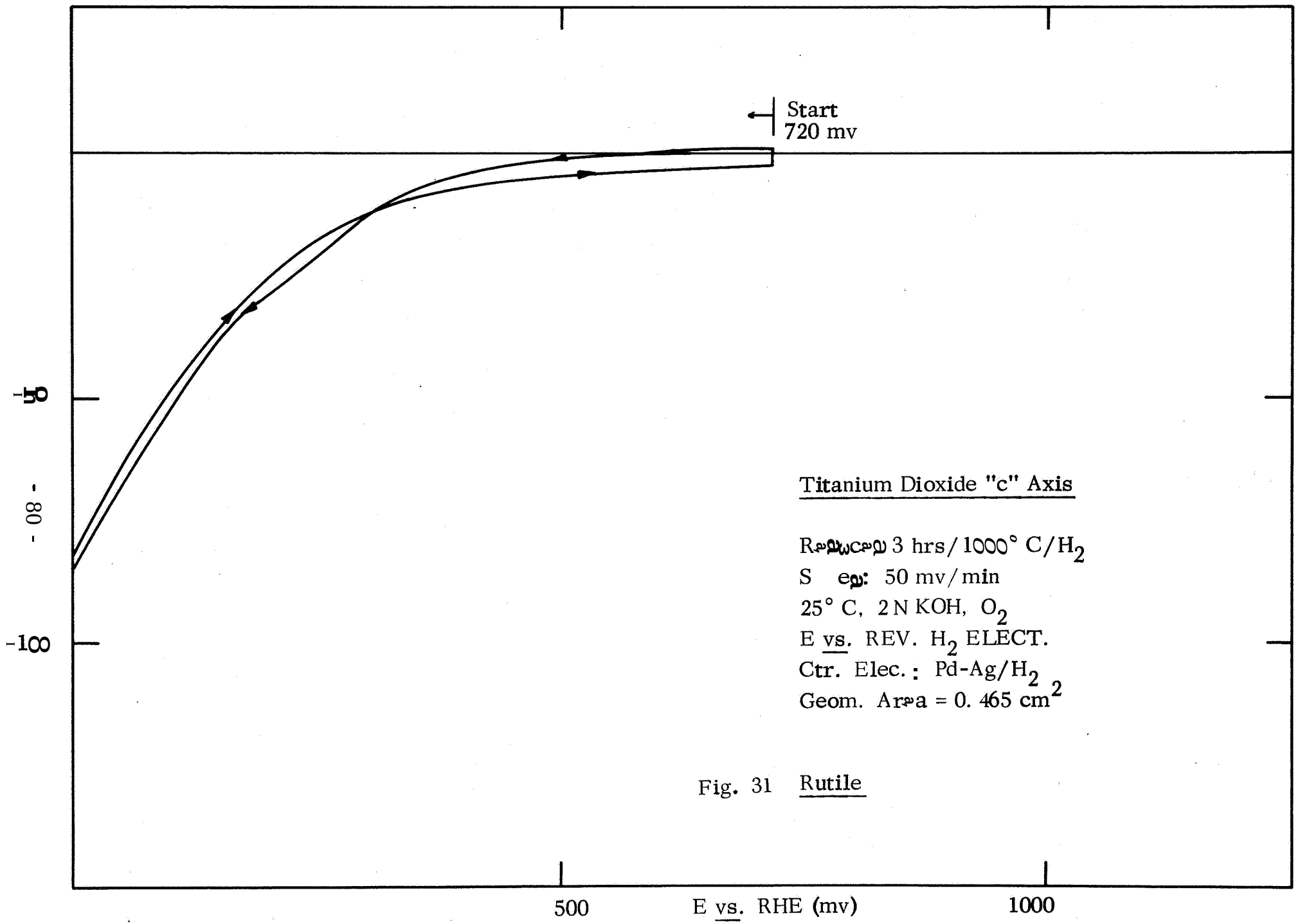

Fig. 31 Rutile

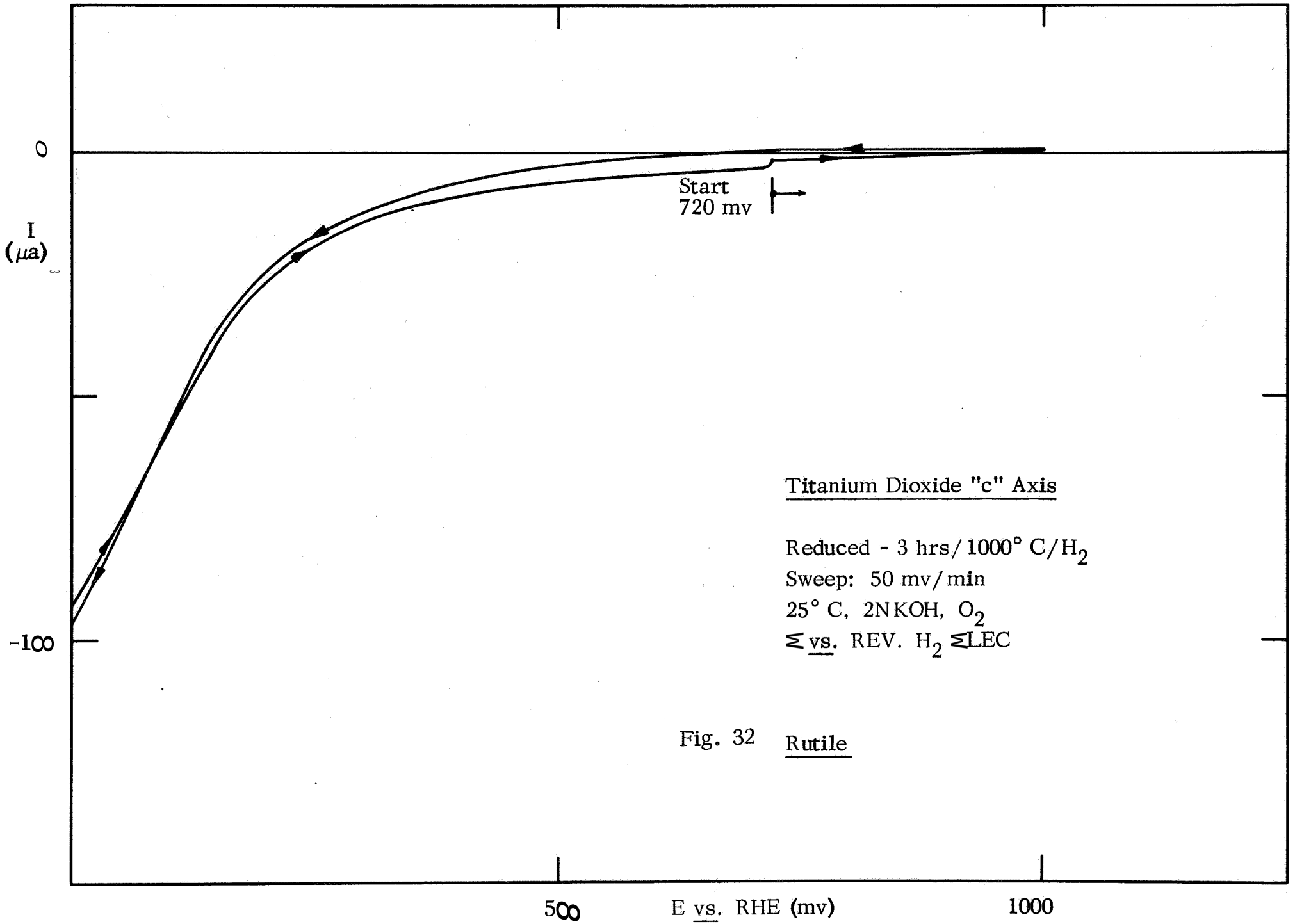

Fig. 32 Rutile

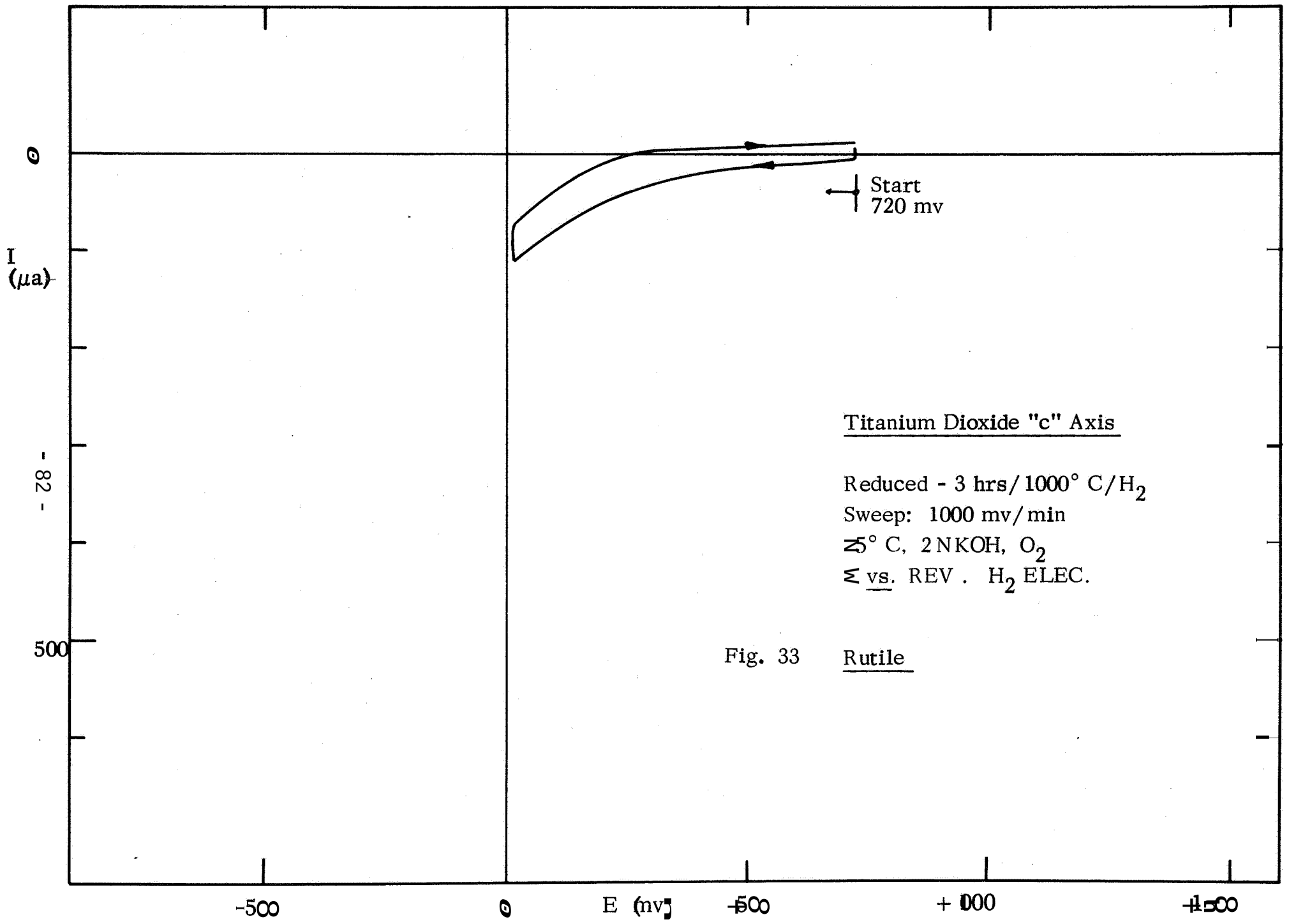

Fig. 33 Rutile

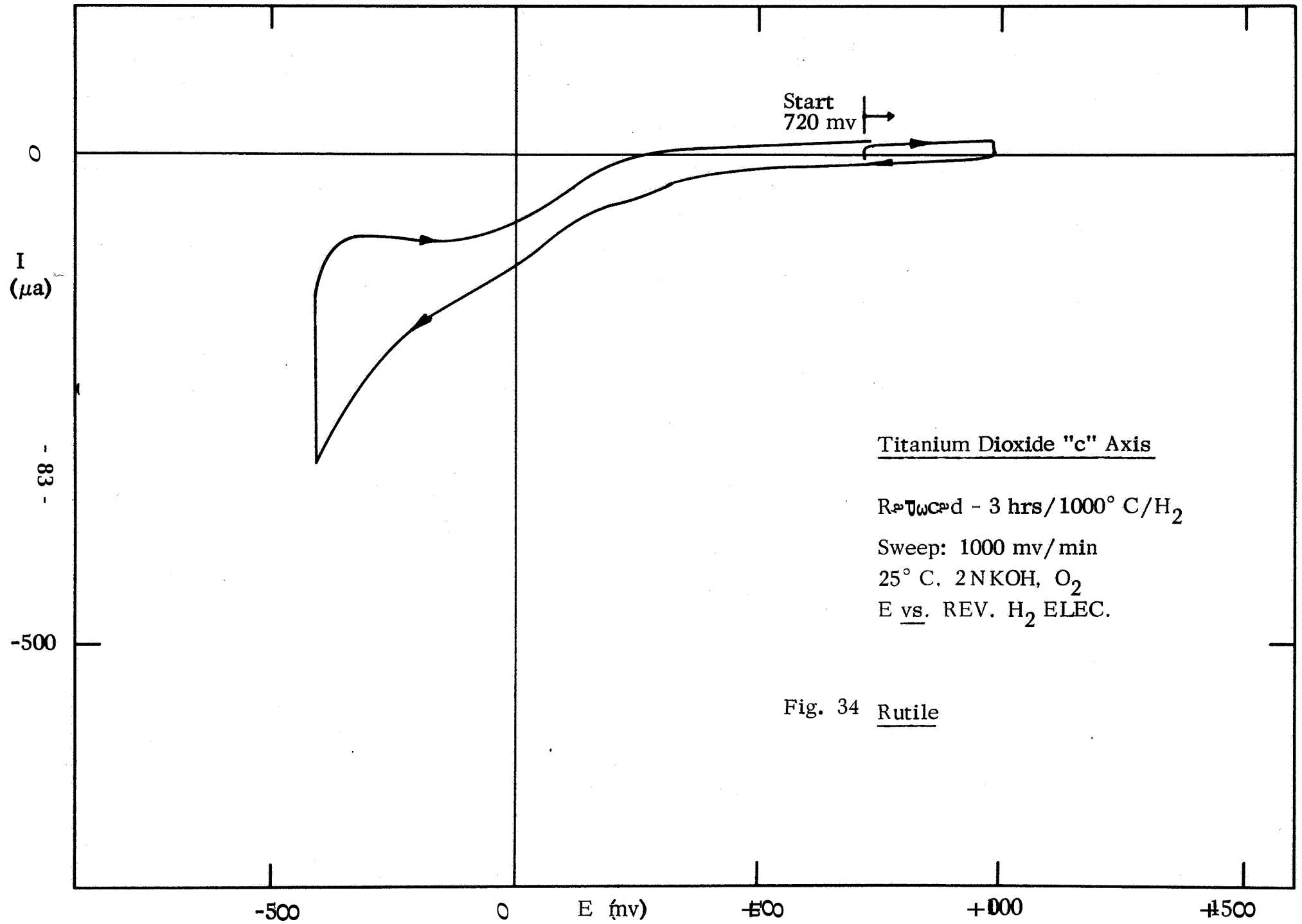

Fig. 34 Rutile

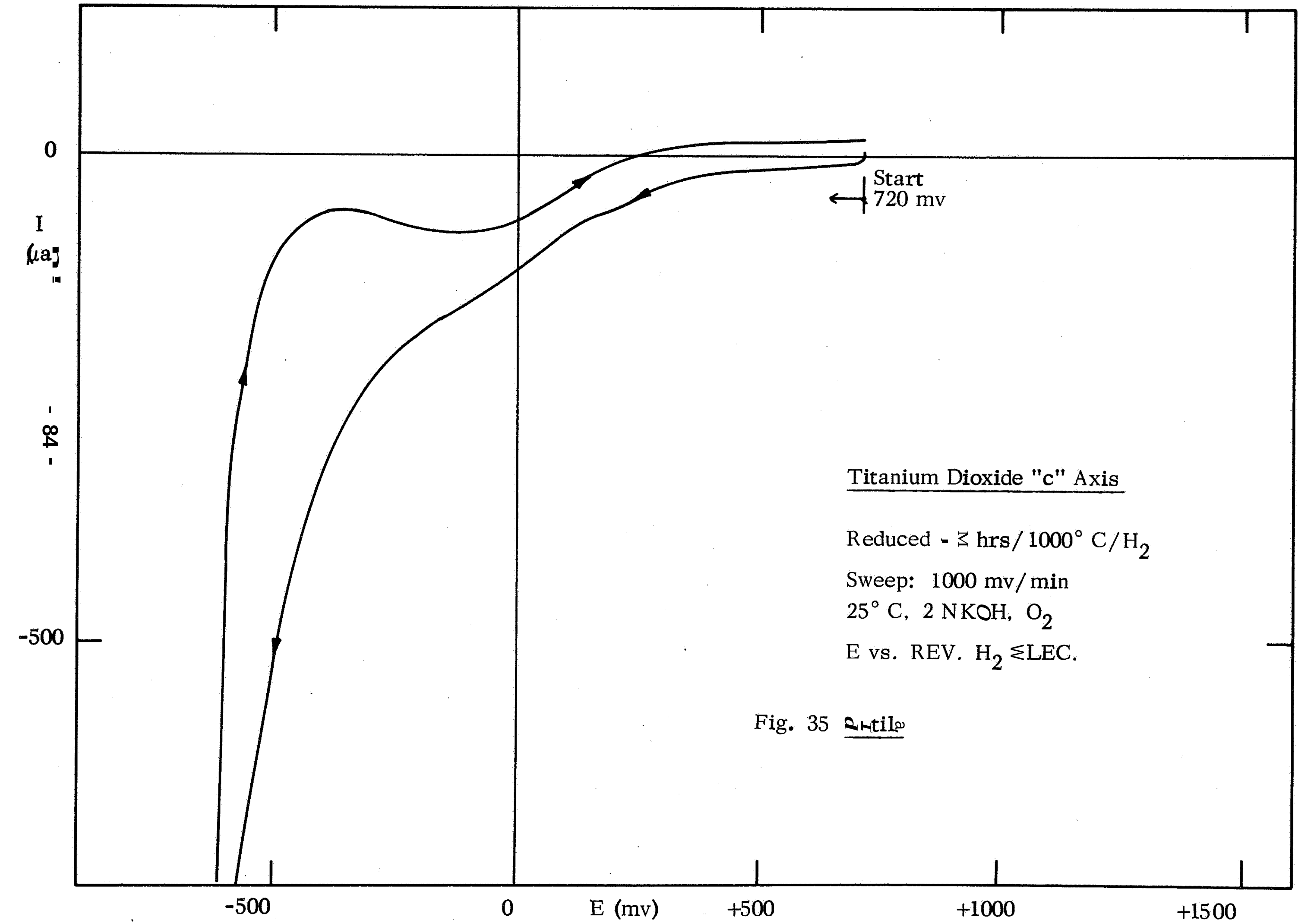

Fig. 35 Rutile

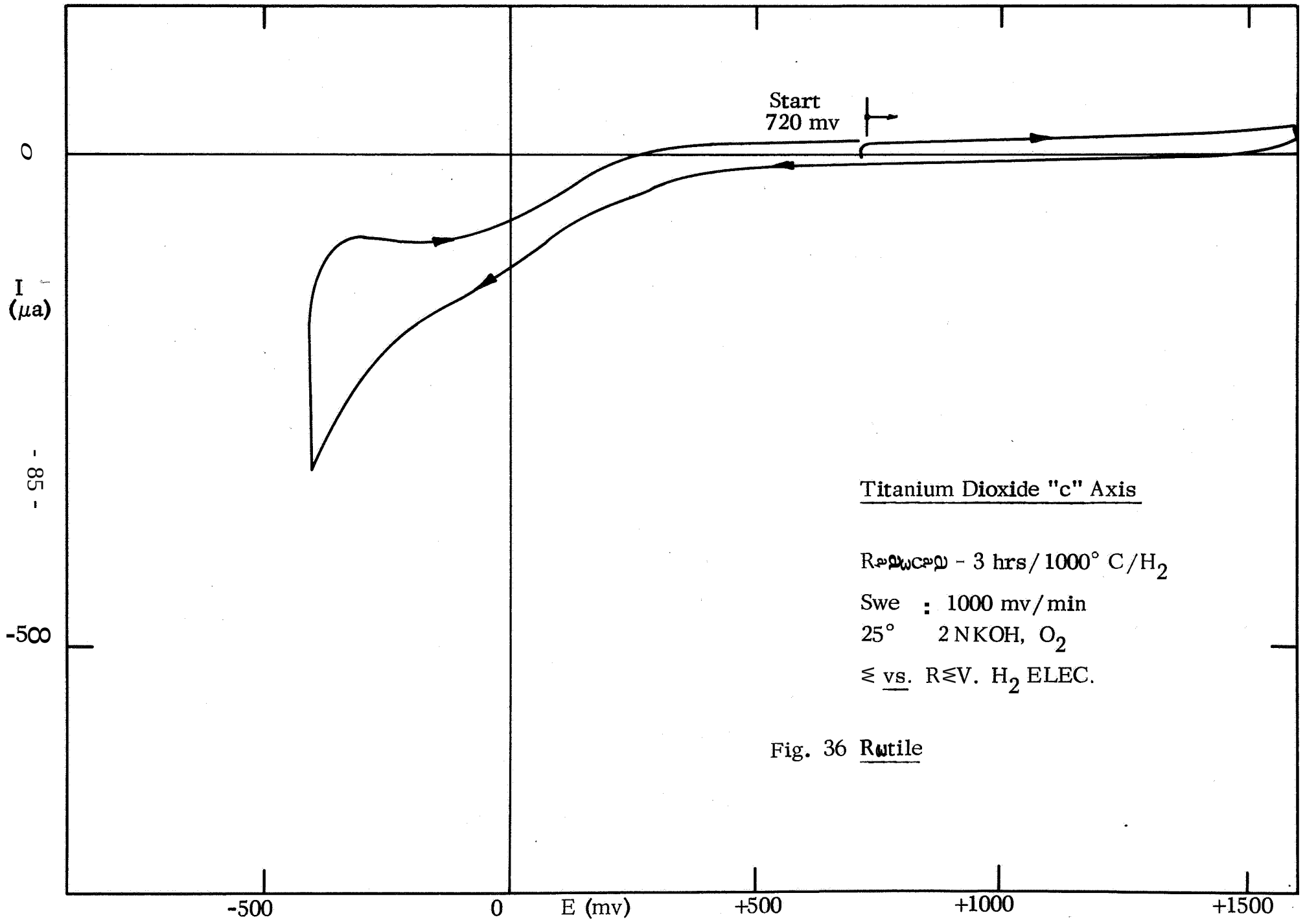

Fig. 36 Rutile

One of the tentative conclusions of the survey of intermetallic compounds was that the activity could be related to the activity of the components. The electronic or geometric properties of the intermetallic compound seem to be important only in special cases. It is tempting in the case of Ti_3Au to relate its activity to the near reversible behavior of gold for the reduction of oxygen to peroxide (O_2H^-) and to identify the titanium oxide as a peroxide decomposition catalyst. This point will be discussed further in the next part of this report in conjunction with the related studies of TiAu and $TiAu_2$.

E. Intermetallic Compounds Related to Ti_3Au

The materials tested are listed below; the experimental methods are as described in the first section of this report, except that the temperature of measurement was 25°C. Some of the materials were tested previously at 75°C.

1. $TiAu_2$

This material, a brittle intermetallic compound, was tested as a rotating disc electrode in 2N KOH at 25°C. The results are presented in Fig. 37.

2. TiAu

The test conditions were as for $TiAu_2$ above; the results are presented in Fig. 38. This material had previously shown significant activity at 75°C (Fig. 39) but with a much reduced corrosion rate compared with TiAu; this needed confirmation. A comparison of the results is given in Table XIV.

3. $TiRh_{1.5}Au_{1.5}$

The test conditions were as for $TiAu_2$ above, the results are presented in Fig. 40 and the previous measurement is shown in Fig. **41** for qualitative comparison (75°C *vs.* 25°C).

TABLE XIV

Activity of Titanium and Related Intermetallic Compounds

	$E_{\frac{1}{2}}$ (mv)(1)	E_i (mv)(2)	i_L (μa/cm^2)	Capacity μf/cm^2	Corrosion
Ti_3Au	810	910	698	69. 8	some corrosion
Ti_3Au*	840	900	1050	164.	particularly > 800 mv
TiAu	745	925	746	50.7	
TiAu*	800	860	833	56. 7	
$TiAu_2$	725	800	665	46. 8	some corrosion > 700 mv
$TiRh_{1.5}Au_{1.5}$	825	920	658	225.	v. small
$TiRh^*_{1.5}Au^*_{1.5}$	570(3)	790	1296	109.	v. small
$TiPt^*_3$	820	870	882	132.	"
$TiRh_3$	610	920	1266	129.	"
$TiRh^*_3$	460	670	1366	116.	"
V_3Au	Corrodes rapidly for E = 400 mv				
Nb_3Au	(825)	(910)	582	-	significant corrosion rate
Pt*	845	925	1350	115.	
Au	785	900	(1340)	96.	
Rh	544	675	1370	340.	

* Previous measurements (at 75°C)

(1) $E_{\frac{1}{2}}$-half wave potential

(2) E_i-potential at which initial cathodic current observed

(3) Low $E_{\frac{1}{2}}$ value due to high anodic starting potential forming a thick oxygen film not completely removed during the initial part of the potential sweep.

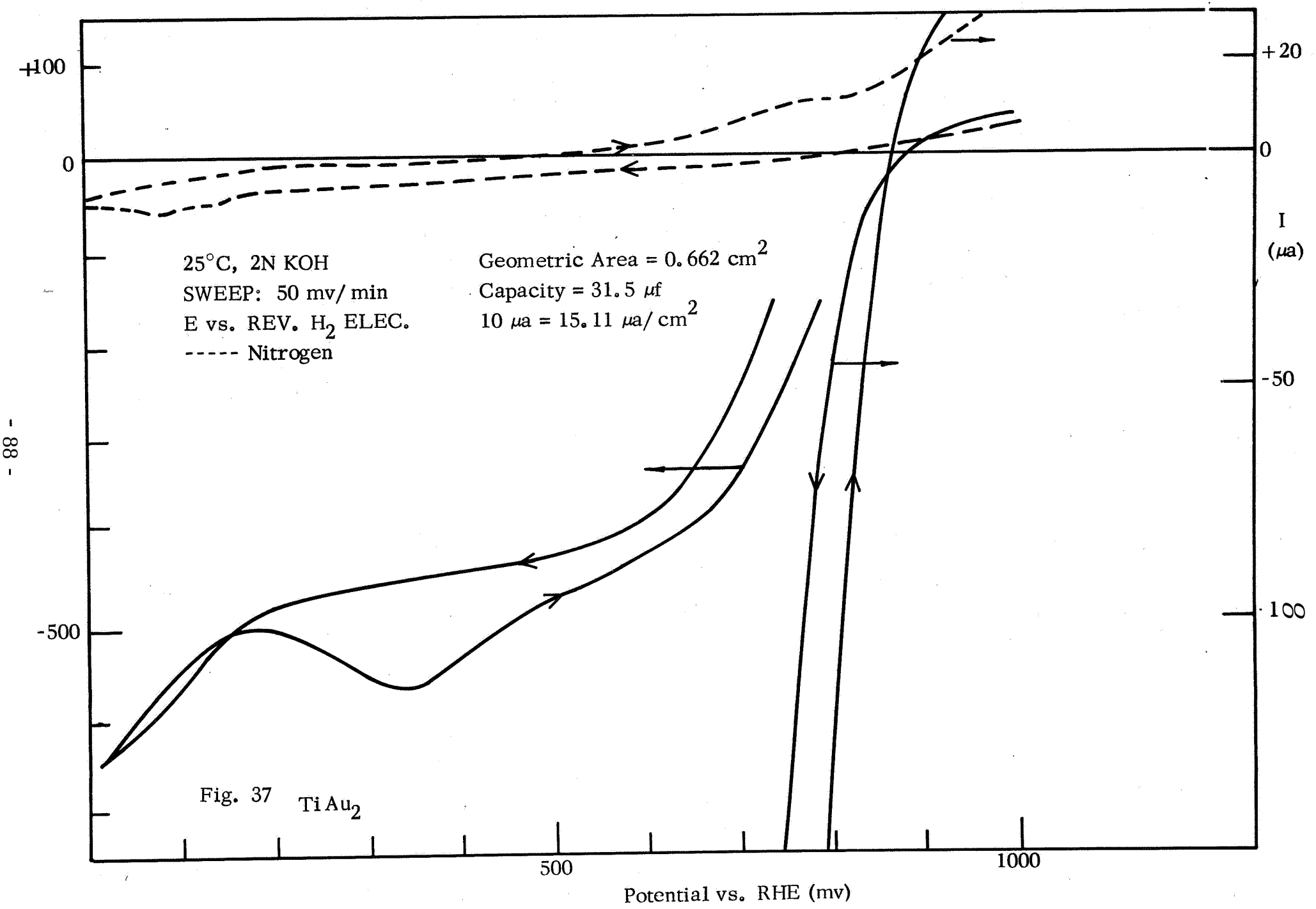
+100
0
-500
+20
0
-50
-100
I
(μa)
25°C, 2N KOH
SWEEP: 50 mv/ min
E vs. REV. H_2 ELEC.
----- Nitrogen
Geometric Area = 0.662 cm^2
Capacity = 31.5 μf
10 μa = 15.11 μa/ cm^2
500
1000
Potential vs. RHE (mv)

Fig. 37 $TiAu_2$

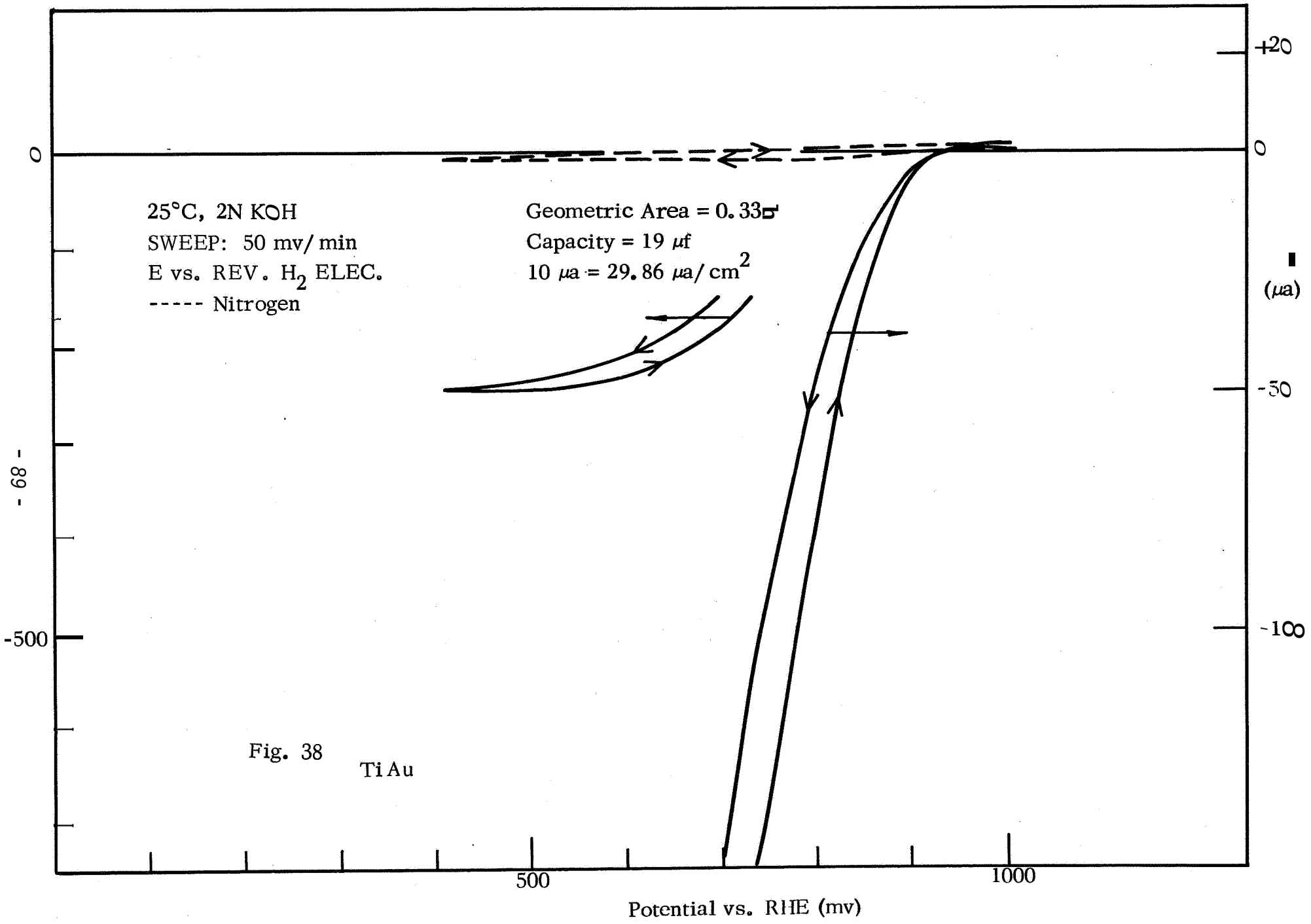
25°C, 2N KOH
SWEEP: 50 mv/ min
E vs. REV. H_2 ELEC.
----- Nitrogen
Geometric Area = 0.33
Capacity = 19 μf
10 μa = 29.86 μa/ cm^2
+20
0
-50
-100
(μa)
0
-500
500
1000
Potential vs. RHE (mv)

Fig. 38

Ti Au

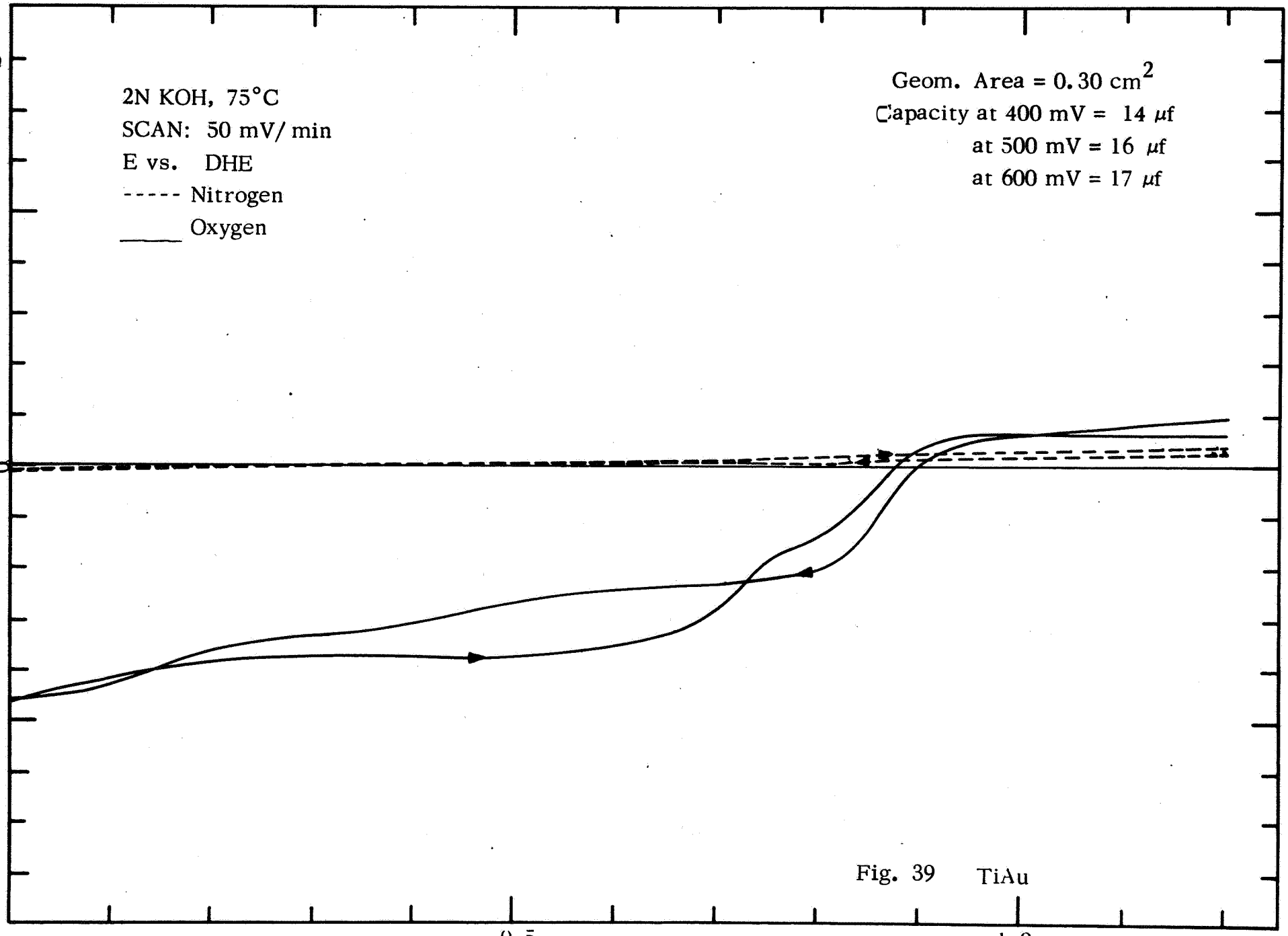
2N KOH, 75°C
SCAN: 50 mV/ min
E vs. DHE
----- Nitrogen
_____ Oxygen
Geom. Area = 0.30 cm2
Capacity at 400 mV = 14 μf
at 500 mV = 16 μf
at 600 mV = 17 μf
Current
Curr. Dens.
+ 0.5 mA
1.67 mA/ cm2
0
- 90 -
-0.5 mA
1.67 mA/ cm2
0.5
1.0
POTENTIAL vs. DHE (volts)

Fig. 39 TiAu

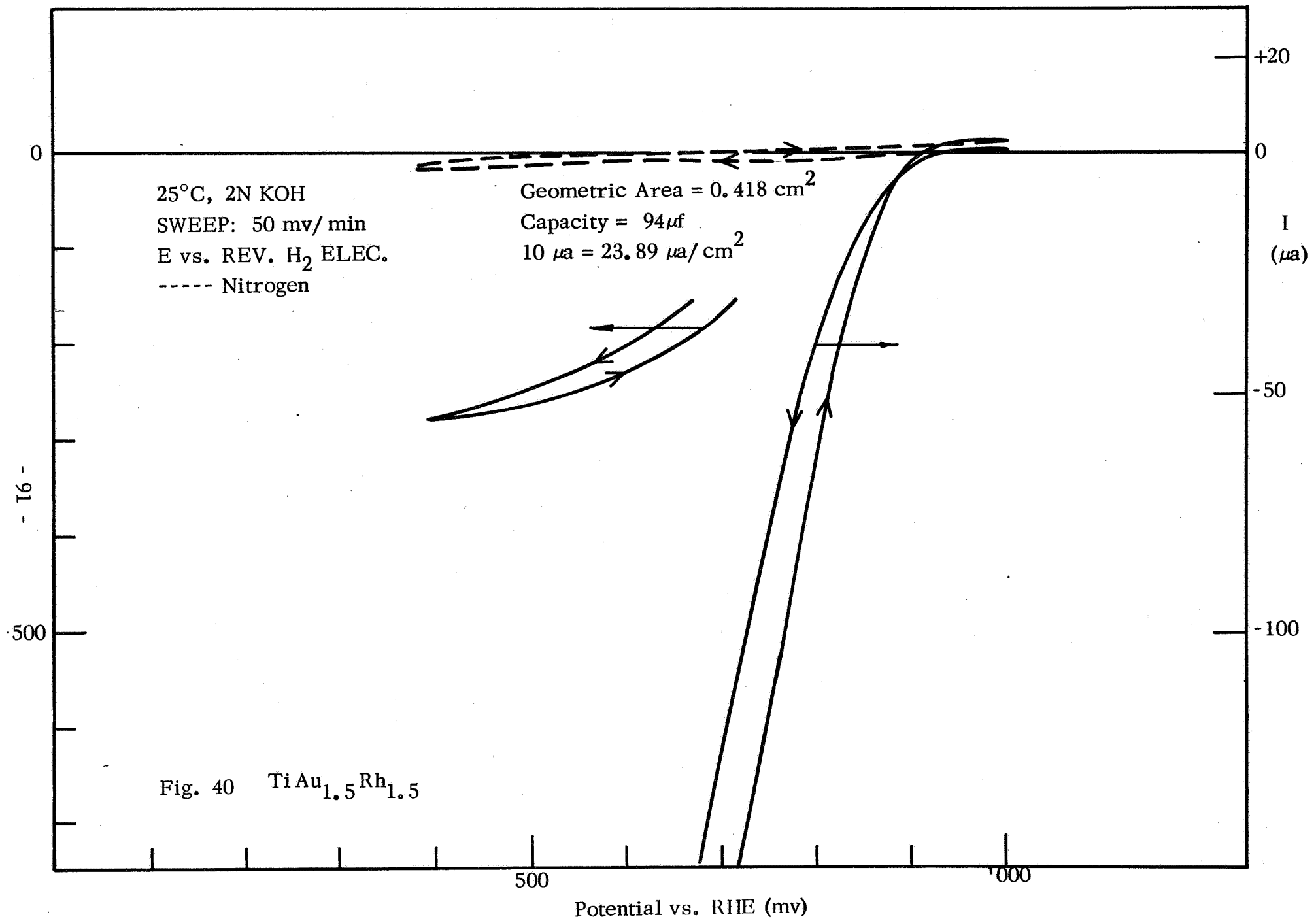

Fig. 40 $TiAu_{1.5}Rh_{1.5}$

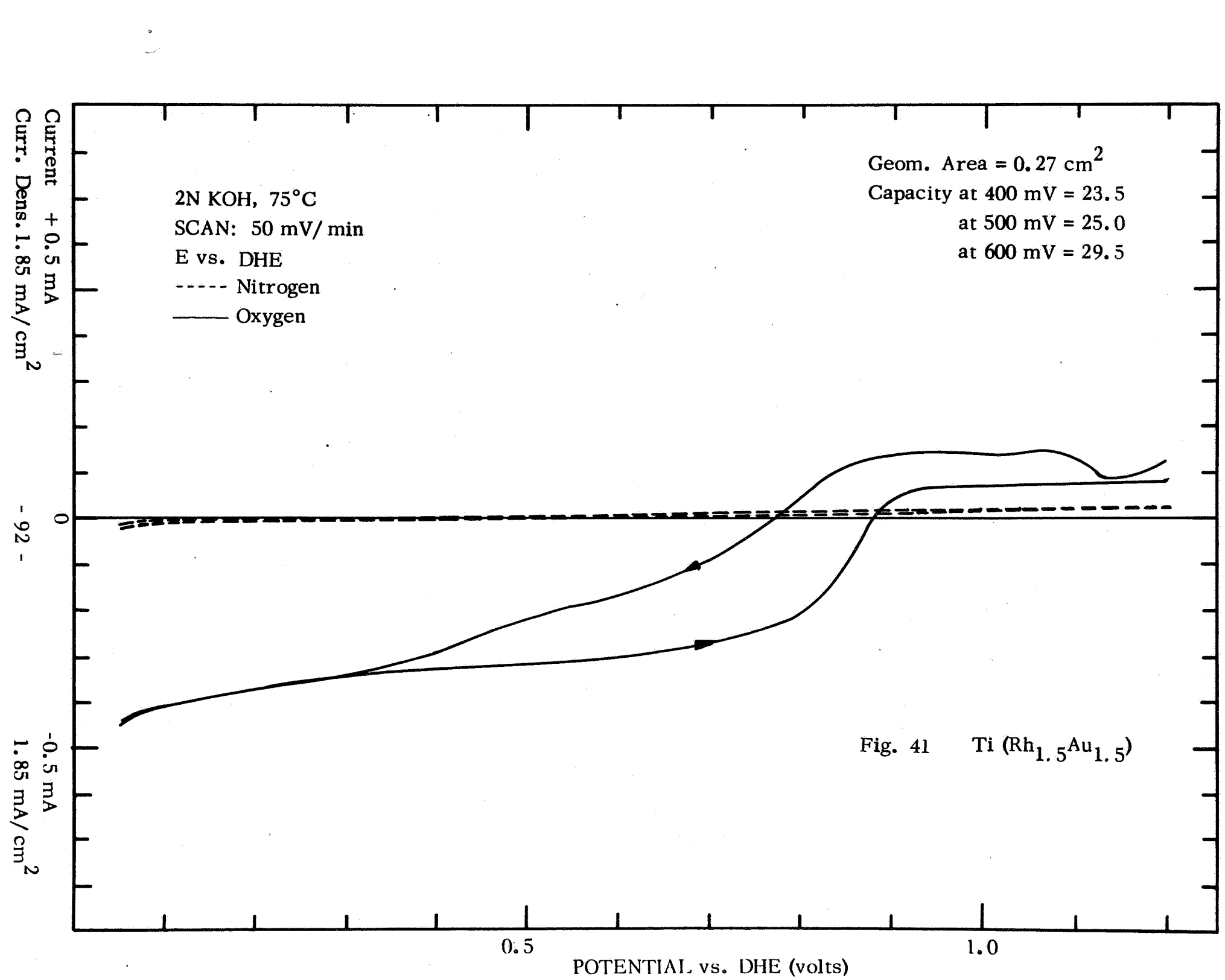

Fig. 41 Ti ($Rh_{1.5}Au_{1.5}$)

4. $TiRh_3$

This material was tested as $TiAu_2$ above; the present and previous results (75°C) are presented in Figs. 42 and 43, respectively.

5. V_3Au and Nb_3Au

These materials were tested as rotating disc electrodes in order to compare their behavior with Ti_3Au. The results are presented in Figs. 44 and 45.

6. Ti_3Au

A sample of Ti_3Au was rerun at lower temperatures.

The results are summarized in Table VII and Figs. 46 and 47, including earlier work at 75°C. The activity is lower at lower temperature, as expected, except for $Ti(Rh_{1.5}Au_{1.5})$ which now shows a half wave potential ($E_{\frac{1}{2}}$) 355 mv more positive. This however is not a temperature effect and is probably due to a thick oxide film formed in the earlier experiments by the high starting potential.

For the three titanium gold compounds Ti_3Au, TiAu, and $TiAu_2$, the $E_{\frac{1}{2}}$ values (810 mv, 745 mv and 725 mv respectively) decrease as the titanium content decreases. If the principal electrochemical reaction is O_2 reduction to O_2H^- on the gold component, then the titanium content limits the accumulation of peroxide in the solution in the immediate vicinity of the electrode, The effect of peroxide is to establish a potential between the reversible potentials of the O_2/OH^- reaction (1. 23v) and the O_2/HO_2^- (0. 75v) reaction i. e. a less positive potential (increased polarization) for increasing peroxide concentration.

$TiRh_{1.5}Au_{1.5}$ is of particular interest since the Rh/Au combination has the same electron density as $TiPt_3$. The comparison of Au/Ir is not possible, and the Rh/Au can only be compared as the titanium intermetallic because Rh and Au are not mutually soluble to any great extent. When $TiRh_{1.5}Au_{1.5}$ is compared'with $TiPt_3$, it can be seen that the half wave potentials ($E_{\frac{1}{2}}$) are identical but that the E_i value is larger for the rhodium gold intermetallic (920 mv compared to 870 mv). This behavior is closer to that of the titanium gold series than to that of the $TiPt_3$.

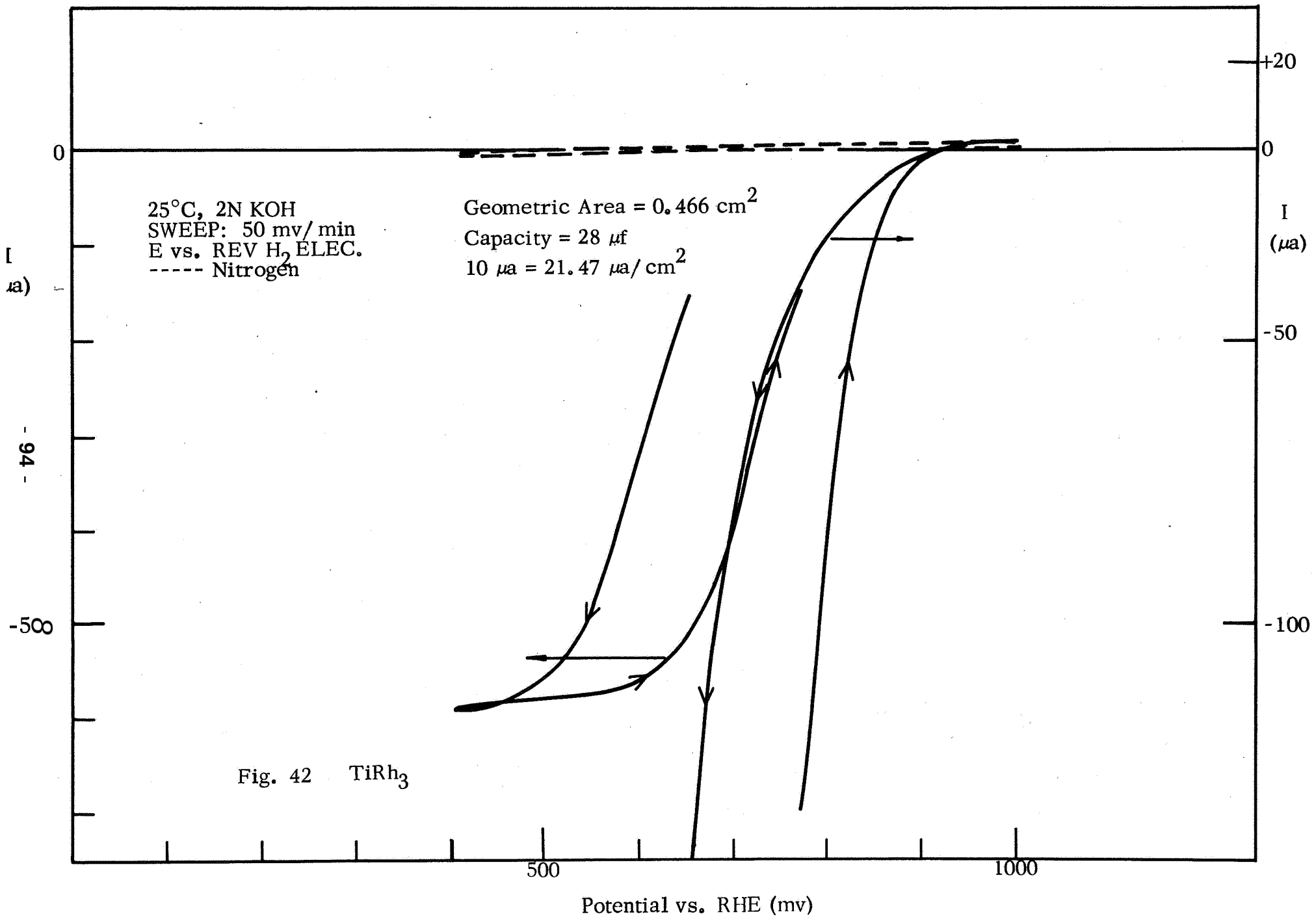
25°C, 2N KOH
SWEEP: 50 mv/ min
E vs. REV H_2 ELEC.
----- Nitrogen
Geometric Area = 0.466 cm^2
Capacity = 28 μf
10 μa = 21.47 μa/ cm^2
+20
0
-50
-100
I (μa)
-500
500
1000
Potential vs. RHE (mv)

Fig. 42 $TiRh_3$

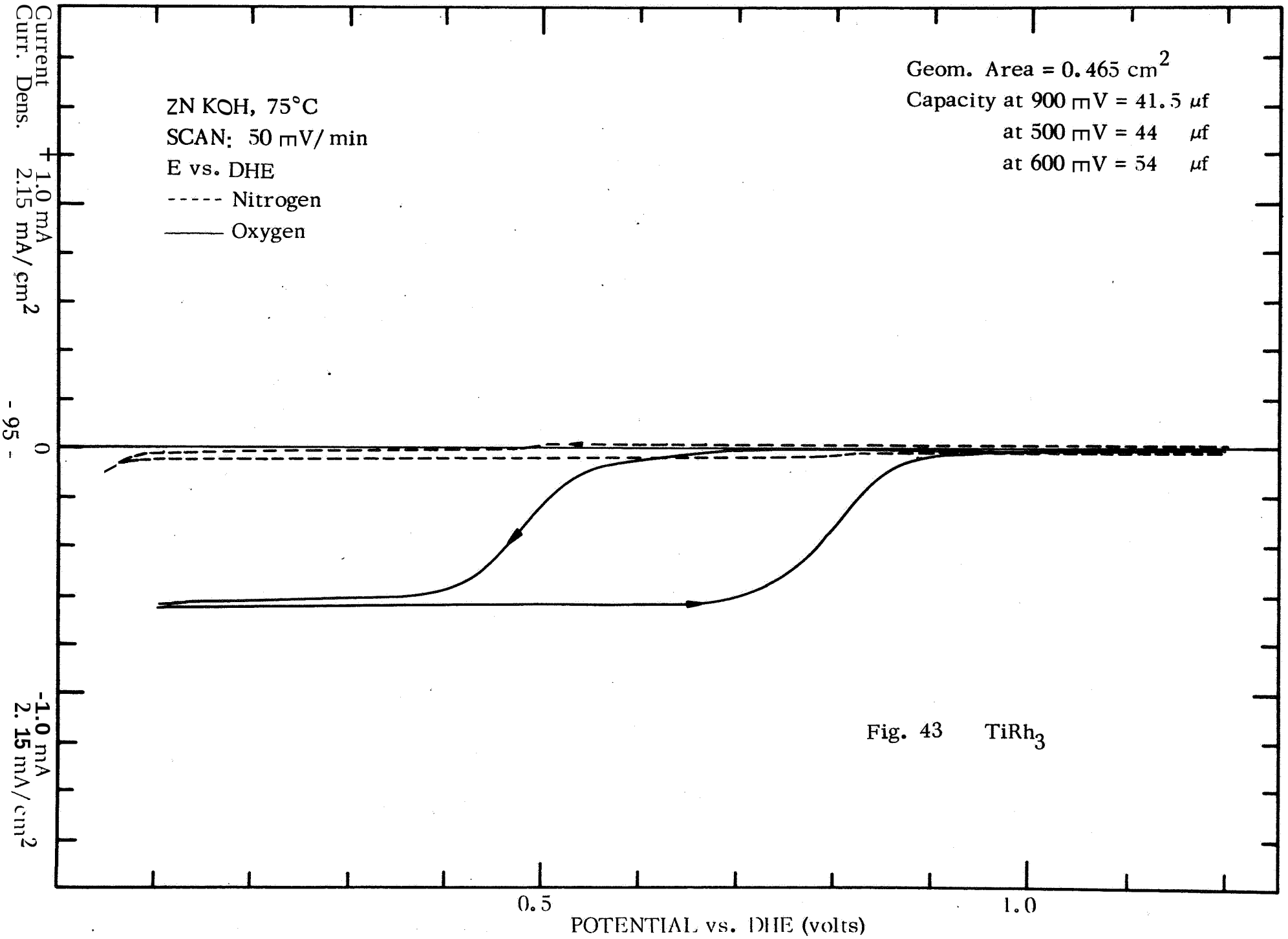
Current
Curr. Dens.
+1.0 mA
2.15 mA/cm²
0
-1.0 mA
2.15 mA/cm²
ZN KOH, 75°C
SCAN: 50 mV/min
E vs. DHE
----- Nitrogen
—— Oxygen
Geom. Area = 0.465 cm²
Capacity at 900 mV = 41.5 μf
at 500 mV = 44 μf
at 600 mV = 54 μf
0.5
1.0
POTENTIAL vs. DHE (volts)

Fig. 43 $TiRh_3$

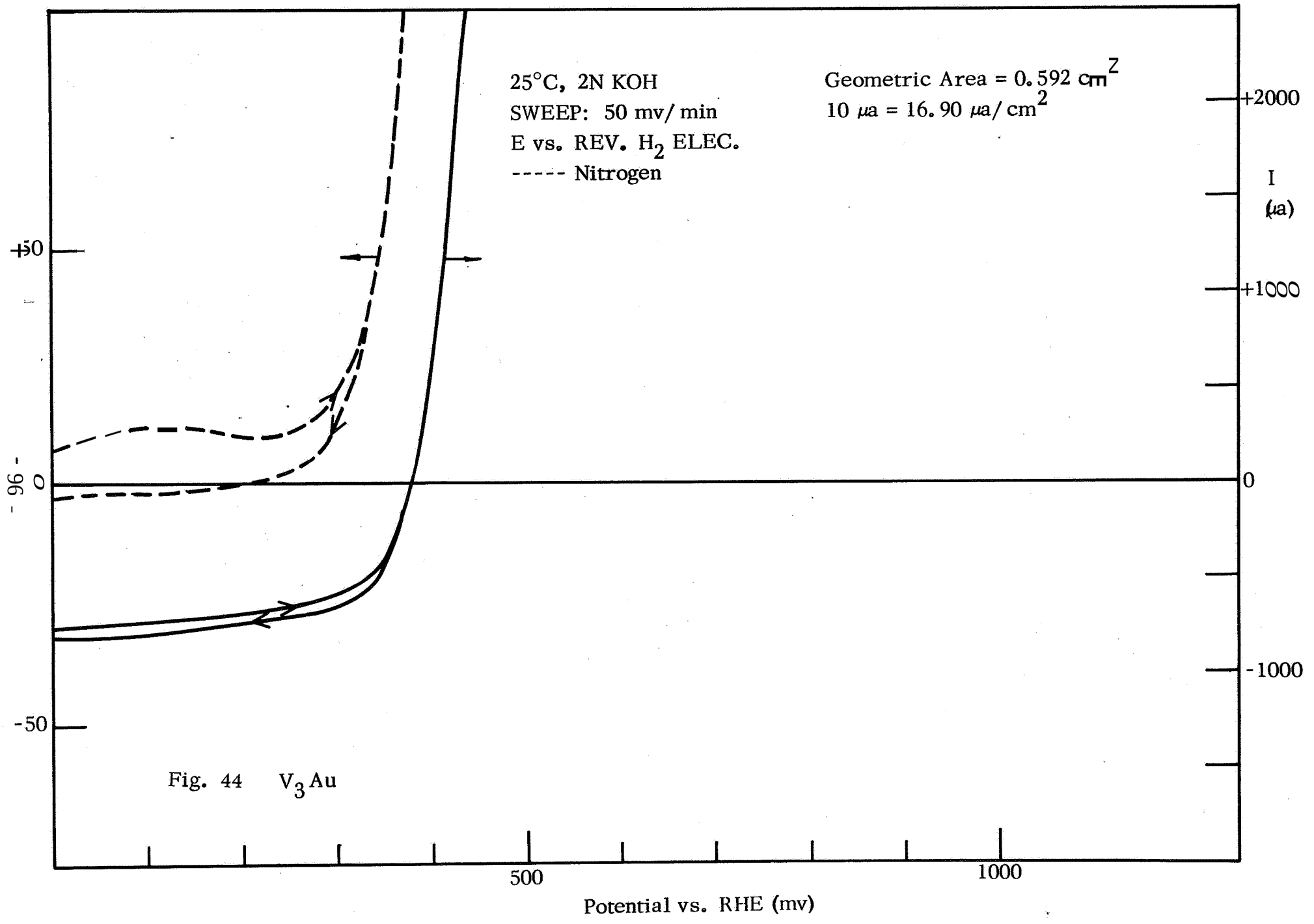
25°C, 2N KOH
SWEEP: 50 mv/ min
E vs. REV. H_2 ELEC.
----- Nitrogen
Geometric Area = 0.592 cm^2
10 μa = 16.90 μa/ cm^2
+2000
I
(μa)
+1000
+50
- 96 -
0
0
-1000
-50
500
1000
Potential vs. RHE (mv)

Fig. 44 V_3Au

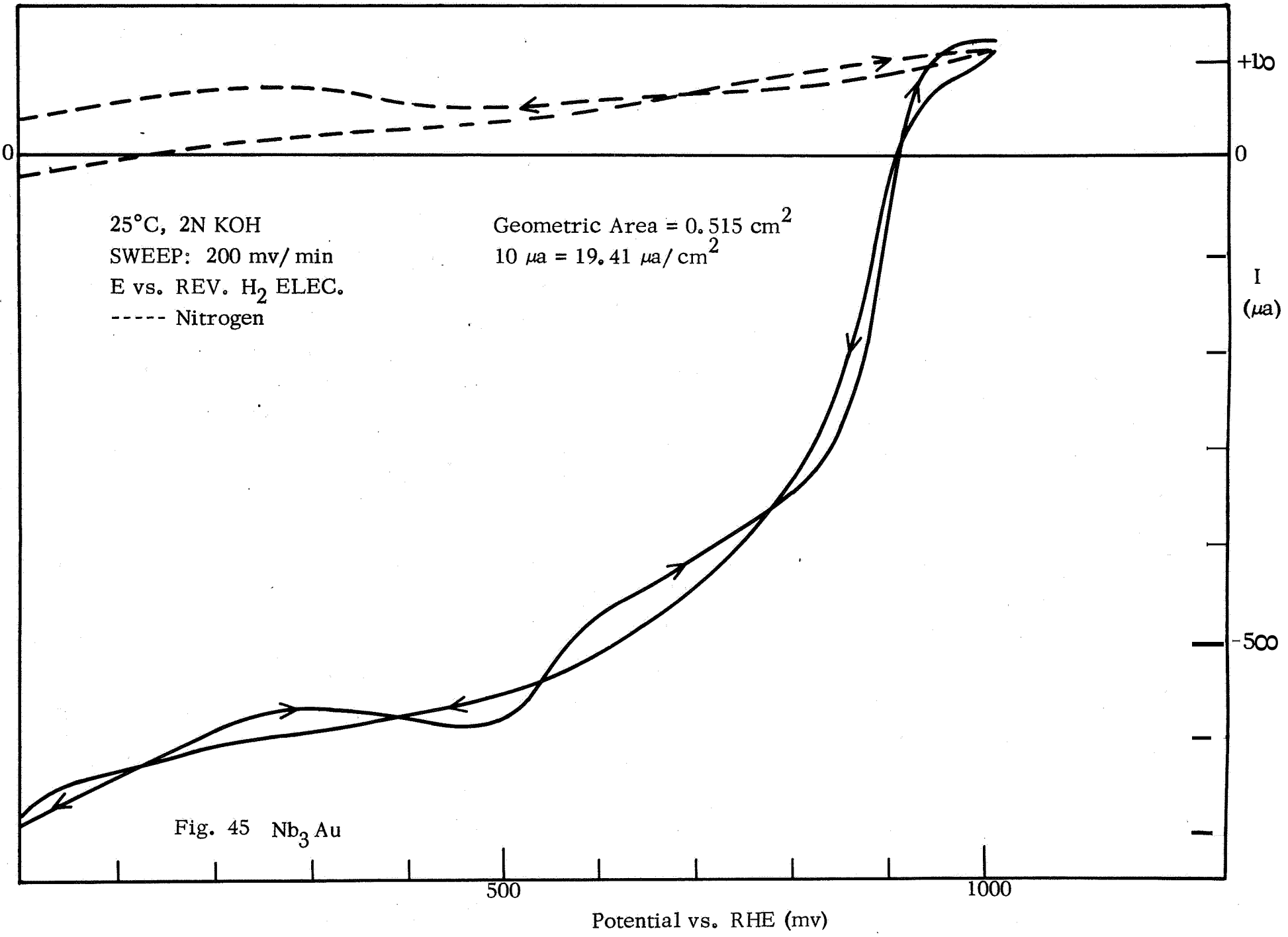
25°C, 2N KOH
SWEEP: 200 mv/ min
E vs. REV. H_2 ELEC.
----- Nitrogen
Geometric Area = 0.515 cm^2
10 μa = 19.41 μa/ cm^2
+100
0
0
I
(μa)
-500
500
1000
Potential vs. RHE (mv)

Fig. 45 Nb_3Au

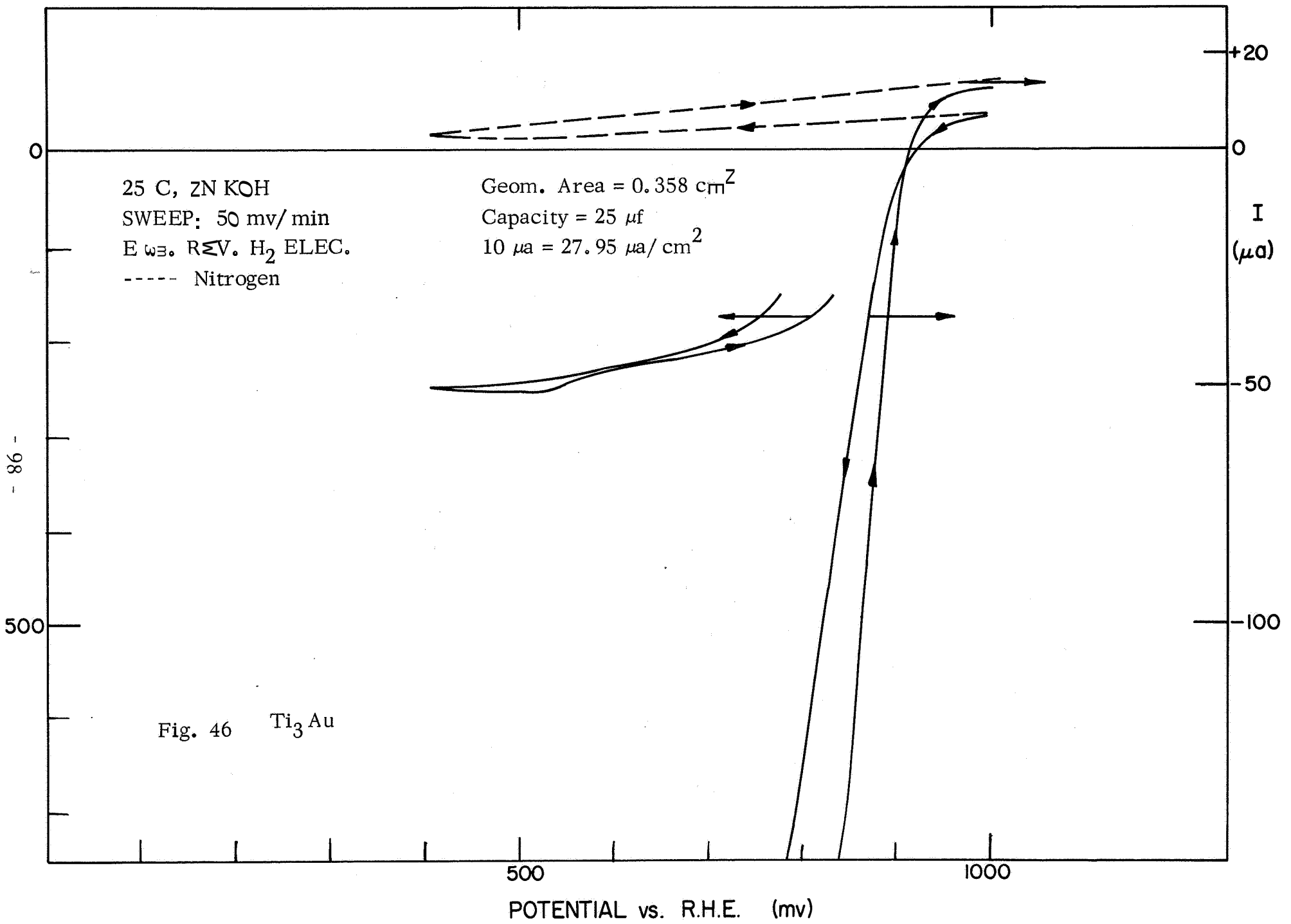
25 C, ZN KOH
SWEEP: 50 mv/ min
E ωɜ. RΣV. H_2 ELEC.
----- Nitrogen
Geom. Area = 0.358 cm^2
Capacity = 25 μf
10 μa = 27.95 μa/ cm^2
+20
0
-50
-100
I
(μa)
0
500
500
1000
POTENTIAL vs. R.H.E. (mv)

Fig. 46 Ti_3Au

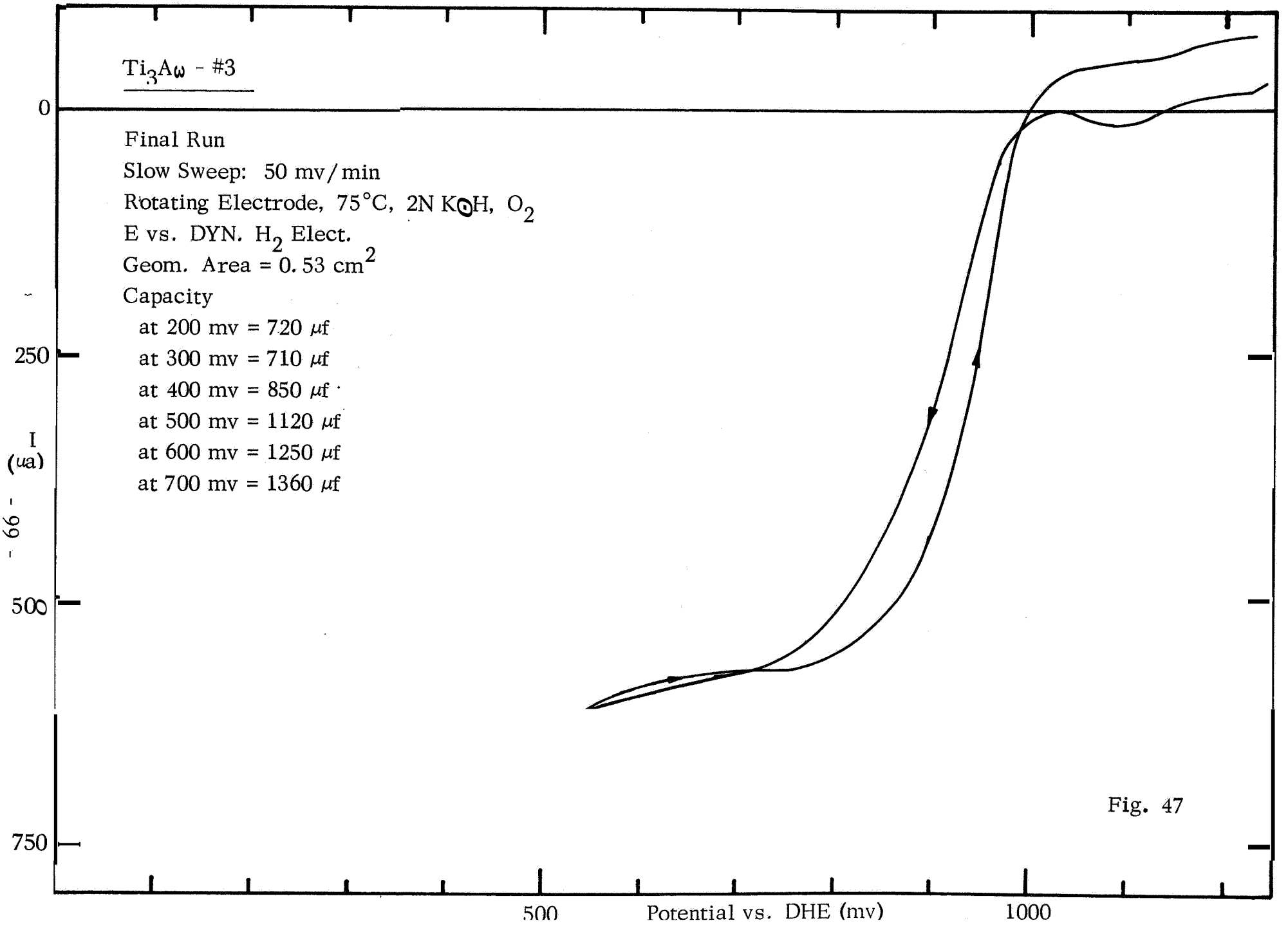
Ti_3Au - #3
Final Run
Slow Sweep: 50 mv/min
Rotating Electrode, 75°C, 2N KOH, O_2
E vs. DYN. H_2 Elect.
Geom. Area = 0.53 cm^2
Capacity
at 200 mv = 720 μf
at 300 mv = 710 μf
at 400 mv = 850 μf
at 500 mv = 1120 μf
at 600 mv = 1250 μf
at 700 mv = 1360 μf
0
250
500
750
I (μa)
500
Potential vs. DHE (mv)
1000

Fig. 47

V_3Au and Nb_3Au corrode too rapidly to be considered as practical catalysts. $TiRh_3$ shows an initial cathodic current at 920 mv, but the $E_{\frac{1}{2}}$ value at 610 mv is well below the titanium gold values.

III. SILVER-MAGNESIUM ALLOYS

A. Introduction

We have tested silver-magnesium alloys under similar experimental conditions to those described for the gold alloys;. The principal reason for this was that Beer and Sandler[28] have examined these catalysts for the oxygen-reduction reaction silver, with different surface pretreatments, and have reported improved performance for a 1.7% Mg:Ag alloy. This was considered to be related to its enhanced secondary electron emission. This work did not include a determination of the real surface area of these materials. A comparison of the real surface areas of Ag and the alloy was carried out in this laboratory in conjunction with activity tests on these materials.

B. Experimental

The silver-magnesium alloy was obtained as foil from Handy and Harmaii Co. , New York, and silver foil was purchased from Williams Metals. The foils, welded to an Ag-wire and sealed in glass, were polished to a bright finish with alumina and tested in a rotating electrode cell as 1 cm by 1 cm squares.

C. Results

The current potential curves for these materials are shown in Figs. 48 and 49. A comparative figure for the real surface areas of the Ag and Ag:Mg foils was obtained from the ratio of their double-layer capacities. The capacities were measured with a 50 mv triangular sweep at 400 and 700 mv at the beginning and at the end of each activity determination. The ratio of the real surface areas ranged from 3.2 to 6, the Ag:Mg alloy having the higher surface area, A series of experiments at different sweep rates showed that the surface was substantially free of adsorbed impurities.

A comparison of the potentials at a current density of 200 $\mu a/cm^2$ (corrected for the difference in surface roughness), where there are no mass transfer limitations, shows no greater intrinsic activity for the Ag:Mg alloy (Table XV).

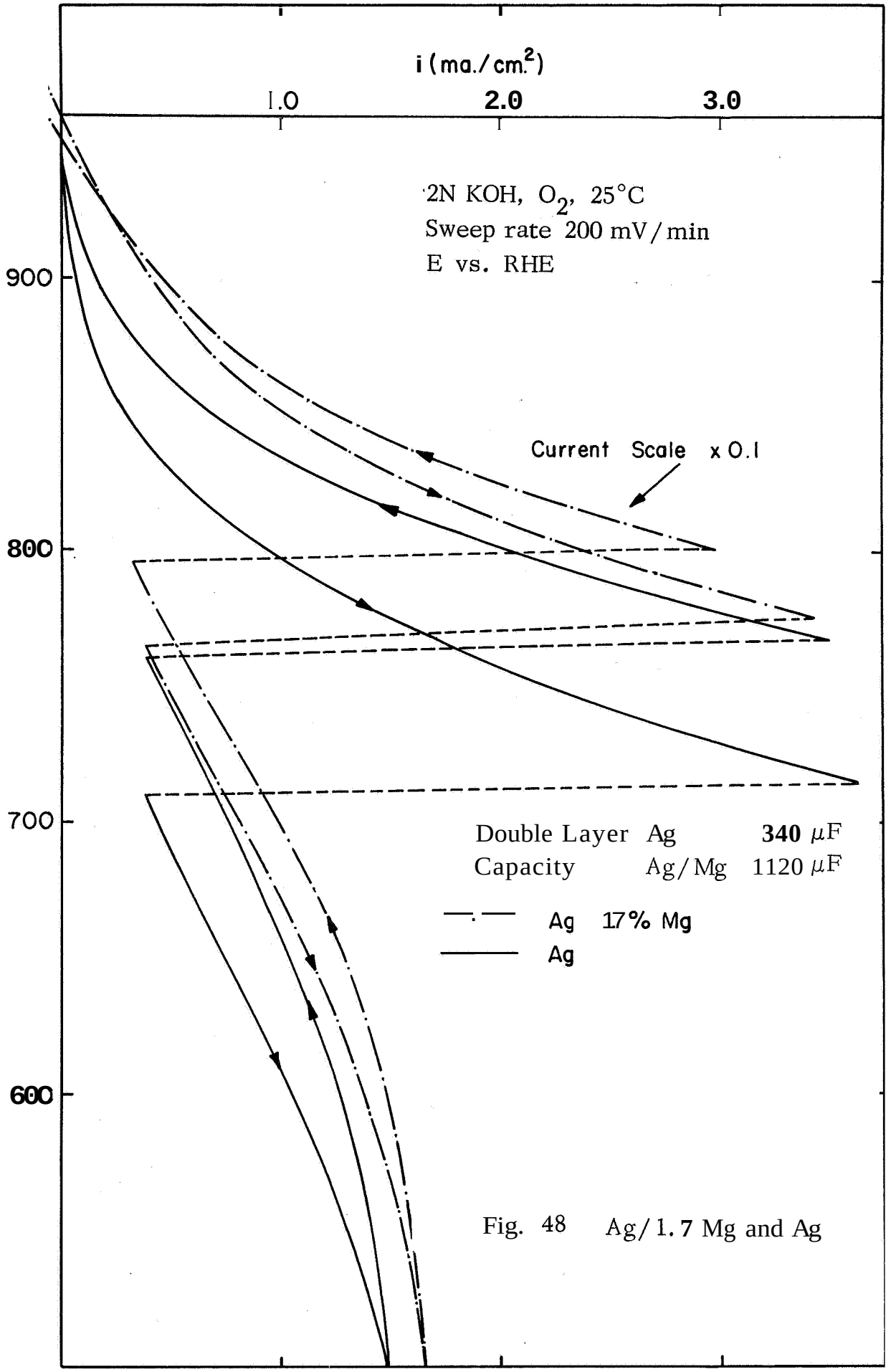

Fig. 48 Ag/1.7 Mg and Ag

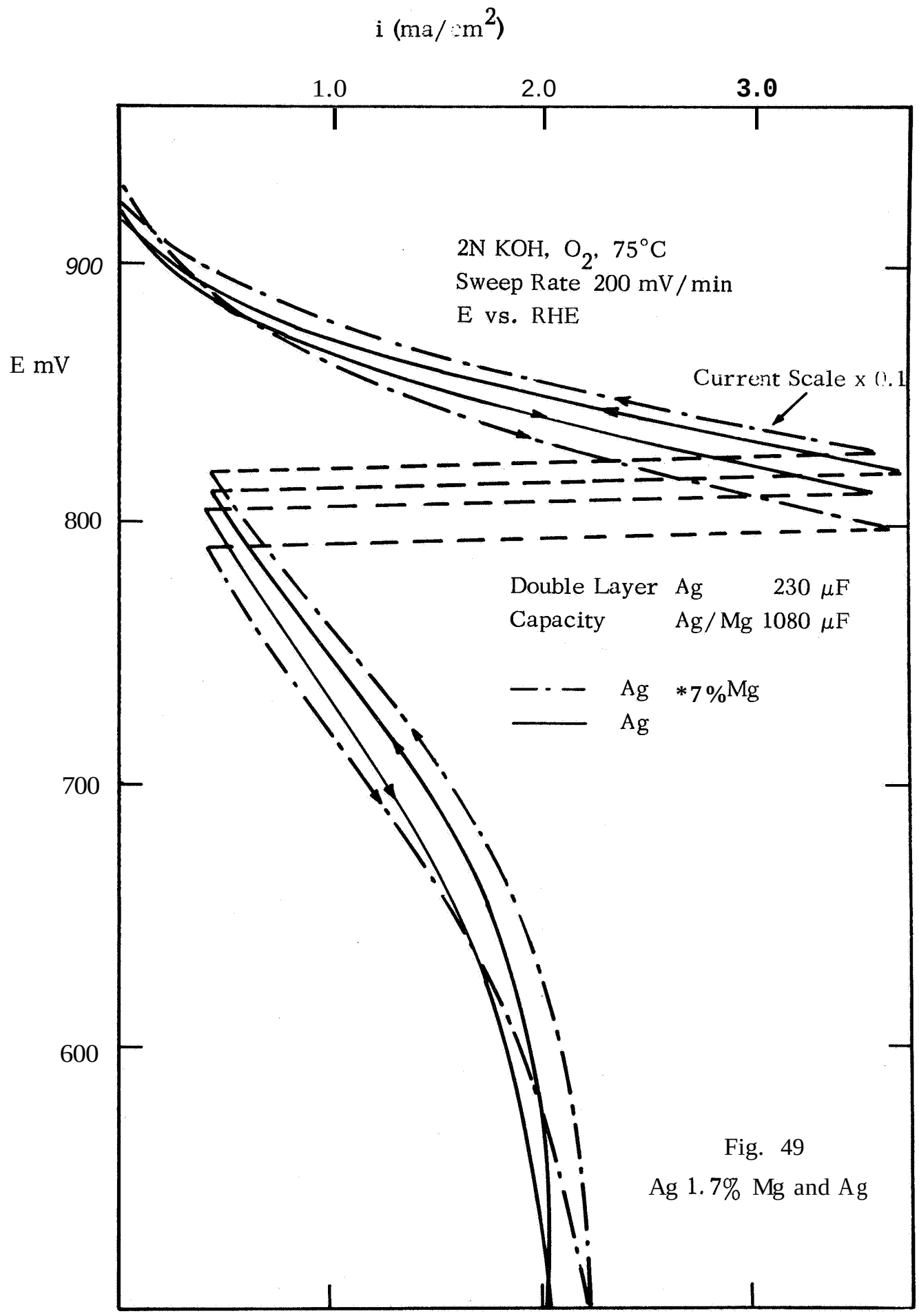

Fig. 49
Ag 1.7% Mg and Ag

TABLE XV

Comparison of Silver and Silver-Magnesium Alloys

		E vs. RME	
		Ag	Ag:Mg
25°C	i = 200 μa/cm2"	863	8S8 mv
75"C	i = 200 μa/cm2"	900	880 mv

* Corrected for difference in surface roughness.

IV. OSMIUM AND Pt/Os ALLOYS

The initial measurements on osmium[4] showed a low half-wave potential but an initial cathodic current at potentials more positive than the initial current with Pt.

More extensive tests were made at 25° and 75°C to explore this behavior in more detail. The measurements made are reported in Figs. 50 to 54. The half-wave potentials (at 370 mv) are in good agreement with previous results, but the cathodic current close to 1000 mv was not observed in any of these measurements. We can only conclude that the initial results presented in the Fourth Quarterly Report were misleading.

A Pt/Os 80/20 alloy (after careful annealing to insure uniform composition) gave results that were identical to that of Pt. Similarly, electrodes prepared from a coprecipitated Pt/Os 80/20 black gave performances (Figs. 55 and 56) that were typical of Pt electrodes prepared in the same way.

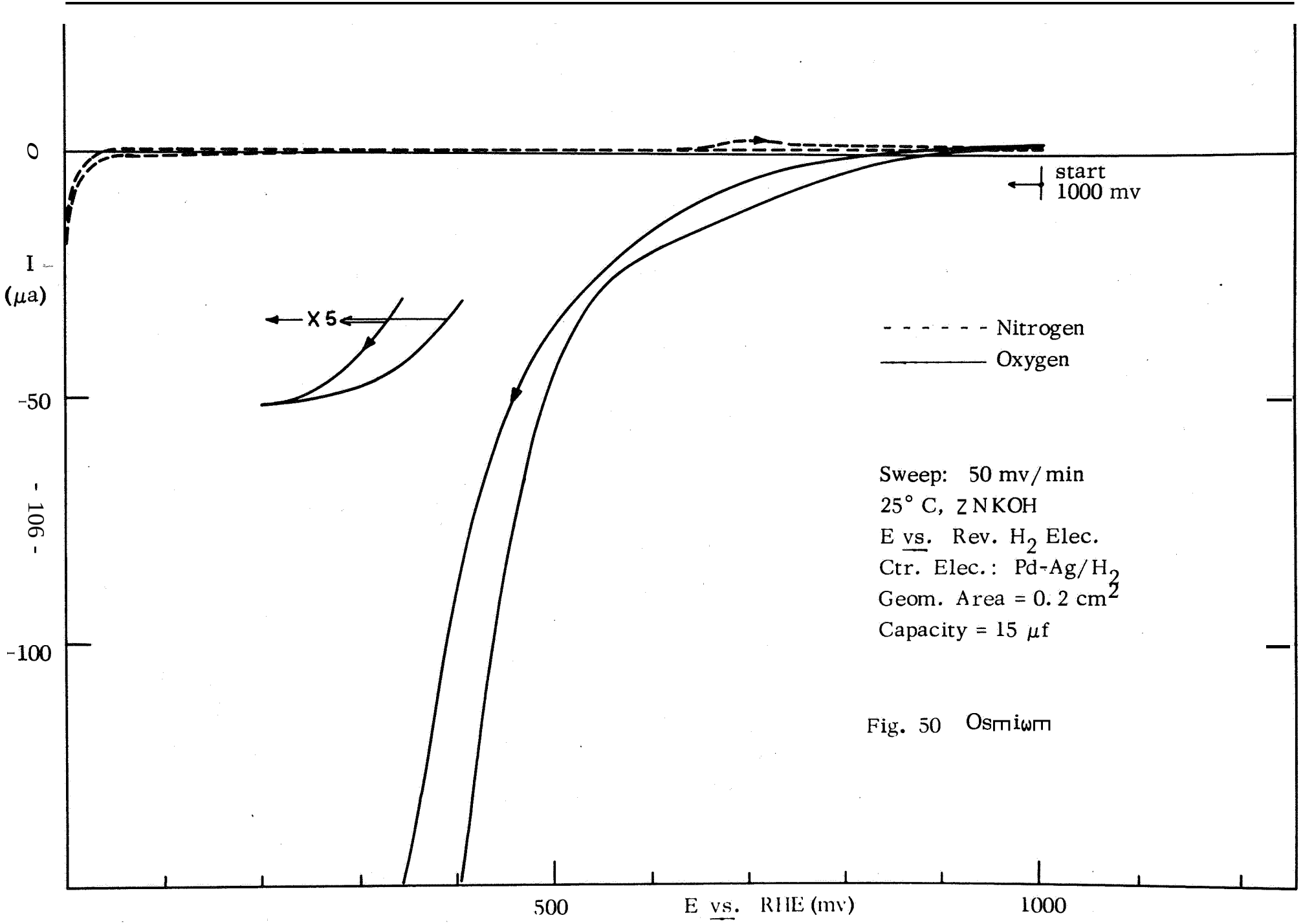

Fig. 50 Osmium

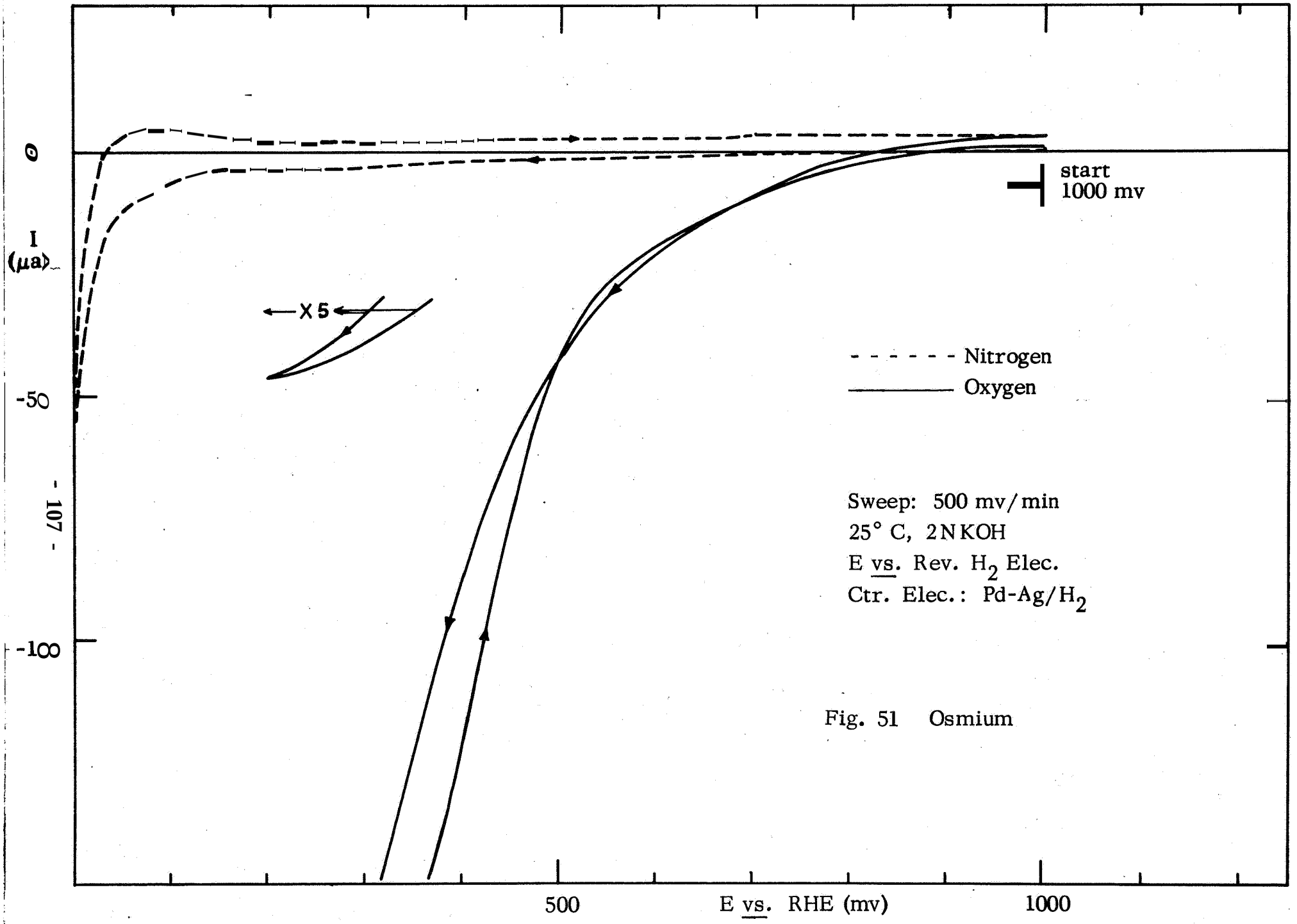

Fig. 51 Osmium

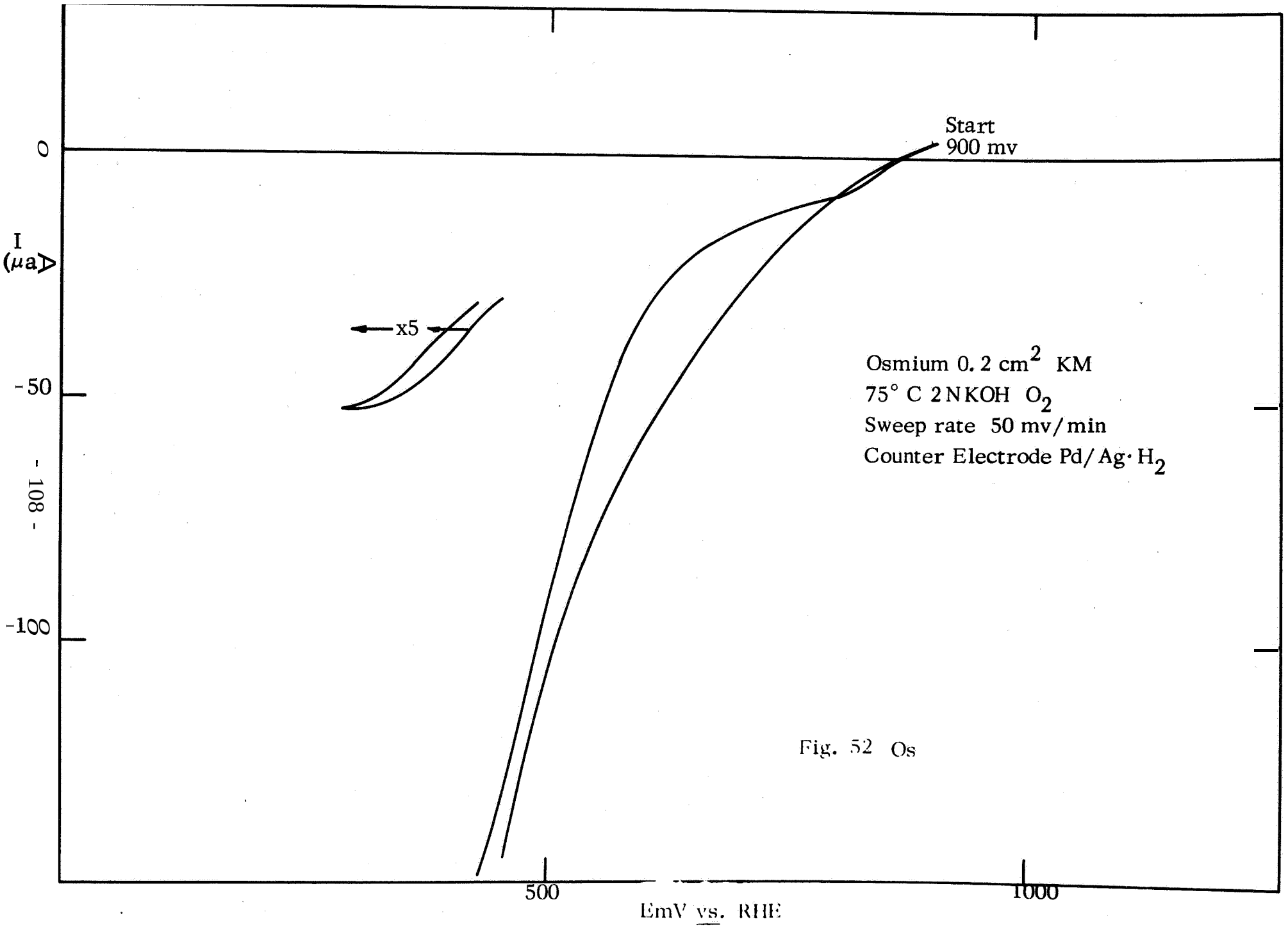
Start
900 mv
0
I
(μa)
-50
-100
x5
Osmium 0.2 cm² KM
75° C 2N KOH O₂
Sweep rate 50 mv/min
Counter Electrode Pd/Ag·H₂
500
1000
EmV vs. RHE

Fig. 52 Os

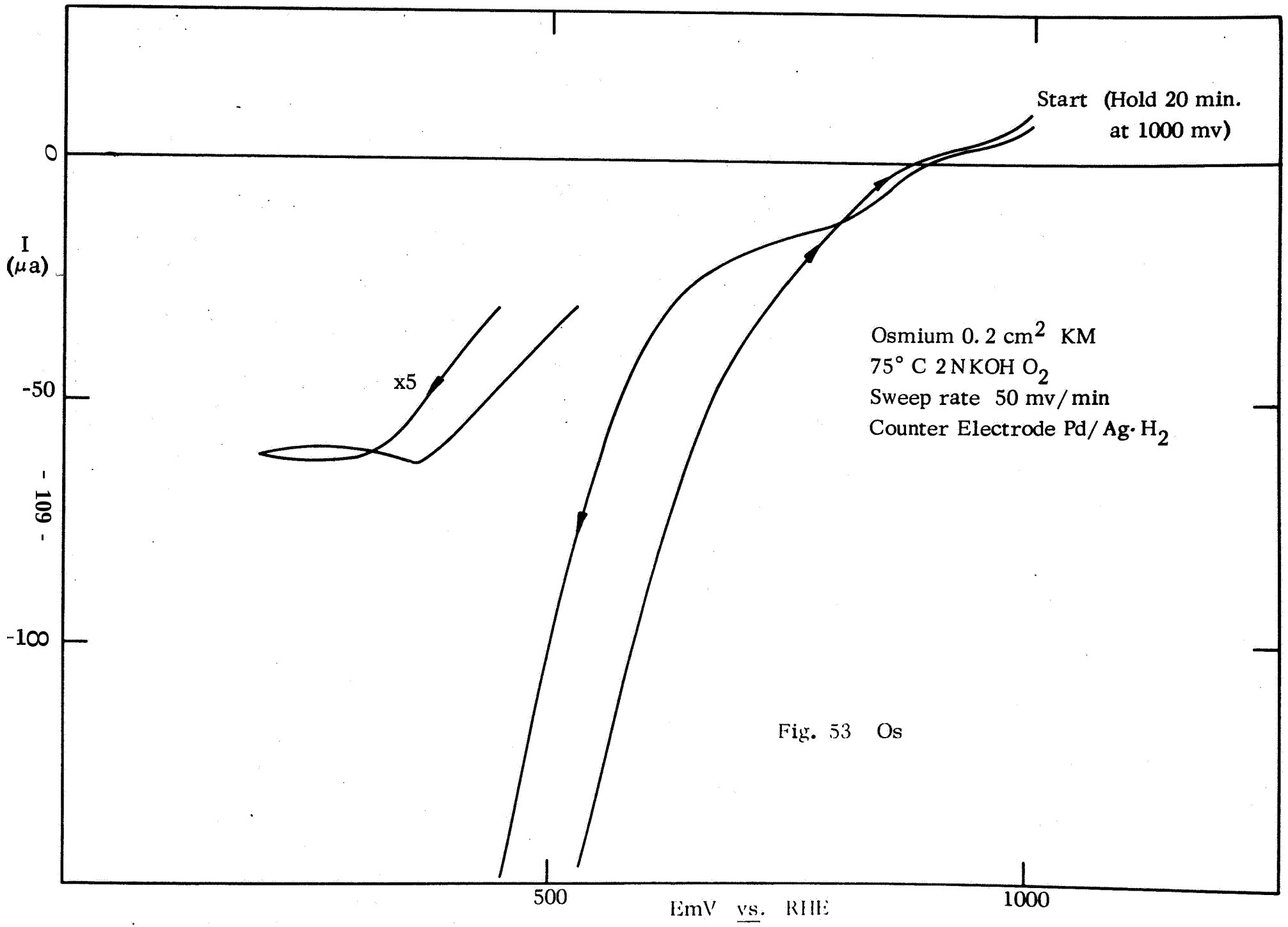
Start (Hold 20 min.
at 1000 mv)
0
I
(μa)
-50
- 109 -
-100
x5
Osmium 0.2 cm² KM
75° C 2NKOH O₂
Sweep rate 50 mv/min
Counter Electrode Pd/Ag·H₂
500
1000
EmV vs. RHE

Fig. 53 Os

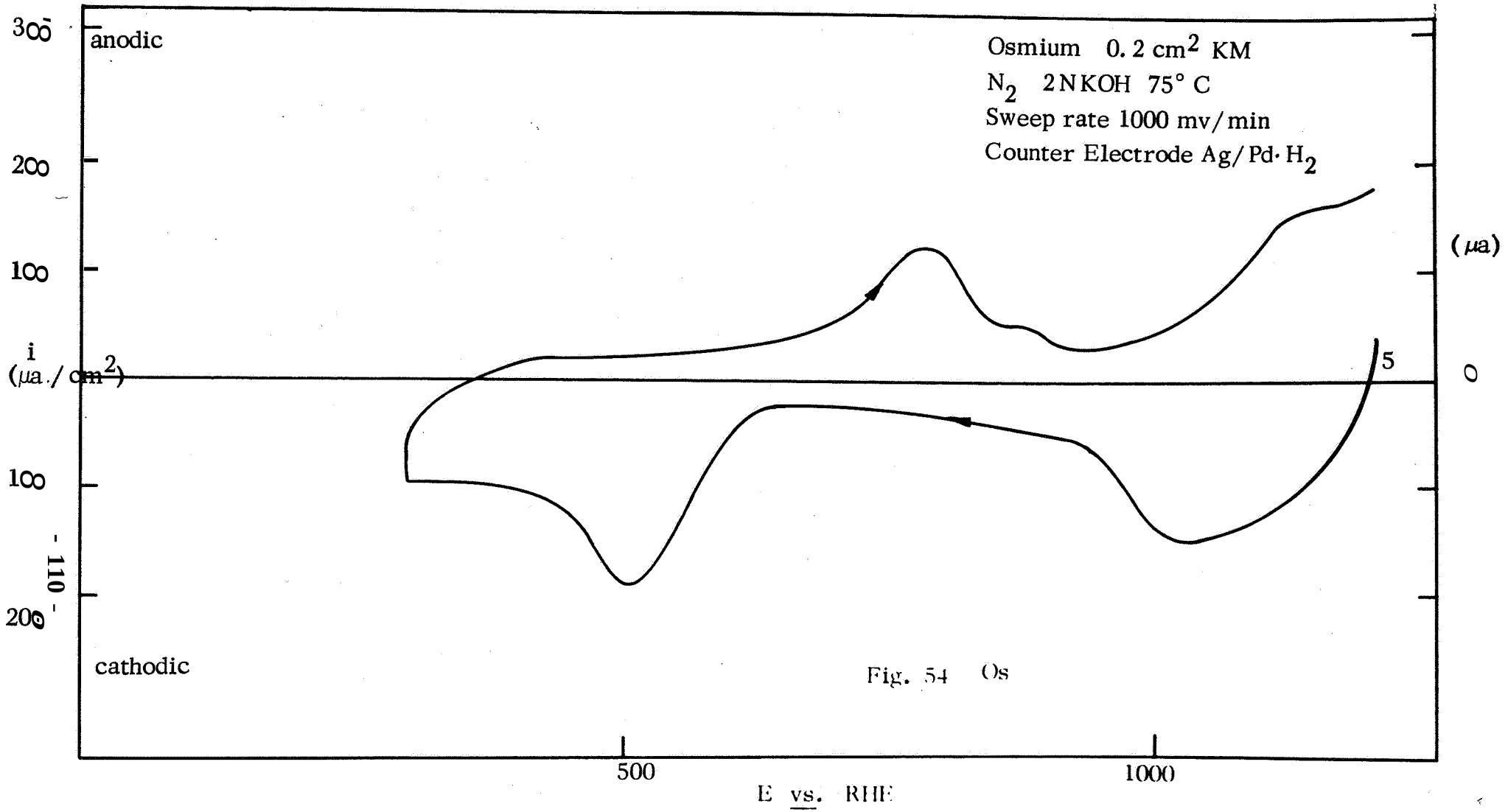
anodic
Osmium 0.2 cm2 KM
N2 2NKOH 75° C
Sweep rate 1000 mv/min
Counter Electrode Ag/Pd·H2
300
200
100
i
(μa./cm2)
100
- 110 -
200
(μa)
0
5
cathodic
500
1000
E vs. RHE

Fig. 54 Os

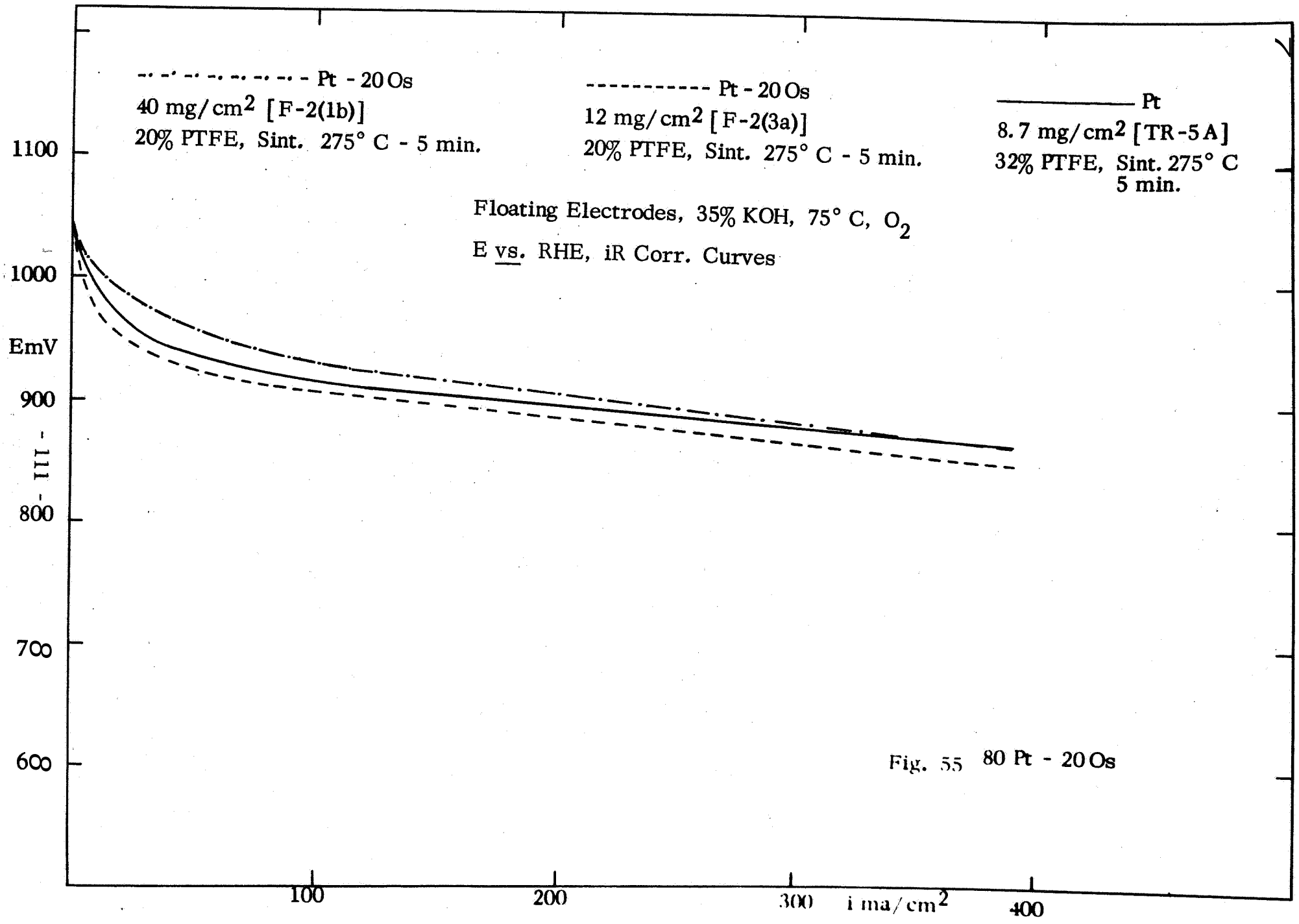

Fig. 55 80 Pt - 20 Os

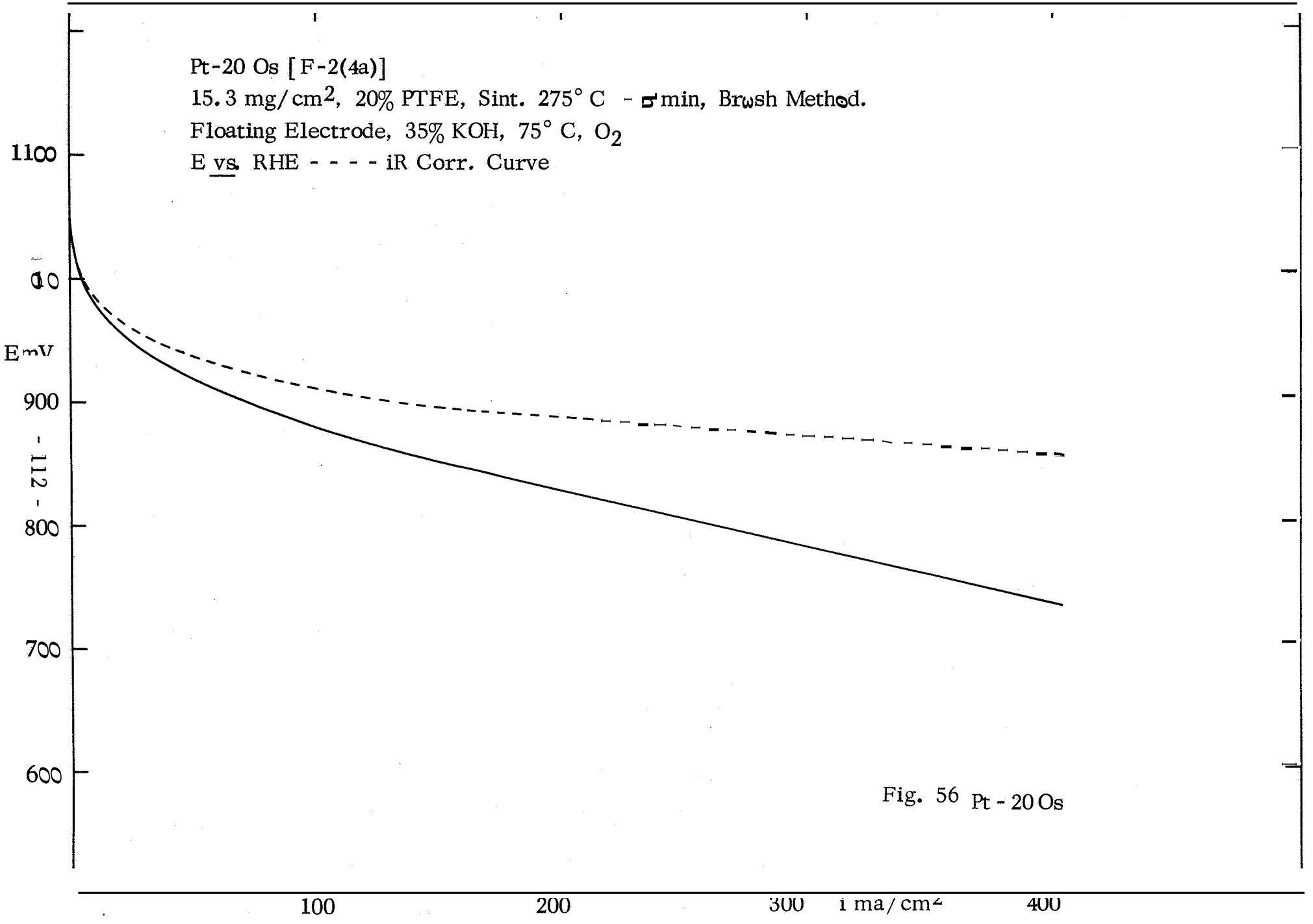

Fig. 56 Pt - 20 Os

V. SINGLE CRYSTALS OF SILICON CARBIDE

A. Introduction

Single crystalline 6H-a!-silicon carbide most frequently grows in the direction of the c-axis, and consequently the largest surfaces will be the (0001) planes. These surfaces are monatomic, one side showing silicon atoms and the opposing parallel surface only carbon atoms. The surface composition is unalterable (by polishing or grinding) in a direction perpendicular to these planes; consequently, it should be possible to prepare a monatomically surfaced sample of SiC by cutting and polishing a platelet in a direction normal to the growth direction. The electrochemical behavior of SiC prepared in this manner will exhibit equal or different characteristics, depending on the relative importance of continuum or atomic properties of this catalyst. The actual orientation can be verified by observing the etch pit formation obtained in ClF_3.

B. Experimental

A piece of silicon carbide was obtained which exhibited one flat face and appeared to be a single crystal throughout the area of this surface. The polycrystalline material extending parallel to this face was cut off; the opposing side was ground parallel to the flat surface and polished. One side of the sample was then vapor-plated with gold and topped with highly conductive silver epoxy for optimum electrical contact to the silicon carbide. The sample was then mounted in Koldmount and tested in the rotating electrode assembly in 2N KOH at 25°C. The same procedure was used to mount and test the opposing side of the crystal. When the testing was completed, the crystal orientation with respect to silicon and carbon was determined by the etch pit formation in ClF_3; (the silicon side shows hexagonal pits).

C. Results and Conclusions

Both surfaces, carbon and silicon, of the SiC crystal showed activity for O_2-reduction. However, there are some differences between the two surfaces which could be related to the surface composition. The open circuit

potential, though not a completely reliable parameter here, is higher on the carbon side of the crystal (700 mv vs. 500 mv). The initial cathodic current on the carbon side is observed at 525 mv vs. **RHE,** compared with 375 mv for the silicon side. The cathodic current at 0.0 mv is 34 μa for the carbon side and 15 pa for the silicoii side (same geometric area on both sides), Figs. 57 and 58. The sweeps made at 50 mv/min, from which the above data were taken, were started from the observed open circuit potentials. The subsequent sweeps, run at 500 mv/min, show the effects of sweeps between different potentials (Figs. 59-64). For example, the effect of sweeping to 1000 mv is different for the two sides of the crystal; On the silicoii side the activity is increased in the subsequent down sweep, whereas the activity on the carbon side is somewhat decreased under the same conditions (Figs. 59 and 60).

These differences suggest that for SiC continuum factors are not the dominant factor in the rate of reduction of O_2.

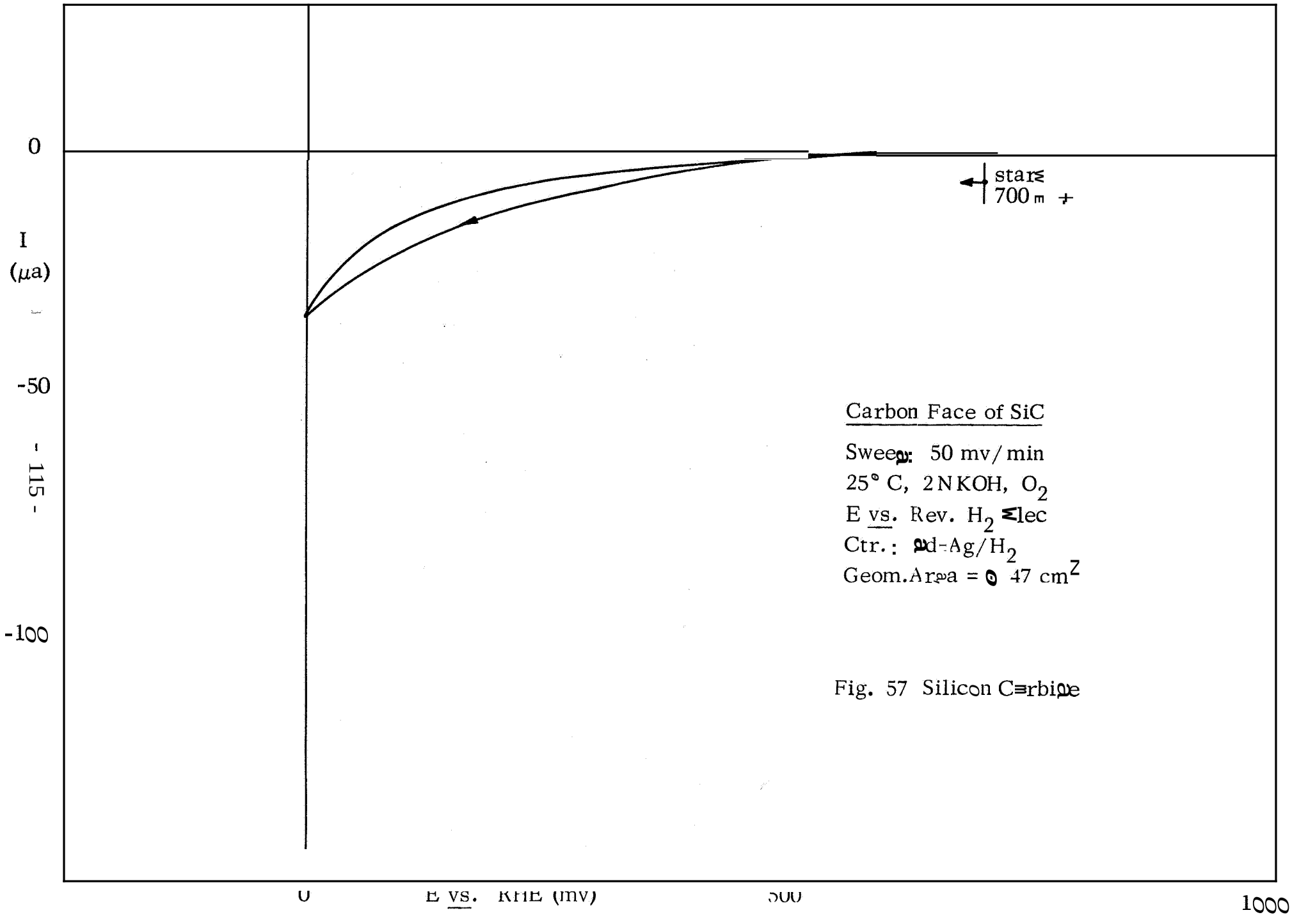

Fig. 57 Silicon Carbide

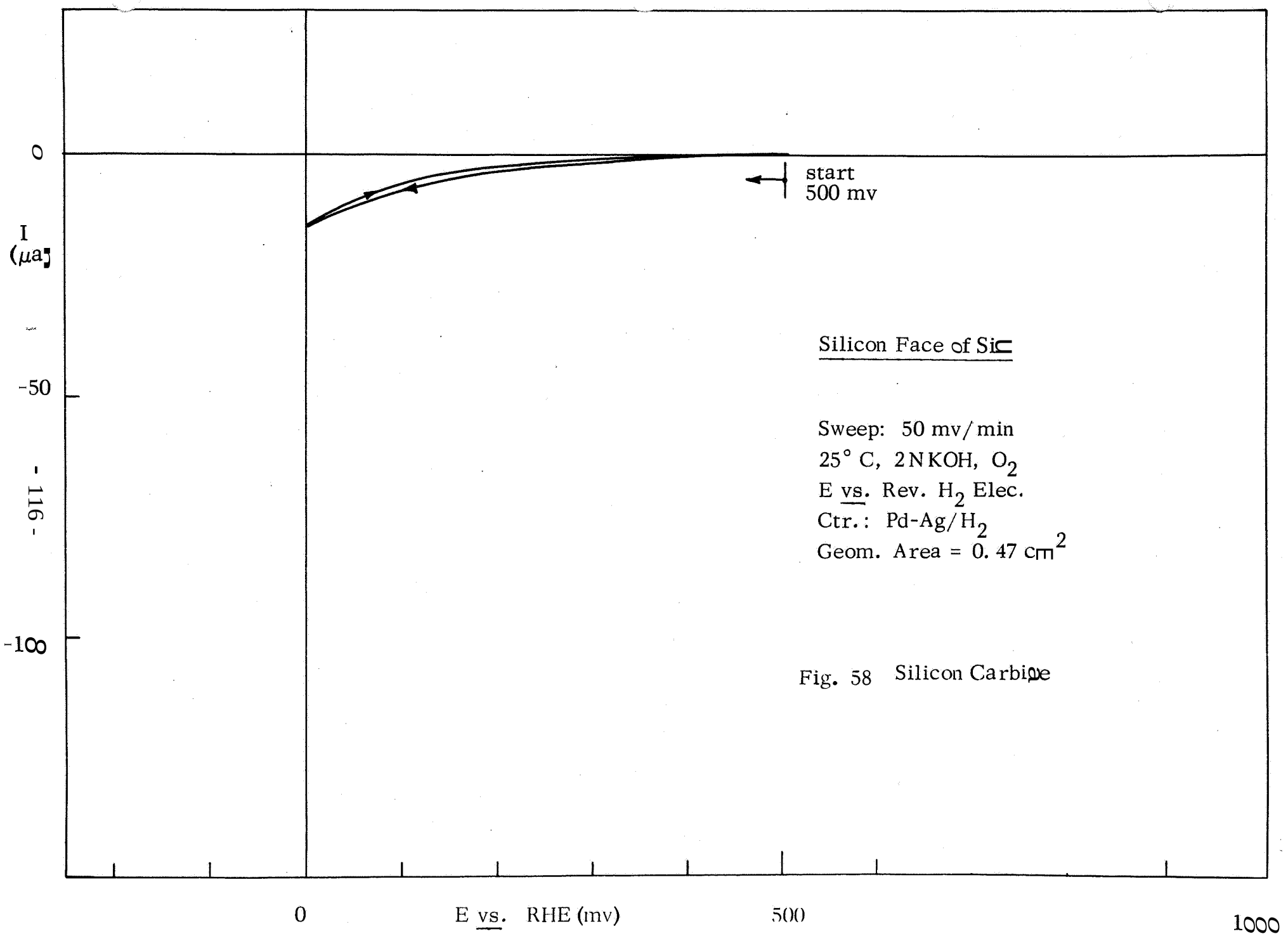

Fig. 58 Silicon Carbide

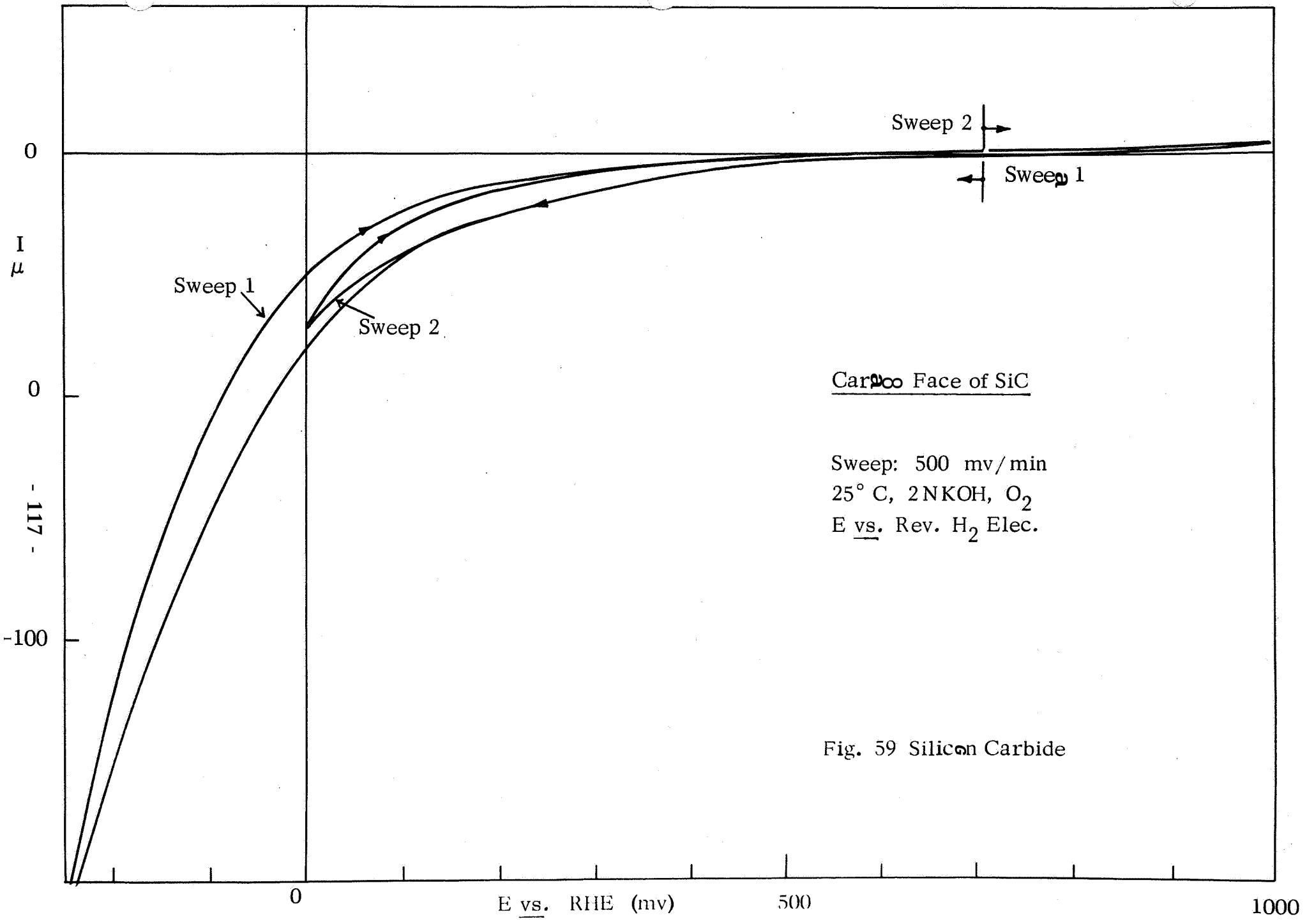

Fig. 59 Silicon Carbide

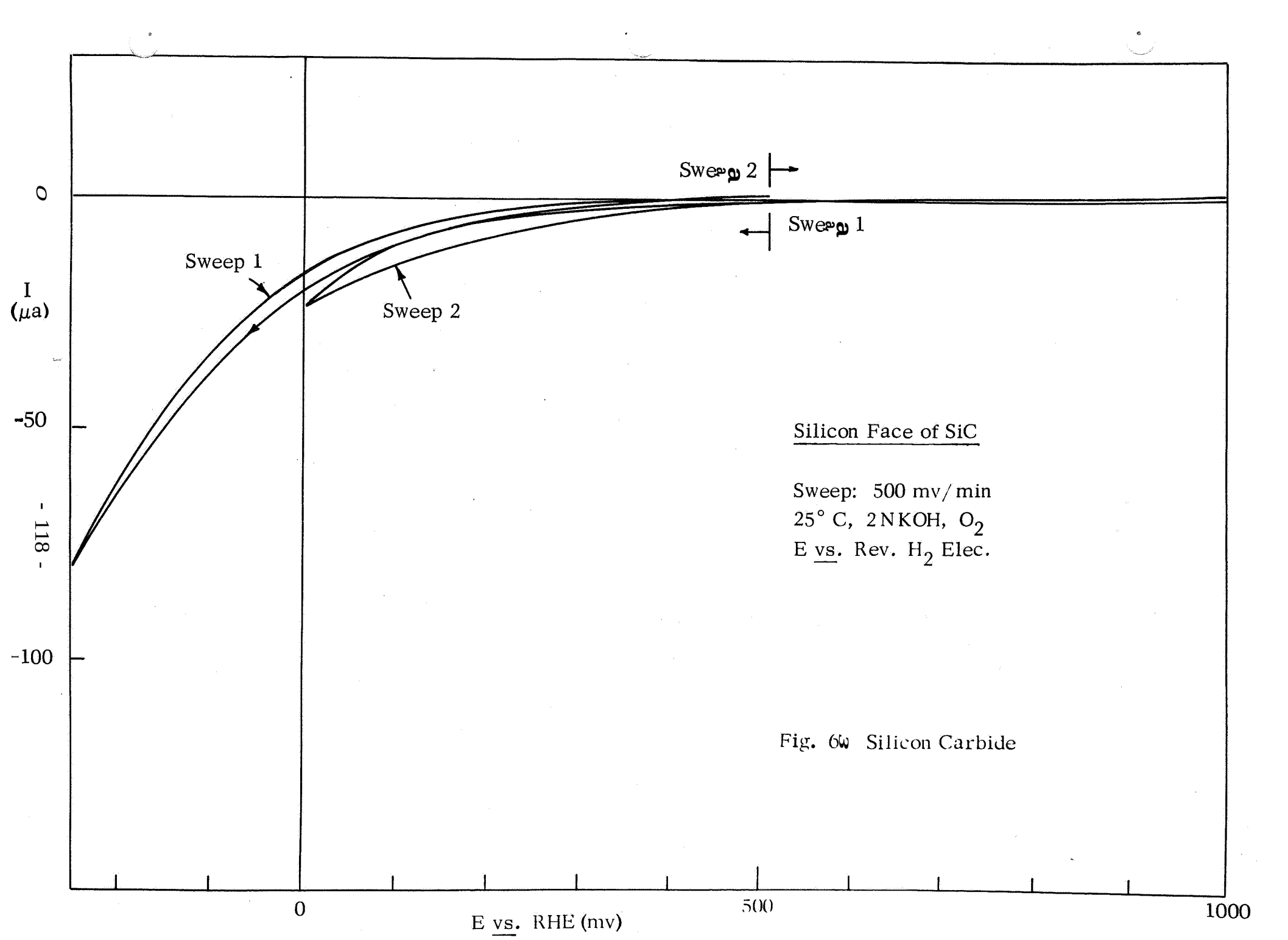

Fig. 6ω Silicon Carbide

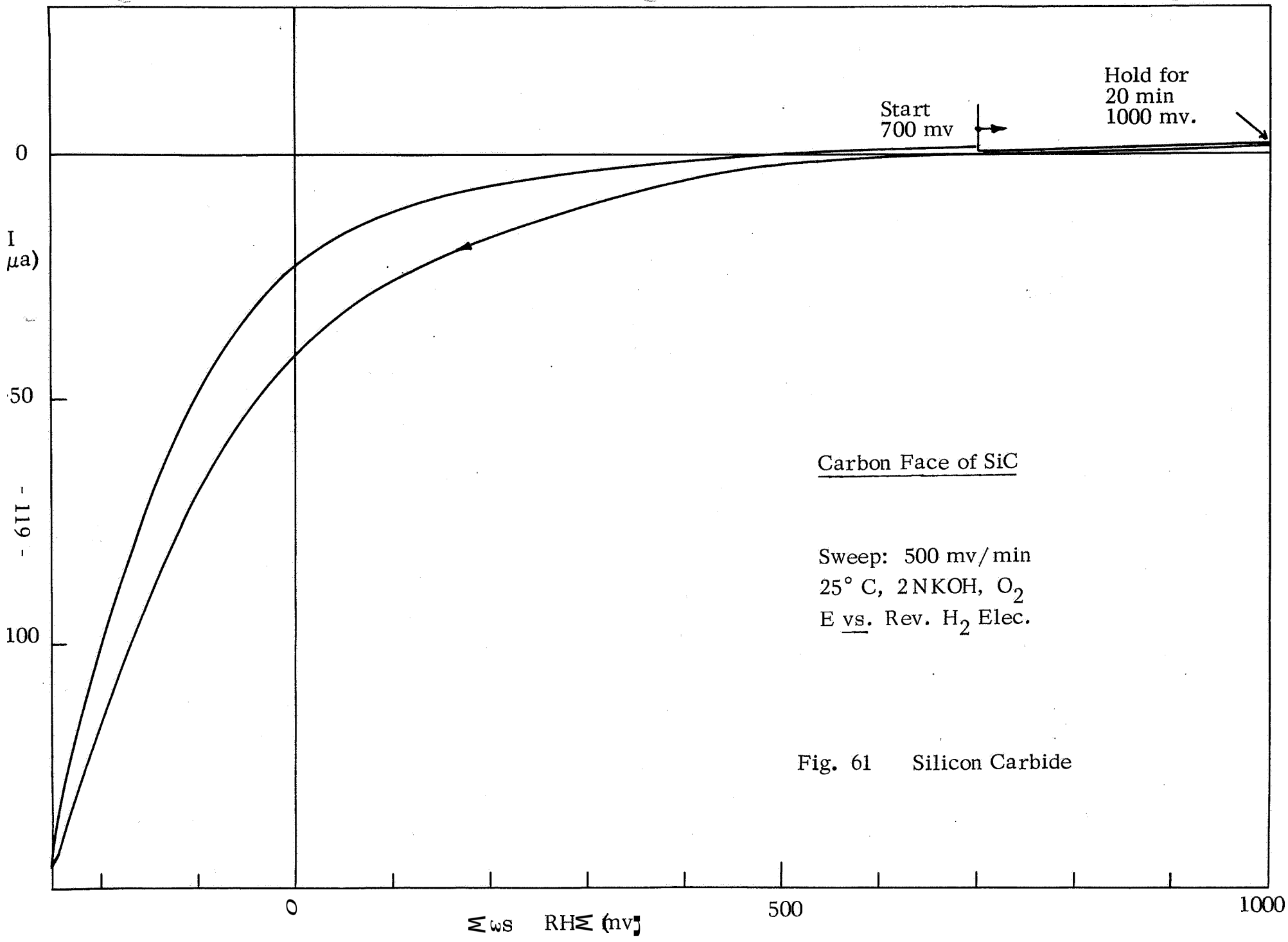

Fig. 61 Silicon Carbide

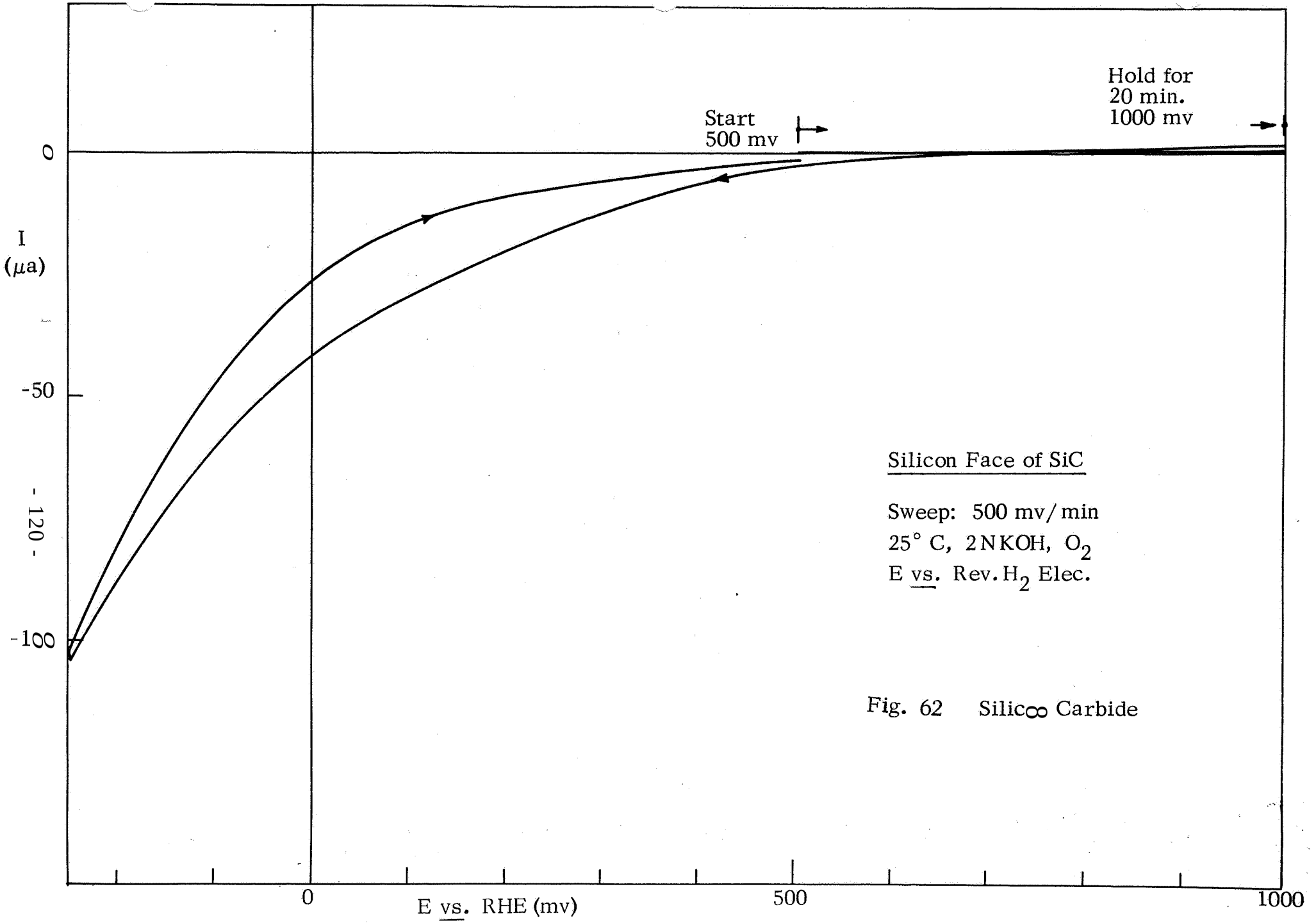

Fig. 62 Silicoo Carbide

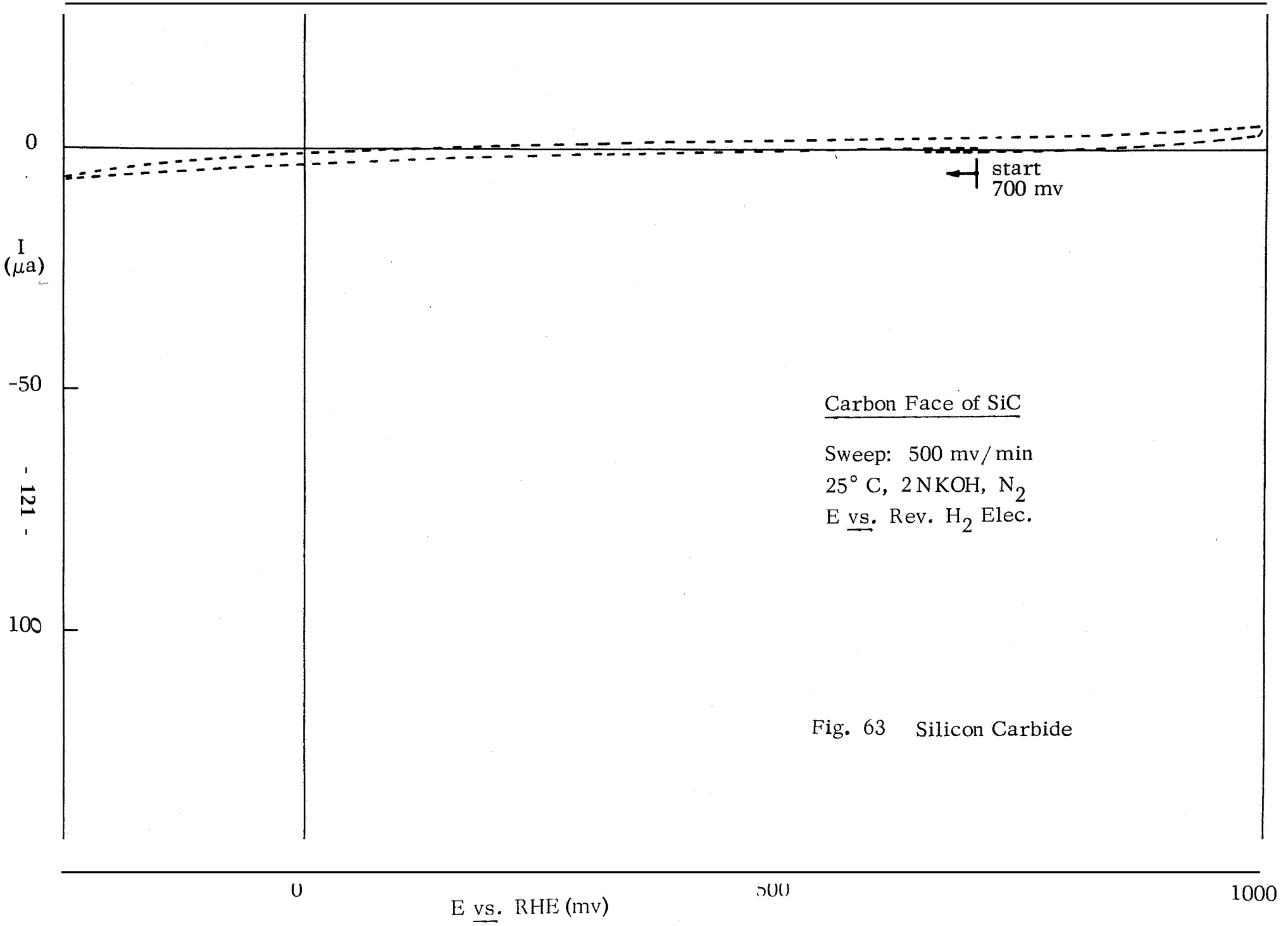

Fig. 63 Silicon Carbide

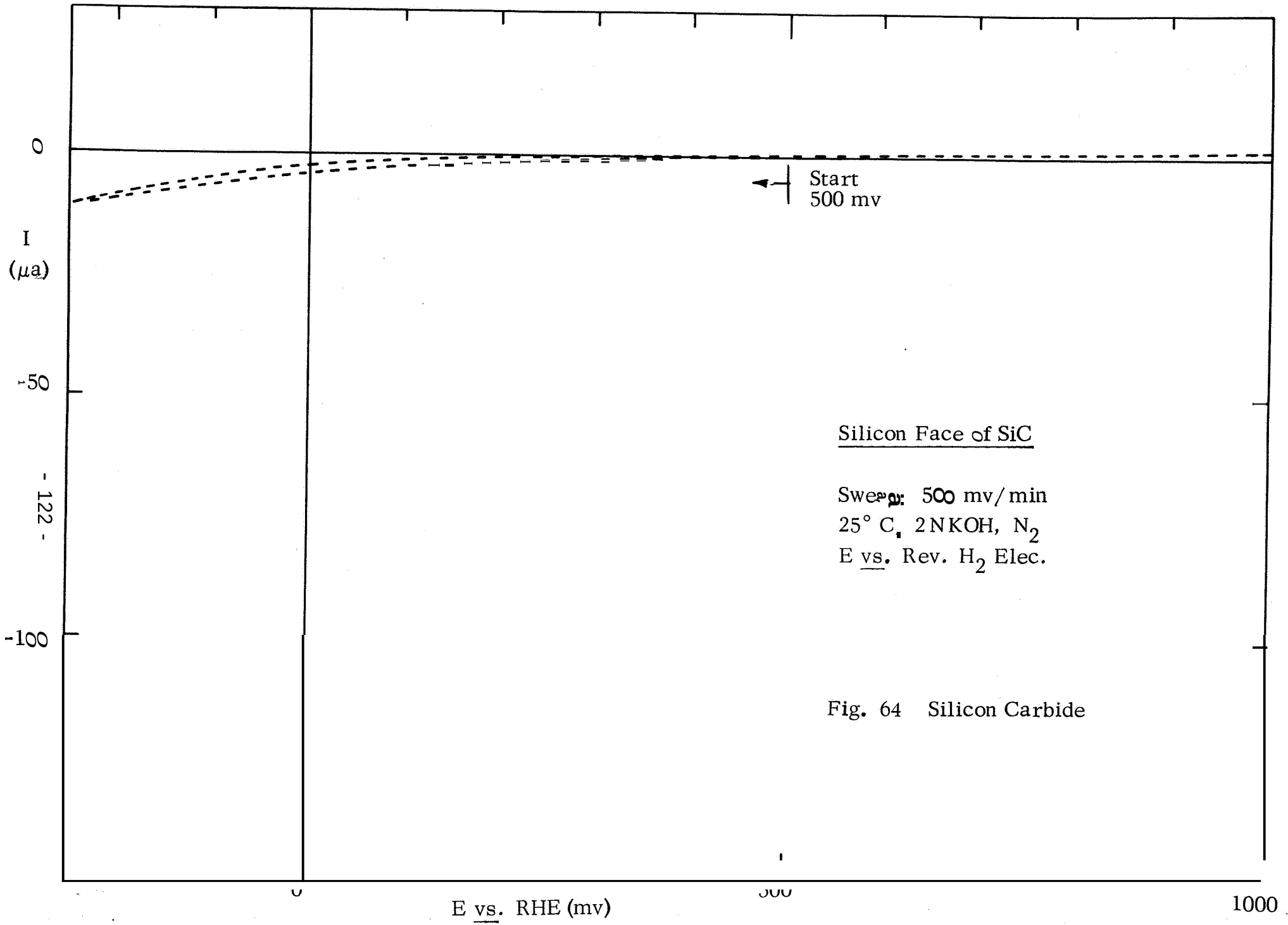

Fig. 64 Silicon Carbide

VI. BARIUM TANTALATE

Figures 65-68 show the results obtained on a sample of $BaTiO_3$ in gold supplied by the University of Pennsylvania. The main characteristics observed were those of Au. The sample, a solid cylinder, was tested as a rotating disc exposing only the base of the cylinder. Both faces were tested. One side (Figs. 65 and 66) shows basically Au behavior with some corrosion. Under N_2 (Fig. 67), the other side showed large residual currents which will be further investigated. Under O_2 (Fig. 68) the behavior was essentially the same except for the addition of the cathodic current due to O_2 reduction on Au. The University of Pennsylvania will be approached to obtain pure $BaTaO_3$ (without Au).

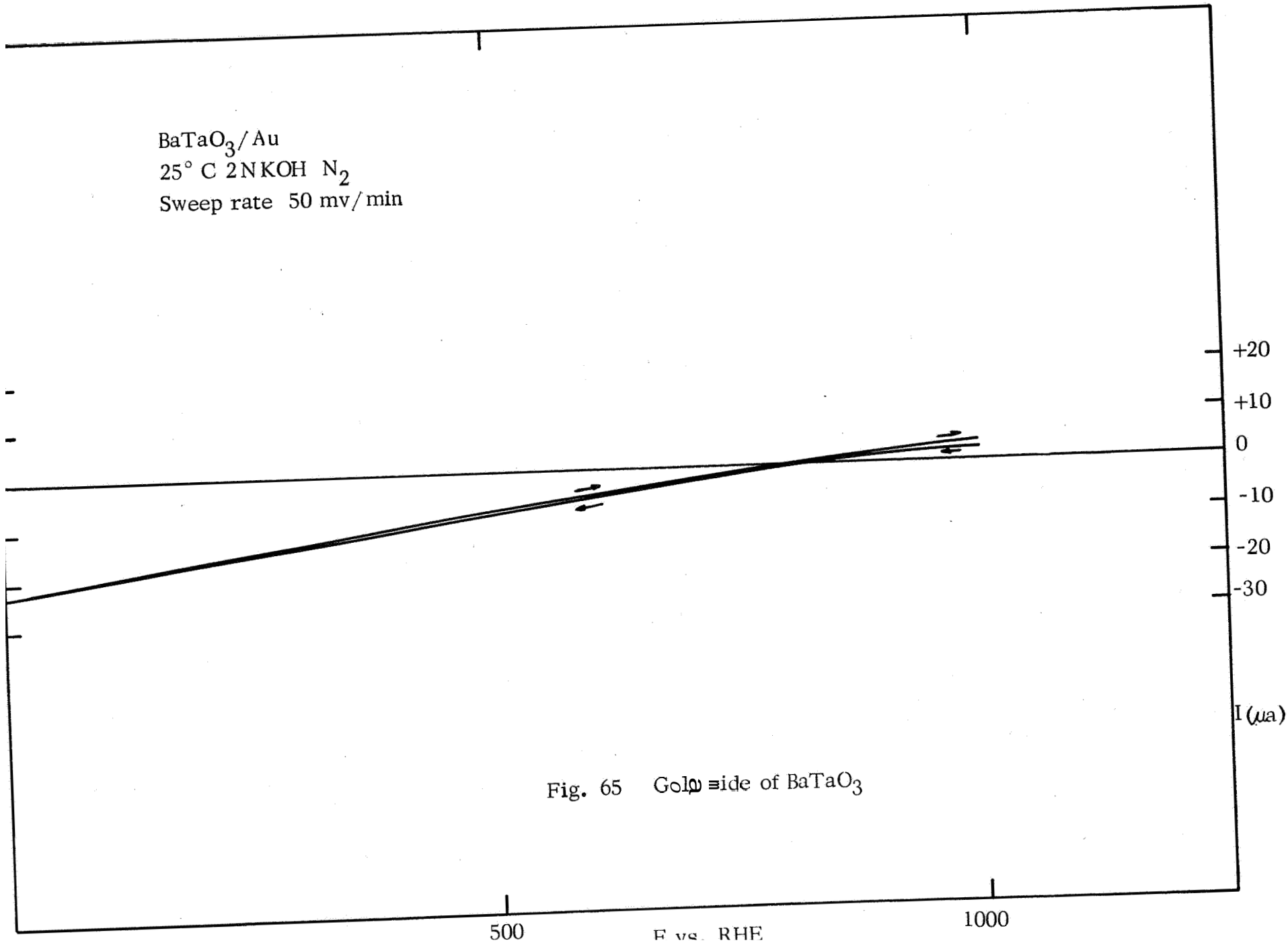

Fig. 65 Gold side of $BaTaO_3$

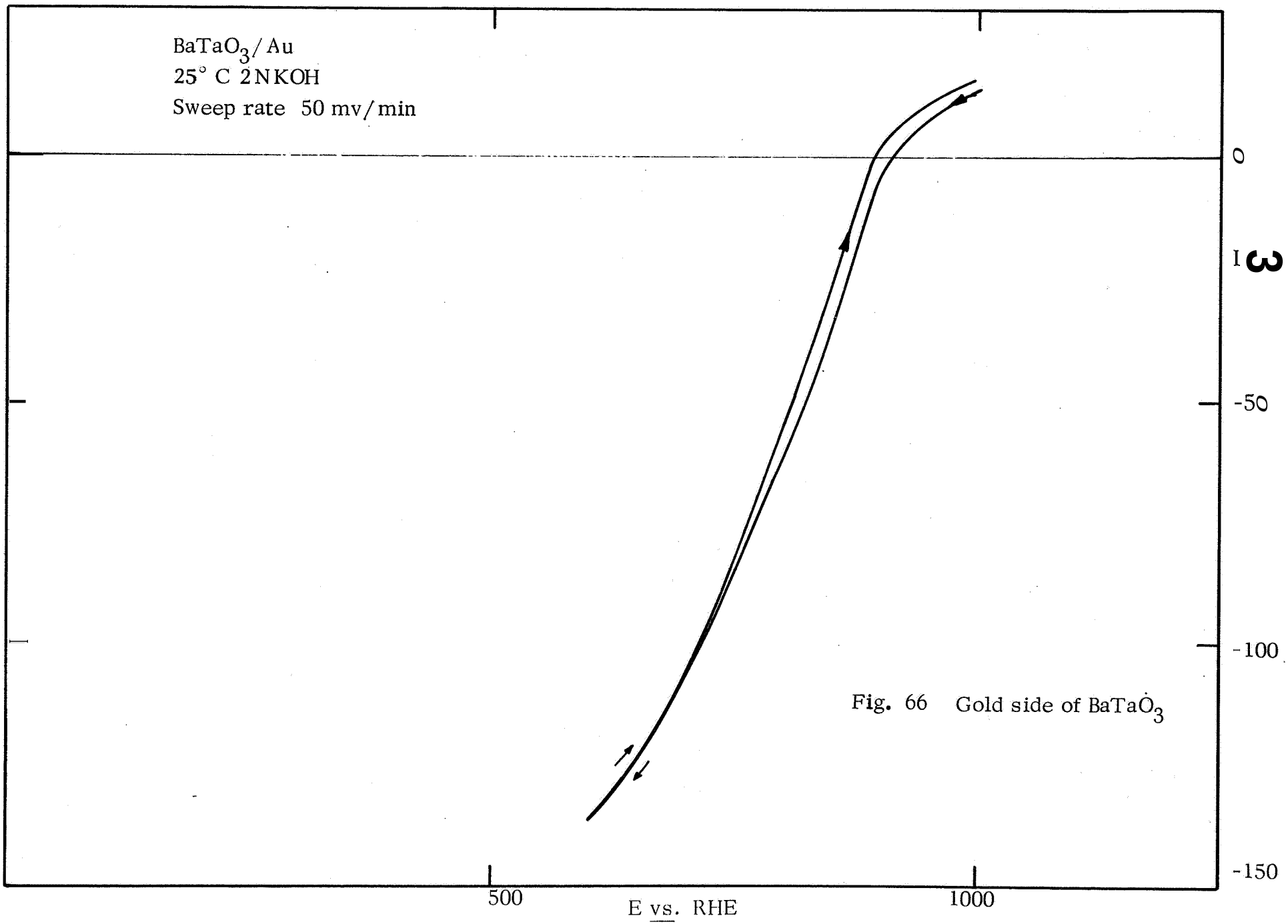

Fig. 66 Gold side of $BaTaO_3$

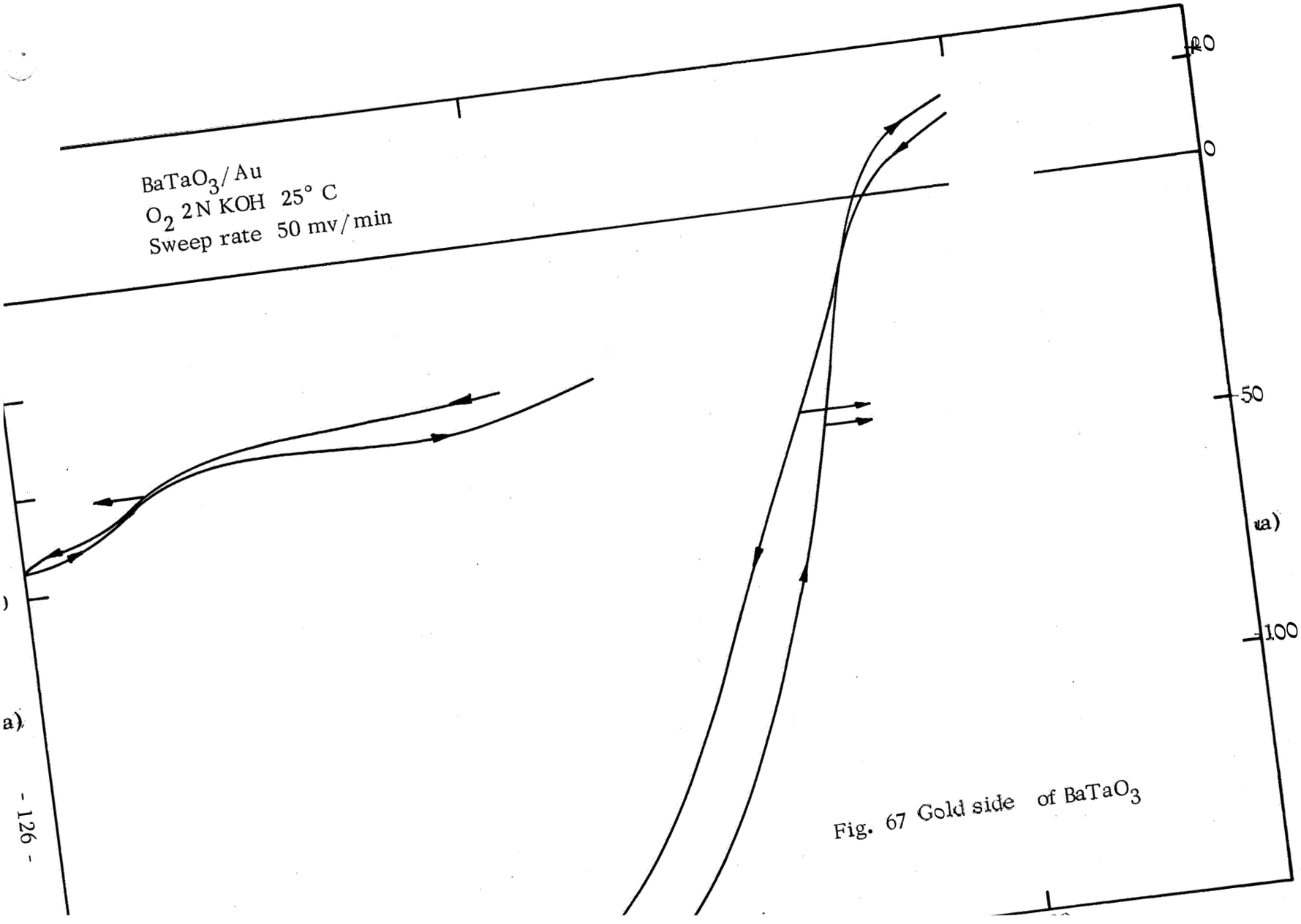

Fig. 67 Gold side of $BaTaO_3$

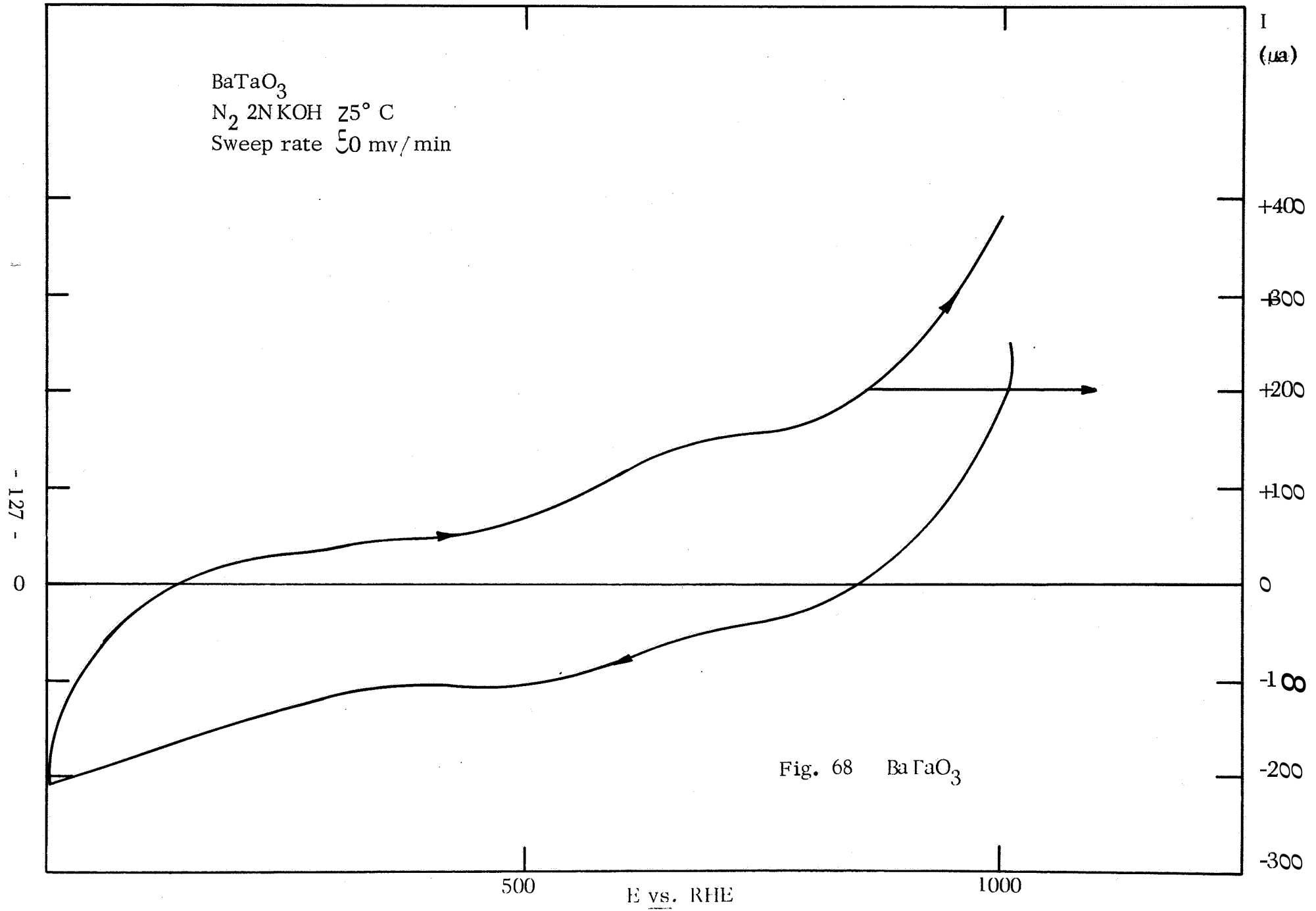

Fig. 68 $BaTaO_3$

SECTION 3

INTERSTITIAL COMPOUNDS OF GROUP VIII METALS (POROUS ELECTRODES)

I. BUREAU OF MINES' CATALYSTS

A. Introduction

The carbides, nitrides, carbonitrides and nitrocarbides of iron, nickel, and cobalt are an interesting group of catalysts many of which have been investigated in detail in connection with the Fischer-Tropsch reaction[29]. Because of their metallic properties and their possible enhanced resistance to oxidation as compared with their parent metals, this class of materials presented attractive possibilities as oxygen reduction electrocatalysts. Measurements with porous Ni_3C electrodes described in the previous section showed very high activity for O_2-reduction, at least for short-term measurements. In addition, initial measurements on an iron rod carbided on the surface demonstrated that iron carbide had a somewhat higher activity than pure Fe.

A range of interstitial compounds of Fe, Ni, and Co in finely divided form were prepared by the Bureau of Mines as part of a cooperative program. A total of 178 electrodes based on these catalysts were tested at Tyco. These are listed, with a guide to their activity and corrosion resistance, in Table XVI. Several samples of Ni_3C were also prepared in our laboratory; these are listed separately and discussed later.

B. Experimental

The testing of highly dispersed catalysts presents many problems that are not experienced with the testing of solid electrodes. These are discussed in detail before the presentation of the data on the interstitials, because the interpretation of the data depends to a great extent on an appreciation of these problems.

TABLE XVI

Iron Carbides

	Catalyst	Inducted	mg/cm^2	% PTFE	ma/cm^2 at 900 mv	ma/cm^2 at 750 mv	ma/cm^2 at 600 mv	Comments
2C (i)	≤ Fe_2C/Fe_3O_4	No	~ [illegible]	[illegible]% *	---	---	---	Anodic
2C (ii)a		Yes	~ [illegible]	[illegible]%	---	---	1.0	
2C (ii)b		Yes	~ [illegible]	[illegible]%	---	---	11.0	
4[illegible]	× Fe_2C/Fe_3O_4	No	~ 10	[illegible]%*	---	---	1.0	
6C (i)	χ $Fe_2C + \theta Fe_3C$	Yes	~ 10	[illegible]% *				Anodic
6C (ii)		No	~ 10	19%			4.0	
10C	θ-Fe_3C + Fe	Yes	~ 10	10%*	---	---	3.4	
11C	See TABLE XX							

* Elvax bonding

TABLE XVI (Cont.)

Iron Nitride

Electrode	Catalyst	Inducted	mg/cm^2	% PTFE	ma/cm^2 at 900 mv	ma/cm^2 at 750 mv	ma/cm^2 at 600 mv	Comments
2N (i)	γ Fe_4N + ε - Fe_3N	Yes	~ 30	10*			6	
2N (ii)	"	No	~ 30	19			3	
5N (i)	ε-Fe_3N + γ Fe_4N	Yes		10 *			6	
5N (i)	"	No		10			58	
6N (i)a	ε-Fe_3N + ζ-Fe_2N	Yes		10*			1.3	
6N (i)b	"	Yes		10*			2.5	
6N (ii)a	"	No		19			53.0	
6N (ii)b	"	No		19			2.6	
8N	γ Fe_4N	Yes		10*			6.4	
9N (i)	ζ-Fe_2N	Yes		10*			3.0	
9N (i)	"	No		10			7.0	
11N	ε Fe_3N + Ag	Yes		10 *			14.8	Fe/Ag = 3/1
13N (i)a	ε Fe_3N	"		10*			12.4	
13N (ii)a	"	Yes		10			Anodic	
15N	ε Fe_3N + Ag	Yes		10*			19.4	Fe/Ag = 1/1
16N	ε-Fe_3N + Ag	Yes		10*			14.4	Fe/Ag = 1/3
18N	ζ Fe_2N + ε Fe_3N	Yes		10*			Anodic	

* Elvax bonded

TABLE XVI (Cont.)

Iron Nitrocarbides

Electrode	Catalyst	Inducted	mg/cm^2	% PTFE	ma/cm^2 at 900 mv	ma/cm^2 at 750 mv	ma/cm^2 at 600 mv	Comments
1 NC (i)	≤ Fe_2X + Fe_3O_4	Yes		10*			3.2	
1NC (ii)		Yes		[illegible]			3.2	
2 NC (i)a	χ Fe_2X + ≤ Fe_2X + C	Yes		10*			3.5	
2NC (i)b		Yes		[illegible] *			0.4	
2NC (ii)a		Yes		[illegible]			68.0	
2NC (ii)b		Yes		[illegible]			5.2	
3NC	≤ Fe_2X	Yes		10 *			1.6	
4NC	≤ Fe_2X	Yes		10*			Anodic	
5NC	θ Fe_3X	Yes		10 *			5.4	
6NC	χ Fe_2X	Yes		[illegible]*			1.2	
7NC (i)	θ Fe_3X	Yes		10*			Anodic	
7 NC (ii)		Yes		10			Anodic	

* Elvax bonded
X = C, N

TABLE XVI (Cont.)

Iron Carbonitrides

Electrode	Catalyst	Inducted mg/cm^2	% PTFE	ma/cm^2 at 900 mv	ma/cm^2 at 750 mv	ma/cm^2 at 600 mv	Comments
1CN	ϵ Fe_2X	No	[illegible]			1.0	
2CN (i)	ϵ Fe_2X	Yes	10			2.9	
2CN (ii)	"	Yes	[illegible]*			Anodic	
3CN	ϵ Fe_2X	Yes	[illegible]*			Anodic	
6CN	ϵ-Fe_2X +Ag	Yes	10*			7.0	Fe/Ag = 3/1
7CN	ϵ-Fe_2X +Ag	Yes	[illegible]*			11.6	Fe/Ag = 1
8CN	ϵ-Fe_2X +Ag	Yes	10*			5.4	Fe/Ag = 3/1
9CN	γ'-Fe_4X	Yes	[illegible]*			Anodic	
[illegible]CM	γ'-Fe_4X	Yes	[illegible]*			1.9	

* Elvax bonded
X = C.N

TABLE XVI (Cont.)

Coprecipitated Iron and Silver Catalysts

Electrode	Catalyst	Inducted	mg/cm^2	% PTFE	ma/cm^2 at 900 mv	ma/cm^2 at 750 mv	ma/cm^2 at 600mv	Comments
1 CP	$Fe(OH)_3 + Ag_2O$	No	20	5*			1.0	Fe/Ag = 3/1
2 CP	"	No	20	10*			92	Fe/Ag = 1/1
3 CP	"	No	20	8*			59	Fe/Ag = 1/3

* Elvax bonded

TABLE XVI (Cont.)

Raney Alloys of Ni and Co

(with A Silver Gold Palladium and Platinum

Electrode	Ca	Impregnated	mg/cm^2	% PTFE	ma/cm^2 at 900 mv	ma/cm^2 at 750 mv	ma/cm^2 at 600 mv	Comments
RAL 1 (i)a		No	37.0	20		17/20	5/5.6	
RAL 1 (ii)a		Yes	51 0	20		3.4/2	6.3/3.5	
RAL 1 (ii)b		Yes	37.0	20		3.6/2.8	7.0/6.0	
RAL 2 (i)a		No	45.2	20		20.6/3.2	13/12	
RAL 3 (ii)a		Yes	45.0	20		1/0.5	2.3/3.6	
RAL 2 (ii)b		Yes	34.0	20		3.6/3.6	10.8/13.5	
RAL 3 (i)a	3 N	No	36.0	20		32/36	60/64	
RAL 3 (ii)a		Yes	32.0	20		4.8/6.0	12.9/16.2	
RAL 3 (ii)b		Yes	35.0	20		7/11 5	19/26.5	
RAL 4 (i)a	N	Yes	31	20	10/11	39/44	39/44	

TABLE XVI (Cont.)

Electrode	Catalyst	Inducted	mg/cm^2	% PTFE	ma/cm^2 at 900 mv	ma/cm^2 at 750 mv	ma/cm^2 at 600 mv	Comments
RAL 4 (i)b	Ni/3Ag	Yes	33.0	20	27/32			
RAL 4 (ii)a	"	No	46.3	20		26/26	76/84	
RAL 4 (i)c	"	Yes	33.0	20		40/82	140/191	
RAL 5	Ni/Ag	No	3[illegible].9	20		4/4	12/30	
RAL 5	"	Yes	38.0	20	18/75			
RAL 5	"	Yes	31 0	20	11.5/27.5	96/168		
RAL 14 (i)a	Ni P[illegible]	No	21 0	30		0	0.25	
RAL 14 (ii)a	"	Yes	26.0	30		0.2	0.2	
RAL 17 (i)a	Ni Au Pd	No	3	30		80/100	145/162	
RAL 17 (ii)a	"	Yes	18	30	45/65	300/315		
RA> 21 (i)a	Ni Ag [illegible]	No	21	30	22.5/47	170/250		
RAL 21 (ii)a	"	Yes	20	30	15/48	132/232		

TABLE XVI (C t.)

Carbides of Nick◎l and Cobalt

Electrode	Catalyst	Inducted	mg/cm^2	% PTFE	ma/cm^2 at 900 mv	ma/cm^2 at 750 mv	ma/cm^2 at 600 mv	Comments
19C (i)	Ni_3C	Yes	51	20	---	/4	21/14	
19C (ii)		No	49	20	---	/3.5	46/18	
19C (iii)		No	68	E	---	13/2.5	19/7	
19C (iv)		No	48	20	---	14/10	55/29	
19C (v)		No	60	15	---	37/14	94/44	
19C (vi)		No	79	10		16/8	38/18	
19C (vii)		No	58	E		20/9	69/38	
20C (i)	Co_2C	Yes	35.5	10	---	0.4/0.4	0.8/1.0	electrolyte turned blue
20C (ii)		No	57.4	10	---	10/9	43/35	"
25C (i)a	Ni/Co C	Yes	60 4	20	---	16/2	43/6	
25C (ii)a		No	49.5	20	---	6/2	19/6	

TABLE XVI (Conω)

Electrode	C	Inducted	mg/cm^2	% PTFE	ma/cm^2 at 900 mv	ma/cm^2 at 750 mv	ma/cm^2 at 600 mv	Comments
26C	N CoC	No	45.5	30	---	12/6	28/15	
26C (i)b	N CoC	No	41 0	30		6/10	16/23	
26C (ii)a		Yes	55.0	30		4/anodic	11/2	
26C (iii)a		No	56.0	20		7/anodic	13/1	
26C (iv)a		Yes	61.0	20		anodic	18/2	
26C (iv)b		Yes	39.0	20		7/0.3	16/1	
27C (i)a	N CoC	Yes	46.7	20		24/24	72/72	sweep metho
27C (i)b		Yes	51.4	20		14/15	44/44	"
27C (ii)a		No	63.4	20		13/14	36/40	"
27C (ii)b		No	45.1	20		14/13	34/34	"
28C	N C N	Yes	----	Partially Impregnated		1.2/12	5/19	Carbided Ni plaque
28C (ii)	N C N	No		Partially Impregnated		1.8/7.2	5/8.5	

TABLE XVI (Cont.)

Electrode	Catalyst	Inducted	mg/cm^2	% PTFE	ma/cm^2 at 900 mv	ma/cm^2 at 750 mv	ma/cm^2 at 600 mv	Comments
38C (iii)	Ni_3C + Ni	No		None		0.3/0.6	0.7/1.1	
	Ni			Partially Impregnated		0.9/2.9	3.8/10.8	
36C (i)a	Ni_3C	Yes	38.0	20		3/3	8/8	
36C (ii)a	"	Yes	22.0	40		10/12	29/30	sweep method
36C (iii)a	"	No	40.0	20		0.25/0.25	0.5/0.5	"
36C (iv)a	"	No	29.0	40		1.5/2	5.5/6.5	"
40C (i)a	Ni/Co/AgC	Yes	24.0	20		2.5/4	7.0/9.5	"
40C (ii)a	"	No	30.0	20		1.5/1.5	2.5/2.5	"
40C (iii)a	"	No	26.0	30		0.7/0.7	1.0/1.0	"
40C (iv)a	"	Yes	32.0	30		0/0.2	0.5/1	"
40C (iv)b	"	Yes	25.0	30		2/2.5	2.5/3.0	"
41C (i)a	Ni/Co/AuC	No	24.0	30		3/2	6/4.5	"
41C (ii)a	"	Yes	31.0	30		19/35	53/72	"
41C (ii)b	"	Yes	36.0	30		20/25	44/51	"

TABLE XVI (Cont.)

Electrode	Catalyst	Inducted	mg/cm^2	% PTFE	ma/cm^2 at 900 mv	ma/cm^2 at 750 mv	ma/cm^2 at 600 mv	Comments
44C (i)a	Ni/Ag/AuC	No	18.0	30	17.5/18.5	90/95	177/180	sweep method
44C (i)a	"	Yes	20.0	30	48/48	355/355		limiting current at 750 mv
45C (i)a	Co/Ag/AuC	No	15.0	30		40/60	113/140	sweep method
45C (i)a	'	Yes	12.0	30		28/39	82/95	"
50C (i)a	3 Ni/Co C	No	10.9	30		4/8	11/17	"
50C (i)b	"	No	5.2	30		12/14	28/31	"
50C (i)a	"	Yes	9.7	30		14/16	33/37	"
50C (i)b	"	Yes	11.3	30		3.5/4	7.5/9	"
53C (i)a	Ni/AgC	No	20.6	30		18/26	41.5/50	"
53C (ii)a	'	Yes	24.4	30		23/12	25/21	"
54C (i)a	Ni_3C	No	23.4	20		22.5/49	100/126	"
55C (i)a	Ni C	No	20.2	30		0.5/0.5	1/1	"
55C (i)b	'	No	16.4	30		23/34	48/64	"

TABLE XVI (C t.)

Electrode	Catalyst	Inducted	mg/cm^2	% PTFE	ma/cm^2 at 900 mv	ma/cm^2 at 750 mv	ma/cm^2 at 600 mv	Comments
55C (ii)a	Ni/Pd C	Yes	24.8	30		10/14	19/23	slow sweep method
58C (i)a	3 Ni/Co C	No	10	30		52/50	125/120	"
58C (ii)a	"	Yes	13.4	30		3/3	3.5/3.5	"

TABLE XVI (Cont.)

Nitrocarbides of Nickel and Cobalt

Electrode	Catalyst	Inducted	mg/cm^2	% PTFE	ma/cm^2 at 900 mv	ma/cm^2 at 750 mv	ma/cm^2 at 600 mv	Comments
11 NC (i)a	Ni_3NC	Yes	45.4	20		8/1.5	23/5	
11 NC (ii)a	"	No	57.4	20		10/9	43/35	
12 NC (i)a	Co_2NC	No	45.5	10		0 1	0 7	
12 NC (ii)a	'	Yes	37.0	10		0 2	0 5	
13 NC (i)a	Ni/3 Co NC	No	45.0	20		anodic/5	49/12	
13 NC (ii)a		Yes	50.0	20		10/anodic	27/1	
15 NC (i)a	3 Ni/Co NC	Yes	56.4	20		14/11	33/28	sweep method
15 NC (i)b		Yes	52.0	20				corrosion test see Fig.
15 NC (ii)a	3 Ni/Co NC	No	49.2	20		18/16	44/42	sweep method
16 NC (i)a	Ni/Co NC	Yes	49.7	20		11/13	37/27	"
16 NC (ii)a	'	No	53.2	20		25/22.5	68/68	"
24 NC (i)a	Ni_3NC	No	23.0	30		3/3	7/7.5	"

TABLE XVI (Cont.)

Electrode	Catalyst	Inducted	mg/cm^2	% PTFE	ma/cm^2 at 900 mv	ma/cm^2 at 750 mv	ma/cm^2 at 600 mv	Comments
24 NC (ii)a	Ni_3NC	Yes	28.0	30		2.5/3	7.5/9	sweep method
27 NC (i)a	Ni/Co/Ag NC	No	23.0	30		3/4	6.5/9.5	"
27 NC (ii)a	"	Yes	28.0	30		1/1.5	2/2.5	"
27 NC (ii)b	"	Yes	17.0	30		1/3	4/8.5	"
29 NC (i)a	Ni/Co/Au NC	No	30	30		0.5/0 5	1/1	"
29 NC (ii)a		Yes	25	30		5/6.5	11.5/13.5	"
29 NC (i)b	Ni/Co/Au NC	Yes	34.0	30		5.5/7	12.5/15	"
30 NC (i)a	Ni Ag Au NC	No	22.0	30	45/45	325/325		"
30 NC (ii)a	"	Yes	23.0	30	49/49	340/340		"
33 NC (i)a	Co Ag Au NC	No	16.0	30		82/115	230/257	"
33 NC (ii)a	"	Yes	20.0	30		70/90	200/225	"
37 NC (i)a	3 Ni/Co NC	No	10.2	30		9/21	28/49	"
36 NC (ii)a	"	Yes	20 6	30		18/26	41.5/50	"

TABLE XVI (Cont.)

Electrode	Catalyst	Inducted	mg/cm^2	% PTFE	ma/cm^2 at 900 mv	ma/cm^2 at 750 mv	ma/cm^2 at 600 mv	Comments
37 NC	3 Ni/Co NC	No	16.7	30		3/3	4/4	Sweep method
37 NC	"	Yes	9.4	30		1.5/2	3.5/4	"

TABLE XVI (Cont.)

Catalysts from Alternative Starting Materials to Raney Alloys

Electrode	Catalyst	Inducted	mg/cm^2	% PTFE	ma/cm^2 at 900 mv	ma/cm^2 at 750 mv	ma/cm^2 at 600 mv	Comments
50R (i)a	3 Ni/Co	No	8.2	30		33/37	85/92	sweep method
50R (i)b	"	No	9.9	30		40/46	105/112	"
50R (ii)a	"	Yes	10.1	30		22/22	44/44	"
50R (ii)b	"	Yes	11.5	30		43/90	185/225	"
53R	Ni/Ag	No	12.6	30		95/100	195/207	"
53R	"	Yes	16.3	30		100/105	200/210	"
54R	Ni	No	22.5	30		43/48	130/145	"
54R	Ni	Yes	22.7	30		83/92	150/160	"

The high area surface of a catalyst is not used to its full advantage unless the electrode structure into which it is incorporated offers good mass transport characteristics to all regions of the surface. The plastic (PTFE) bonded electrode[30] undoubtedly comes closest to realizing this objective for a practical catalyst.

In these electrodes the catalyst is mixed with a dispersion of PTFE and spread on a nickel screen. The effectiveness of this structure depends on (a) the hydrophobic nature of the binder to provide gas contact to the interior surfaces of the electrode and (b) the porosity of the catalyst (the pores fill with electrolyte by capillary action) to provide electrolyte contact at all the reaction sites of the surface. Thus a catalyst of good intrinsic activity, in a highly dispersed form, must also have a pore structure conducive to the mass traiisport requirements of normal operation.

In more detail, most of the spaces between the agglomerates are wetproofed by the PTFE dispersion and provide good gas traiisport; some remain hydrophillic (depending on the % PTFE in the catalyst mix) and permit electrolyte penetration in depth into the electrode. However, contact between the electrolyte and a large percentage of the catalyst surface depends on a network of fine pores (pore diameter $< \sim 500$ Å) in the catalyst. These do not become wetproofed because the particle size of the PTFE dispersion ($\sim 0.1\mu$) is larger than the pore diameter.

Even with a catalyst of good activity and ideal structure, the performaiice of a PTFE bonded electrode can vary with its method of preparation. The main variables are the percentage of plastic binder, the sintering time, and the sintering temperature. The distribution of the catalyst binder mixture on the supporting metal screen can also be carried out in several ways. Before the Bureau of Mines' catalysts were tested, a familiarization program was carried out with platinum and carbon to explore these variables. Brief details are presented below.

1. Effect of Manufacturing Techniques on Performance of Porous Electrodes

a. Platinum Electrodes

Platinum electrodes were prepared by spraying, brushing, spreading, and rolling methods. All preparations to date have been made with approximately 30% Teflon, considered from previous work to be optimum, and a Pt loading of about 10 mg/cm^2. Deviations from the 10 mg/cm^2 loading are due to uncertainties in the expected loss of material for each fabrication method. All electrodes are cut from larger pieces to 1 cm^2 for testing.

b. Catalyst Distribution Methods

(1) Spraying Technique

Electrodes numbered 1, 2a, TR-1, TR-2, TR-3A, TR-3B, TR-4A, TR-4B, TR-6, TR-7, and TR-8 were sprayed with an air gun to determine the relation between loading and spraying techniques. Electrodes 1and 2a were prepared on 100 cm^2 of screen, and 50% excess platinum was used for a projected 10 mg/cm^2 loading after losses. These electrodes were sintered at 260°C and had 10 mg/cm^2 Pt. Electrodes TR-1, TR-2, TR-3 and TR-4 were prepared on 36 cm^2 of screen, and 20% excess platinum was used for a projected 10 mg/cm^2. These electrodes had approximately 3-7 mg/cm^2 of platinum. Electrodes TR-3A and TR-4A were sintered at 260°C and showed extremely low performance; subsequently, electrodes TR-3B and TR-4B, sintered at 310°C, showed improved performance. Electrodes TR-6, TR-7 and TR-8 were also sprayed on 36 cm^2 screens with 20% excess platinum but with the following changes in technique: Cab-o-SiL was added to the platiiium-Teflon mix on a 1:1 volume ratio. Since this extended the liquid volume and produced a thicker spraying mix, continuous drying was employed. These electrodes had a good uniform physical appearance and loadings (8-10 mg/cm^2) were closer to the projected loading. However, the Cab-o-SiL may have had an adverse effect on the wetting characteristics of the electrodes. The

electrodes were sintered at 285°C, since 260°C seems to be on the borderline of the critical minimum sintering temperature. The influence of sintering temperature is considered in more detail below.

(2) Spreading Technique

It has been found that spraying produces the most uniform distribution of catalyst but does not work well with a small quantity of material. The spreading process (spreading a thick paste with a spatula) lends itself better to small quantities but usually does not yield uniform electrodes. Electrode TR-5 was made in this manner on 8 cm^2 of screen starting with no excess material; 13% of the material was lost.

(3) Brushing Technique

Electrode TR-9 was made by applying a paste with a small brush to 12 cm^2 of screen mounted on a portable jig for weighing "in situ." An excess of 100% was used in order to work with a paste of the same consistency throughout application. The performance of the electrode was exceptionally high, surpassing all previous runs. This method, however, has proved to be of limited application, being restricted to very finely divided catalysts.

(4) Rolling Technique

Electrode TR-10 was made by forming the platinum-Teflon into a rubbery dough and rolling it between Teflon sheets over the defined area of screen. This electrode was not made specifically for this program and consequently did not have a 10 mg/cm^2 loading. It has been found that the rolling method produces uniform electrodes with no loss of material, but they show comparatively low performance. No duplication of runs has been made.

The results are summarized in Fig. 69. The variation in performance was assumed to be mainly related to sintering temperature. This was examined as described below.

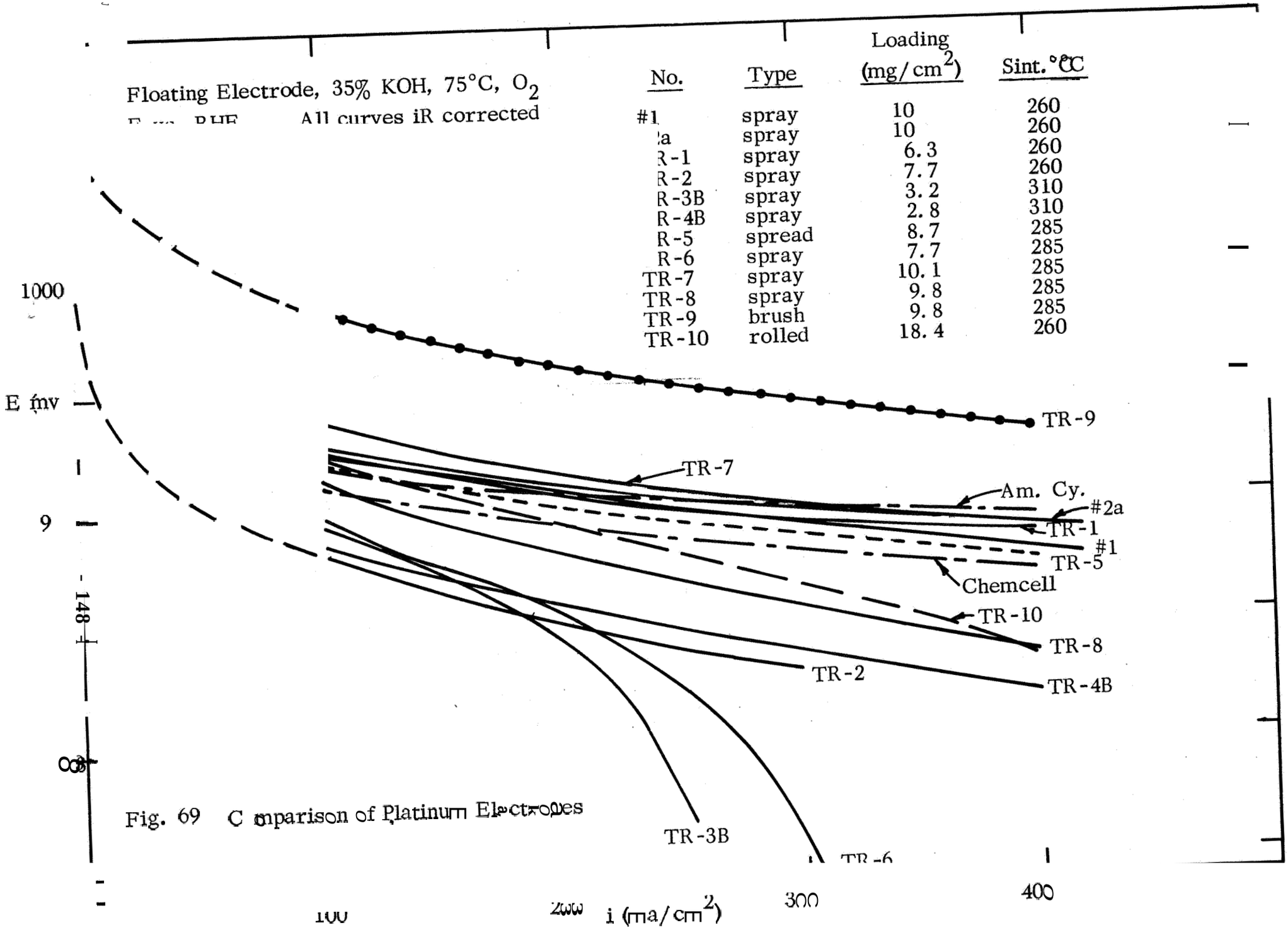

Fig. 69 Comparison of Platinum Electrodes

2. Effect of Sintering Temperatures

A number of electrodes cut from a single sheet of electrode material prepared by the spray method were sintered at 250°C, 275°C, 300°C, and 325°C for five-minute and fifteen-minute intervals. The sintering temperatures in these experiments were accurately defined. In previous work the thermocouple controlling the sintering furnace was influenced by radiant heat. Since the electrodes were effectively shielded from the radiant heat by aluminum foil, the true sintering temperature was some 26" lower than that registered on the controller/indicator.

The two electrodes sintered at 250°C were not hydrophobic and were not tested. On the basis of these results summarized in Table XVII the sintering technique was improved and made more reliable and the optimum sintering conditions (for platinum) defined as 275°C for 15 minutes. Results obtained under these conditions compare favorably with the best previously reported for electrodes prepared in the same way. The change in real surface area during this sintering process at 275°C was measured by a BET technique. The figures before and after sintering were 22.6 m^2/g and 15.6 m^2/g respectively; the platinum black from which the electrodes were prepared had a surface area of 29.0 m^2/g.

3. Carbon and Graphite Electrodes

The performance of carbon and graphite powders were initially of interest as a basis for comparison of metal carbides. They also present a good opportunity for studying techniques of preparing high surface area electrodes, because of the wide range of samples available with such different physical properties as bulk density and surface area. They were consequently used to examine the influence of PTFE/catalyst ratio on performance. The bulk densities of the catalysts were measured to discover if a better correlation could be made in terms of a volume rather than a weight ratio. The following samples were examined; graphite with 22.5%, 25%, 27.5%, 30%, 35%, 40% PTFE content and acetylene black with 45%, 50%, 60%, 70% PTFE content. A summary of performance is given in

TABLE XVII

Effect of Sintering Time and Temperature

		E = 950 mv	E = 900 mv
250°C	---------- not tested ----------		
275°C	5 min	i = 4	5 ma/cm^2
	15 min	28	242 "
300°C	5 min	5	10 "
	15 min	18	130 "
325°C	5 rnin	20	214 "
	15 min	25	230 "

Table XVIII. The optimum PTFE contents were deduced to be 27.5% for graphite and 50% for acetylene black, although the curves showed fairly flat maxima so that these figures are not too critical.

The bulk densities were measured after vibration and after centrifuging. Each method is reproducible to about 5%, but as can be seen from Table XIX, the agreement between the two methods is not good. This is not an unusual occurrence in the determination of bulk densities, since the particle shape factor has a different effect in the various methods of measurement[31]. The data available to correlate bulk density and PTFE content are shown in Fig. 70. It is apparent that the correlation is a useful guide and that the centrifuging method gives the more consistent data.

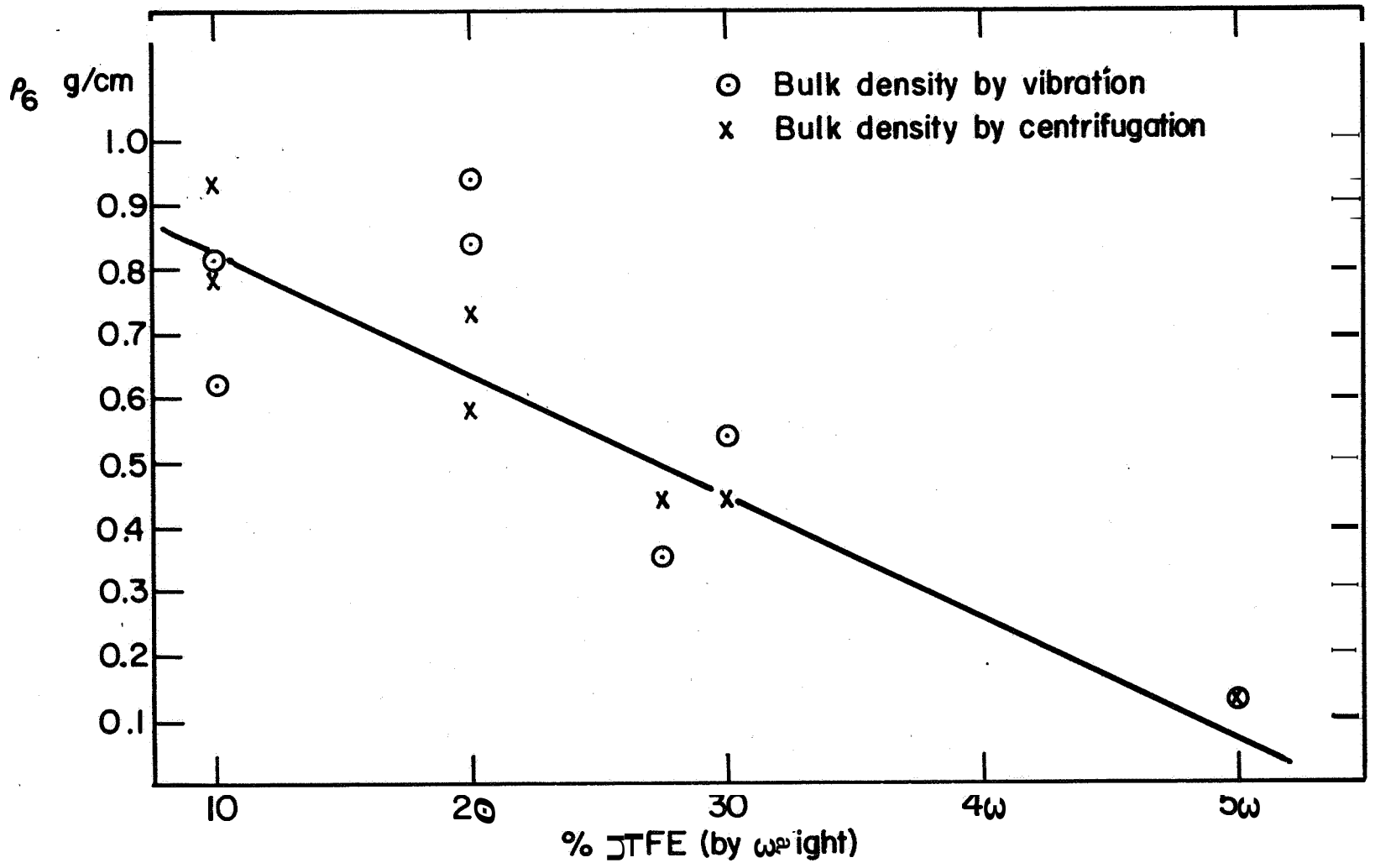

Fig. 70 Plot of Bulk Density vs. PTFE Content of Electrodes

TABLE XVIII

Performance as a Function of PTFE Content

Graphite	20	22.5	25	27.5	30	35	40	% PTFE
Current at 800 mv	----	9	7	22.2	5	61	4	ma/cm2
Current at 600 mv	----	44.5	78	95.5	68	26.6	22	ma/cm2

Acetylene Black	45	50	55	60	70	% PTFE
Current at 800 mv	2.4	7	5	4	3	ma/ cm^2
Current at 600 mv	21.4	94.5	45	48	42	ma/ cm^2

TABLE XIX

Bulk Density Measurements

Material	Bulk Density (gm/cc) Vibration	Centrifuge	% PTFE
Acetylene black	0.125	0. 130	50
Graphite	0.350	0.425	27.5
Engelhard Pt black	0.540	0.435	30
Carbon #7706	0.940	0.73s	20
Carbon #8946	0.830	0.580	20
Ni_3C	0.689	0.927	10
$Ni_3C + Co_2C$	0.814	0.780	10

4. Electrode Preparation

Electrode fabrication consisted of the mixing of the catalyst (after induction or exposure, see below) with a dispersion of PTFE (DuPont, Teflon 30) in a known weight ratio, This mixture was pasted on a nickel screen (100 mesh) to produce an electrode of ~ 6 cm2 area. The electrodes were dried in a vacuum oven at 100°C and subsequently sintered in a stream of N_2 at 275°C. Several test electrodes of 1 cm2 area could be cut from the sintered structure.

5. Electrochemical Testing

The fabricated electrodes were tested in a floating electrode cell configuration (Fig. 71) in 35% KOH at 75°C using as reference a dynamic hydrogen electrode. Current-voltage curves were determined under potentiostatic conditions using the following procedures. The electrode made contact with the electrolyte at a controlled potential of 1000 mv; the potential was almost immediately reduced to 850 mv and the current noted. The current was measured again after five minutes, the potential was adjusted to 750 mv, and the current measured as before. The current voltage curve was then determined at 50 mv intervals, each held for 5 min in the sequence 750 mv → 400 mv → 850 mv. For the cobalt and nickel-cobalt alloys the procedure was modified to include an anodic induction at 1600 mv for 10 min. The anodic pretreatment induction should produce complete oxidation of the surface and effectively reduce the corrosion rate during oxygen reduction, particularly with the cobalt catalysts. In the case of the nickel-cobalt alloys, the high pretreatment potentials (which may be imagined as being equivalent to heating in an oxidizing atmosphere) could contribute to the formation of a surface spinel ($NiCo_2O_4$), reported[32] to exhibit good conductivity and catalytic activity for oxygen reduction. The complete E (i) curve 850 mv → 400 mv → 850 mv was measured as before.

Further modifications to the technique were introduced when experiments described in detail below showed that the activity of these electrodes

FLOATING ELECTRODE CELL

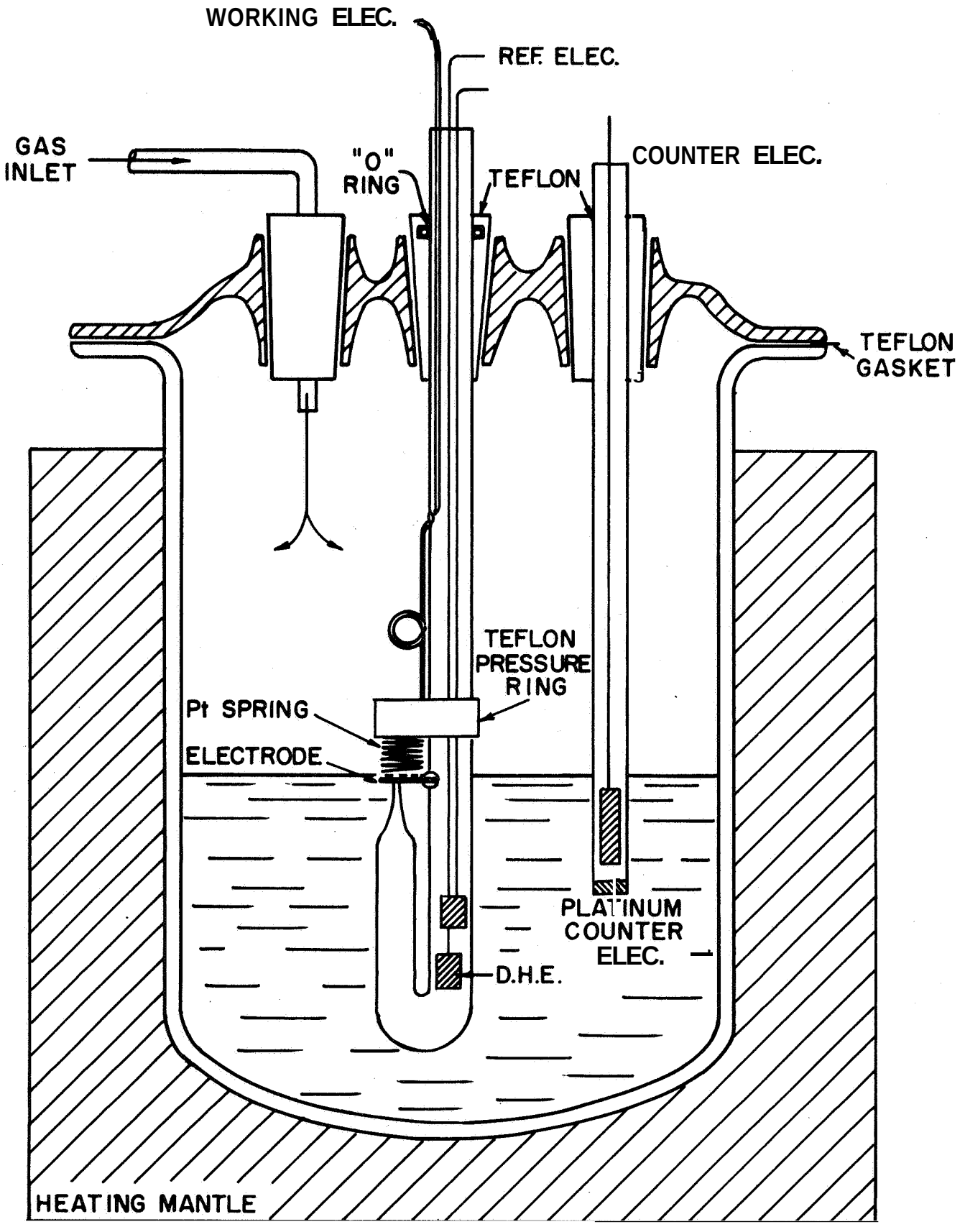

Fig. 71

varied with time in an unusual manner (see Fig. 72). The current at constant potential initially increased, then remained constant for a period of time before decaying to a constant value somewhat below the initial current.

In order to compare the catalytic activity of individual samples, it was obvious that the measurements had to be made at identical points on this time curve. Since this behavior must be related to the surface oxide, two factors probably need to be taken into account: the total time the catalyst was exposed to air before testing (whether inducted or directly exposed) and the total time of exposure to electrolyte during tests.

After the initial examples the first factor was easily eliminated by preparing each electrode individually and testing as soon as possible (usually within 24 hours). Total contact time with the electrolyte was more difficult. If the fabricated electrodes were fully reproducible, complete information could have been obtained by measuring first a decay curve on one electrode and then the E (i) characteristic on another. Since good reproducibility cannot be guaranteed with PTFE bonded electrodes, the approach adopted was to make several successive determinations of the E (i) curve sufficiently rapidly to display the pattern of the activity change with time. This necessitated the use of a slow potential sweep method. After preanodization the electrode was subjected to a 100 mv/min potential sweep between 1000 mv and 400 mv. A complete curve of increasing and decreasing potential could then be obtained in about ten minutes. The sweeps were continued until the pattern of increase and decrease in current at a particular potential was observed; the tabulated values (see below) represent the highest observed activity. A careful comparison was made of the manual and sweep methods to ensure that the E (i) curves were equivalent.

C. Material Handling

The materials were delivered in sealed containers under an atmosphere of CO_2; the first process was to divide the sample into eight approximately equal lots. The subdivision was carried out in a glove box in a

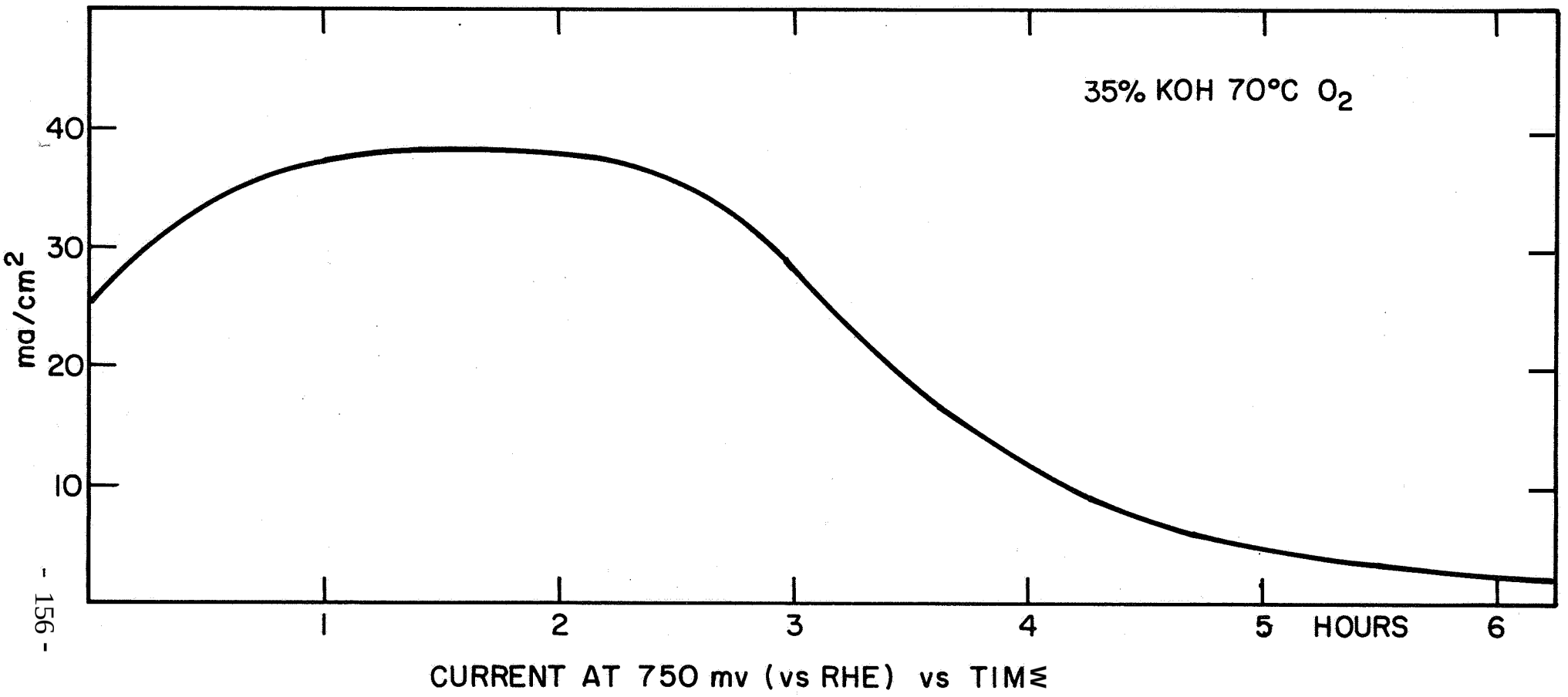

Fig. 72 #47 Ni_3C

nitrogen atmosphere; the individual samples were contained in plastic snap top bottles that were further sealed in paraffin wax as the bottles were brought out of the inert atmosphere. A freshly prepared sample of Raney nickel was subjected to exactly the same procedures as the Bureau of Mines' materials up to the stage of wax sealing. The Raney nickel was then exposed to air and on each occasion the sample was pyrophoric, indicating the effectiveness of the glove box in each case. (The surface of Raney nickel is easily passivated by exposure to very small amounts of O_2 and becomes noiipyrophoric.)

Also, during the subdivision of the samples, the resistance of the powder was measured. The sample was contained between two pieces of Pt foil by an O ring 1/2" O.D. and 5/16" I.D. The sample was then compressed at constant pressure in a jig using a torque wrench (Sturtevant Model F-21-1 at 15 inch pounds) and the resistance measured. The resistance of exposed and inducted samples was measured in an attempt to measure the need for, or the effectiveness of, the induction procedure, The method was only used to determine major changes in conductivity (see below).

D. Induction Methods

In a finely divided state (BET surface areas in the range 10-27 m^2/g) many of these materials were pyrophoric. Pyrophoric oxidation probably results in the complete oxidation of the sample and, for finely divided materials, the loss of a large proportion of their surface area. Special techniques were developed to induct the materials prior to exposure to oxygen during electrochemical testing. The basis of these techniques was to carry out the initial oxidation process as slowly as possible. Thus it was hoped to limit the extent of oxidation and any significant increase in temperature to avoid appreciable loss of surface area by sintering. Some loss of surface area of the catalyst could also be expected from the heat treatment of the electrode to sinter the PTFE. This factor was examined simultaneously with the development of the induction procedure. The

induction procedure was based on the fact that the rate and extent of the initial oxidation of the surface was thought to be dependent on how and at what stage of the electrode fabrication process the catalyst was first exposed to air.

The experiments carried out are detailed in Table XX . The effectof exposure to air when covered with methanol or water is believed to produce slow oxidation of the surface, either by reaction with dissolved O_2 or by progressive exposure to air during evaporation of the liquid layer. Elvax (a duPont polyvinyl resin) was substituted for PTFE as a plastic binder in the tests to investigate the effect of sintering. Elvax electrodes were prepared by dissolving the appropriate quantity of the resin in trichloroethylene at 70-80°C; after cooling to 35°C, the catalyst was added and the mix distributed on a nickel screen. The electrodes required no sintering and were tested after evaporation of the residual solvent, The results obtained with Elvax bonded Pt electrodes were equivalent to some of the better results obtained with PTFE bonded Pt electrodes, indicating that this was an effective method of catalyst testing. The life of the Pt electrode was, however, limited to about two hours, probably due to oxidation of the Elvax under the test conditioiis (35% KOH at 75°C). The life of Elvax-bonded electrodes prepared from the interstitial compounds was somewhat longer (3-4 hours). Other plastic binders are being examined in order to obtain longer lived electrodes.

The main coiiclusioii drawn from these experiments was that careful induction of the catalyst produces a more active electrode and also that resistance measurements as described earlier on the dry powder are not sensitive enough to relate to activity.

The electrodes made with PTFE, in which the catalyst was exposed to air in the first case (#3, Table XX) after sintering and in the second case (#4, Table XX) before sintering, showed no signficant difference. Both were comparable to electrode #1 (i) made with Elvax. However, this

TABLE XX

Inducting Methods For Catalysts 11-C

		Activity ma/cm2 at 600 mv
ELVAX ELECTRODES		
1. Electrode made in N_2 then		
(i) Exposed to air slowly		10
(ii) Exposed to air in water		4
(iii) Exposed to air in methanol		4
2. Catalyst inducted by		
(i) Exposure to air slowly	Electrodes made in air	10
(ii) Exposure to air in water		3
(iii) Exposure to air in methanol		32
PTFE ELECTRODES		
3. Electrode made and sintered in N_2		10
4. Electrode made in air sintered in N_2 using catalyst 2 (iii)		12

cannot be regarded as a conclusive indication that the sintering process is not detrimental, since the test was not conducted with the catalyst in its most active form.

The induction method was further refined by the use of the following techniques:

(1) Slow oxidation in the gas phase

(2) Extension of the liquid phase induction in methanol to a sequence of organic solvents (petroleum, ether, diethyl ether, aceton and methanol), a sequence in which the reactivity and solubility of oxygen increases.

The slow gas phase oxidation was carried out by the Bureau of Mines with a second sample of material 11C. Three samples of 11C were supplied: an untreated sample, one that had been oxidized in 0. 1% O_2 in N_2 for 100 hours at room temperature, and another in 1% O_2 in N_2 for 100 hours at room temperature. All were tested as Elvax bonded electrodes and compared with further samples that had been subjected to the liquid phase induction described above. The details of the tests and the results are presented in Table XXI. The uniformity of the results (all except one produced close to 20 ma/cm^2 at 600 mv) indicates that all attempts, both at Tyco and at the Bureau of Mines, to induct this material were of no consequence. This is in direct contrast to the results reported previously. Further, the activity of the uninducted sample A is higher than previously observed, suggesting that the surface was in some way conditioned prior to the induction processes. The improved efficiency of the extended liquid phase induction process was demonstrated by the induction of the original sample of 11C to produce an activity of 40 ma/cm^2 at 500 mv; this compares to 33 ma/cm^2 observed with simple methanol induction.

The induction method for the protection of the activity of Raney nickel described in German Patent 1, 185,589 (Doehren and Jung to Varta Petrix-Union G. m. b. H.), in which the catalyst was immersed in a polyhydric alcohol such as ethylene glycol, was not successful for induction of catalyst 11C.

TABLE XXI

11C – Oxygen Induction Series (B. O. M).

Sample	A	B	C	A	B	C
B. O. M. Pretreatment	None	Inducted in N_2 with 0. 1% O_2 100 hours	Inducted in N_2 with 1. 0% O_2 100 hours	None	Inducted in N_2 with 0. 1% O_2 100 hours	Inducted in N_2 with 1. 0% O_2 100 hours
Tyco Pretreatment	None	None	None	Catalyst Inducted in Pet. Ether etc.	Catalyst Inducted in Pet. Ether etc.	Catalyst Inducted in Pet. Ether etc.
Binder	10% Elvax	10% Elvax	10% Elvax	10% Elvax	10% Elvax	10% Elvax
Electrode Activity ma/cm^2 at 600 mv	19. 3	18. 2	18. 0	18. 4	14. 4	19. 8

E. Results

A complete listing of the activity of the interstitial compounds was presented in Table XVI (p. 129). The electrodes are described by identification numbers – the first number and letter, e.g. 26, corresponds to the Bureau of Mines' identification number of the catalyst. The italic number in parenthesis describes the electrode preparation, i.e. 2C (ii), and the final letter identifies the test (e.g. 2C (ii)a and 2C (ii)b are tests carried out on separate samples cut from electrode 26 (ii). The tables also record the induction of the catalyst, and the nature and amount of the plastic binder used. The activity is presented as the current density at selected potentials. The less active materials (mainly Fe interstitials) are compared at 600 mv; most others are compared at 750 mv, with additional figures at 900 mv for those catalysts containing Ag, Au, or Pd. When two figures are quoted, these are the current densities for increasing and decreasing potentials respectively. These can differ due to differences induced in the oxide films at the lower potentials (minimum potential for these tests was 400 mv). In the case of Ni interstitials, it was noted that the pattern of activity was an initial increase, followed by a plateau of steady current and steady decay. To insure that peak activity was recorded in these cases the repetitive potential sweep method described earlier was used. The results obtained by this method are identified in Table XVI.

Brief details of the preparation of each sample are given in Table XXII. Complete information and experimental techniques are documented in the Bureau of Mines' Reports, Q-1 to Q-4. (33)

F. Discussion

The results obtained for the interstitial compounds of iron were disappointingly low. The highest activities were 53 and 58 ma/cm^2 at 600 mv vs. RHE for samples 5N and 6N.

Error

An error occurred while processing this page. See the system log for more details.

TABLE XXII (Cont.)

Nitride Preparations

Run no	Iron source	Hourly space velocity of NH_3, hr^{-1}	Average bed temp, °C	Duration of nitriding, hrs	Discharge wt, g	Phases by x-ray diffraction	Chemical analyses, wt-%	
							Total Fe	Total N
1N	Hematite	750	356	6	49.1	ϵ-Fe_3N, γ'-Fe_4N	89.90	5.92
2N	〃	750	366	6	51.3	γ'-Fe_4N, ϵ-Fe_3N	83.20	5.47
4N	〃	1000	339	7	48.9	ϵ-Fe_3N, γ'-Fe_4N	81.90	7.61
5N	〃	1000	340	7	52.3	ϵ-Fe_3N, γ'-Fe_4N	82.80	6.57
6N	〃	1000	338	12	51.5	ϵ-Fe_3N, ζ-Fe_2N	82.4	6.35
7N	〃	1000	381	6	50.2	γ'-Fe_4N	83.53	5.04
8N	Raney iron	1000	347	7½	46.5	γ'-Fe_4N		
9N	Magnetite	1000	342	24	46.6	ζ-Fe_2N		
10N	〃	1000	345	24	55.5	ε-Fe_3N	80.28	7.94
11N	Coprecipitated 3Fe/1Ag	1000	350	25	50.5	ϵ-Fe_3N, Ag		4.85
13N	Raney iron	1000	350	12	46.1	ε-Fe_3N	86.47	9.75
14N	〃	1000	347	24	44.6	ε-Fe_3N		9.61
15N	Coprecipitated 1Fe/1Ag	1000	352	24	58.1	ϵ-Fe_3N, Ag		4.35
16N	〃	1000	349	24	57.7	Ag, ε-Fe_3N		2.81
17N	Raney iron	1000	352	12	49.1	ε-Fe_3N		9.12
18N	〃	1000	294	24	99.1	ζ-Fe_2N, ϵ-Fe_3N		

* Taken from Bureau of Mines Quarterly Report - Contract No. NASW 12300

TABLE XXII (Cont.)

Nitriding of Iron Carbides

Run no	Charge	Charge wt, g	X-ray analysis	Gas	Hourly space velocity, hr^{-1}	Average bed temp, °C	Duration of nitriding, hrs	Discharge wt, g	X-ray analysis	Chemical analysis, wt-%		
										Total C	Free C	Nitrogen
1NC	3C	50.41	χ-Fe_2C, Fe_3O_4,	NH_3	1000	345	28	-	ϵ-$Fe_2X(C,N)$, Fe_3O_4	-	-	-
2NC	9C	107.85	χ-Fe_2C	NH_3	1000	349	24	109.18	χ-$Fe_2X(C,N)$, ϵ-$Fe_2X(C,N)$	11.76	5.93	2.26
3NC	8C	101.58	θ-Fe_3C, ϵ-Fe_2C	NH_3	1000	352	24	104.40	ϵ-$Fe_2X(C,N)$	-	-	-

Carbiding of Iron Nitrides

Run no	Charge	Charge wt, g	X-ray analysis	Gas	Hourly space velocity, hr^{-1}	Bed temp, °C	Duration of carbiding hrs	Discharge wt, g	X-ray analysis	Chemical analysis, wt-%		
										Total C	Free C	Nitrogen
1CN	4N	46.05	ϵ-Fe_3N, γ'-Fe_4N	CO	100	309-346 (335) 302-352 (347) 292-315 (307)	11	46.67	ϵ-$Fe_2X(C,N)$	-	-	-
2CN	7N	43.14	γ'-Fe_4N	CO	100	210-295 (273) 295-343 (319)	4 9	43.32	ϵ-$Fe_2X(C,N)$	-	-	-
3CN	14N	42.51	ϵ-Fe_3N	CO	100	180-345 (249) 345	4 7	43.43	ϵ-Fe_2X	-	-	-

a/ First figure is temperature at which reaction starts; second figure is maximum temperature of carbiding; third figure is the average temperature of carbiding.

* Taken from Bureau of Mines Quarterly Report - Contract No. NASW 12300

TABLE XXII (Cont.)

Carbiding of Iron Nitrides

Run No.	Charge	Charge wt.,g.	X-ray analysis	Gas	Hourly space velocity $hr.^{-1}$	Bed temp., °C a/	Duration of carbiding, hrs.	Discharge wt.,g.	X-ray analysis	Chemical analysis wt.-% Total C	Free C	Nitrogen
6CN	11N	30.4	ε-Fe$_2$N, Ag	CO	100	225-350(319) 350	3 7	30.4	ε-Fe$_2$X(C,N), Ag			
7CN	15N	37.6	ε-Fe$_2$N, Ag	CO	100	185-350(306) 350	5 5	37.6	ε-Fe$_2$X(C,N), Ag			
8CN	16N	37.6	Ag, ε-Fe$_3$N	CO	100	202-350(305) 350	4 6	37.2	Ag, ε-Fe$_2$X(C,N)			
9CN	21N	40.1	γ'-Fe$_4$N, ε-Fe$_3$N	CO	100	200-250(243) 250	½ 3½	40.1	γ'-Fe$_4$X(C,N)			
10CN	8N	17.7	γ'-Fe$_4$N, ζ-Fe$_2$N	CO	100	200-250(223) 250	1 3	17.1	γ'-Fe$_4$X(C,N)			

a/ First figure is temperature at which reaction started, second figure is maximum temperature of carbiding, third figure is the average temperature of carbiding.

* Taken from Bureau of Mines Quarterly Report - Contract No. NASW 12300

TABLE XXII (Cont.)

Nitriding of Iron Carbides

Run No.	Charge	Charge wt.,g.	X-ray analysis	Gas	Hourly space velocity, $hr.^{-1}$	Average bed temp., °C	Duration of nitriding, hrs.	Discharge, wt., g.	X-ray analysis	Chemical analysis, wt.-%		
										Total C	Free C	Nitrogen
4NC	5C	34.5	χ-Fe_2C, α-Fe	NH_3	1000	350	20	35.3	ϵ-$Fe_2X(C,N)$	3.84	1.09	6.64
5NC	14C	35.1	θ-Fe_3C	NH_3	1000	294	6	35.0	θ-$Fe_3X(C,N)$	8.13	3.53	0.78
6NC	7C	15.0	χ-Fe_2C	NH_3	1000	280	15	14.7	χ-$Fe_2X(C,N)$	7.35	6.0	1.13
7NC	15C	29.9	θ-Fe_3C	NH_3	1000	300	6	29.8	θ-$Fe_3X(C,N)$			
8NC	21C	13.0	Ag, χ-Fe_2C	NH_3	1000	280	19	13	Ag, χ-$Fe_2(C,N)$			
9NC	22C	15.0	Ag, χ-Fe_2C	NH_3	1000	280	15	14.9	Ag, χ-$Fe_2(C,N)$			
10NC	24C	15.0	Ag	NH_3	1000	280	15	14.9	Ag			0.37[a]

a/ Fe 25.0%.

* Taken from Bureau of Mines Quarterly Report - Contract No. NASW 12300

TABLE XXII (Contd.)

Coprecipitation and Reduction of Mixed Oxides of Iron and Silver

Run no	Reactants other than H_2O, g						Washings	Fe/Ag weight ratio of product	Reduction				
									Charge, g	Gas	Hourly space velocity, hr^{-1}	Average bed temp, °C	Duration of reduction, hrs
I-CP	$Fe(NO_3)_3 \cdot 9H_2O$	46.62	$AgNO_3$	3[illegible]3	$2CO_3$	[illegible]	H_2O, [illegible]ethanol, [illegible]ether	3.04/1	65.35	H_2	2,500	450	18
II-CP	$Fe(NO_3)_3 \cdot 9H_2O$	1.0[illegible]	$AgNO_3$	[illegible].93	Na_2CO_3	[illegible]0	H_2O, [illegible]cetone, ethanol, and ether	1/1	71.12	H_2	2,500	453	7
III-CP	$Fe(NO_3)_3 \cdot 9H_2O$	[illegible].2[illegible]	$AgNO_3$	19 [illegible]	Na_2CO_3	[illegible]	H_2O, [illegible]cetone, ethanol, and ether	1/3.0	66.25	H_2	2,500	450	3.3

* Taken from Bureau of Mines Quarterly Report - Contract No. NASW 12300

TABLE XXII (Contd.)

Pretreatment and Carbiding

Run No.	Pretreatment						Carburization						
	Charge	Charge wt., g.	Gas	Hourly space velocity, $hr.^{-1}$	Temp., °C.	Time, hr.	Gas	Hourly space velocity, $hr.^{-1}$	Temperature, °C. Front of bed	Temperature, °C. Rear of bed	Time, hr.	Discharge, wt., g.	X-ray diffraction
21C	38CP	33.95	H_2	2500	443	14	88	100	170-357	157-329	45	27	Ag, X-Fe_2C
22C	39CP	42.41	H_2	2500	446	11	88	100	170-350	167-343	45	36	Ag, X-Fe_2C
24C	40CP	57.61	H_2	2500	452	13	88	100	170-350	151-329	45	49	Ag
17C	Leached Raney nickel	44.78					8	100	160-249(232)	155-244(229)	7		
									250	228	24	46.1	Ni_3C, Ni trace
		42.80					88	100	250	228	48	43.8	Ni_3C, Ni trace
		43.2					88	100	300	257	24	49.8	Ni_3C, Ni trace
18C	Leached Raney cobalt	40.54					8	100	200-[illegible]0	[illegible]-27	22		
									[illegible]0	27	49	47.2	C $_2$C Co
19C	Leached Raney nickel	53.19					8	100	180-250	[illegible]236	29		
									250	236	48	55.2	Ni_3C, Ni
		54.33					8	100	251	233	20	55.2	Ni_3C, Ni trace
20C	Leached Raney cobalt	49.95					8	100	[illegible]0-250	167-240	4		
									250	240	48	51.0	Co_2C, Co
		50.41					8	100	260	241	27	50.1	Co_2C, Co

* Taken from Bureau of Mines Quarterly Report - Contract No. NASW 12300

TABLE XXII (Contd.)

Preparation of Carbides

Carbiding gas --------- CO
Hourly space velocity - 100

Run No.	Charge 1/	Duration of carbiding, hrs.	Temperature, °C	Chemical analysis, weight percent	
				Total C	Free C
25C	RAL-1	13	170-225		
	(1Ni-1Co)	216	250	9.78	6.18
26C	RAL-2	13	170-228		
	(1Ni-3Co)	144	250	8.86	4.86
27C	RAL-3	13	170-225		
	(3Ni-1Co)	144	250	9.33	7.48
29C	RAL-4	5	170-230		
	(1Ni-3Ag)	104	250	1.21	0.7
30C	RAL-5	6	160-220		
	(1Ni-1Ag)	102	250	2.31	1.12
	60-250 mesh				
31C	RAL-5	6	160-220		
	(1Ni-1Ag)	100	250	2.04	1.06
32C	RAL-6	5	160-220		
	(3Ni-1Ag)	102	250	3.42	0.8
33C	RC-1	26	160-240		
	(Raney Co)	72	250	3.59	0.54
34c	RAL-9	5	160-220		
	(3Co-1Ag)	105	250	4.67	1.75
35C	RN-2B2	22	160-220		
	(Raney Ni)	72	250	10.78	6.55
36C	RNL-4	11	160-220		
	(Raney Ni, <mesh)	72	250		
38C	RAL-7	6	160-220		
	(1Co-3Ag)	100	250	1.82	0.72
39c	RAL-8	13	160-230		
	(1Co-1Ag)	100	250	2.56	0.66
40C	RAL-10	13	160-230		
	(1Ni-1Co-1Ag)	100	250	0.84	0.33
41C	RAL-11	22	160-220		
	(1Ni-1Co-1Au)	102	250		
42C	RAL-1	21	160-220		
	(1Ni-1Co)	101	250		
43c	RAL-5	4	160-250		
	(1Ni-1Ag)	102	250		
44c	RAL-12	4	160-250		
	(1Ni-1Ag-1Au)	103	250		

1/ Mesh size 150-250, unless otherwise stated.

* Taken from Bureau of Mines Quarterly Report - Contract No. NASW 12300

TABLE XXII (Contd.)

Preparation of Carbides

Carbiding gas: CO
Hourly space velocity: 100

Run no.	Charge[1/]	Duration of carbiding, hrs.	Temp., °C	Chemical analysis, weight-percent Total C	Free C	X-ray analysis
53c	1Ni-1Ag	5 102 106	160-250 250 260	1.92	0.12	Ni_3C, Ag
56C	Ni	6 102 36	160-250 250 260	0.94	0.20	Ni_3C, Ni
57c	1Ni-1Pd	6 37 103	160-250 250 260	1.19	0.95	
59c	co	5 100	160-250 250			Co_2C

1/ Reduced precipitated/coprecipitated hydroxides.

Space velocity of CO: 100 hr^{-1}

Run no.	Charge	Duration of carbiding, hrs	Temp, °C
45c	1Co-Ug-1Au	4 104	160-250 250
46C	3Ni-1Ag	6 101	160-250 250
55c	1Ni-1Pd	4 106	160-250 250

* Taken from Bureau of Mines Quarterly Report - Contract No. NASW 12300

TABLE XXII (Cont.)

Preparation of Nitrocarbides

Nitriding gas ---------- NH_3
Temperature ---------- 260°C
Hourly space velocity ----- 1000

Run No.	Charge	Duration of nitriding, hrs	Chemical analysis, weight-percent N	Total C	Free C
11NC	19C (Ni_3, trace of Ni)	15	1.08		
12NC	20c (Co_2C, α-Co, Cub. Co)	39	0.90	5.33	2.50
13NC	26C (Carbided 1Ni-3Co)	48	0.92	8.88	4.50
15NC	27C (Carbided 3Ni-1Co)	48	1.01	9.30	6.38
16NC	25C (Carbided 1Ni-1Co)	48	0.87	9.45	6.46
17NC	29C (Carbided 1Ni-3Ag)	48			
18NC	30C (Carbided 1Ni-1Ag, 60-250 mesh)	48			
19NC	31C (Carbided 1Ni-1Ag, 150-250 mesh)	48			
20NC	32C (Carbided 3Ni-1Ag)	58			
21NC	33c (Co_2C, α-Co)	48			
22NC	34c (Carbided 3Co-1Ag)	48			
23NC	35c (Ni_3C)	48			
24NC	36C (Ni_3C, <250 mesh)	48			
25NC	38C (Carbided 1Co-3Ag)	48			
26NC	39c (Carbided 1Co-1Ag)	48			
27NC	40C (Carbided 1Ni-1Co-1Ag)	48			
28NC	42C (Carbided 1Ni-1Co)	48			
29NC	41C (Carbided 1Ni-1Co-1Au)	48			
30NC	44c (Carbided 1Ni-1Ag-1Au)				

* Taken from Bureau of Mines Quarterly Report - Contract No. NASW 12300

After the initial low results with the carbides, the testing method was examined closely to eliminate all possible steps in the process that could be detrimental. These were the oxidation of the catalyst surface and the possible sintering of the catalyst at the "curing" temperature of PTFE bonded electrodes. The experimental approach to these problems was described in the previous section, together with an assessment of their effectiveness. For the testing of the nitrides, carbonitrides, and nitrocarbides, all the electrodes were prepared by the preferred method using an inducted catalyst with Elvax as a binder. In addition, several uninducted samples were tested and occasional electrodes were prepared with PTFE. The results were uniformly bad with only one electrode showing a current density > 10 ma/cm^2. This electrode 2 NC (ii)a showed an activity of 68 ma/cm^2 on first test, but this figure was not reproduced in a subsequent test. Though this activity represents the best observed for this class of materials, it does not approach the activity required of a practical catalyst. The general picture of activity for these materials, though not clearly defined, is nitrides > carbonitrides > carbides > nitrocarbides. Except where noted in Table XVI, these materials did not show significant currents under N_2. Prolonged exposure to air (after induction) for several days was found to have an adverse effect on performance.

Poor physical structure of the catalyst, particularly in the form of pore size distribution, could contribute to the low activity shown by these electrodes, but it is unlikely that a substantial increase in current density could be expected even if this were improved. The results are considered to be a reliable guide to the activity of the iron interstitials, and it must be concluded that these materials do not meet the requirements for a practical catalyst of the reduction of oxygen in a basic electrodes.

Three catalysts prepared by the coprecipitation of $Fe(OH)_3$ and Ag_2O showed relatively high activity, particularly for the two high Ag content materials (92 and 59 ma/cm^2). This is most probably related to the silver content. The nitride and carbonitride forms of these catalysts showed lower activity ~ 20 ma/cm^2 and 11 ma/cm^2 respectively, probably due to the adverse effect of the heat treatment associated with the nitriding and carbiding processes.

The carbides of nickel, and nickel cobalt alloys were in general, more active than were the iron compounds. The best activity of a series of tests with Ni_3C (19C(v)) was 94 ma/cm^2 at 600 mv. This does not compare with the activity obtained with catalysts prepared by decomposition of nickel acetate which give currents in excess of 300 ma/cm^2 at 600 mv (as discussed below). Cobalt carbide (20C) showed lower activity coupled with substantial corrosion (electrolyte became blue), preanodization at 1600 mv for 10 mins reduced the extent of corrosion but did not result in improved activity.

The carbided nickel cobalt Raney alloys (25C, 26C, 27C) showed activities in the range 20 to 70 ma/cm^2 at 600 mv, the order of activity being 3 Ni/Co > Ni/Co > 3 Ni/Co. All these materials were preanodized at 1600 mv. Conditions that could give rise to the formation of the nickel cobalt spinel at the surface improved conductivity and enhanced catalytic activity, as has been reported for the spinel. The nitrocarbides of nickel and cobalt 11 NC, 13 NC, 15 NC, 16 NC showed activity of the same order of magnitude as that of the carbides, though in the case of the nickel cobalt alloys the observed order of activity was Ni/Co > 3 Ni/Co > Ni/3 Co. It should also be noted for the uiicarbided Raney nickel cobalt alloys (RAL 1, 2 and 3) the activity was in the same range, the Ni/3 Co alloy giving 60 ma/cm^2 at 600 mv. For the Raney alloys the activity pattern was Ni/3 Co > Ni/Co = Ni/3 Co.

In view of the demonstrated capabilities of Ni_3C catalysts prepared from the acetate, the much lower activity of the alloys prepared from the Raney alloys was unexpected. X-ray characterization showed the catalysts from both sources to be very similar (Fig. 73). The acetate material had a higher free nickel content; the Raney material was obviously composed of smaller crystallites as evidenced by the line broadening of the X-ray pattern. The difference in activity can most probably be attributed to differences in the physical structure of the catalysts prepared by the two methods. A second sample of Ni_3C (36C) was prepared from the Raney alloy pulverized to < 250 mesh, to check whether *gross* particle size could affect electrode

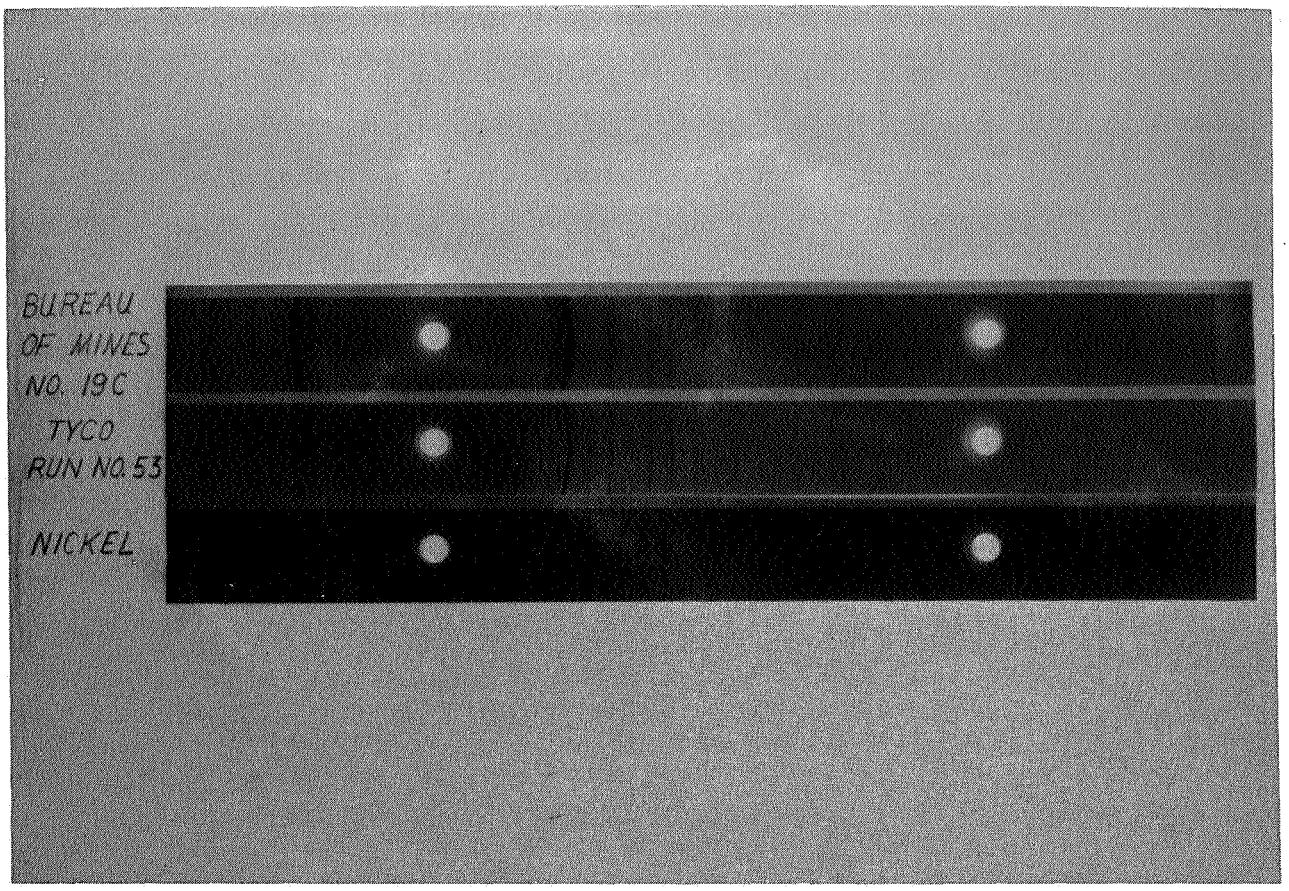

Fig. 73

performance. The results, a maximum activity of 30 ma/cm2 at 600 mv, were not encouraging. Sample 50C represented an attempt to carbide a Ni/Co alloy obtained by decomposition of nickel formate and cobalt acetate. The activity was still very low (33 ma/cm^2), but a second sample carbided at a lower temperature showed considerable improvement at 125 ma/cm^2 at 600 mv. Further experiments are in progress at the Bureau of Mines in which the temperature of carbiding will be further reduced and the carbiding time shortened.

Several catalysts were prepared in which gold, silver and palladium were added to the Ni and Co. The performance of these catalysts themselves and as carbides was, in some cases (e. g. 44C), very good. Probably this is due to the activity of the precious metal itself, though the presence of the precious metal could improve the utilization of the nonnoble metal component by providing a lower resistance current path in the electrode structure. In these cases the structure of the Raney alloy catalyst was capable of supporting limiting currents of 350 ma/cm^2 (44C (ii) but this could easily be adversely affected by the carbiding process. Carbided porous nickel plaques were used for three tests on Ni_3C (28C). This electrode configuration gives a high surface area catalyst without the possibility of the high resistance that could occur with the particle-to-particle contact of the highly dispersed catalyst. The difficulty in testing these electrodes is to establish the gas electrolyte interface throughout the electrode structure. In the results reported, this was attempted by partial wetproofing, with PTFE dispersion, so that the electrodes could be run in the floating electrode cell. The recorded performance shows that the attempt to produce an extended interface was not very successful. The material will be tested in a conventional fuel cell configuration with a matrix electrolyte. This test equipment is presently under construction. Under these conditions the pressure differential between the electrode and the electrolyte can be varied to obtain optimum performance.

The unusual decay pattern associated with the activity measurements on nickel and nickel cobalt catalysts was described above. A tentative explanation for this can be given as follows:

Error

An error occurred while processing this page. See the system log for more details.

II. NICKEL CARBIDE PREPARED BY ACETATE DECOMPOSITION

A. Introduction

Several samples of Ni_3C and Ni/Co carbide were prepared at Tyco by thermal decomposition of nickel and cobalt acetates in N_2, according to the method of Liecester and Redman[34]. The initial experiments based on this method were to a large extent responsible for the interest in the survey of interstitial compounds, described above.

B. Experimental

The acetate crystals were first dehydrated by heating to 100°C on a hot plate for 1 hr. The thermal decomposition was carried out in a furnace with N_2 flowing over the sample. The times and temperatures of decomposition of the active samples is listed in Table XXIII. The inactive samples, many of which were prepared under conditions apparently identical. to the active catalysts, are not listed. For the Ni/Co alloy carbides the starting material was either a solution of the acetates evaporated to dryness or the crystals ground together in a pestle and mortar.

The method of electrochemical testing was identical to that reported for the Bureau of Mines' catalysts.

C. Results

The best result obtained with Ni_3C catalysts was an activity of 100 ma/cm^2 at 750 mv vs. RHE, with a limiting current > 300 ma/cm^2. Figures 74, 75, and 76 show the current voltage curves of the most active catalysts. Other results are presented in summary form in Table XXIII. For the nickel cobalt catalysts ($Ni_3C + Co_2C$) activities of 45 and 105 ma/cm^2 were measured at 750 mv vs. RHE. The latter electrode showed a limiting current greater than 350 ma/cm^2. Ten samples of Ni_3C and two samples of Ni/Co carbide showed very low activity (i_L < 50 ma/cm^2).

TABLE XXIII

Activity of Ni_3C Prepared by Acetate Decomposition in N_2

Sample No.	Catalyst Preparation[1]			Electrode[2]		
	Time hrs.	Temperature °C	Induction	Loading mg/cm^2	Activity ma/cm^2[3] at 750 mv	Activity ma/cm^2[3] at 600 mv
	3	200				
20	4	275	No	≲7	≲0	≲10
	4	300				
39	3	300	No	24	90	290
44[4]	6	300	No	30	105	≻350
48[4]	6	300	No	26	50	150
53	3	300	No	30	44	310
55	3	350	No	43	20	87
56	3	350	No	9	18	58
58	3	300	Yes	28	30	125
59	3	300	Yes	23	16	82
62	3	300	No	27	40	300
63	3	300	Yes	10	100	≻350

(1) All preparations based on Liecester & Redman

(2) All electrodes contained 20% PTFE and were sintered 5 mins at 275°C

(3) Best figures when more than one electrode tested

(4) 3 Ni/Co carbides.

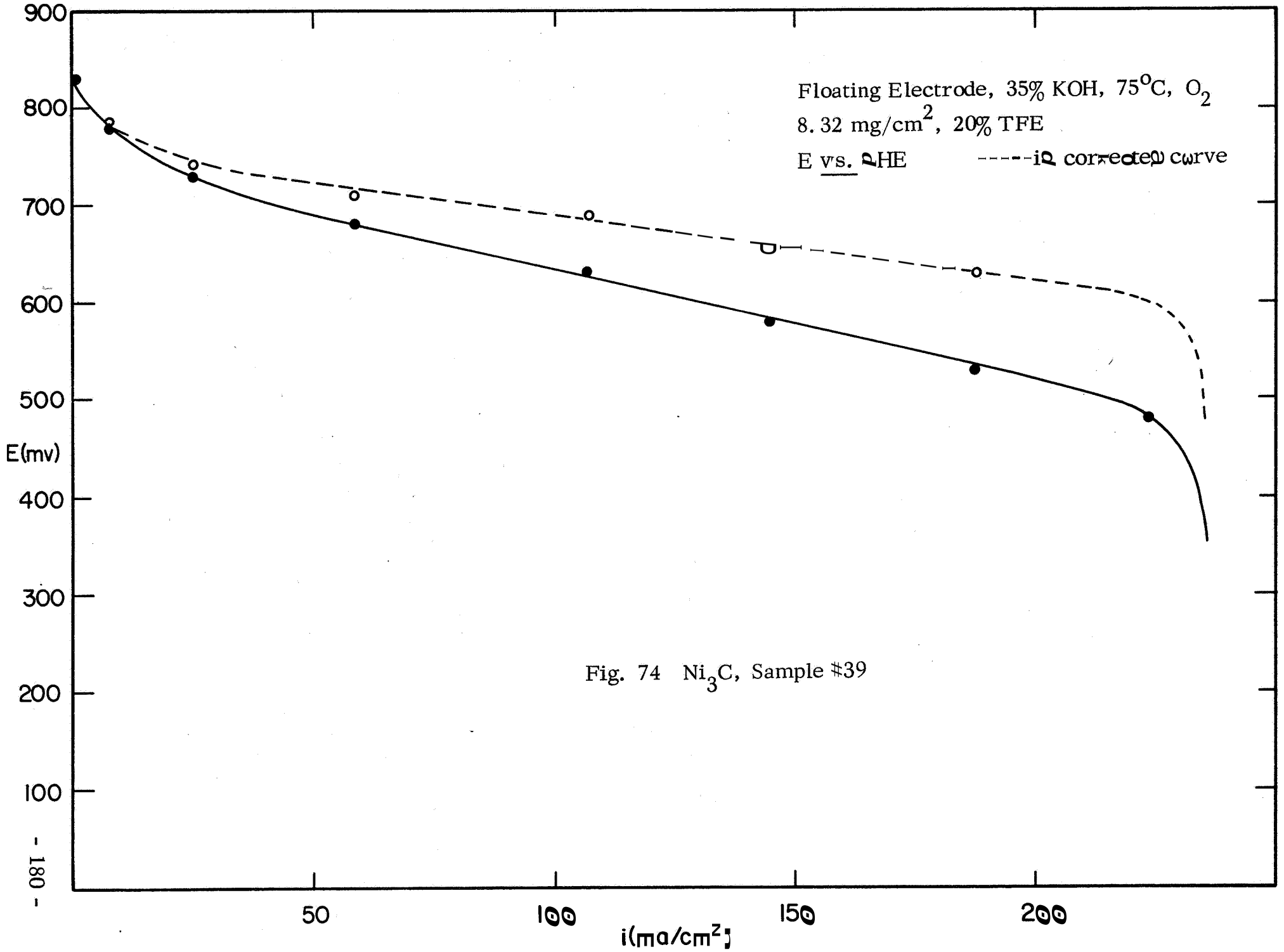

Fig. 74 Ni_3C, Sample #39

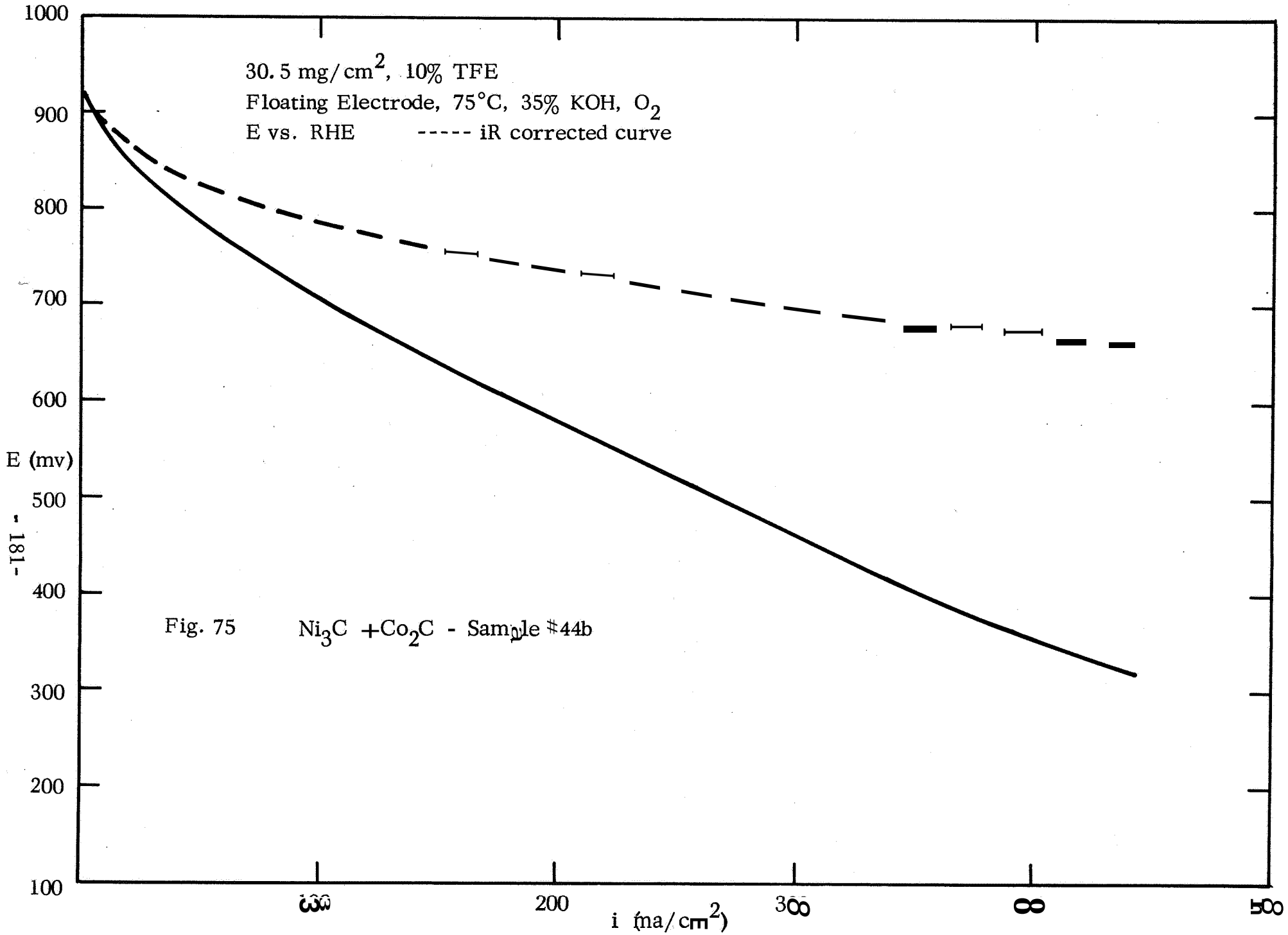

Fig. 75 $Ni_3C + Co_2C$ - Sample #44b

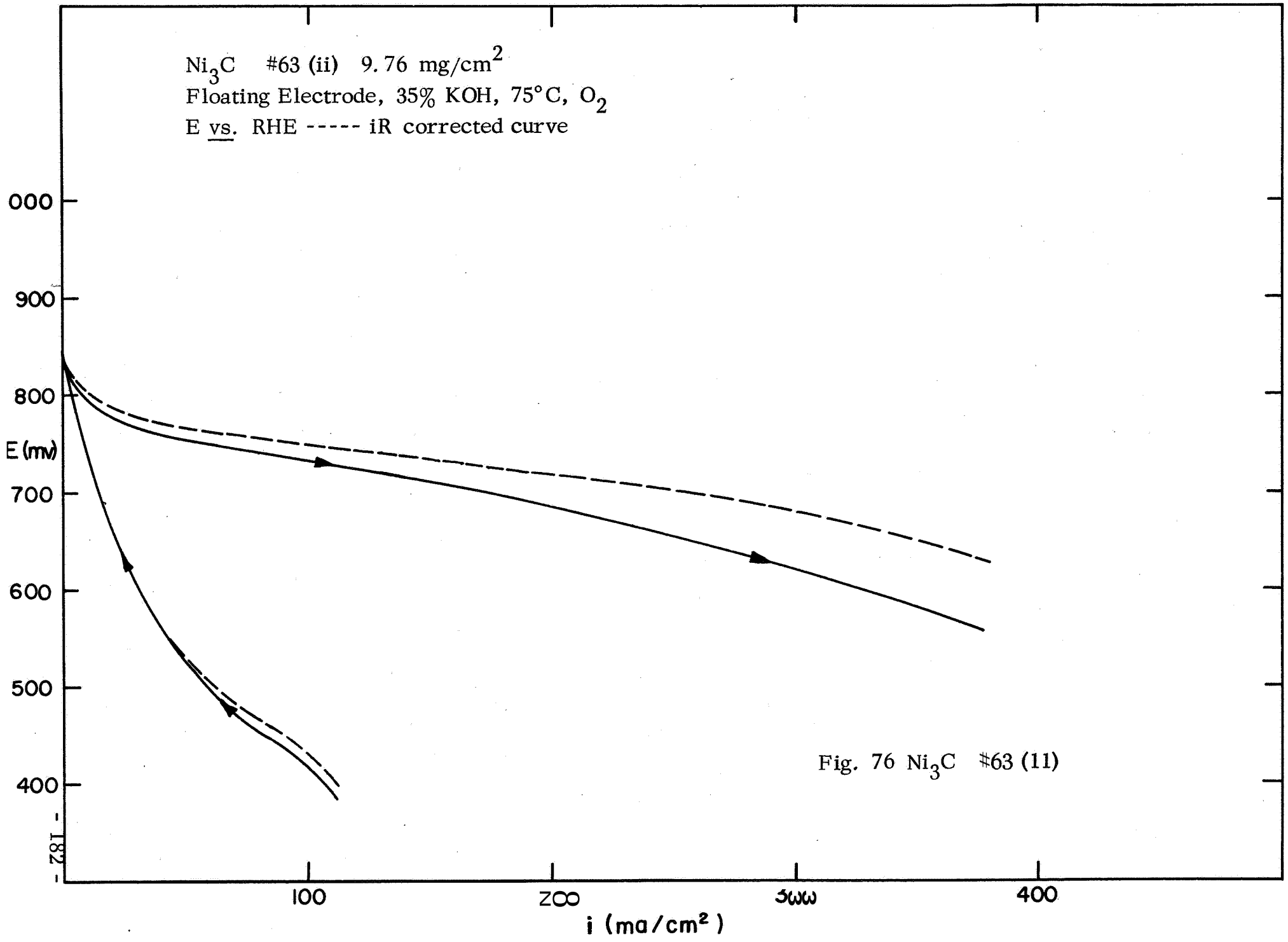

Fig. 76 Ni_3C #63 (11)

D. Discussion

The observed activities of these catalysts are very encouraging. However, the irreproducibility of the performance of electrodes and catalysts prepared in an apparently identical manner is difficult to explain. Where variations do exist in terms of the preparation of the catalysts method of induction, or electrode fabrication, no logical pattern was observed. It is possible that in the preparation of the catalyst the position of the sample in the furnace or the gas flow rate may be critical. These factors were not rigidly controlled.

The discrepancy between the best results obtained with these catalysts and nickel and nickel cobalt carbides prepared by the Bureau of Mines is of greater significance and can probably be related to physical differences between the catalysts. The main difference is probably that of pore structure, which is of considerable importance in the efficient operation of the PTFE bonded electrode.

111. NICKEL NITRIDE

Only one successful preparation of nickel nitride was made. This was based on the reduction of carbonyl nickel in H_2 at 450°C for 24 hrs followed by nitriding at 300°C with NH_3 for 48 hours. X-ray measurements showed 58% Ni_3N. Five other attempts to reproduce this preparation were unsuccessful.

The activity of the Ni_3N + Ni catalyst as a PTFE bonded electrode was quite low (16 ma/cm^2 at 600 mv vs. RHE).

REFERENCES

1. See, for example, M. L.B. Rao, A. Damjanovic, and J. O'M. Bockris, J. Phys. Chem. 67, 2508 (1963); J. P. Hoare, J. Electrochem, Soc. 111, 232 (1964); A. Kranse, J. Slawck and Z. Winowski 2 Physik. Chem. 40, 261 (1964).
2. M. Stern and A.C. Makrides, J. Electrochem. Soc. 107, 782 (1960).
3. J. Giner, J. Electrochem. Soc. 111, 377 (1964).
4. Fourth Quarterly Report, this contract.
5. R. Parsons, Trans, Far. Soc. 47, 1332 (1951).
6. M. L. Kronenberg, J. Electroanal. Chem. 12, 168 (1966).
7. J. H. Fishman and E. F. Rissmann, Extended Abstracts, Spring Meeting of the Electrochemical Society, San Francisco, May 1965.
8. M. L.B. Rao, A. Damjanovic, and J. Bockris, J. Phys. Chem. 67, 2508, (1963).
9. D. L. Douglass, D.R. St. Pierre, and R. Spieser, Met. Soc. Conf. 8, 705 (1961).
10. J.C. Gilles, A. M. Lejus, R. Collonguy, Corrosion and Anticorrosion 12, (3) 99 (1964).
11. L. E, Hollander, and P. L. Castro, Phys. Rev. 119, 1882 (1960).
12. V. A. Dorin, and F. M. Tartakovskaya, Zhur. Neorg. Khim. 4, 2635 (1959).
13. B.I. Boltaks, F.I. Vesenin, and A.E. Salunina, Zhur. Tekh. Fiz. 21, 532 (1951).
14. E.H. Greener, Diss. Abstr. 21, 1514 (1960).
15. S. M. Ariya, and N. I. Bogdanova, Fiz. Tverdogo Tela 1, 1022 (1959).
16. F. J. Morin, Phys. Rev. Letters 3, 34 (1959).
17. I. Sawai, K. Terada, T. Okamura, and A. Ueno. Repts. Inst. Chem. Research Kyoto Univ. 17, 55 (1949).

REFERENCES (Cont.)

18. H. Grunewald, Z. Ann. Physik 14, 121 (1954).

19. J. Long, and S. J. Tiechner, Bull.Soc. Chim. France, (9) 2625 (1965).

20. I. A. Mysanikov, Zhur. Fiz. Khim. 33, 2564 (1959).

21. F. Mazza, T. Mussoni, and S. Trasatti, Chim, eInd. (Milan) 45, (4), 417 (1963).

22. F. Mazza, Chim. eInd. (Milan) 43, 1424 (1961).

23. R. S. Dean, and I. Hornstein, U.S. Government Research Reports 32, 251 (1959).

24. M.V. Smirnov, L. E. Ivanovskii, and Yu. N. Krasnov, Akad, Nauk. S.S.S.R., Ural Filial, 2, 177 (1958).

25. J. Schmets, and M. Pourbaix, Proc. 6th Meeting C. I. T. C. E. p. 118 (1955).

26. R.C. DeVries, and R. Roy, Ceramic Bulletin 33, 370 (1954).

27. H.V. Philipsborn, and R. Laves, Acta Cryst. 17, 213 (1964).

28. S. Z. Beer, and Y.R. Sandler, J. Electrochem. Soc. 112, 113 (1965).

29. J. F. Schultz, L. J. E. Hofer, E. M. Cohn, K. C. Stein, and R. B. Anderson Bulletin 578, 1959, Bureau of Mines, Synthetic Liquid Fuels from the Hydrogenation of CO.
J. F. Schultz, L. J. E. Hofer, K. C. Stein, and R. B. Anderson Bulletin 612, 1963, Bureau of Mines, Nitrides and Carbonitrides of Iron as Catalysts in the Fischer Tropsch Synthesis

30. L. W. Niedrach, H. R. Alford, J. Electrochem. Soc. 112, 117 (1965).

31. Particle Size: Measurement Interpretation and Application, Irani and Callis, Wiley, New York (1963) p. 9.

32. G. Feuillade, Proceedings of the International Meeting on Fuel Cells Brussells 1965, Vol. IV, p. 49 Contract NASA-W 12,300.

33. Bureau of Mines Reports Q-1 to Q-4, July 1st 1966 to June 30th 1966.

34. J. Leicester, and M. J. Redman, J. Appl. Chem. 12. 356 (1962).

Tyco Laboratories, Inc.
Waltham, Massachusetts

INDEX

to

Q-8

Eighth Quarterly Report

Development of Cathodic Electrocatalysts for Use in Low Temperature H_2/O_2 Fuel Cells with an Alkaline Electrolyte

Contract No.

NASW 1233

For
National Aeronautics and Space Administration
Headquarters, Washington, D. C.

This index is subdivided in the following manner:

(1) Elements

(2) Alloys and Intermetallic Compounds

(3) Interstitial Compounds-Carbides, Nitrides and Oxides

(4) Interstitial Compounds-Borides and Silicides

(5) Barium Tantalate

(6) Interstitial Compounds of Group VIII Metals

(1) ELEMENTS	FIG. NO,	PAGE NO.
Ag	12	12, 24–27, 29, 31, 37, 40, 46, 51–53, 58, 102–04, 162 173, 176
Au	3(a, b, c), 4, 10–13	2, 12, 24–27, 29, 37, 39, 40, 42–44, 46, 51–53, 55, 57–58, 87, 123, 162, 176
C		20, 24, 27, 29, 38, 149, 152
co		12, 26, 30–32, 37–39, 128, 174, 176, 178
Cr		12, 19, 26, 27, 30, 31, 34, 35, 39, 46
CU		12, 24–27, 31, 46
Fe		12, 20, 24–27, 32, 34, 37, 46, 128, 162, 173
Graphite		12, 20, 37, 41, 46, 149, 150, 152
Hf		12, 19, 26, 30, 33, 35–37, 39
Ir		12, 24, 26, 27
Mn		12, 24–28, 31, 37, 39
MO		12, 20, 26, 30, 31, 34, 35
Nb		12, 19, 25–27, 30–33, 35, 37
Ni		12, 20, 24–27, 32, 34, 37–39, 51, 128, 162, 174, 176, 178
OS	50–54	12, 24, 26–28, 31, 105–10
Pd	11	12, 24–28, 40, 47, 51–53, 58, 142, 176
Pt	5, 10, 13	2, 12, 24–28, 37, 38, 40, 41, 46–48, 51–55, 87, 105, 146, 148, 149, 152
Re		12, 24, 26, 27, 31
Rh		12, 26, 31, 87

(1) ELEMENTS (cont'd.)

(2) **ALLOYS** AND INTERMETALLIC COMPOUNDS

(2) ALLOYS AND INTERMETALLIC COMPOUNDS (cont'd.)

(2) **ALLOYS AND** INTERMETALLIC COMPOUNDS **(cont'd.)**

(2) ALLOYS AND INTERMETALLIC COMPOUNDS (cont'd.)

(2) ALLOYS AND INTERMETALLIC COMPOUNDS (cont'd.)

(2) ALLOYS AND INTERMETALLIC COMPOUNDS (cont'd.)

(3) INTERSTITIAL COMPOUNDS-CARBIDES, NITRIDES & OXIDES

(4) INTERSTITIAL **COMPOUNDS**- BORIDES AND SILICIDES

(4) INTERSTITIAL COMPOUNDS-BORIDES AND **SILICIDES**

(5) BARIUM TANTALATE

(6) INTERSTITIAL COMPOUNDS OF GROUP VIII METALS · (porous electrodes)

DISTRIBUTION LIST

July 12, 1967

NASA and JPL

National Aeronautics & Space Admin.
Scientific and Technical Information Facility
College Park, Maryland 20740
Attn: NASA Representative
Send **2** copies plus 1 reproducible

National Aeronautics & Space Admin.
Washington, D. C. 20546
Attn: RNW/E. M. Cohn

National Aeronautics & Space Admin.
Washington, D. C. 20546
Attn: FC/A. M. Greg Andrus

National Aeronautics & Space Admin.
Goddard Space Flight Center
Greenbelt, Maryland 20771
Attn: Thomas Hennigan, Code 716.2

National Aeronautics & Space Admin.
Langley Research Center
Langley Station
Hampton, Virginia 23365
Attn: John Patterson

National Aeronautics & Space Admin.
Lewis Research Center
21000 Brookpark Road
Cleveland, Ohio 44135
Attn: Mr. Robert Miller

National Aeronautics & Space Admin.
Washington, D. C. 20546
Attn: Office of Technology Utilization

National Aeronautics & Space Admin.
Lewis Research Center
21000 Brookpark Road
Cleveland, Ohio 44135
Attn: M. J. Saari
MS 500-202

National Aeronautics & Space Admin.
Lewis Research Center
21000 Brookpark Road
Cleveland, Ohio 44135
Attn: Mr. N. D. Sanders

National Aeronautics & Space Admin.
Marshall Space Flight Center
Huntsville, Alabama 35812
Attn: Mr. Richard Boehme
R-ASTR-E

National Aeronautics & Space Admin.
Marshall Space Flight Center
Huntsville, Alabama 35812
Attn: Mr. Charles Graff
R-ASTR-EAP

National Aeronautics & Space Admin.
Ames Research Center
Pioneer Project
Moffett Field, California 94035
Attn: Mr. Jon Rubenzer

National Aeronautics & Space Admin.
Manned Spacecraft Center
Houston, Texas 77001
Attn: Mr. William R. Dusenbury

National Aeronautics & Space Admin.
Manned Spacecraft Center
Houston, Texas 77001
Attn: Mr. Hoyt McBryar
EP-5, Building 16

National Aeronautics & Space Admin.
Manned Spacecraft Center
Houston, Texas 77001
Attn: Mr. Forrest Eastman

National Aeronautics & Space Admin.
Electronics Research Center
575 Technology Square
Cambridge, Mass. 02139
Attn: Dr. Sol Gilman

Jet Propulsion Laboratory
4800 Oak Grove Drive
Pasadena, California 91103
Attn: Paul Goldsmith

Department of the Army

U. S. Army Engineer R & D Labs.
Fort Belvoir, Virginia 22060
Attn: Energy Conversion
Research Lab.

Commanding General
U. S. Army Electronics R & D Labs
Attn: Code AMSEL-KL-P
Fort Monmouth, New Jersey 07703

Harry Diamond Labs.
Room 300, Building 92
Conn. Ave. & Van Ness Street, N. W.
Washington, D. C. 20438
Attn: Mr. Nathan Kaplan

U. S. krmy Natick Laboratories
Clothing & Organic Materials Div.
Natick, Massachusetts 01760
Attn: Leo A. Spano

Department of the Navy

Office of Naval Research
Department of the Navy
Washington, D. C. 20300
Attn: Dr. Ralph Roberts/H. W. Fox

U. S. Naval Research Laboratory
Washington, D. C. 20390
Attn: Dr. J. C. White
Code 6160

Commander, Naval Ship System Comm.
Department of the Navy
Washington, D. C. 20350
Attn: Mr. Bernard B. Rosenbaum

Commander, Naval Ship System Comm.
Department of the Navy
Washington, D. C. 20350
Attn: Mr. C. F. Viglotti

Naval Ordnance Laboratory
Department of the Navy
Corona, California 91720
Attn: Mr. William C. Spindler
Code 441

Naval Ordnance Laboratory
Silver Spring, Maryland 20910
Attn: Mr. Philip B. Cole
Code 232

U. S. Navy Marine Engineering Lab.
Special Projects Division
Annapolis, Maryland 21402
Attn: J. H. Harrison

Department of the Air Force

Wright-Patterson AFB
Aeronautical Systems Division
Dayton, Ohio 45433
Attn: James E. Cooper, APIP-2

A F Cambridge Research Lab.
Attn: CRE
L. G. Hanscom Field
Bedford, Massachusetts 01731
Attn: Francis X. Doherty
Edward Rasking (Wing F)

Rome Air Development Center
Griffiss AFB, New York 13442
Attn: Mr. Frank J. Mollura
(RASSM)

Other Government Agencies

Mr. Donald A. Hoatson
Army Reactor, DRD
U. S. Atomic Energy Commission
Washington, D. C. 20545

Office of Assistant Director
(USW & Battle Support System)
Defense Research & Engineering
3D-1048 Pentagon
Washington, D. C. 20301

Mr. D. Bienstock
Bureau of Mines
4800 Forbes Avenue
Pittsburgh, Pa., 15213

Private Organizations

Aeronautronic Division of Philco Corp.
Technical Information Services
Ford Road
Newport, California 92663

Allis-Chalmers Mfg. Co.
1100 S. 70th Street
Milwaukee, Wisconsin 53214
Attn: John W. McNeil
Mgr. Marketing Research Div.
#3349

American Cyanamid Company
1937 W. Main Street
Stamford, Connecticut 06901
Attn: Dr. R. G. Haldeman

American Machine & Foundry
689 Hope Street
Springdale, Connecticut 06879
Attn: Dr. L. H. Shaffer
Research Division

Arthur D. Little, Inc.
Acorn Park
Cambridge, Mass. 02140
Attn: Dr. Ellery W. Stone

Aerospace Corp.
P. O. Box 95085
Los Angeles, California 90045
Attn: Tech. Library Acquisition
Group

Atlantic Refining Co.
500 South Ridgeway Ave.
Glenolden, Pa. 19036
Attn: H. Shalit

Atomics International Division
North American Aviation, Inc.
8900 De Soto Avenue
Canoga Park, California 91304
Attn: Dr. H. L. Recht

Battelle Memorial Institute
505 King Ave.
Columbus, Ohio 43201
Attn: Dr. C. L. Faust

Bell Telephone Laboratories, Inc.
Murray Hill, New Jersey 07971
Attn: U. B. Thomas

ChemCell Inc.
150 Day Road
Wayne, New Jersey 07470
Attn: Peter D. Richman

Clevite Corporation
Mechanical Research Division
540 East 105th Street
Cleveland, Ohio 44108
Attn: D. J. Berger

Consolidated Controls Corporation
15 Durant Avenue
Bethel, Connecticut 06801
Attn: Miss Carol R. Naas
(NsG-325 reports only)

G. & W. H. Corson, Inc.
Plymouth Meeting
Pennsylvania 19462
Attn: Dr. L. J. Minnick

Douglas Aircraft Company, Inc.
Astropower Laboratory
2121 Campus Drive
Newport Beach, California 92663

Dynatech Corp.
17 Tudor Street
Cambridge, Mass, 02139
Attn: Dr. A. R. Reti

Electromite Corp.
562 Meyer Lane
Redondo Beach, California 90278
Attn: R. N. Sparks

Electrochimica Corp.
1140 O' Brien Drive
Menlo Park, California 94025
Attn: Dr. Morris Eisenberg

Electro-Optical Systems, Inc.
300 North Halstead Street
Pasadena, California 91107
Attn: Martin Klein

Engelhard Industries, Inc.
497 Delancy Street
Newark, New Jersey 07105
Attn: Dr. J. G. Cohn

Esso Research and Engineering Co.
Government Division
P. O. Box 8
Linden, New Jersey 07036
Attn: Dr. C. E. Heath

The Franklin Institute
Philadelphia, Pennsylvania 19103
Attn: Mr. Robert Goodman

Garrett Corporation
1625 Eye St., N. W.
Washington, D. C. 20013
Attn: Mr. Bowler

General Dynamics/Convair
P. O. Box 1128
San Diego, California 92112
Attn: Mr. R. P. Mikkelson
Electrical Systems Dept. 988-7

General Electric Company
Direct Energy Conversion Operation
930 Western Ave.
Lynn, Massachusetts 01901
Attn: P. Schratter

General Electric Company
Research & Development Center
P.O. Box 8
Schenectady, New York 12301
Attn: Dr. H. Liebhafsky

General Electric Company
777-14th St., N. W.
Washington, D. C. 20005
Attn: Philip C. Hargraves

General Motors Corp.
G. M. Technical Center
Warren, Michigan 48090
Attn: Library, Research Lab.

Globe-Union, Inc.
P.O. Box 591
Milwaukee, Wisconsin 53201
Attii: J. D. Onderdonk,
V, P., Marketing

Ionics, Incorporated
65 Grove Street
Watertown, Massachusetts 02172
Attn: Dr. Werner Glass

Institute for Defense Analyses
Research and Engineering Support
Division
400 Army Navy Drive
Arlington, Virginia 22202
Attii: Dr. George C. Szego

Institute for Defeiise Analyses
Research & Engineering Support Div.
400 Army Navy Drive
Arlington, Virginia 22202
Attii: Dr. R. Briceland

Institute of Gas Technology
State and 34th Streets
Chicago, Illinois 60616
Attn: Mr. B. S. Baker

John Hopkins University
Applied Physics Laboratory
8621 Georgia Avenue
Silver Spring, Maryland
Attn: Richard Cole

LTV Research Center
P. O. Box 5907
Dallas, Texas 75222
Attn: Madison Reed
(Contract W12, 300 only)

Johns-Manville R & E Center
P. O. Box 159
Manville, New Jersey 08835
Attn: J. S. Parkinson

Leesona Moos Laboratories
Lake Success Park
Community Drive
Great Neck, New York 11021
Attn: Dr. A. Moos

Livingston Electronic corporation
Route 309
Montgomeryville, Pennsylvania 18936
Attn: William F. Meyers

Lockhead Missiles & Space Company
Technical Information Center
3251 Hanover Street
Palo Alto, California 93404

The Martin Co.
Electronics Research Department
P. O. Box179
Denver, Colo. 80201
Attn: William B. Collins
Mail No. 1620

Midwest Research Institute
425 Volker Boulevard
Kansas City, Missouri 64110
Attn: Physical Science Library

Monsanto Research Corporation
Boston Laboratories
Everett, Massachusetts 02149
Attn: Dr. J. O. Smith

Monsanto Research Corporation
Dayton Laboratory
Dayton, Ohio 45407
Attn: Librarian

North American Aviation Co.
S & ID Division
Downey, California 90241
Attn: Dr. James Nash

Oklahoma State University
Stillwater, Oklahoma 74075
Attn: Prof. William L. Hughes
School of Electrical Eng.

Power Information Center
University of Pennsylvania
3401 Market Street
Philadelphia, Pennsylvania 19104

Radio Corporation of America
Astro Division
P. O. Box 800
Highstown, New Jersey 08540
Attn: Dr. Seymour Winkler

Rocketdyne
6633 Canoga Avenue
Canoga Park, California 91304
Attn: Library, Dept 086-306 Zone 2

Speer Carbon Company
Research & Development Lab.
Packard Road at 47th Street
Niagara Falls, New York 14304
Attn: Dr. W. E. Parker

Stanford Research Institute
820 Mission Street
SO. Pasadena, California 91108
Attn: Dr. Fritz Kalhammer

Texas Instruments, Inc.
P. O. Box 5936
Dallas, Texas 75222
Attn: Dr. Isaac Trachtenberg

TRW, Inc.
23555 Euclid Avenue
Cleveland, Ohio 44115
Attn: Dr. R. A. Wynveen

TRW Systems
One Space Park
Redondo Beach, California 90278
Attn: Dr. A. Krausz

Tyco Laboratories, Inc.
Bear Hill
Hickory Drive
Waltham, Massachusetts 02154
Attn: Dr. A. C. Makrides

Unified Science Associates, Inc.
826 S. Arroyo Parkway
Pasadena, California 91105
Attn: Dr. Sam Naiditch

Union Carbide Corporation
Electronics Division
P. O. Box 6116
Cleveland, Ohio 44101
Attn: Dr. George E. Evans

United Aircraft Corporation
400 Main Street
East Hartford, Connecticut 06108
Attn: Library

University of Pennsylvania
Electrochemistry Laboratory
Philadelphia, Pennsylvania 19104
Attn: Prof. John O'M. Bockris

University of Pennsylvania
Institute for Direct Energy Conversion
260 Towne Building
Philadelphia, Pennsylvania 19104
Attn: Dr. Manfred Altman

Western Reserve University
Department of Chemistry
Cleveland, Ohio 44101
Attn: Prof. Ernest Yeager

Research & Development Center
Westinghouse Electric Corporation
Churchill Borough
Pittsburgh, Pennsylvania 15235
Attn: Dr. A. Langer

Whittaker Corporation
Narmco R & D Division
3540 Aero Court
San Diego, California 92123
Attn: Dr. M. Shaw

Yardney Electric Corp.
40 Leonard Street
New York, New York 10013
Attn: Dr. George Dalin

Zaromb Research Corp.
376 Monroe Street
Passaic, N. J. 07055
Attn: Dr. S. Zaromb